Analysis, Monitoring and Control of Voltage Stability In Electric Power Systems

by

Miroslav M. Begovic

Dissertation submitted to the Faculty of the

Virginia Polytechnic Institute and State University

in partial fulfillment of the requirements for the degree of

PhD in Electrical Engineering

in

The Bradley Department of Electrical Engineering

APPROVED:

Arun G. Phadke, Chairman

Saifur Rahman

Jaime De La Ree Lopez

Kwa Sur Tam

John W. Layman

July, 1989

Blacksburg, Virginia

Analysis, Monitoring and Control of Voltage Stability In Electric Power Systems

by

Miroslav M. Begovic

Arun G. Phadke, Chairman

The Bradley Department of Electrical Engineering

(ABSTRACT)

The work presented in this text concentrates on three aspects of voltage stability studies: analysis and determination of suitable proximity indicators, design of an effective real-time monitoring system and determination of appropriate emergency control techniques. A simulation model of voltage collapse was built as analytical tool on 39-bus, 10-generator power system model . Voltage collapse was modeled as a saddle node bifurcation of the system dynamic model reached by increasing the system loading. Suitable indicators for real-time monitoring were found to be the minimum singular value of power flow Jacobian matrix and generated reactive powers. A study of possibilities for reducing the number of measurements of voltage phasors needed for voltage stability monitoring was also made. The idea of load bus coherency with respect to voltage dynamics was introduced. An algorithm was presented which determines the coherent clusters of load buses in a power system based on an arbitrary criterion function, and the analysis completed with two proposed coherency criteria. Very good agreement was obtained by simulation between the results based on accurate and approximate measurements of the state vector. An algorithm was presented for identifi-

cation of critical sets of loads in a voltage unstable power system, defined as a subset of loads whose changes have the most pronounced effect on the changes of minimum singular value of load flow Jacobian or generated reactive powers. Effects of load shedding of critical loads were investigated by simulation and favorable results obtained. An investigation was also done by sensitivity analysis of proximity indicators of the effects that locations and amounts of static var compensation have on the stability margin of the system. Static compensation was found to be of limited help when voltage instabilities due to heavy system loading occur in power systems. The feasibility of implementation of the analyses and algorithms presented in this text relies on development of a feasible integrated monitoring and control hardware. The phasor measurement system which was designed at Virginia Polytechnic Institute and State University represents an excellent candidate for implementation of real-time monitoring and control procedures.

Dedication

Acknowledgements

Writing this section for a dissertation is one of the more pleasant duties. As with any large study of this nature, it was necessary for me to obtain the help and support of many persons. It is difficult to meaningfully thank all the people who have made this long sought dream a reality. I could not possibly do justice to all who have helped in large and small ways; whether they know it or not they have my gratitude.

Heartfelt thanks are due to Professor Arun G. Phadke, Chairman of my dissertation committee. His suggestions did much to help me define this project and his comments provided support through to its completion. In addition, the other members of my committee also deserve many thanks. Prof. Saifur Rahman, Prof. Jaime De La Ree Lopez, Prof. Kwa Sur Tam and Prof. John W. Layman were helpful and supportive of my work throughout its duration.Many thanks are due to for valuable discussions and help in some of the computational aspects of my studies.

My colleagues also provided worthy assistance to this work. I wish to acknowledge the helpful comments and support of my project teammates, , , and , provided during crucial developmental stages. , who also serves as the system manager of our workstation, is thanked for supplying some of the software used in this venture. I appreciate the help of who always provided all of us in the Power Systems Laboratory with prompt service.

The financial support for this work, provided by Bonneville Power Administration and National Science Foundation, is also gratefully acknowledged.

Last, but certainly not least, many thanks and love is extended to my family, whose commitment to the completion of my studies has been as complete as my own. My wife has worked, worried and endured throughout the process. She brightened many dark days through valued friendship. My son had to endure my absence during the past months and for that I apologize. My heartfelt appreciation and endless gratitude is owed to my parents, and , for their love, understanding, patience and unwaivering support.

Table of Contents

List of Illustrations

Chapter 1. Introduction

Voltage stability problem in power systems was approached by many researchers in the recent past. A variety of analytical and modeling techniques were applied in power system analysis to grasp the mechanism of development of voltage collapse. A number of sources were identified which deteriorate power system voltage stability margin. Different aspects of power system dynamics were found to contribute to the loss of voltage stability in different ways. Virtually all of the reports of actual cases of voltage instability in power systems as well as the results of theoretical analyses stress the fact that loading level is very high in power systems which operate near voltage stability boundary. Another important observation is that development of voltage instability is linked to slow dynamic modes in power systems, sometimes taking several minutes to produce voltage collapse after first symptoms are identified.

The trend of increasing consumption of electricity in power systems of many countries seems to climb ahead of forecasts. It is accompanied by a lag in con-

struction of new generation facilities which is due to difficulties arising in the process of finding new natural energy resources to compensate for the lack of traditional ones (coal, oil) and growing environmental concerns which are imposing severe regulatory constraints on the utilities. Nuclear energy, once promising generation technology, is practically bogged down in endless disputes between utilities and regulatory commissions about security measures. Many utilities suffered substantial financial losses because of the astronomical budgets for construction, maintenance and subsequent security reinforcement of new nuclear facilities which were not licensed to operate (or at least not licensed to operate at full power) after construction was completed. The expansion of the transmission nework also does not follow the expansion of the system. Complicated legal procedures which precede construction of a transmission line create many delays. It is not uncommon that the construction of a new transmission line is completed 10 years after the initial design. In addition to the above concerns, deregulation in power system operation creates new difficulties and makes planning and control much more complicated. Wheeling is introducing new and unpredictable patterns of power transfer which may sometimes overload parts of the transmission network. It is therefore inevitable to expect power systems to operate in steady states which are very close to stability boundary. Stability margins are sometimes so small that protective equipment trips in normal operating regimes. Under such operating conditions, the problem of power system voltage stability, which was virtually unknown two decades ago, becomes an important factor for reliable and uninterrupted operation.

Although the above mentioned difficulties in power system operation cannot be avoided, there are possibilities to reinforce the security aspects. Developments of new and promising computer technologies (of which the power utilities are among the most dedicated and appreciative users) allow much faster analysis of system operation than was imaginable some time ago. The processing speed of new generation of computers is being greatly increased by introduction of parallel processing architectures, more powerful processors with reduced instruction sets, faster bus designs etc. On the software side, many new algorithms and analytical procedures were developed which support better new computer architectures and/or speed up the calculations which used to take much more. It is becoming within reach of new generation of integrated hardware and software to undertake the task of acquiring and processing data about the system at rates which are fast enough to allow control of system dynamic behavior.

The main motivation for the work presented in this text is development of a feasible integrated monitoring and control system for power system voltage stability. The hardware base for phasor measurement system, which is a backbone of such a system, was designed at Virginia Polytechnic Institute during the past four years. It consists of modular components which provide the ultimate performance that current computer technology offers. Fast 32-bit microprocessors coupled with math coprocessors, A/D converters with multiplexers and extensive communication hardware were implemented in a VMEbus environment. Sophisticated software relies on a real-time DFT algorithm for processing of measurement data, which is implemented in assembly language. The accurate

synchronization of measurements is accomplished by using GPS satellite time dissemination signals (recently made available to nonmilitary users). The distributed phasor measurement microcomputers are linked to more powerful central processing computers which can be chosen to suit the requirements of custom designs. Although the development of phasor measurement system was a substantial team effort to which the author of this text made a contribution, it is not reflected here to a major extent. The purpose of this dissertation is to propose an application which can be accomodated by presently available hardware and software and to propose a design of a monitoring and control system which can take the best advantage of the inherent properties and sophistication of the phasor measurement system. Voltage stability is an excellent candidate for such an application.

Chapter 2 of this text reviews briefly some of the most widely known reported cases of voltage instabilities in actual power systems. It gives an overview of the modeling aspects related to the particular problem of voltage stability analysis and control and mentions some of the important contributions and analytical techniques used by other authors.

Chapter 3 gives the analysis of voltage stability on a 39-bus model of an actual power system which did experience voltage stability related problems. The underlying theory is a static bifurcation theory and the method of attack was chosen to be by simulation. Reason for these choices is the author's belief that some of very commonly encountered cases of voltage collpase can be appropri-

ately described using the static bifurcation theory. It is also notable that the extensive literature on voltage stability is very poorly documented by examples and simulations, most of which are done on very small power system models. Modeling aspects which are relevant for the simulation approach are discussed in Chapter 3. The voltage collapse model was developed on a 39-bus test system and tested by steady state and dynamic simulation for a variety of loading conditions. Indicators of proximity of the system state to voltage stability boundary are identified and tested in numerical examples. Their choice was influenced by the desired objective of real-time application. It was concluded that minimum singular value of a load flow Jacobian matrix and generated reactive powers should be monitored on-line for the assessment of stability margin.

Chapter 4 is a proposal to establish a monitoring system for voltage stability margin based on a phasor measurement system and proposed proximity indicators. A new concept of load bus coherency with respect to voltage dynamics is introduced with the objective to accomplish the real-time stability monitoring using reduced set of measurements. Coherency graph on a set of load buses is defined and an algorithm for determination of coherent clusters of buses is proposed. Two choices for definition of coherency relationship between load buses are analyzed and simulations performed to assess the performance of the algorithm. The obtained results are encouraging and call for further research. The algorithm presented in this chapter may lend itself well to a number of other applications, allowing the determination of the minimum (or optimal) measurement set for a given monitoring or control objective.

Chapter 5 presents an approach for emergency control of a stressed power system when the monitoring system detects alarming conditions of proximity to voltage instability. Sensitivity analysis of both proximity indicators is used to identify the sets of critical load buses, which affect most the changes of proximity indicators when power system is operating close to voltage stability boundary. Proposed algorithms are very suitable for real-time application and can be implemented with phasor measurement system. When critical loads are identified, emergency load shedding is proposed to move the system away from instability. The algorithms can also be used for discrete remote control of groups of loads to prevent the occurrence of an emergency. The results of simulations are provided for the algorithms and effects of load shedding calculated for a variety of loading situations.

The effects of static var compensation on stability boundary are investigated in Chapter 6. Sensitivity analysis similar to the one used for identification of critical loads is developed and used for identification of the most suitable locations for var support as well as the amounts of compensation capacity installed at particular locations. Different compensation setups and extents of compensation were investigated and their effect on voltage stability boundary established. Conclusions were drawn that only substantial amounts of var compensation may provide significant relief in a stressed power system and conditions established for optimal utilization of a given amount of static compensation in terms of their allocation and distribution.

Various issues appropriate for further research are emphasized throughout the text. Although the presented material is an integrated framework for a feasible application of voltage stability monitoring and control system, it remains a matter of continuing research interest of the author.

Chapter 2. A Survey of Research On Voltage Instability

2.1 Introduction

Although the complexity of the voltage stability problem has been studied by many researchers, many questions still remain unanswered and need to be discussed further. Controversies exist about the mechanisms of the development of voltage collapse, important aspects of system modeling (modeling of generators and loads in particular), relevance of system dynamics with respect to voltage stability etc. The apparent multitude of approaches have resulted in a large number of papers published on various aspects of voltage stability analysis, monitoring and control. Many of them are listed herewith in the bibliography of this text. The purpose of this section is to briefly present a few reported scenarios of voltage collapse cases, review some modeling considerations relevant for volt-

age stability studies in power systems, point out the most important contributions, evaluate their likely impact on the future research, and define the framework and motivation for the work done here and the results which will be presented later.

2.2 *Voltage Collapse: Observations*

The first reported cases of voltage collapse occurred in France [1][2][3]. They were linked to the inappropriate voltage regulation of parts of the system which were topologically equivalent to long radial transmission lines (in French Brittany). The inability of the system to supply enough reactive power and the aggravating action of under load tap changing transformers (ULTCs) were found to be the most likely reasons for the collapse. The analysis in reference [1] was based on a simple system connecting a generator to the load through one transmission line. The familiar P-V curves were drawn for different loading conditions and the maximum power transfer associated with the voltage instability. The described case of voltage collapse, which occurred on December 19, 1978 in the French system, was characterized by a slow descent of voltages in the 400kV system during a 25 minute period. Voltages dropped well over 10% during that time, after which one line was tripped on account of overloading. The conditions that preceeded collapse included the heavy East-West power transfer from foreign systems and a very low voltage profile in most of the French system, which

maintained voltages in the regions near foreign systems while the part of the system near Paris was much more vulnerable to voltage instability.

The reasons associated with collapse were: low initial voltage profile, high consumption, heavy transmission system loading, long distances between most of the generation and loads and insufficient reactive power compensation facilities. The situation was worsened by the fact that some of the generators reached their rective generation capability limits and could not maintain voltages with increasing demand. The analysis of French collapses (there were several of them) was concentrated around the maximum power transfer capability of the long radial transmission links, their reactive power support and the action of ULTCs at the loads. One of the most important consequences of the voltage collapse was that it triggered a massive research effort in the general area of voltage stability analysis. Some of those results will be mentioned later and their importance discussed.

The Swedish blackout occurred on December 27, 1983. The Swedish power system is largely a radial system which extends in the north-south direction. The disturbance which caused blackout was a contingency (an outage) in a heavily loaded system. Therefore, changes occurred in network topology as well as system loading which influenced the development of voltage instability. The power transfer in one of the important north-south links was 5.6 GW, just 0.2 GW below the precalculated critical level that can withstand certain types of possible contingencies. The ground fault at one 400 kV bus in the eastern part of the country produced tripping of one 400 kV substation, thus severing the ties to a

major part of 220 kV network through which a part of the power supply to Stockholm and southern regions was channelled. In the first few seconds after the fault, load was redistributed in the network and the transient swings died out fast, leaving as a consequence lower voltages in the southeastern part of the country. About 8 seconds later, the only remaining 220 kV link to the eastern part of the system was tripped because of overloading, increasing further the heavy transmission in the north-south direction. While voltages in the southern part of the system continued to decrease, one more 400 kV line tripped after 50 seconds, triggering cascade tripping of other lines in north-south direction and leaving the southern part of the country with local generation able to supply only 50% of the connected load. Generators in the south tripped soon afterwards due to large shifts of frequency and voltages. Service restoration took several hours.

The above described voltage collapse, reported in [102], is an example of the blackout caused by the changes in network topology rather than due to an increase in load. The importance of this example is that the subsequent stability analyses failed to produce conditions that lead to the collapse, so that the research was largely oriented toward determining the modeling considerations relevant for voltage instability caused by contingencies. Some important conclusions were drawn regarding the modeling of loads: accuracy of load models at low voltages associated with voltage instability situations plays a crucial role in the accurate assessment of the system state. The authors of reference [102] have therefore undertaken an effort to analyze various load models under such conditions and have proposed some new load models, including the dynamic induction

motor model. A suggestion was also made to incorporate the operation of tap changers, generator current limiters, and protective relaying equipment into the simulation models.

A very interesting case of voltage collapse occurred in the Japanese power system (in the zone of Tokyo) on July 23, 1987. It is indicative for a whole category of voltage instabilities in that it was caused solely by changes in load, without any contingencies or topological changes in the system. The demand forecast for that day was 38.5 GW, but high temperatures contributed to the increase in demand. Japanese power system has two nominal operating frequencies, 50 Hz and 60 Hz, interfaced by HVDC converter stations. The zone in which voltage instability was observed was operated by Tokyo Electric Power Company (TEPCO). It serves an area of over 40 square km containing 20.8 million customers. Most of it's 186 power plants are in the eastern region, transmitting power through a 500 kV network to the consumers in the western region of Tokyo.

On July 23, 1987, temperatures were higher than projected ($100°F$ instead of $91°F$) and TEPCO committed 3.8% generation as spinning reserve. The combination of the usual increase of demand after lunch break and the highest daily temperatures (recorded at 12:55 PM) on that day contributed to the high demand of 36.5 GW from 12:40 to 38.2 GW at 1:00, when demand started to grow at the rate of 400 MW/min. Voltages started to fall gradually, all shunt capacitors were switched on and reactive power generation was increased to its maximum. The demand reached a record level of 39.3 GW by 1:10 PM, followed by a voltage

drop to 460 kV in the 500 kV network at 1:15 PM and 370 kV at 1:19 PM, after which three substations tripped, leaving 3 million people without electricity. The recovery of the 8.2 GW lost during the disturbance took about 3 hours, after which the system continued to operate normally. Figure 1 shows the voltage profile at 4 substations which was followed by a general voltage collapse.

This example shows a type of voltage instability quite different from the previous one. The fact that the incident was not triggered by a contingency nor by any kind of human error (all available reactive power support was operating 10 minutes before collapse) shows that its causes must be different. In fact, Japanese collapse is an excellent example of the power system undergoing saddle node static bifurcation. It is possible that this type of voltage instability may become more common in the future, for demand seems to be increasing faster then the long term forecasts while the transmission network and reactive power support do not follow the same trend. Another aspect of this incident is the dominant type of load prevailing at the time of collapse. Due to weather conditions, large portions of the load consisted of the air conditioning equipment with the characteristic very close to constant power. This type of load aggravates the system condition as the load power increases. A power system model based on this example was used in a simulation study of voltage collapse presented later in this text.

Finally, a scenario will be presented for a hypothetical voltage collapse case presented in [81] as a simulation on a portion of Southwestern Ontario power system

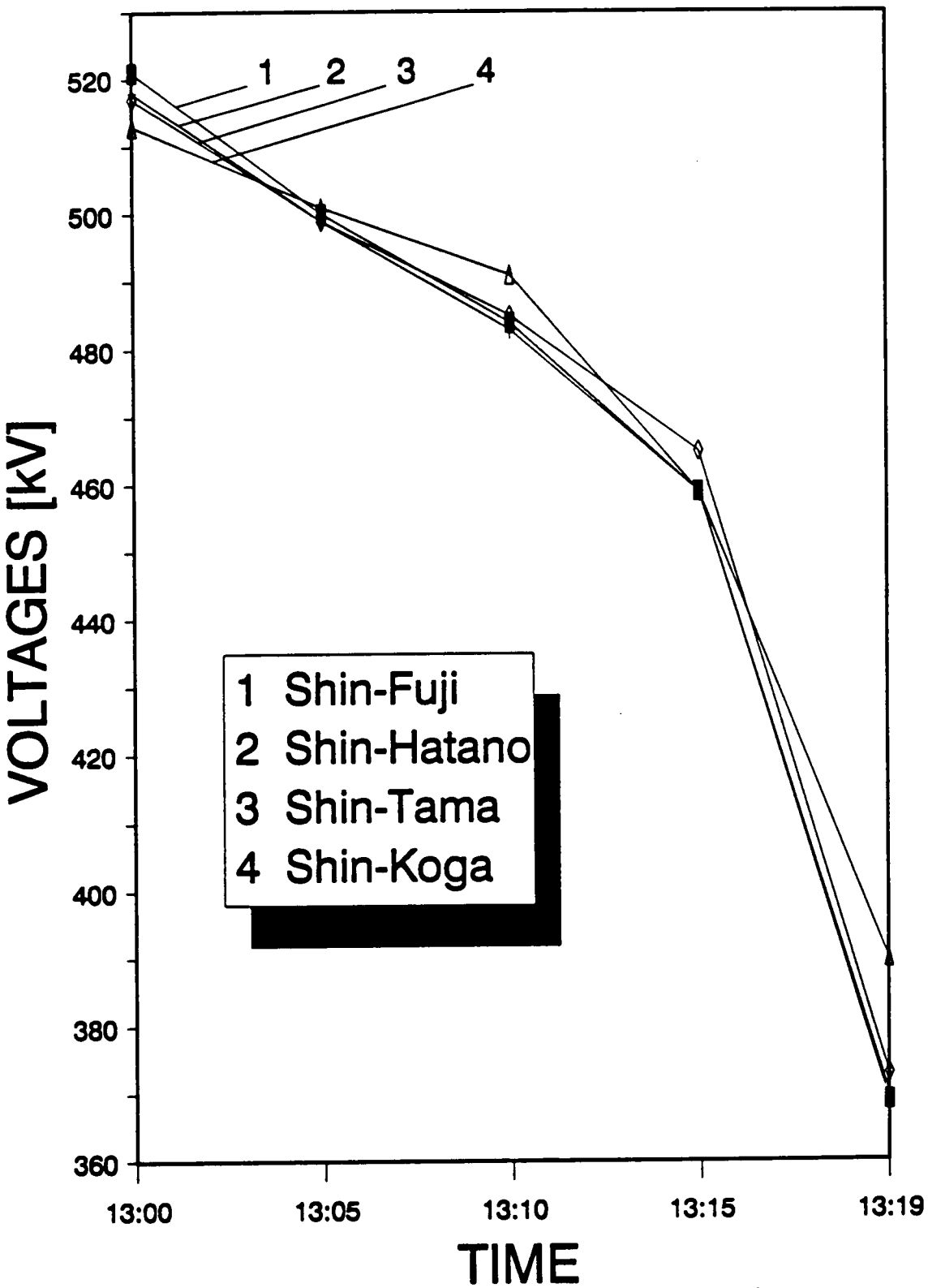

Figure 1. Voltage profile in major 500 kV substations of TEPCO system before the collapse.

which is subjected to heavy power transfer patterns during the winter load peaks. The 4000 bus system model was used with power flows close to their maximum allowable limits with respect to voltage stability. The contingency was modeled as stuck breaker fault which trips two 500 kV lines. The system would settle down in a new steady state after the relay operation following the fault, leaving the two generating units closest to load centers producing reactive power beyond their capabilities. After withstanding such operation for about 10 seconds, their reactive output was gradually reduced to within their VAr capabilities and the compensation was achieved by increasing reactive power generation at two plants farther away from load centers. That increase in VAr output placed those two units beyond their allowable operating limits, which led to gradual decrease of VAr production of one of them after 5 more seconds. The balance was picked up by a remaining unit, which was forced into VAr reduction of its own 5 seconds later, producing a systemwide voltage collapse. The sequence of actions which produced collapse was the decrease of the required VAr production of several generators required to keep their operation within VAr limits $Q_{min} \leq Q \leq Q_{max}$. It was achieved by the gradual reduction of their excitation voltage as a consequence of the increased VAr demand following the violent contingency. This example shows the important role that is played by reactive power generation in voltage instability situation. Similar observations will be presented in the simulation studies later in the text.

2.3 Power System Modeling and Voltage Instability

The modeling aspects of power system voltage stability analysis are very important issues and a matter of disagreement among power system researchers. This is partly caused by the fact that differences still exist in approaches to the problem of voltage instability: as a quasi-steady state, or a dynamic behavior of the system. The emphasis given to particular features which influence most the deterioration of stability margin can also contribute to determining some of the modeling aspects.

Modeling is affected by the size of the system model under investigation. In the first papers which dealt with the issue of voltage instability [1][2][3], the observations pertained to systems having long radial transmission links. The model was therefore chosen to be a network equivalent of a generator connected to the impedance load through a tap-changing transformer and a transmission line. The generator was modeled as a simple voltage source. The inherent dynamics of the tap- changers was implicitly taken into account through the sequence of step-by-step calculations, thus emphasizing the quasi-steady state nature of the adopted approach.

In one of the first attempts to analyze the problem of steady state stability in a power system of arbitrary topology [41], the system model consisted of load flow equations

$$W(x, u) = 0 \tag{2.3.1}$$

where $W: R^{n+m} \rightarrow R^m$ is a set of nonlinear algebraic equations describing the balance of active and reactive powers in the system, while $x \in R^n$ and $u \in R^m$ are vectors of dependent and independent (controlled) variables. The solution of the load flow by Newton method involves the iterative solution of the equation

$$\left[\frac{\partial W}{\partial x}(x^{(i)})\right]\Delta x^{(i)} = -W(x^{(i)}) \tag{2.3.2}$$

where (i) denotes the iteration number. All generators are treated as voltage controlled (P-V) buses while load buses are treated as P-Q buses and multiple slack buses are allowed for situations when several infinite buses are present in the system. The load flow model similar to (2.3.1) is common to most of the approaches based on steady state analysis. Variations include the treatment of the loads as impedances (when they are incorporated into the system admittance matrix with ground connections), or nonlinear functions of voltage (described later). Some recent studies [102] suggest that a careful load modeling, including nonlinearities (for steady state approach) and dynamics (for dynamic approach) are essential in assessing the voltage stability limits without substantial error.

2.3.1 Modeling of loads

Some authors propose voltage dependent loads of the form

$$P = P_0 V^{N_P} \tag{2.3.3}$$

$$Q = Q_0 V^{N_Q} \tag{2.3.4}$$

where exponents N_P and N_Q are constants which depend on the load structure (mostly influenced by the changes in weather). Typical values for the summer season are reported to be $(N_P, N_Q) \sim (1.0, 3.0)$ while winter patterns are $(N_P, N_Q) \sim (1.5, 3.0)$. Authors of [66] have found that, below certain critical values of (N_P, N_Q) , system behavior (damping and synchronizing torques in particular) become highly sensitive to load changes. It should be noted that $N_P = 0, 1, 2$ correspond to constant impedance, constant current, and constant power loads respectively. Some authors [147] propose that a mix of the three types of loads be represented by

$$P = AV^2 + BV + C \tag{2.3.5}$$

The system admittance matrix is used in [147] to relate current injections to voltage magnitudes. When admittance matrix is reduced to internal nodes only, constant impedance parts of the loads are already incorporated into the reduced admittance matrix. The calculation continues with the incorporation of currents corresponding to constant current and constant MVA portions of the load. This

iterative procedure continues until a convergence is reached. It is mostly used in dynamic power system models for transient stability analysis and has recently been incorporated into transient stability analysis using energy functions [147]. It is not clearly established, however, how the changes in load behavior affect the model (2.3.5).

Some authors [102][126][130] consider dynamic load models in their studies. Practical results can be found [102] about the load dependence on voltage variations for various types of loads - motor loads, refrigerators, freezers etc., as well as composite loads. Tests were performed in the Royal Institute of Technology in Stockholm, Sweden, as a consequence of an unsuccessful attempt to reproduce scenarios of voltage instabilities in Sweden using conventional stability analysis methods. Conclusions drawn in [147] suggest that the failure of conventional stability analysis techniques was caused by: i) not observing the load characteristics at low voltage; ii) not modeling the action of ULTC transformers in the system; iii) not modeling the field current limits of generators and iv) disregarding the relay protection. It should be noted that the nature of voltage instabilities discussed in [102] was inherently dynamic (caused by system contingencies). The following dynamic model was proposed for induction motors

$$P = k_{pf} f + k_{pu}(V + T_{pu}\dot{V}) \tag{2.3.6}$$

$$Q = k_{qf} f + k_{qu} V \tag{2.3.7}$$

where k_{pf}, k_{pu}, T_{pu}, k_{qf}, k_{qu} are constants determined by load testing. Some typical values are proposed in the reference cited. V and f are voltage magnitude and frequency at the load bus. The nature and existence of time constant T_{pu} are explained in terms of the inertia of the motor.

Some recent observations [131], however, suggest that the modeling of loads as constant P-Q corresponds to normal operating conditions. This is especially true when a significant portion of the system load consists of voltage controlled devices, which makes them consumers of constant power even when the operating conditions are causing the voltage profile in the high voltage transmission network to sag. Such was the case of the above mentioned voltage collapse in Tokyo, presented in [131], where most of the load consisted of recently developed air-conditioning equipment with almost constant power characteristics over a wide range of voltages. The action of tap-changing transformers at the interface of high voltage transmission and distribution networks could also contribute to making the loads constant power consumers, because their action changes the equivalent impedance 'seen' from the HV transmission network. Due to the control law inherent to ULTC transformers, which tends to maintain a constant secondary voltage, loads tend to consume constant power even when they are constant impedances on the secondary bus.

Constant power load characteristic is generally considered as 'stiff'. Impedance loads consume less power as their voltage decreases. That relieves the system of a part of its burden and represents a natural way of stabilization. Constant

impedance loads can therefore be considered to be 'flexible' loads. When loads are consuming constant power, lower voltages in a strained system cause them to draw more current to preserve the constant power consumption. Higher currents increase losses in transmission network, contributing to further reduction of voltages and bringing the system operating state closer to instability. These phenomena are described and analyzed in [25].

2.3.2 Generator modeling

Detailed models of generators have long been used in transient stability analyses. Some models relevant for voltage stability studies have been proposed, but their complexity varies widely. The model of one-axis generator with zero stator resistances and no saliency can be writen in the following form

$$\frac{dE'_q}{dt} = \frac{1}{T'_{d0}}\left[-E'_q - (X_d - X'_d)I_d + E_{fd}\right] \tag{2.3.8}$$

$$\frac{d\delta}{dt} = \omega \tag{2.3.9}$$

$$\frac{d\omega}{dt} = \frac{1}{2H}\left[-E'_q I_q - D + T_m\right] \tag{2.3.10}$$

$$\frac{dV_r}{dt} = \frac{1}{T_a}\left[K_a R_f - \frac{K_a K_f E_{fd}}{T_f} - V_r - K_a V_t + k_a V_{ref}\right] \tag{2.3.11}$$

$$\frac{dR_f}{dt} = \frac{1}{T_f}\left[- R_f + \frac{k_f E_{fd}}{T_f} \right] \tag{2.3.12}$$

$$\frac{dE_{fd}}{dt} = \frac{1}{T_e}\left[- (k_e + a_{sat} e^{B_{sat} E_{fd}}) + V_r \right] \tag{2.3.13}$$

The notation used above is standard [179]. Equation (2.3.8) represents dynamic behavior of the flux linkages. Equations (2.3.9) and (2.3.10) are models of rotor dynamics driven by the imbalance between electrical and mechanical torques applied to the shaft. Equations (2.3.11 - 13) describe the automatic voltage regulator. E'_q is the generator internal voltage, δ and ω are phase angle and frequency that correspond to the phasor E'_q, while V_r, R_f and E_{fd} are the parameters of the exciter and automatic voltage regulator , which usually consist of dc generator driven by the amplifier circuit whose input is reference voltage (set point), stabilization feedback from the exciter circuit, and rectified feedback from the generator terminal voltage. The values of time constants associated with voltage regulator dynamics are typically a fraction of a second (i.e. T_a and T_e are of the order of 0.1s, and T_f is less than 1s). Their effect on voltage dynamics can therefore be neglected, because voltage dynamics is characterized by transients whose time constants are several seconds to several minutes. Typical values for T'_{d0} are of the order of 5s, while transient swings of phase angles and frequency of a period of 1s or longer.

It seems reasonable to consider only the equations (2.3.8 - 10) as candidates for generator dynamic model pertinent to voltage stability studies. If voltage instability is triggered by a system contingency (line outage, loss of generation etc.) then (2.3.8 - 10) may be necessary to capture all the relevant dynamics in the system response which may have transients whose time constants are very short (less than 1 s). If, however, the voltage instability is caused by migration of a stable equilibrium point due to the change of operating parameters (power requirements of the loads etc.) until a stable equilibrium is lost, then the dynamics of the system descent into collapse may as well be described by equations (2.3.9 - 10) only. The solutions of those equations (for $\ddot{\delta} = \dot{\delta} = 0$) coupled with the algebraic equations describing active and reactive power balance at load buses are the system equilibria. When a smooth transition of the parameters brings the system to the point where no stable equilibrium exists, the system is at a static bifurcation, characterized by the singularity of the Jacobian matrix describing linearized power flow equations. In the first approach to model voltage instability described above, the process is inherently dynamic, caused by a disturbance which moves the system along a trajectory in the state space which contains some stable equilibria that the system may eventually settle in. In the second approach, the changes of system parameters shrink the regions of attraction of stable equilibria until they vanish, causing the system to embark on a center manifold trajectory in post-bifurcation dynamics which may or may not end up in another stable equilibrium point. It seems likely that the generator dynamics (2.3.8)(2.3.11-13) plays a minor role in the post-bifurcation system response. This

opinion is shared by a number of other researchers who use similar generator models in their studies [19][20][23][34][35][38][40][42][70][71][86][149][150], but there are opinions that the flux decay dynamics of (2.3.8) should also be taken into consideration [44][60][74]. The exclusion of the flux decay mode presents a convenience in analysis of complicated power system dynamics, and the present discussion should be viewed as an argument in favor of the model simplification rather then an attempt to disregard the effects that the flux decay mode has on the overall system dynamics. Present studies do not offer a definite answer to the issue of defining the minimum generator model relevant for voltage stability studies. A useful analytical tool will be presented here without a proof. It was presented in [29] as a means of decoupling the systems with widely different dynamics into a two time scale system. For a system

$$\varepsilon \dot{y} = g(x, y) \tag{2.3.14}$$

$$\dot{x} = f(x, y) \tag{2.3.15}$$

decoupled solutions may be expressed as

$$x = \bar{x}(t) + O(\varepsilon) \tag{2.3.16}$$

$$y = \bar{y}(t) + \hat{y}(\tau) + O(\varepsilon) \tag{2.3.17}$$

provided that the equilibrium $\hat{y}(\tau) = 0$ is uniformly asymptotically stable in the fast (boundary layer) dynamics

$$\frac{d\hat{y}}{dt} = g(\bar{x}(t_0), \bar{y}(t_0) + \hat{y}(\tau), 0, t_0) \tag{2.3.18}$$

and $\hat{y}(0) = y(t_0) - \bar{y}(t_0)$ belongs to its domain of attraction

$$\lim_{\tau \to \infty} \hat{y}(\tau) = 0 \tag{2.3.19}$$

Also, the eigenvalues of $[\partial g/\partial y]$ for $\varepsilon = 0$ along $\bar{x}(t)$ and $\bar{y}(t)$ should have real parts smaller then a fixed negative number

$$Re\,\lambda\left[\frac{\partial g}{\partial y}\right] < -A < 0 \tag{2.3.20}$$

The above technique can be used to determine the model of the fast system dynamics moving on a zero order manifold consisting of the values of the slow system variables. The condition (2.3.20) assures that asymtotically stable zero order manifold exists for all values of $\varepsilon \in [0, \varepsilon^0]$. This technique was used in [60] to extract (2.3.8) as the only part of the generator model relevant for stability studies incorporating ULTC dynamics. An open area for research is the determination of the zero order manifold for a study incorporating generator dynamics (2.3.8 - 10) which was not pursued before because of the complexity of the problem. Such an approach would provide a rigourous analytical justification for time scale based decoupling of generator dynamics.

2.3.3 Modeling of ULTC transformers

The under load tap changing (ULTC) transformers have long been recognized as one of the possible sources of voltage instabilities in power systems. It is therefore very important to pay due attention to modeling of tap changers in order to account for their influence on voltage stability studies. One problem associated with ULTCs is the discrete nature of their operation, which does not lend itself to easy integration into the power system model whose dynamics can be modeled by differential equations in continous time domain. In one of the first attempts to analyze the ULTC operation [14], the assumption was made that relatively long time intervals between the tap changes justify the steady state model, which was analyzed in a few typical applications.

In [4], however, an attempt was made to generate a discrete model for the analysis of uncoordinated tap changer dynamics, without consideration for the dynamics of the other power system components. The objective of the paper [4] was to show that the ULTC control law based on the local voltage measurement can produce systemwide destabilizing action. The discrete model of the tap position was proposed as

$$a_{i_j}(k+1) = a_{i_j}(k) - d_i f(X_i - X_i^{ref}) \tag{2.3.21}$$

where the nonlinear control law is given as

$$f(X_i - X_i^{ref}) = \begin{cases} 1, & if \ X_i - X_i^{ref} > \Delta V_i \\ 0, & if \ |X_i - X_i^{ref}| \le \Delta V_i \\ -1, & if \ X_i - X_i^{ref} < -\Delta V_i \end{cases} \tag{2.3.22}$$

Equation (2.3.21) shows the tap position $a_{ij}(k+1)$ of a tap changing transformer connected between nodes i and j at the instant $k+1$. The minimum tap change is d_i and nonlinear control function $f: R \rightarrow \{1,0,-1\}$ transforms the difference between the measured voltage X_i and the reference voltage X_i^{ref} into a tap change, if that difference is bigger than some threshold ΔV_i . The subsequent system analysis was based on the application of the linearized $Q-V$ decoupled equations with discrete tap changer model (2.3.21-22). The results obtained suggest that conditions may arise in the system when the decentralized control law of ULTC would actually destroy the stability of the voltage profile in the system. Those conditions were derived by analysis of the above described discrete system with the relay - type nonlinearity. The drawbacks of this method are the use of linearized system equations over a wide range of system states and the assumption that the action of ULTCs is highly synchronized, which is not true. The authors of [4] refinced their model later [8] by assuming that the control time intervals of different ULTCs in the system are multiples of some shorter time interval T_1 and can therefore be expressed as

$$\begin{aligned} T_2 &= m_2 T_1 \\ T_3 &= m_3 T_1 \\ &\cdots \\ T_n &= m_n T_1 \end{aligned} \tag{2.3.23}$$

That was a more appropriate model, although the linearization of the power flow equations remains a debatable assumption for this kind of analysis.

A different approach was adopted by authors of [24][25][46][126]: they modeled ULTCs as continously acting devices, justifying it by a relatively small tap change (typically 0.625%) and the continous effect of the systemwide ULTC action which can be well approximated by equations of the form

$$\frac{dn}{dt} = \frac{1}{T}\left\{V - V^{ref}\right\} \tag{2.3.24}$$

where n represents the tap position, T is the time constant associated with the first order delay model, and V and V^{ref} are the measured and reference voltages. The authors [24] considered constant voltage sources and constant impedance loads to derive conditions for unstable operation based on the linearized system matrices. Similar were the assumptions in [25], where the objective of the study was the assessment of voltage stability regions. A nonlinear dynamic load was included in a similar study [126].

The modeling aspects of ULTCs and their dynamics are important, because they can explain part of the problems which lead to voltage instability. Considering their operating time of 5 - 100 s, they cannot be neglected in analysis of the events which precede the final system descent into collapse (those events may take up to several minutes). The voltage collapse itself cannot be explained through ULTC action, the least of the reasons being that their operating range is limited

to a relatively narrow range of voltages around a nominal voltage. None of the authors who analyzed their operation recognized this fact, because it would create models whose complexities would far exceed the objectives of the studies. One should bear in mind, however, that ULTCs are important parts of the voltage control activity in power systems and that their dynamics may contribute significantly to the worsening of the voltage stability margin.

2.3 Voltage stability studies

The extensive research in the domain of power system voltage stability have generated considerable literature about the nature of voltage collapse, modeling aspects, determination of stability regions and development of techniques for monitoring and control of stressed power systems.

An attempt to analyze voltage collapse in long radial transmission networks was made in [1], where the first observed case was presented. Regulation of voltages in power systems based on the conclusions in [1] was discussed in [2][3][11]. No attempts were made to extend the analysis to a power system of arbitrary topology. Relationship between loss of power system steady state stability and the singularity of the associated Jacobian matrix of the load flow equations was reported in [41]. Similar observations were made in [49].The phenomenon of multiple load flow solutions was investigated in [22], along with the associated voltage

instability, the proximity of multiple load flow solutions, change of sign of the determinant of load flow Jacobian, and the analysis of stored energy in the system for stability assessment of the solutions. These concepts were refined in [88][94][125][65], where the voltage instability proximity index was proposed as the angular measure between the vectors representing the high and the low voltage solutions in the state space. The analysis of voltage stability was done on Q-V curves (instead of P-V) of the power system load nodes in [87]. The reactive area identification was proposed in [93] based on the system topology and the properties of disturbance spreading was reported in [9]. Another static stability index for the proximity of voltage collapse was analyzed and proposed in [89][90][91]. It was also based on the multiple load flow solutions: an estimate of the critical state on a P-V curve for a certain node of a power system was found as the intersection of the tangents to low- and high voltage solution curves at that particular state. A relationship between the total reactive power generated and consumed in the system was proposed as an alarm against the incipient voltage instability in [17]. Two optimal load flow solutions were proposed for the estimate of stability margin at any operating steady state. A simple approximate proximity indicator based on the load flow calculation was proposed in [21]. Convergence properties of the load flow in the vicinity of voltage stability limit were investigated in [53] and it was concluded that higher initial voltage estimates and calculation in polar coordinates improve solution stability and convergence properties. Conditions for voltage stability were presented as signs of gradients of load bus voltage magnitudes vs. changes in generator voltages and shunt

capacitances. In [24], tap changer based dynamics of the power system (continous time model) was used to investigate stability conditions by checking whether linearized system matrices are M-matrices. Similar modeling was used in [25][46] to demonstrate the possibility of unstable operation of tap changers and propose the calculation of the stability regions as largest hypercubes in the system state space which are contained within the true domain of stability. The modeling was extended in [126] to incorporate nonlinear dynamic motor loads [102] in the analysis of a simple two bus system. The discrete dynamics of the tap changers was analyzed in [4][8] based on the steady state modeling [14] and conditions derived for unstable operation. Based on the linearized and decoupled power flow equations, an algorithm was proposed to use the optimization of the Chebyshev norm for determination of the reduced set of monitoring (pilot) points in the power system for stability tracking and control [6][7]. The approach was based on the French concept of secondary voltage control by use of pilot points [11] determined by analyzing the nodes in network which have the maximum short circuit power and behave like 'centers of coherency' to neighboring nodes with respect to voltage changes in the system. Properties of the spreading of the effects of Q-V disturbances in power networks were further investigated in [5][9][10]. In [45][92][107], voltage instability is associated with the loss of voltage controllability, defined as a property of the voltage magnitude at every node to increase for positive reactive power disturbances and increases of voltages at generator nodes. Static conditions for voltage instability were used in [26][32] and loads modeled as random variables with Gaussian distribution. The probability

of voltage collapse could then be derived from the linearized system model with the intention to incorporate voltage stability risk analysis at the planning level. The singularity of a load flow Jacobian was recognized as a condition for voltage collapse [19] and the minimum singular value of the Jacobian proposed as a proximity indicator. The implementation of an algorithm for calculation of the minimum singular value in a parallel processing environment was analyzed. The strategy for redistribution of generated powers following the disturbance was analyzed in [61] based on the results of [19]. The model was extended to dynamic voltage instabilities by using the dynamic induction motor model in [71].

The small disturbance stability analysis was introduced in [30][31][50] on linearized equations of generator swing dynamics on a structure preserving model [96]. Structure preserving model does not reduce the equivalent system to generator buses only, but keeps track of system topology on buses without dynamics as well. That model was successfully used for transient stability analysis [97][98] and was favored by a number of authors for voltage stability analysis. The accuracy of generator modeling for voltage stability analysis was investigated in [44][59][60][74]. The flux decay mode was found relevant for coupling with the dynamics of tap changers. In the analysis on a model with generator dynamics only, flux decay mode was determined to be critical in the analysis of the linearized dynamics for the eigenvalues which correspond to flux decay modes in a multimachine system. These eigenvalues were found to be the first ones to cross the imaginary axis into the region of instability. Very important results were presented in [40][86][129], where the conditions for voltage collapse were derived

as a static bifurcation of the equilibria of a power system model based on swing dynamics and loads modeled as constant complex power. The distinction was emphasized between conditions for development of steady state instability, characterized by a high sensitivity of phase angles to changes of system parameters, and voltage instability, characterized by a high sensitivity of load voltage magnitudes to the change of system parameters. Both voltage and steady state instability regions belong to the hypersurface in state space which corresponds to the singularity of the linearized dynamics at the equilibrium point (power flow Jacobian). The degree of degeneracy of Jacobian may produce a variety of system behaviors, including the voltage collapse. A Lyapunov-Schmidt reduction technique was proposed for local description of the bifurcation equation in the form of a polynomial whose degree is dependent on the degree of degeneracy of Jacobian. A few types of bifurcations were analyzed on a small three bus system example and it was suggested that a majority of the voltage instability cases were caused by a saddle node bifurcation of the equilibria (characterized by codimension one, or a single eigenvalue of the Jacobian crossing the imaginary axis under the influence of changing system parameters). This model seems to be well supported by many reports of the collapse cases, although the author warns [86] that other types of bifurcations are quite possible in power systems. Voltage collapse models in small power systems which were based on static bifurcation were presented in [54][64][130][171], while the simulation models on a 39 bus system were presented in [168][169] and will be explained in detail later in the text.

Finally, a complete dynamic model of a power system with randomly changing loads was analyzed in [20][23][42][123][175] as a set of stochastic differential equations. The system state was modeled as continously changing in a sort of 'potential well' of energy while the change of system parameters was shrinking the size and depth of a 'well' as the system approaches the bifurcation. The exit time was introduced as an estimate of time within which the system would jump out of the 'well' with a probability of one. This dynamic model, although very appealing, presents many difficulties in analysis and did not lend itself to efficient analysis on large models. It is an important concept, however, because it is probably the best description of the process that leads to voltage instability (or any other instability caused by a bifurcation) and proposes the use of direct stability analysis methods.

Very good reviews of the voltage stability analysis methods and techniques was presented in [18][43][128][163] and categorized according to the modeling aspects and other assumptions.

2.4 Conclusion

The examples presented in 2.2 show the seriousness of the consequences of voltage instability in power systems. Another factor of the importance for voltage stability analysis is that instabilities are occurring more frequently due to in-

creasing loads, slow increase of generation, and a slow expansion of transmission networks. It seems likely that a number of voltage instability cases may be expected in the future without any human errors, or contingencies in the system, but simply because of the sharp increase of demand caused by changing weather conditions or some other significant event. Wheeling and the unpredictable patterns of power flows it causes may also contribute to the reduction of stability margins. As an illustration of the rate at which voltage instability cases are occurring in the US, just a few recent ones will be named here: northeast voltage depression on June 11, 1984, southeast Florida disturbance on May 17, 1985, Utah disturbance on July 6, 1985 and Indiana/Illinois low voltage conditions on July 20, 1987 [81]. It seems very likely that the research on voltage stability will have to expand in the near future and take on some new directions. The analysis of modeling aspects and development of new analytical techniques for assessment of power system voltage stability will have to resolve many of the present dilemmas and find some new answers to the issues which are still a matter of debate. Growing needs of utilities will direct some of the research toward development of practical applications which could be used to protect power systems from voltage instabilities. At this time, commercially available hardware is more than able to allow effective stability monitoring of the slow voltage dynamics at the system level. Development of monitoring systems is a first step toward controlling voltage stability. The availability of the monitoring system [165][166] for direct systemwide acquisition of state vector was one motivation for the work that is presented in this text. Once the monitoring is successfully accomplished and im-

plemented in a power system, the fast control applications will be needed as an extension of the monitoring systems. The work in the following chapters was motivated by feasibility for implementation in the near future.

Chapter 3. Voltage Stability Analysis: Simulation Approach

3.1 Introduction

The research in power system voltage stability, part of which was discussed in the previous chapter, represents a substantial although somewhat controversial body of knowledge. Some of the results [40][70][86] combined with reports of actual observations of voltage instability [131] may be used as a framework toward building a reasonably accurate model of voltage collapse mechanism, which could be used as a first step toward development of the monitoring and control system for voltage stability.

Several issues are to be resolved before the simulation model may be formed. The purpose of this chapter is to present the reasoning that leads towards building the simulation model:

i) The first question is to define a mathematical model of the power system of a reasonable size which can provide significant results and practical observations. Such a system should have several generators and a complex topological structure which cannot be approximated by a long radial transmission line. Many of the previous attempts to explain voltage collapse were based on such an approximation and many examples were presented on simple models with one load and one, or two generators. Voltage instability is a much more complex network behavior and more complex models are needed to capture its properties. One should bear in mind, however, that the purpose of establishing the simulation model is to implement the results in a real-time monitoring system, which means that the simulation model should be as simple as possible. This requires that modeling issues of the generators and loads be resolved in a way efficient enough to lend itself to easy implementation. An algorithm for simulation will then be presented which is based on the modeling assumptions and robust enough to produce accurate results near stability boundary. Conditions will also be derived which bring the system state to the stability boundary and produce the loss of steady state stability, or voltage instability.

ii) Another important issue is to establish a scenario which would move the power system state trajectory towards voltage instability. Since virtually all reports

stress the heavy system loading which preceded blackouts, loading patterns need to be determined which end in voltage instability. It will be shown how different loading patterns affect the system behavior and that different loading patterns lead to different types of instablities. The loading in the pre-collapse period can be conveniently simulated by a quasi-steady state analysis since it represents a relatively slow process. Dynamic simulation is useful in a narrow time frame before the instability, when alarm and emergency control actions in a system need to be triggered.

iii) Finally, an analysis of the simulation results will provide an insight into the development of voltage instability and provide important information about the choice of indices for stability margin which could be captured by a real time monitoring system.

3.2 Model definition

The choice of a model, as discussed above, is determined by two important considerations: it should represent with sufficient accuracy the conditions and dynamics reported in many actual cases of voltage instability and should also be kept to a level of simplicity which is acceptable for future implementations in a real-time environment. The modeling of components is the first issue to be resolved. Transmission lines do not need special consideration since voltage dy-

namics is not associated with very fast transients nor unbalanced operation of the power system. Therefore, single phase (positive sequence) representation of the balanced network with transmission lines modeled as pi-sections is appropriate. The transformers play a major role in deterioration of the voltage profile, as it was mentioned in the previous chapter. Tap changing action is certainly important when security issues are investigated. In the pre-collapse conditions, tap changers are persistently trying to maintain constant secondary voltages at interfaces of HV and distribution networks, as well as between networks of different voltage levels. Their operation may be viewed as slightly delayed action toward keeping constant consumption of the impedance loads in the secondary network. That translates into conclusion that in a voltage stability oriented analysis, the approximate modeling of loads is linked with modeling of tap changing action. A convenient approach is to abandon explicit modeling of ULTC dynamics for the dynamic simulation algorithm and assume that loads are 'stiff'. This is justified by reports on typical loads in some systems which suffered from voltage instability [131] as well as the above described effect of ULTCs. The convenience of using the composite model for load [102] which was used in [126][130] does not provide an accurate picture of the voltage instability problem. Its dynamics mainly relies on the assumption that induction motors represent a significant portion of every load in the system, which is debatable. If all the loads are assumed to have dynamics, then the dynamic model of the power system may be represented in the equivalent form

$$\dot{x} = f(x, \lambda) \tag{3.2.1}$$

where $x \in R^n$ and $\lambda \in R^k$ are the system state and parameter vectors consisting of elements describing dynamics of generators and loads, while f: $R^n \times R^k \rightarrow R^n$. In case when some (or all) of the loads do not have dynamics, the model is represented by

$$\begin{aligned} \dot{x} &= f(x,y,\lambda) \\ 0 &= g(x,y,\lambda) \end{aligned} \tag{3.2.2}$$

where $x \in R^n$, $y \in R^m$ and $\lambda \in R^k$ are vectors of state variables which correspond to generator dynamics, elements of the vector field that describe the power balance imposed by non-dynamic loads as the rest of the system and parameter vector. Functions f: $R^n \times R^m \times R^k \rightarrow R^n$ and g: $R^n \times R^m \times R^k \rightarrow R^m$ are nonlinear power flow equations. The analysis of the model (3.2.2) is more complicated than the analysis of (3.2.1), although both models can be brought to the state of voltage instability [126][130][168][169]. The model chosen for simulation analysis is therefore of the form (3.2.2), with loads modeled as constant complex powers.

Generator model is chosen to be a voltage source behind synchronous reactance, but with one additional assumption: it is not the voltage behind the synchronous reactance, but the generator terminal voltage which is assumed constant. This is equivalent to the assumption that the time constants in differential equations (2.3.8) (2.3.11-13) are close to zero, i.e. that the automatic voltage control and flux decay modes are acting much faster than the system voltage dynamics. Thus the model does not represent equations (2.3.9-10) only but a fast acting voltage control as well (Figure 2).

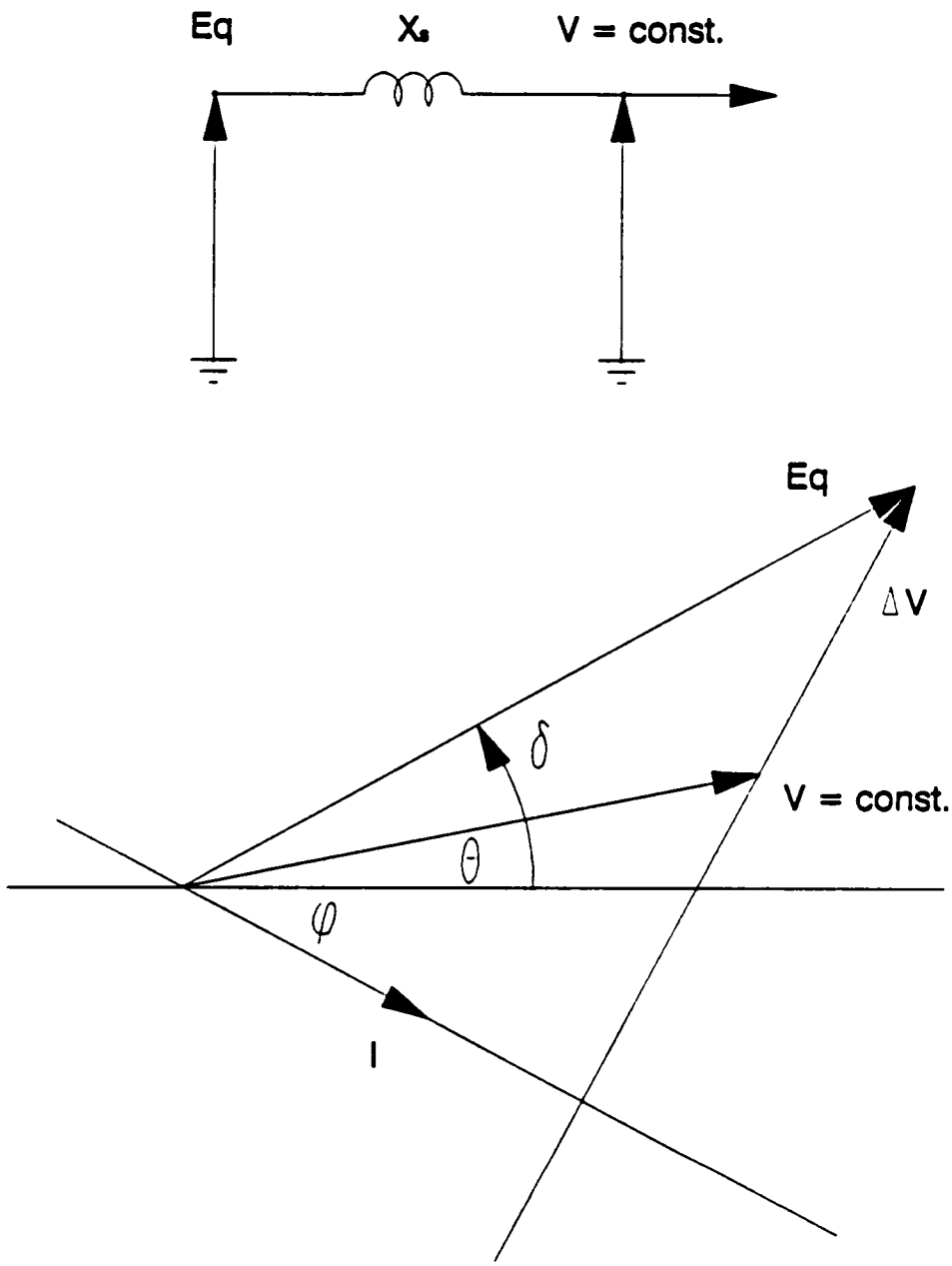

Figure 2. Phasor diagram of the generator model

3.3 Simulation algorithm

Let us assume that the power system consists of n generators and m loads. Generator dynamics can be expressed in terms of swing equations, while two additional algebraic equations are needed per load bus to impose active and reactive power balance constraints

$$\begin{aligned} M_i\ddot{\delta}_i + D_i\dot{\delta}_i + f_{ri}(\delta, \theta, V, \lambda) &= 0\,, \quad i = 1, \ldots, n \\ g_{rj}(\delta, \theta, V, \lambda) &= 0\,, \qquad j = 1, \ldots, m \\ g_{ql}(\delta, \theta, V, \lambda) &= 0\,, \qquad l = 1, \ldots, m \end{aligned} \tag{3.3.1}$$

where $M_i\,(M_i \geq 0)$ are generator moments of inertia, $D_i\,(D_i \geq 0)$ are generator damping factors, $\delta \in R^n$, $\theta \in R^m$, $V \in R^m$ and $\lambda \in R^k$ are vectors of generator phase angles behind synchronous reactances, load bus phase angles, load bus voltage magnitudes and the rest of the system parameters respectively, consisting of the transmission line parameters, tap changer positions and transformer parameters, as well as the active and reactive load requirements. Besides load requirements, the rest of paremeters are assumed constant for the purpose of our simulation. Generator terminal buses are treated as load buses with zero power requirements. Adopting a shorter notation

$$\begin{aligned}\delta &= [\delta_1\, \delta_2, \ldots, \delta_n]^T \\ \theta &= [\theta_1\, \theta_2, \ldots, \theta_m]^T \\ V &= [V_1\, V_2, \ldots, V_m]^T \\ \lambda &= [\lambda_1\, \lambda_2, \ldots, \lambda_m]^T\end{aligned} \tag{3.3.2}$$

Nonlinear functions

$$\begin{aligned} f_{ri}&: R^n \times R^m \times R^m \times R^k \to R \quad , i = 1, \ldots, n \\ g_{rj}&: R^n \times R^m \times R^m \times R^k \to R \quad , j = 1, \ldots, m \\ g_{qi}&: R^n \times R^m \times R^m \times R^k \to R \quad , l = 1, \ldots, m \end{aligned} \tag{3.3.3a}$$

represent active and reactive power balance equations. If we denote

$$\begin{aligned} f_r &= [f_{r1} f_{r2}, \ldots, f_{rm}]^T \\ g_r &= [g_{r1}\, g_{r2}, \ldots, g_{rm}]^T \\ g_q &= [g_{q1}\, g_{q2}, \ldots, g_{qm}]^T \\ M &= diag\{M_1\, M_2, \ldots, M_n\} \\ D &= diag\{D_1\, D_2, \ldots, D_n\} \end{aligned} \tag{3.3.3b}$$

we can express the power system dynamic model (3.3.1) in the compact form

$$\begin{aligned} M\ddot{\delta} + D\dot{\delta} + f_r(\delta, \theta, V, \lambda) &= 0 \\ g_r(\delta, \theta, V, \lambda) &= 0 \\ g_q(\delta, \theta, V, \lambda) &= 0 \end{aligned} \tag{3.3.4}$$

If we assume

$$\xi = \begin{bmatrix} \xi_1 \\ \xi_2 \\ \cdots \\ \xi_{n+m} \end{bmatrix} = \begin{bmatrix} \delta_1 \\ \delta_2 \\ \cdots \\ \delta_n \\ \theta_1 \\ \theta_2 \\ \cdots \\ \theta_m \end{bmatrix}$$

$$E = \begin{bmatrix} E_1 \\ E_2 \\ \cdots \\ E_{n+m} \end{bmatrix} = \begin{bmatrix} V_{g1} \\ V_{g2} \\ \cdots \\ V_{gn} \\ V_1 \\ V_2 \\ \cdots \\ V_m \end{bmatrix} \qquad (3.3.5)$$

where V_{gi} represent the voltage magnitude behind the synchronous reactance for generator i , power balance equations f_r, g_r and g_q can be expressed as

$$
\begin{aligned}
f_{ri} &= P_{mi} - E_i \sum_{j=1}^{n+m} E_j [G_{ij} \cos(\xi_i - \xi_j) + B_{ij} \sin(\xi_i - \xi_j)] \\
g_{ri} &= P_i - E_i \sum_{j=1}^{n+m} E_j [G_{ij} \cos(\xi_i - \xi_j) + B_{ij} \sin(\xi_i - \xi_j)] \\
g_{qi} &= Q_i - E_i \sum_{j=1}^{n+m} E_j [G_{ij} \sin(\xi_i - \xi_j) - B_{ij} \cos(\xi_i - \xi_j)]
\end{aligned}
\tag{3.3.6}
$$

where G_{ij} and B_{ij} are the admittances and susceptances of the lines connected between buses i and j . P_i and Q_i are active and reactive load requirements at bus i while P_{mi} is mechanical power at the shaft of the generator i . The equilibria of (3.3.4) are obtained when $\ddot{\delta} = \dot{\delta} = 0$ and are calculated using Newton Raphson algorithm in polar coordinates.

The choice of the overall solution technique for the system (3.3.4) is determined by a number of factors. The system (3.3.4) is not equivalent to an ordinary transient stability problem in two main aspects: it is almost always close to being ill-conditionned in the voltage stability oriented simulations and it is necessary to preserve the network topology during the simulations, because it is at load buses where the actual instability happens and the use of the model reduced to the network equivalent connected to generator terminal buses would not be suitable. The first requirement translates into requirement for a differential equation solver which can handle stiff systems. Stifness is defined as the property of those systems which consist of widely varying time constants, or, in more general sense,

property of those systems whose linearized dynamics (Jacobian) is characterized by a large ratio between the largest and the smallest eigenvalues. When swing dynamics of the generators is the only one modeled, stifness is not an issue unless the problems investigated are associated with the loss of stability (as in our case, due to near singularity of the Jacobian which makes it very ill-conditionned).

There are two alternatives in handling the system (3.3.4), which consists of the system of differential equations coupled with a system of algebraic equations. The first one is called the partitionned solution approach and consists of simple alternation of the differential equation solver with the algebraic equation solver, simultaneously taking care that solutions be properly interfaced. The interface between the solutions is the main obstacle in application of partitionned solution techniques, but there is an advantage which makes them a very popular choice: it is the possibility to chose the integration methodes and network solution methods independently. That way, they can be chosen suitably to accomodate specific requirements of the problem being solved. The best of currently known partitionned solution techniques have excellent convergence properties and are very effective. The alternative approach is the use of simultaneous solution approach which is characterized by 'algebrization' of the differential equations and simultaneous solution of the whole system of algebraic equations obtained that way. The advantage of this method is absence of interface problems, but its convergence properties are not superior to the ones of the partitionned solution approach.

When system (3.3.4) is being numerically solved, it can be assumed that the slow dynamics of (θ, V) allows the alternative solving of the system of differential equations (giving a propagation of the solution in time domain) with solving of the system of algebraic equations (giving correction in the state space and the vector field on it). That approximation can be modeled as follows: if we linearize the differential equation (3.3.4) around a point $(\delta_0, \theta_0, V_0, \lambda_0)$ without considering the algebraic part of it and assuming that the parameter vector λ is not changing, we will get

$$\begin{aligned} M\,\Delta\ddot{\delta} + D\,\Delta\dot{\delta} + f_p(\delta_0, \theta_0, V_0, \lambda_0) + \frac{\partial f_p}{\partial \delta}\Delta\delta + \\ + \frac{\partial f_p}{\partial \theta}\Delta\theta + \frac{\partial f_p}{\partial V}\Delta V + O(\|\Delta\delta\|^2) + O(\|\Delta\theta\|^2) + O(\|\Delta V\|^2) = 0 \end{aligned} \tag{3.3.7}$$

where $\Delta\delta = \delta - \delta_0$, $\Delta\theta = \theta - \theta_0$ and $\Delta V = V - V_0$. The expression (3.3.7) is true because f_p is infinitely differentiable. In the above proposed simulation approach, (3.3.7) is simplified by the assumption

$$\Delta\theta \sim 0, \quad \Delta V \sim 0 \tag{3.3.8}$$

over very short time steps of the integration methods used, allowing that the interface of the solution of the integration method and the solution of algebraic equations be done in one iteration. The rigorous interfacing would require that solutions of the differential equation solver and algebraic equation solver be alternately inserted into one another until complete convergence is reached of the whole system (3.3.4). The simplification is justified by the fact that voltages and

phase angles that correspond to load buses are changing relatively slowly if short enough time step is assumed for differential equation solver. That way, an update of the value of δ is made before it changes significantly, while voltage magnitudes and phase angles are barely changing their values. In practice, it means that time steps chosen are of the order of 1 millisecond for simulations of the system descent into voltage instability which typically takes 10-20 seconds.

Of integration methods available, Euler method is the simplest. It is not suitable for power system applications because it is very inefficient and requires very short time steps. More complicated, but much more effective are Runge-Kutta methods, although opinions are divided about its ability to handle stiff systems. Runge-Kutta methods of the orders 3 to 5 are used in many power system applications. Predictor corrector methods of the Adams family, with self starting Euler method at the low order end, are excellent in handling systems whose stiffness is not high. Implicit multistep formulae of the Gear family are excellent for very stiff problems, but not as competitive on non-stiff ones. The combination of variable step, variable order Adams predictor corrector and Gear methods were used as differential equation solvers, because Gear method is suitable for numerically 'stiff' differential equations and adapt the time step and order of the integration method depending on the convergence of the algorithm while Adams method is more effective in the non-stiff dynamic responses (settling into steady state when transients are dying out for example). A control method was used in several simulation cases to check the validity of the results by changing the value of the time step (from 0.1 millisecond to several milliseconds). In all cases, the

produced outputs were indistinguishable from one another due to the fact that the changes of voltage magnitudes and phase angles corresponding to load buses were almost zero between successive time steps. In the vicinity of voltage collapse though, changes of voltage magnitudes may rapidly become excessive and the algorithm generated larger errors, but that effect was reduced as much as possible by shortening time steps. In all the simulations with different time steps, the descent into collapse was achieved in the exact same time intervals (to within one time step), which suggests that time steps and approximate simulation methods were chosen appropriately. Also, the sensitivities of the functions f_p, g_p, and g_q to changes in θ and V are not significant unless the stability boundary is very close. This property is noted and taken advantage of in the following chapter, where the singular value decomposition of the approximate Jacobian matrix was accomplished with remarkably accurate results.

The differential equation solver is just one part of the simulation algorithm. Another important part is the algebraic equation solver which updates (θ, V) after every update of δ by solving $[g_p\ g_q]^T = 0$. Some choices need to be made to obtain a reliable network solution. As suggested by the results of studies on ill-conditionned power systems [53], polar coordinates were chosen for power system representation in non-complex form (algorithms which can handle power system models in complex form are not effective ones for this application). Gauss Seidel method is simple to program and requires very little memory, but its poor convergence would make it prohibitively slow for ill- conditionned systems. Application of Z-matrix based methods is obsolete. They are rarely used, only in

algorithms associated with some kind of network reduction techniques. Newton Raphson method has very good (quadratic) convergence. It can be applied on non-complex power system equations, but frequent refactorization of Jacobian, required to preserve the quadratic convergence, make it very slow. An improvement in speed (at the expense of somewhat poorer, but still very good convergence), may be obtained if Jacobian is refactorized after more iterations. Newton Raphson method was the choice for the network equations solver. It is obviously a modification of the conventional power flow algorithm, but with a few important additions:

i) In a conventional power flow, system buses are usualy split into two groups: voltage controlled (P-V) buses, for which the injected active power and voltage magnitude are specified, and load (P-Q) buses, for which both active and reactive power consumption are specified. The power flow model also has one or more swing buses, generator buses whose power injections are left unspecified to compensate for active transmission losses which cannot be known prior to calculation. A single swing bus has a voltage magnitude specified and its phase angle is usualy set to zero to provide reference for the other phase angles, because of the translational symmetry of the power flow solutions (for every solution $(\delta_0, \theta_0, V_0, \lambda_0)$, there are infinitely many other solutions $(\delta_0 + \Delta_0, \theta_0 + \Delta_1, V_0, \lambda)$ where $\Delta_0 \in R^n$, $\Delta_1 \in R^m$ are any vectors consisting of n , m equal real constants ($\Delta_{oi} = \Delta_{1j} = const.$). This issue is also important for analysis of stability properties of the equilibria, as it will be mentionned later in the text. In the proposed simulation algorithm, the output of the differential equation solver contains the whole

vector δ of the generator phase angles. Since generator voltages are also specified, the situation is equivalent to having all generators specified as swing buses, with angles and voltages given as inputs. This affects the solution algorithm in such a way that no power balance equation is specified for the generator buses. For the above mentioned power system with n generator buses and m load buses, there will be a total of $2(n+m)$ equations specified ($n+m$ for active powers and $n+m$ for reactive powers). Generator terminal buses are specified as load buses with zero P - Q requirements, while n virtual buses are introduced between generator terminal buses and fictitious voltage sources V_{gi} through generator synchronous reactances (Figure 2).

ii) A modification of the algebraic equation solver must be made to take into account the assumption about constant voltages at generator terminal buses. For such a case, voltages are specified at generator terminal buses, which are already specified as zero P - Q buses. This might look like an overspecification, but additional degrees of freedom are achieved by not specifying the generator voltages behind synchronous reactances. Therefore, in the final modification of the Newton Raphson algorithm in polar coordinates, which was used for simulations, generator internal buses were specified as swing buses with only phase angles given, while generator terminal buses were specified with both active and reactive power requirements as well as voltage magnitudes. This problem can be formulated as follows: the linearization of the equations g_p and g_q will produce the following matrix relationship

$$\begin{bmatrix} \Delta P_T^i \\ \Delta P_L^i \\ \Delta Q_T^i \\ \Delta Q_L^i \end{bmatrix} = \begin{bmatrix} D^i_{\theta_T}(g_{PT}) & D^i_{\theta_L}(g_{PT}) & D^i_{V_T}(g_{PT}) & D^i_{V_L}(g_{PT}) \\ D^i_{\theta_T}(g_{PL}) & D^i_{\theta_L}(g_{PL}) & D^i_{V_T}(g_{PL}) & D^i_{V_L}(g_{PL}) \\ D^i_{\theta_T}(g_{QT}) & D^i_{\theta_L}(g_{QT}) & D^i_{V_T}(g_{QT}) & D^i_{V_L}(g_{QT}) \\ D^i_{\theta_T}(g_{QL}) & D^i_{\theta_L}(g_{QL}) & D^i_{V_T}(g_{QL}) & D^i_{V_L}(g_{QL}) \end{bmatrix} \begin{bmatrix} \Delta\theta_T^{(i+1)} \\ \Delta\theta_L^{(i+1)} \\ \Delta V_T^{(i+1)} \\ \Delta V_L^{(i+1)} \end{bmatrix} \quad (3.3.9)$$

where subscripts T, L refer to terminal and load buses respectively, subscripts P, Q refer to active and reactive power balance equations respectively, superscripts i denote the iteration number and operator D represents the linearizing Jacobian matrix. To account for modification (ii), a change is introduced in (3.3.9)

$$\begin{bmatrix} \Delta P_T^i \\ \Delta P_L^i \\ \Delta Q_T^i \\ \Delta Q_L^i \end{bmatrix} = \begin{bmatrix} D^i_{\theta_T}(g_{PT}) & D^i_{\theta_L}(g_{PT}) & D^i_{V_G}(g_{PT}) & D^i_{V_L}(g_{PT}) \\ D^i_{\theta_T}(g_{PL}) & D^i_{\theta_L}(g_{PL}) & D^i_{V_G}(g_{PL}) & D^i_{V_L}(g_{PL}) \\ D^i_{\theta_T}(g_{QT}) & D^i_{\theta_L}(g_{QT}) & D^i_{V_G}(g_{QT}) & D^i_{V_L}(g_{QT}) \\ D^i_{\theta_T}(g_{QL}) & D^i_{\theta_L}(g_{QL}) & D^i_{V_G}(g_{QL}) & D^i_{V_L}(g_{QL}) \end{bmatrix} \begin{bmatrix} \Delta\theta_T^{(i+1)} \\ \Delta\theta_L^{(i+1)} \\ \Delta V_G^{(i+1)} \\ \Delta V_L^{(i+1)} \end{bmatrix} \quad (3.3.10)$$

where subscript G refer to generator internal buses. Therefore, columns $n+m+1$ through $2n+m$ of the Jacobian matrix reduced to P-Q buses will contain partial derivatives of g_p, g_q with respect to the magnitudes of voltage sources behind synchronous reactances instead of the partial derivatives with respect to voltage magnitudes at terminal buses, which are assumed constant. This algorithm was successfuly used as a complement to the above described differen-

tial equation solver for all the simulations which will be presented in this text. Figure 3 is a schematic representation of the procedure described above.

Its convergence properties are excellent, because generator internal buses and terminal buses are tightly coupled by the synchronous reactances and the initial conditions for every calculation are based on the results of the previous solution (usualy very close, so that the convergence is often reached after a few iterations). The convergence became difficult when voltage collapse was approached, leading to very large gradients of voltage magnitudes, when the algorithm began to diverge. In fact, the divergence of algorithm (3.3.10) triggered termination of the simulation of cases which ended in voltage collapse. This effect was produced by the singularity of the Jacobian matrix J_r introduced in equation (3.3.10) which coincided with very high negative values of the load bus voltage gradients. It was then not possible to extend the simulation to the point when voltage magnitudes reach zero. It is worth noting that the protective relaying equipment action was not modeled for simulations, since in any case the simulation was not carried through to drop in voltages to sufficiently low levels without tripping relays and dismantling the system. The patterns of change of load bus voltages, however, indicated in all of the simulated scenarios that voltage collapse was unavoidable, with extremely large negative gradients in time. Many of the simulation results will be presented and discussed later in the text.

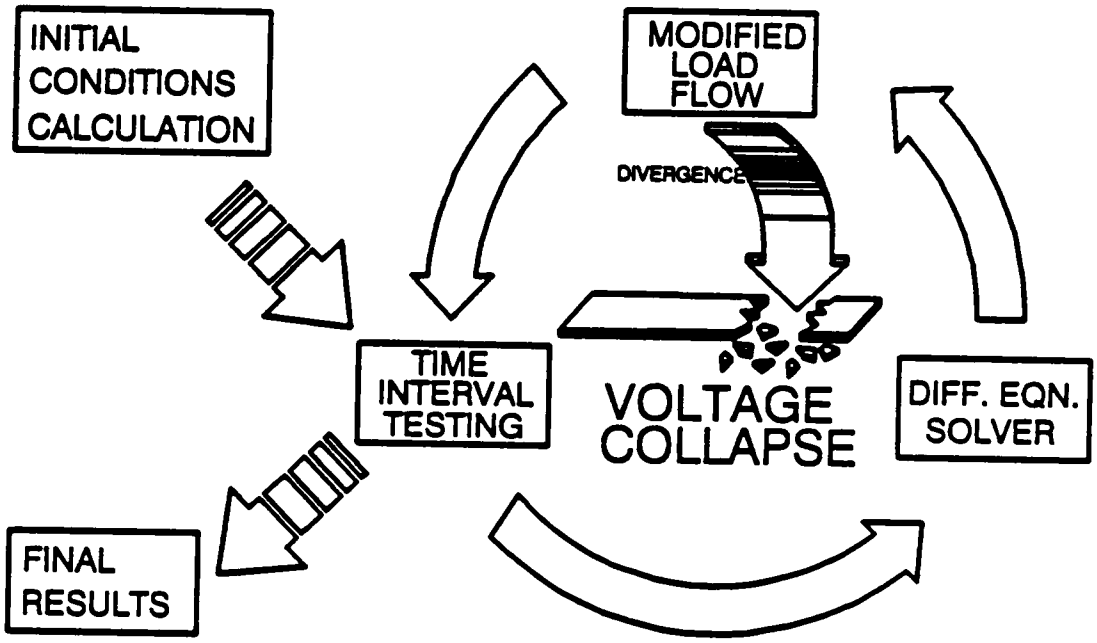

Figure 3. Simulation algorithm

3.4 Power system at static bifurcation

After elaborating on the model and the simulation algorithm, conditions must be defined for the occurrence of voltage instability in power systems which would correspond closely to the reports and observations of the incidents and have a strong mathematical justification. A short overview of the terminology and static bifurcation theory based on [119][40][70][86] will be presented here as a framework for determination of simulation scenarios.

For a dynamical system

$$\frac{dx}{dt} = \dot{x} = f(x, \lambda) \tag{3.4.1}$$

where $x = x(t) \in R^n$ is a vector valued function and $\lambda \in R^m$ is a parameter vector , vector field $f: U \subset R^{n+m} \rightarrow R^n$ generates a flow $\phi_t: U \rightarrow R^n$ for $x \in U$ and $t \in [a, b] \subset R$ such that

$$\frac{d}{dt}(\phi(x, \lambda, t))_{t=\tau} = f(\phi(x, \lambda, \tau)) \tag{3.4.2}$$

The equilibria of the system (3.4.1) are zeroes of f , and the region of attraction of an equilibrium point x_s is defined as

$$A(x_s) = \{x \in R^{n+m} : \phi(x, \lambda, t) \rightarrow x_s \ as \ t \rightarrow \infty\} \tag{3.4.3}$$

When the following conditions are satisfied

$$
\begin{aligned}
f(x, \lambda) &= 0 \\
\det\left\{D_x f(x, \lambda)\big|_{x=x_0,\, \lambda=\lambda_0}\right\} &= 0
\end{aligned}
\tag{3.4.4}
$$

where $D_x f$ is a Jacobian matrix of f, then the point (x_0, λ_0) is a bifurcation. The value λ_0 is called a bifurcation value of λ . Closely related with the above are stable, unstable and center manifolds of the system equilibria. Stable and unstable manifolds of the equilibrium $\bar{x}$ are defined as

$$
\begin{aligned}
W^s(\bar{x}) &= \left[x \in U \mid \phi(x, \lambda, t) \to \bar{x} \text{ as } t \to \infty\,,\ \phi(x, \lambda, t) \in U\,,\ t \geq 0\right] \\
W^u(\bar{x}) &= \left[x \in U \mid \phi(x, \lambda, t) \to \bar{x} \text{ as } t \to -\infty\,,\ \phi(x, \lambda, t) \in U\,,\ t \leq 0\right]
\end{aligned}
\tag{3.4.5}
$$

Center manifold cannot be defined in terms of asymptotic behavior like (3.4.5). It is associated only with those equilibria which are also bifurcations. Let $\bar{x}$ be a bifurcation of (3.4.1)

$$
\begin{aligned}
f_{\bar{\lambda}}(\bar{x}) = f(\bar{x}, \bar{\lambda}) &= 0 \\
\det A = \det\{Df_{\bar{\lambda}}(\bar{x})\} &= 0
\end{aligned}
\tag{3.4.6}
$$

Let us divide the spectrum of A into three parts, σ_s , σ_u and σ_c such that the real parts of the eigenvalues satisfy

$$
Re\,\lambda \quad
\begin{cases}
< 0\,, \lambda \in \sigma_s \\
= 0\,, \lambda \in \sigma_c \\
> 0\,, \lambda \in \sigma_u
\end{cases}
\tag{3.4.7}
$$

Let the generalized eigenspaces of σ_s, σ_c, σ_u be E^s, E^c, E^u respectively. Then, assuming that f is r times differentiable, there exist r times differentiable stable and unstable manifolds W^s and W^u tangent to E^s and E^u at $\bar{x}$ and $r-1$ times differentiable center manifold W^c tangent to E^c in $\bar{x}$ The manifolds W^s, W^c, W^u are all invariant for f. The stable and unstable manifolds are unique, but W^c need not be. As can be seen from its definition, determination of the center manifold for many systems may be a difficult, if not impossible task, but they are closely associated with the system behavior in the bifurcation points.

Among many types of bifurcations, very interesting for our study are those which are generic for one parameter families (a property is generic in certain set if it is true for almost all members of that set). Those bifurcations are called saddle node bifurcations. Let $(\bar{x}, \bar{\lambda})$ be a bifurcation of (3.4.1) with assumption $\lambda \in R$. If its Jacobian has a simple zero eigenvalue, the center manifold theorem permits the reduction of the study of the bifurcation problem to the one where x is unidimensional [119]. The properties of the center manifold $\Sigma \subset R^n \times R$ passing through the bifurcation $(\bar{x}, \bar{\lambda})$ are the following:

i) Tangent space of Σ at $(\bar{x}, \bar{\lambda})$ is spanned by an eigenvector of Jacobian which corresponds to zero eigenvalue and by a vector parallel to λ axis.

ii) For any finite integer r, Σ is r times differentiable if restricted to small enough neighborhood of the bifurcation.

iii) The vector field of (3.4.1) is tangent to Σ.

iv) There is a neighborhood U of the bifurcation point $(\bar{x}, \bar{\lambda})$ such that all trajectories contained entirely in U for all time lie in Σ. Property (iv) says that trajectories originating from the bifurcation point are embedded on a center manifold. Let us get back now to our particular system model (3.3.4), whose equilibria are given as

$$\begin{aligned} f_p(\delta, \theta, V, \lambda) &= 0 \\ g_p(\delta, \theta, V, \lambda) &= 0 \\ g_q(\delta, \theta, V, \lambda) &= 0 \end{aligned} \tag{3.4.8}$$

The equation $f_p = 0$ is satisfied only at system equilibria while the two other equations must be satisfied for every possible system state at all times. The equilibria are called strongly causal if g_p, g_q accept solutions $\theta = \theta(\lambda, \delta)$, $V = V(\lambda, \delta)$. They are called strictly causal if those solutions are unique. Equilibria are regular if they have unique solutions for δ, θ, V for a given value of parameter λ. Statically stable equilibrium point is a regular equilibrium which is also stable in the sense of Lyapunov. A bifurcation of

$$\begin{aligned} f_\lambda(x) &= 0 \\ f &= [f_p \ g_p \ g_q]^T \\ x &= [\delta \ \theta \ V]^T \end{aligned} \tag{3.4.9}$$

is a point $\bar{x}$ in whose every neighborhood there are at least two system equilibria $x_1 \neq x_2$ such that $f_\lambda(x_1) = f_\lambda(x_2) = 0$. Therefore, an infinitesimal change of param-

eter λ creates multiple zeroes (which is equivalent to previously introduced definition of bifurcation as an equilibrium where the linearized system is singular. In fact, if the system Jacobian matrix is nonsingular in equilibrium, the solution is unique by implicit function theorem and the equilibrium is not a bifurcation). Since bifurcation point corresponds to a singular Jacobian and is not regular, it is also not statically stable.

If $F = [f_p \; g_p \; g_q]^T$ is linearized around an equilibrium point [40], the following relationship holds

$$D_\delta F d\delta + D_\theta F d\theta + D_V F dV = - D_\lambda F d\lambda \tag{3.4.10}$$

Assuming $[d\xi] = [d\delta \;\; d\theta]^T$, it can be represented as

$$\begin{bmatrix} D_\delta f_p & D_\theta f_p & D_V f_p \\ D_\delta g_p & D_\theta g_p & D_V g_p \\ D_\delta g_q & D_\theta g_q & D_V g_q \end{bmatrix} \begin{bmatrix} d\delta \\ d\theta \\ dV \end{bmatrix} = - \begin{bmatrix} D_\lambda f_p \\ D_\lambda g_p \\ D_\lambda g_q \end{bmatrix} d\lambda \tag{3.4.11}$$

or

$$\begin{bmatrix} A_1 & A_2 \\ A_3 & A_4 \end{bmatrix} \begin{bmatrix} d\xi \\ dV \end{bmatrix} = - \begin{bmatrix} B_1 \\ B_2 \end{bmatrix} d\lambda \tag{3.4.12}$$

As it was shown in [40], assumption that A_4 is nonsingular allows to form the following matrix relationship

$$\det\{J\} = \det\{A_4\}\ \det\{A_1 - A_2A_4^{-1}A_3\}$$
$$\{A_1 - A_2A_4^{-1}A_3\}d\xi = -\{B_1 - A_2A_4^{-1}B_2\}d\lambda \tag{3.4.13}$$

which means that under the assumption of a nonsingular A_4 the sensitivities of the system phase angles become infinite with respect to an infinitesimal change of the parameter vector λ . This is loss of steady state stability. Such a situation is shown in Figures 4 and 5, where the phase portraits are shown of differential equation which represents the swing dynamics of a single generator connected to an infinite bus. The first phase portrait corresponds to the equation $\ddot{x} + .5\dot{x} + \sin x - \sin .412 = 0$ which has stable equilibria for $x = 0.412 + 2k\pi$ and unstable equilibria for $x = 2.730 + 2k\pi$. The phase portrait clearly shows the region of attraction of one stable equilibrium. Next phase portrait shows a near - bifurcation situation when the constant parameter in the equation is close to one. Stable equilibria are now at $x = 1.56 + 2k\pi$ and unstable at $x = 1.5816 + 2k\pi$. It is shown in that Figure how the region of attraction of the stable equilibrium is shrinking and how the system is approaching the bifurcation which results in phase angle instability (loss of steady state stability).

If matrix A_1 from (3.4.12) is assumed nonsingular, the relationship will become

$$\det\{J\} = \det\{A_1\}\ \det\{A_4 - A_3A_1^{-1}A_2\}$$
$$\{A_4 - A_3A_1^{-1}A_2\}dV = -\{B_2 - A_3A_1^{-1}B_1\}d\lambda \tag{3.4.14}$$

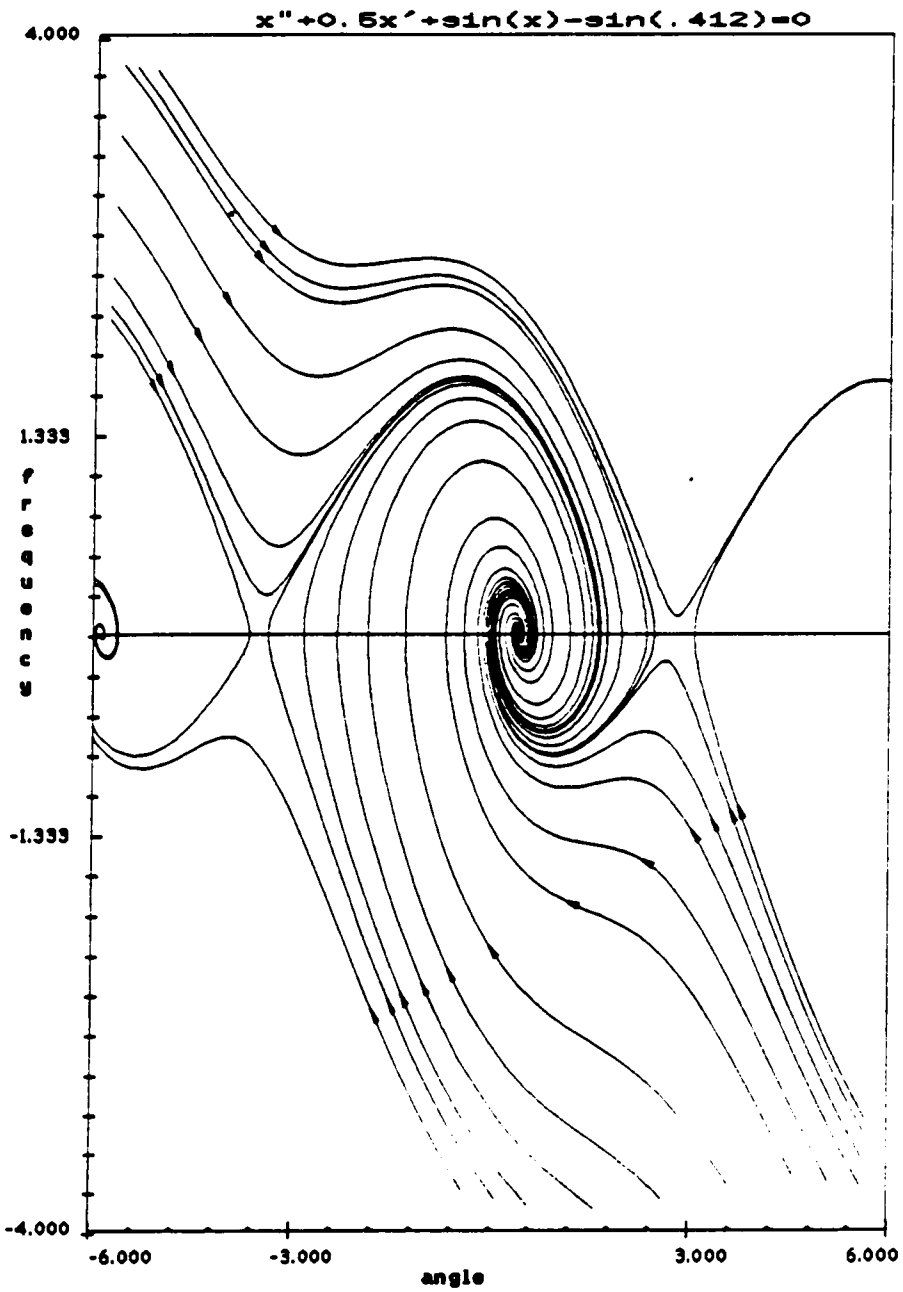

Figure 4. Phase portrait: $x'' + .5x' + \sin x - \sin .412 = 0$.

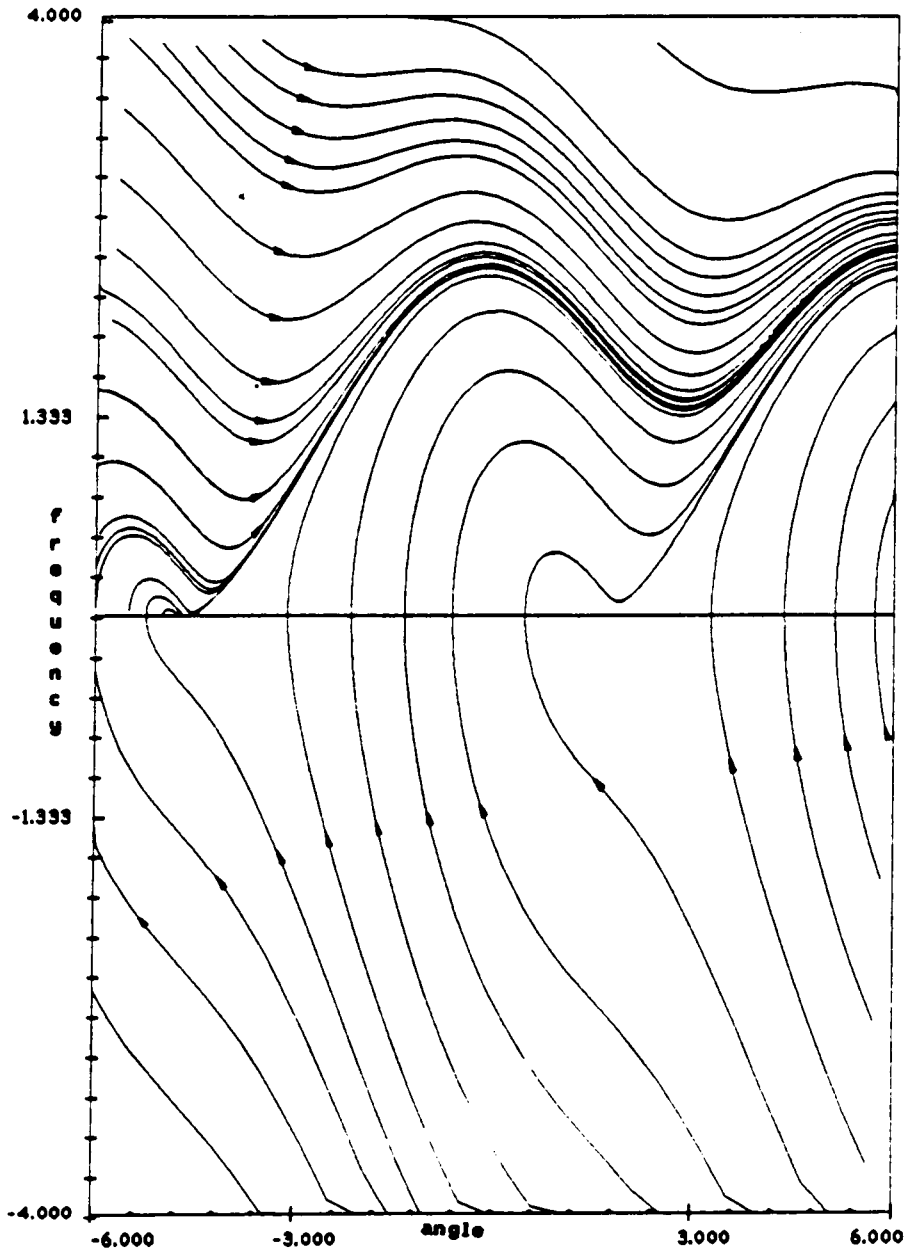

Figure 5. Phase portrait: $x'' + .5x' + \sin x - \sin 1.56 = 0$.

which shows that the sensitivities of voltage magnitudes are becoming infinite (when A_1 is assumed nonsingular) for an infinitesimal change of λ . This is a voltage collapse situation. Both conditions correspond to the singularity of the system Jacobian matrix, but its consequences are quite different depending on the additional assumptions discussed above. It should also be noted that conditions (3.4.14) do not mean that load bus voltage magnitudes should be zero at the bifurcation. Intuitively, one can picture the familiar P-V diagram of one generator - one load system and note that, although voltage gradients become $-\infty$ at the critical power transfer point, voltage itself remains at a nonzero value at a point where the high and low voltage solutions meet. This suggests that the system moves along certain trajectory from the bifurcation to the point where the final collapse occurs, or it settles in another stable equilibrium. Therefore, a bifurcation should be considered as a stability boundary from which the system may descend into voltage collapse, or angular instability, but can also return to the stable state if an appropriate action were taken to prevent the blackout.

The above results were used as guidelines for determination of the voltage unstable situations on the model which will be presented later in the text.

The two generator, three bus power system model used in [40] and many other references was tested for voltage collapse conditions using data from [40]:

Generator 1: $(M_1 , D_1 , V_1 , \delta_1 , P_1) = (1 , 0 , 1 , 0 , 0.5)$;

Generator 2: $(M_2, D_2, V_2, \delta_2, P_2) = (1, 0, 1, 0, 0.5)$;

Transmission lines: $Y_1 = Y_2 = Y = 1$;

Load: $(P, Q, V, \theta) = (1, 0, 1/\sqrt{2}, -\pi/4)$;

Figure 6 shows the time diagram of load voltage after the active load requirement was increased by 0.01 . It can be seen that the voltage trajectory ends in voltage collapse after 0.35 s. Figure 7 shows the changes of phase angles at generator 2 and load during the system descent into collapse. Altghough this power system model is a crude approximation of a real power system, simulation of its dynamics captures some of the essential properties of the observed voltage collapse cases.

It is noticable that a relatively fast descent into collapse is preceeded by a long period of a slow changes of both angles and voltages. This complies well with the observations and also represents the initially slow dynamics of a saddle node bifurcation, from which the system descended into collapse. A likely scenario of the development of voltage instability process can be reconstructed as follows: before any instability occurs, the system is subjected to follow (in quasi - steady state) some pattern of increased loading (change of parameter vector λ) which leads towards condition (3.4.14). The stability of the steady state equilibria may be assessed by linearizing the system model (3.3.4) around the point $(\delta_0, \theta_0, V_0, \lambda_0)$

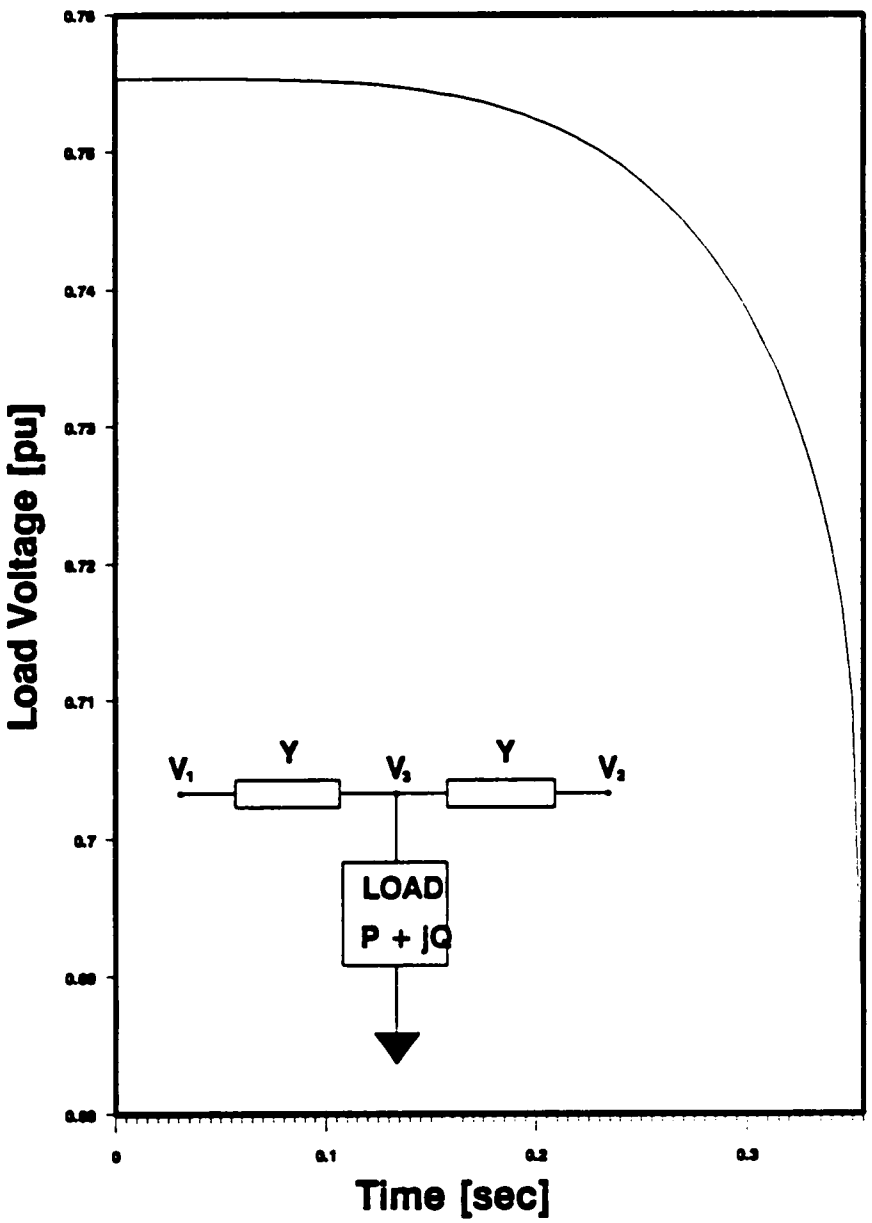

Figure 6. Voltage collapse of a two generator system.

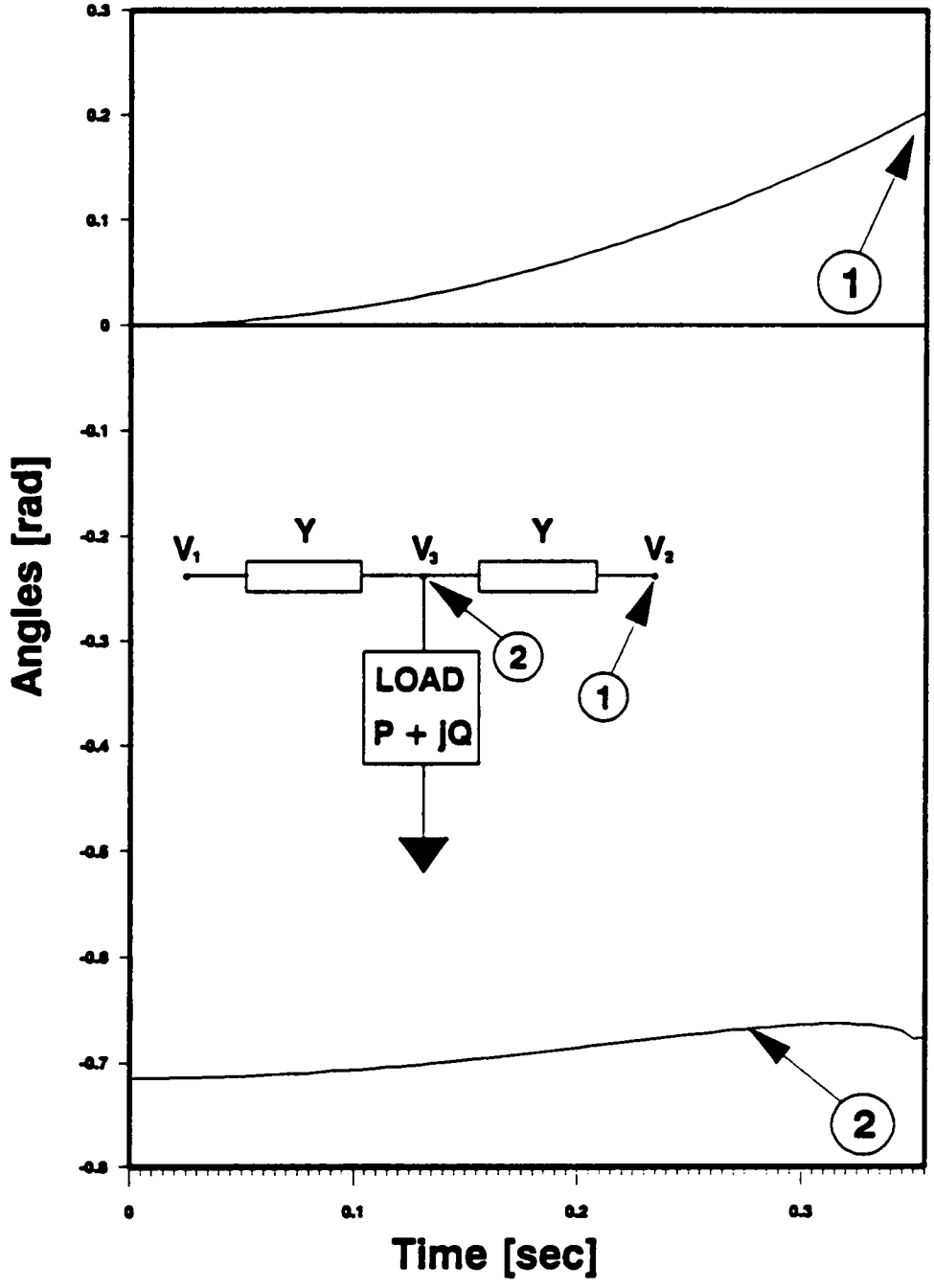

Figure 7. Phase angle changes before voltage collapse.

$$
\begin{aligned}
M\,\Delta\ddot{\delta} + D\,\Delta\dot{\delta} + f_p(\delta_0, \theta_0, V_0, \lambda_0) + \frac{\partial f_p}{\partial \delta}\Delta\delta + \frac{\partial f_p}{\partial \theta}\Delta\theta + \frac{\partial f_p}{\partial V}\Delta V = 0 \\
g_p(\delta_0, \theta_0, V_0, \lambda_0) + \frac{\partial g_p}{\partial \delta}\Delta\delta + \frac{\partial g_p}{\partial \theta}\Delta\theta + \frac{\partial g_p}{\partial V}\Delta V = 0 \\
g_q(\delta_0, \theta_0, V_0, \lambda_0) + \frac{\partial g_q}{\partial \delta}\Delta\delta + \frac{\partial g_q}{\partial \theta}\Delta\theta + \frac{\partial g_q}{\partial V}\Delta V = 0
\end{aligned}
\tag{3.4.15}
$$

The algebraic equations can be solved for ΔV and $\Delta\theta$

$$
\begin{aligned}
\Delta V &= A + B\Delta\delta \\
A &= -\left[\frac{\partial g_p}{\partial v} - \frac{\partial g_p}{\partial \theta}\left(\frac{\partial g_q}{\partial \theta}\right)^{-1} g_p\right]\left[g_p - \frac{\partial g_p}{\partial \theta}\left(\frac{\partial g_q}{\partial \theta}\right)^{-1} g_q\right] \\
B &= -\left[\frac{\partial g_p}{\partial v} - \frac{\partial g_p}{\partial \theta}\left(\frac{\partial g_q}{\partial \theta}\right)^{-1} g_p\right]\left[\frac{\partial g_p}{\partial \delta} - \frac{\partial g_p}{\partial \theta}\left(\frac{\partial g_q}{\partial \theta}\right)^{-1}\frac{\partial g_q}{\partial \delta}\right]
\end{aligned}
\tag{3.4.16}
$$

$$
\begin{aligned}
\Delta\theta &= -\left(\frac{\partial g_q}{\partial \theta}\right)^{-1} g_q - \left(\frac{\partial g_q}{\partial \theta}\right)^{-1}\partial g_q\Delta\delta - \frac{\partial g_q}{\partial V}(A + B\Delta\delta) \\
\Delta\theta &= C + D\Delta\delta
\end{aligned}
\tag{3.4.17}
$$

which can be introduced into differential equation to eliminate $\Delta\theta$ and ΔV

$$
M\Delta\ddot{\delta} + D\Delta\dot{\delta} + \left(\frac{\partial f_p}{\partial \delta} + \frac{\partial f_p}{\partial \theta}B + \frac{\partial f_p}{\partial V}D\right)\Delta\delta = -\frac{\partial f_p}{\partial \theta}A - \frac{\partial f_p}{\partial V}C \tag{3.4.18}
$$

The equation (3.4.18) has a simplified form in an equilibrium

$$
A = C = 0 \tag{3.4.19}
$$

leaving the linearized dynamics of the system in the form

$$M\Delta\ddot{\delta} + D\Delta\dot{\delta} + K\Delta\delta = 0 \qquad (3.4.20)$$

The stability of (3.4.19) requires K to have precisely one zero eigenvalue (to account for the translational symmetry of the solutions) and to have all the other eigenvalues positive, in case when $D = 0$. If $D \geq 0$, the linearized system (3.4.19) is stable if there exists a real, symmetric, positive definite matrix S [40], such that $SK = Q$, where Q is a symmetric matrix with one zero eigenvalue and all the other eigenvalues positive. Therefore, the analysis of the local stability properties may be accomplished by analysis of the matrix K .

The stability margin of the system state may be assessed by calculating the condition number of the system Jacobian in some steady states, or its minimum eigenvalue, or minimum singular value. As the system approaches the stability boundary ($\det\{J\} = 0$), its load bus voltages go down, but without abrupt changes, or early alarms. When the bifurcation point is reached, the system dynamics produces a descent into voltage collapse qualitatively similar to the one shown in Figure 6, whose quantitative measures depend on the system state and the change of the parameter vector λ which brings the system into bifurcation. The simulation of the system descent into collapse is possible for as long as the Jacobian matrix J, used for simulation algorithm remains nonsingular, i.e. as long as the system remains causal. It is interesting to observe simulations of voltage instability on a larger and more realistic power system model. Such an analysis is presented in the next section.

3.5 Steady state analysis

There are two purposes for a steady state analysis of a power system approaching static bifurcation: to assess the quantitative measures of the proximity to instability by analysis of the power flow equations and to calculate initial conditions for the dynamic simulation algorithm of the voltage collapse presented in previous sections. The power system model chosen for simulations is a 39-bus, 10-generator system, whose structure is shown in Figure 8.

The system's 12 transformers are modeled with a fixed tap ratio and 29 loads are constant complex power. Complete system data are presented in Appendix A. An interesting property of the system is that a big part of the consumption (25% of the total active power consumed and 33% of the reactive load requirements) is concentrated in a small portion of the system (buses 4-9) while a big part of the power transfer to that region is accomplished from relatively distant generators. This type of load distribution produces excessive reactive transmission losses as the loading is increased, and make the system susceptible to voltage instability.

The loading pattern which is used to change the system state and move it closer to instability is based on the following: load flow model (3.3.6) is used and the loading defined through a scalar parameter k , called load factor, which is defined as the constant with which some, or all of the loads are multiplied to produce a

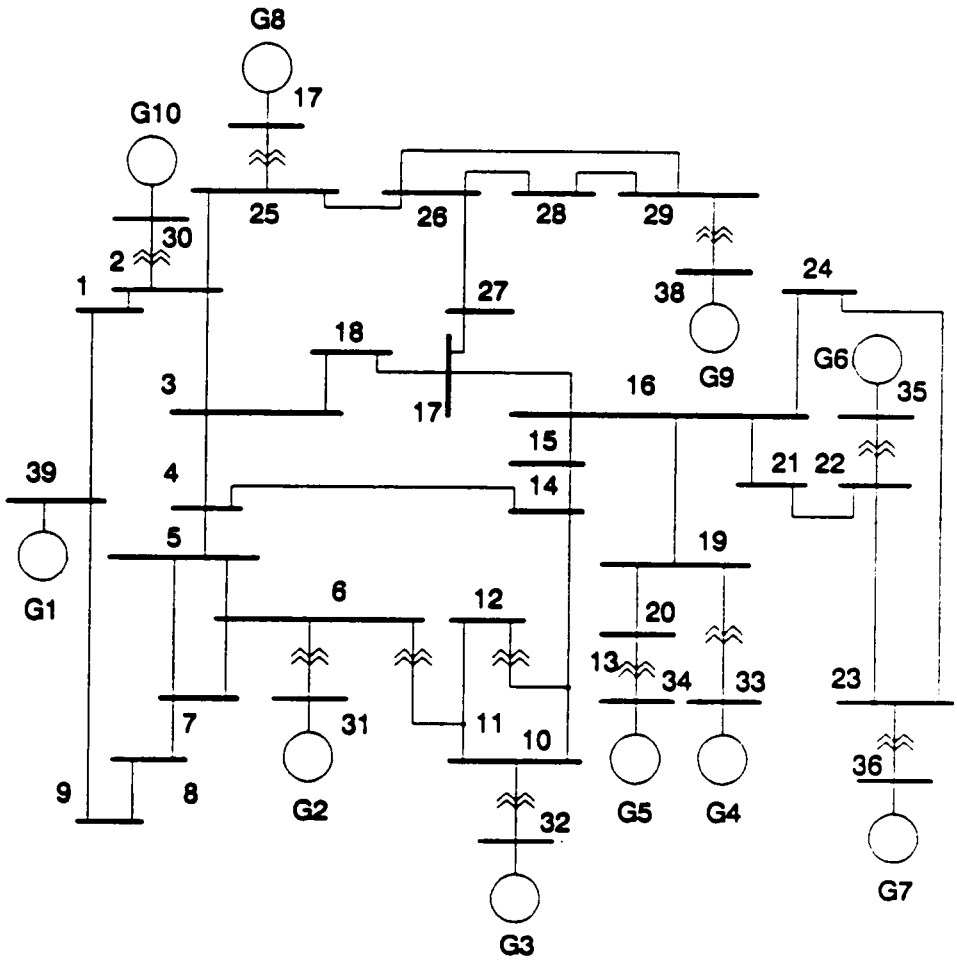

Figure 8. Power system model used for simulations.

new operating state. The system loads and generated powers in a normal operating state are

$$\begin{aligned} P_0 &= [P_1, P_2, \ldots, P_m]^T \\ Q_0 &= [Q_1, Q_2, \ldots, Q_m]^T \\ P_{G0} &= [P_{m1}, P_{m2}, \ldots, P_{m,n-1}]^T \end{aligned} \tag{3.5.1}$$

where generator n is considered a swing bus. A different loading condition corresponding to the load factor k is achieved by

$$\begin{aligned} P(k) &= k \times K_1 \times P_0 \\ Q(k) &= k \times K_2 \times Q_0 \\ P_G(k) &= k \times K_3 \times P_{G0} \end{aligned} \tag{3.5.2}$$

where k_1, K_2, K_3 are diagonal selector matrices

$$K_i = \begin{bmatrix} k_{i1} & 0 & \ldots & 0 \\ 0 & k_{i2} & \ldots & 0 \\ \ldots & \ldots & \ldots & \ldots \\ 0 & 0 & \ldots & k_{kn} \end{bmatrix} \quad i = 1, \ldots, 3 \tag{3.5.3}$$

whose diagonal elements may take values $\{0, 1\}$ and thus select the subset of loads (or generators) on which the loading factor would be applied. The algorithm for approach to the stability boundary is the following:

i) Assume the loading patterns by chosing matrices K_1, K_2, K_3, establish a base load flow case and assume some starting value for the load factor (k_0);

ii) Increase the load factor by a small fixed amount in each subsequent load flow calculation; in the i-th calculation of the load flow, the value of the load factor will be

$$k_i = k_0 + i\Delta k \tag{3.5.4}$$

After each load flow, calculate the minimum eigenvalue, or the minimum eigenvalue of the Jacobian matrix used in the last iteration;

iii) If the last calculated load flow converged, step (ii) should be repeated; if it diverged, it is due to near singularity of Jacobian. The sequence of previously calculated minimum eigenvalues , or minimum singular values can be used for estimating the critical value of the load factor (bifurcation value) for which Jacobian matrix becomes singular, i.e.

$$\lambda_{\min}\{J(\lambda_{crit})\} = 0 \tag{3.5.5}$$

The estimate of the critical load factor is obtained by numerical extrapolation (second, or third degree polynomials are good enough if small enough steps of Δk are taken before divergence of the load flow). It may be used for planning of the dynamic simulation scenarios, which will be presented in the next section. The graph of the minimum eigenvalues of Jacobian vs. load factors for the uniform loading case ($K_1 = K_2 = K_3 = I$) is shown in Figure 9 for a 39-bus system of Figure 8.

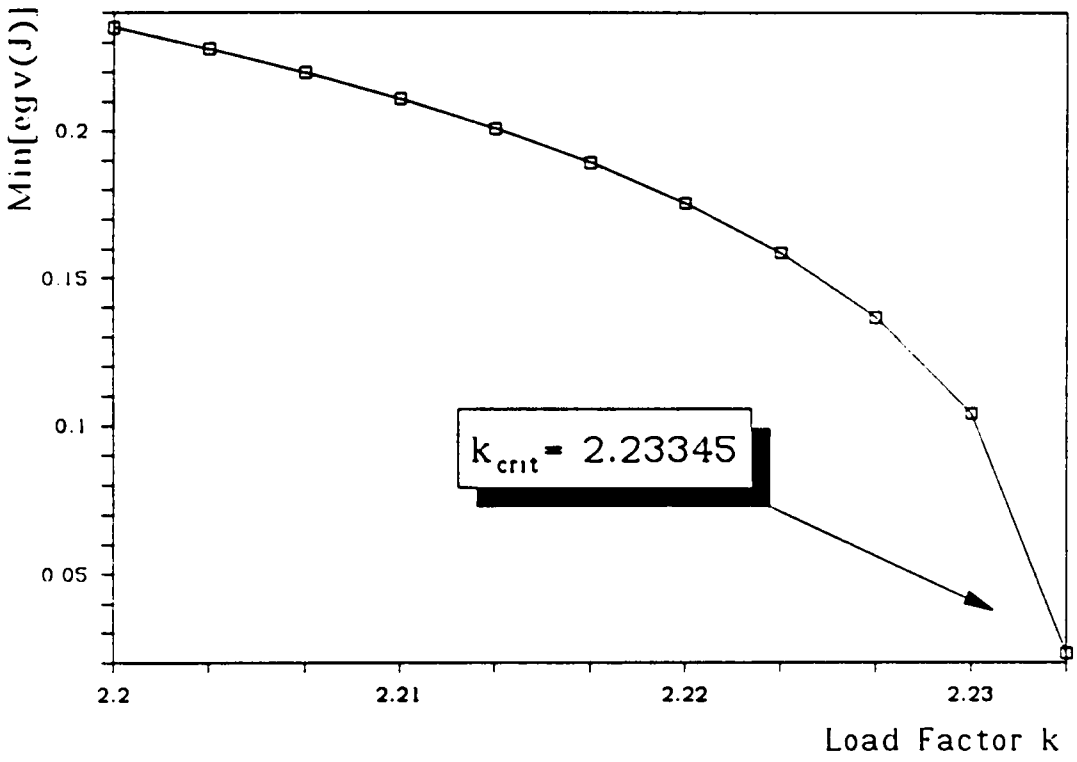

Figure 9. Critical load factor estimation

The last converged load flow is an important source of information about the system state near the stability boundary. It gives the information about system voltages and phase angles near the boundary. It can also be coupled with another load flow calculation with a load factor reduced by a very small amount and both results can be combined to give information about the voltage and phase angle gradients. Some of the results for the 39-bus test system are shown in the following pages.

Figure 10 shows the phasor diagram of the test system in a normal operating condition. Almost all voltages have magnitude 1 pu, or greater and phase angles are concentrated within 20 degrees. The system is well conditioned and stable.

Figure 11 shows the phasor diagram of the system for which it was determined that it was close to static stability boundary (condition (3.4.13)). It was achieved by progressive loading of the active powers (case $K_1 = K_3 = I$, $K_2 = 0$) . The critically convergent load flow was calculated for a load factor $k = 3.061$. It is noticable that the span between phase angles in this case is over 60 degrees and it is to be expected that it would exceed 90 degrees at the exact stability boundary, in which it was not possible to perform a convergent load flow calculation. However, a very small increment of k (less than $\Delta k \leq 0.001$ will move the system across the stability boundary, which suggests that the phase angle gradients in this operating regime are very high). Minimal voltages at load buses are still kept above 0.8 pu, which is acceptable for situations when those voltages are at pri-

mary sides of tap changing transformers connected to a low voltage distribution network, in which voltage levels are maintained closer to nominal levels.

Figure 12 shows the phasor diagram of a test system operating close to voltage stability boundary (condition (3.4.14)). The loading pattern was accomplished by assuming the following values for selector matrices: $K_1 = K_2 = K_3 = I$. The critically convergent load flow was calculated for load factor $k = 2.23345$. The span between phase angles is less then 50 degrees in this case, but the lowest load bus voltage magnitudes are of the order of 0.60-0.65, with very high negative gradients: a change of load factor by $\Delta k = 0.001$ would move the system across stability boundary (into voltage collapse). This operating state was one of those which were used as initial conditions for dynamic simulations of voltage collapse.

Figure 13 shows values of phase angle gradients calculated for buses at two critical regimes shown in Figures 11 and 12. Gradients were approximately calculated by running load flows for load factor levels $\Delta k = 0.001$ below the critically convergent load flows in both cases. The values of gradients are expressed in degrees per unit change of the load factor. It is very noticeable that phase angle gradients which correspond to the case at steady state stability boundary are higher then those which correspond to voltage instability. This is to be expected from conditions derived in (3.4.13-14) for those two types of instability. Swing bus 31 has a zero gradient because it provides a reference for the other buses.

Figure 14 shows voltage gradients calculated for load buses at two critical regimes shown in Figures 11 and 12. Gradients were approximately calculated using the same load flows that were used for calculation of phase angle gradients. The values of the gradients are expressed in per unit changes for unit changes of load factor (linearized). Somewhat surprisingly, voltage gradients at steady state stability boundary were found to be higher then those corresponding to voltage collapse condition. It can be explained, however, by the fact that the voltage instability case showed more difficulty in convergence then the steady state unstable case. Minimum singular values of Jacobians for steady state and voltage instability cases were 0.022 and 0.060 respectively, showing that the load flow calculated for steady state instability was closer to stability boundary. Since system nonlinearities are very emphasized close to stability boundary, linearizations used for calculations of voltage gradients were not good enough indicators of the trends when the states are approaching the boundary. It is to be expected that voltage gradients in the case corresponding to Figure 12 would grow very much and become bigger than those corresponding to steady state instability if a load flow calculation could be performed for both of them in states corresponding to some equal and very small minimum singular values of Jacobian (of the order of 0.001 or less in the test system used here).

Figure 15 shows comparison between voltage profiles and voltage gradients for a test system in normal operating condition (Figure 10) and close to voltage stability boundary (Figure 12). This comparison clearly shows that voltage gradients are typically 100 times bigger at the voltage stability boundary than in

normal conditions and that load buses with highest voltage gradients also have the lowest voltage magnitudes at the boundary. This suggests that the loading pattern assumed for approach to voltage stability boundary produces smooth changes of the voltage profile in the system.

In the steady state simulations, the conditions (3.4.13-14) were used to approach the steady state and voltage stability boundary by progressive loading of the 39-bus test system. The results of dynamic simulations in the next section will show mechanisms of voltage collapse as the system is moving across the stability boundary.

3.6 Dynamic simulation analysis

Dynamic simulations were performed on a test system (Figure 8) in order to get more information about the mechanism of transition into instability. Two series of tests were performed with that objective: the first one is based on the application of a step change of the load factor to the power system in steady state. Depending on the magnitude of the step change and the final value of the load factor, the system would move across stability boundary, or stay in the stable region. This method may be used to determine relatively accurately the exact bifurcation value of the load factor and to monitor the system asymptotic behavior in the critically stable region. The second simulation method is based on

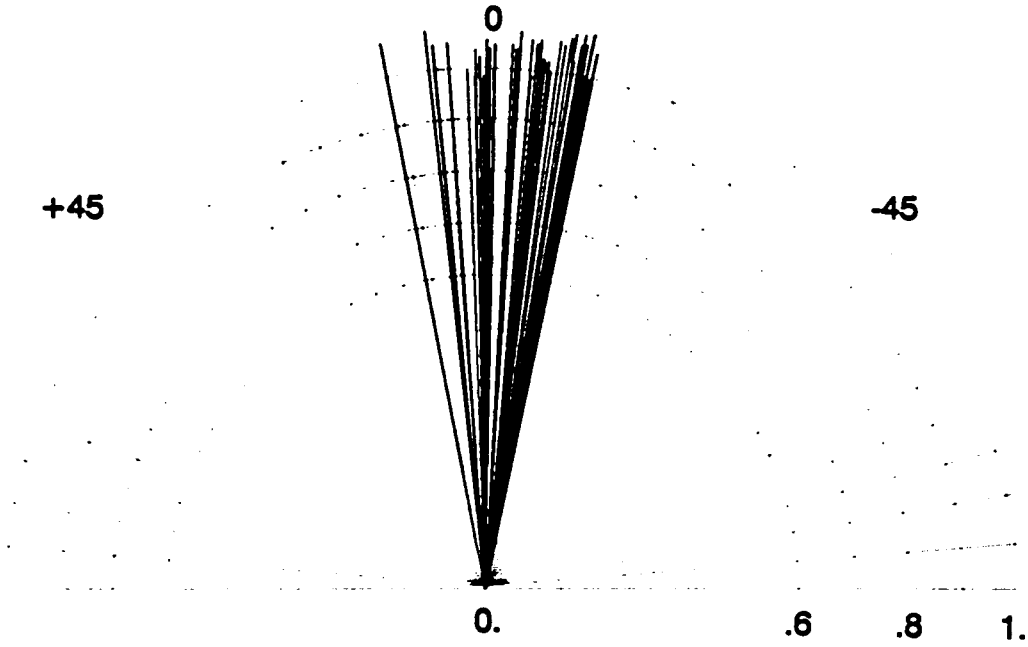

Figure 10. Phasor diagram of the system in normal operating regime.

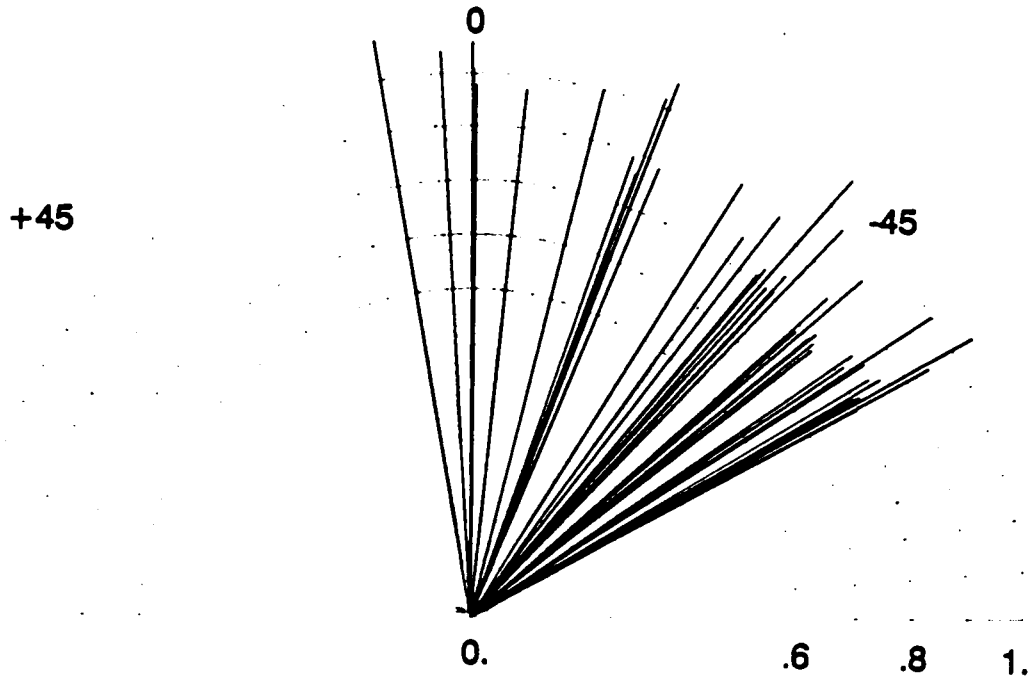

Figure 11. Phasor diagram of the system close to steady state instability.

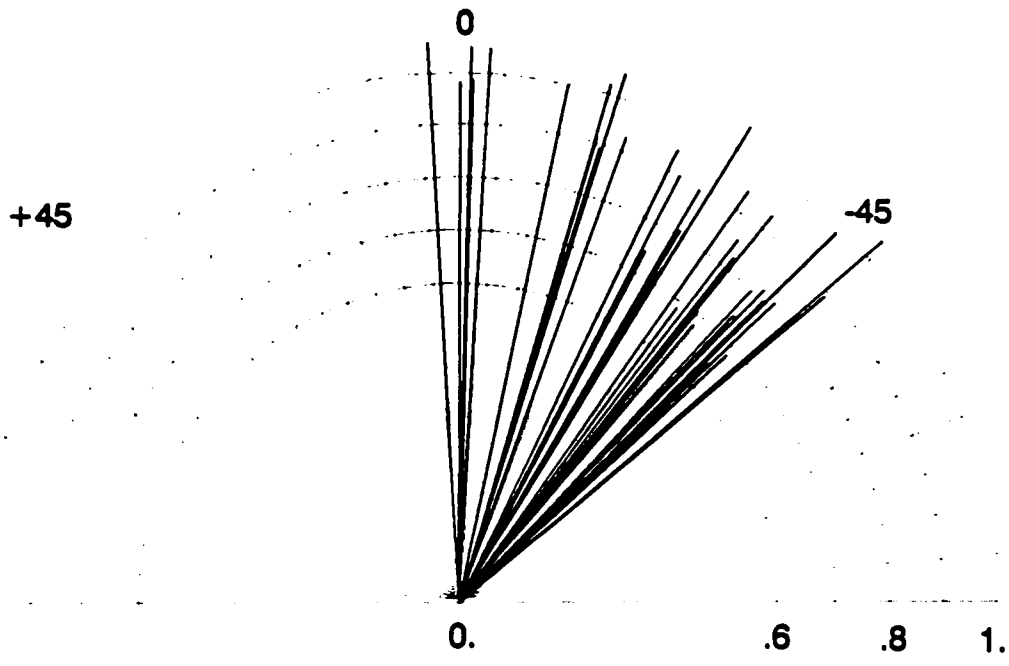

Figure 12. Phasor diagram of the system near voltage stability boundary.

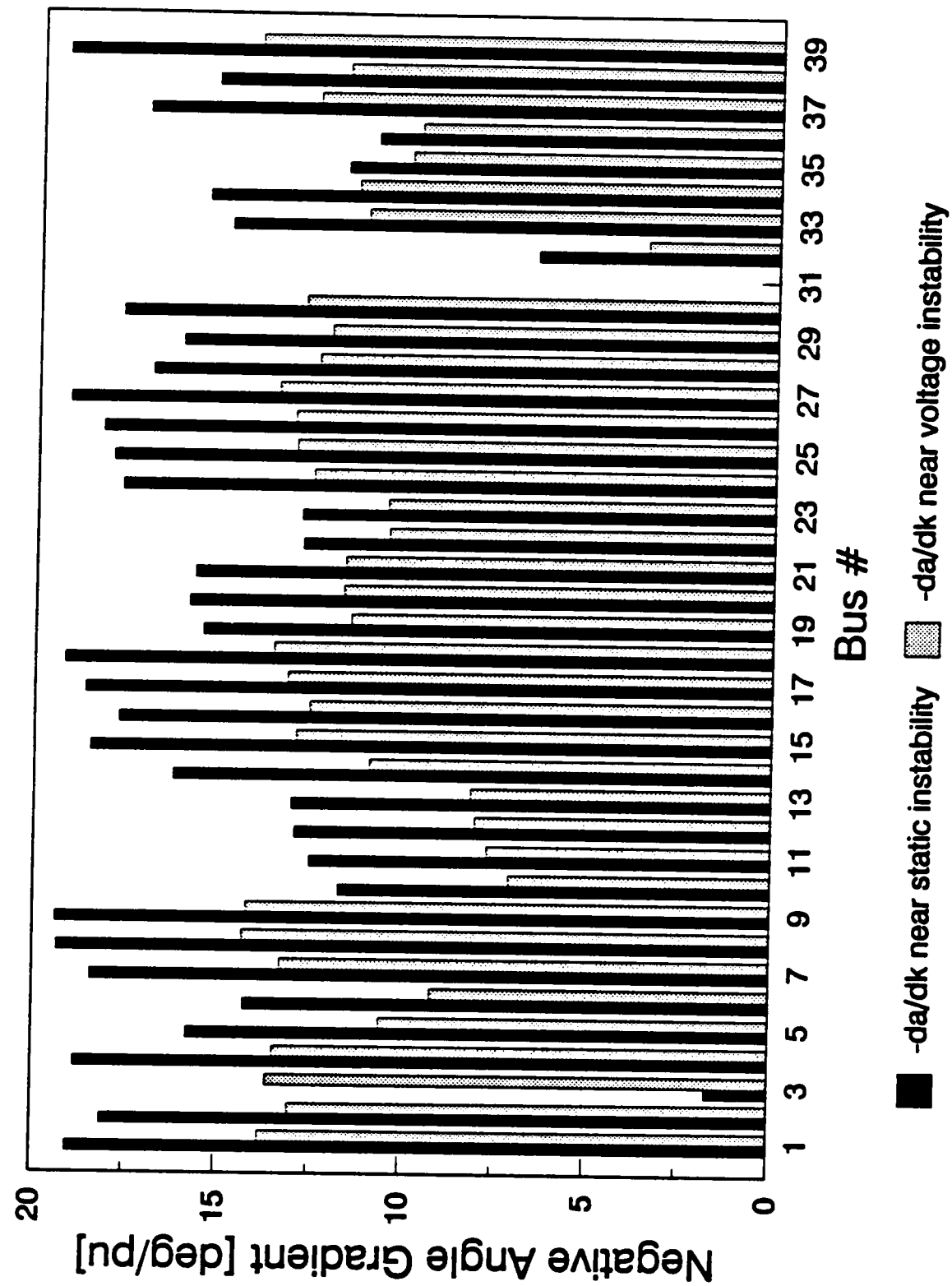

Figure 13. Phase angle gradients near stability boundary.

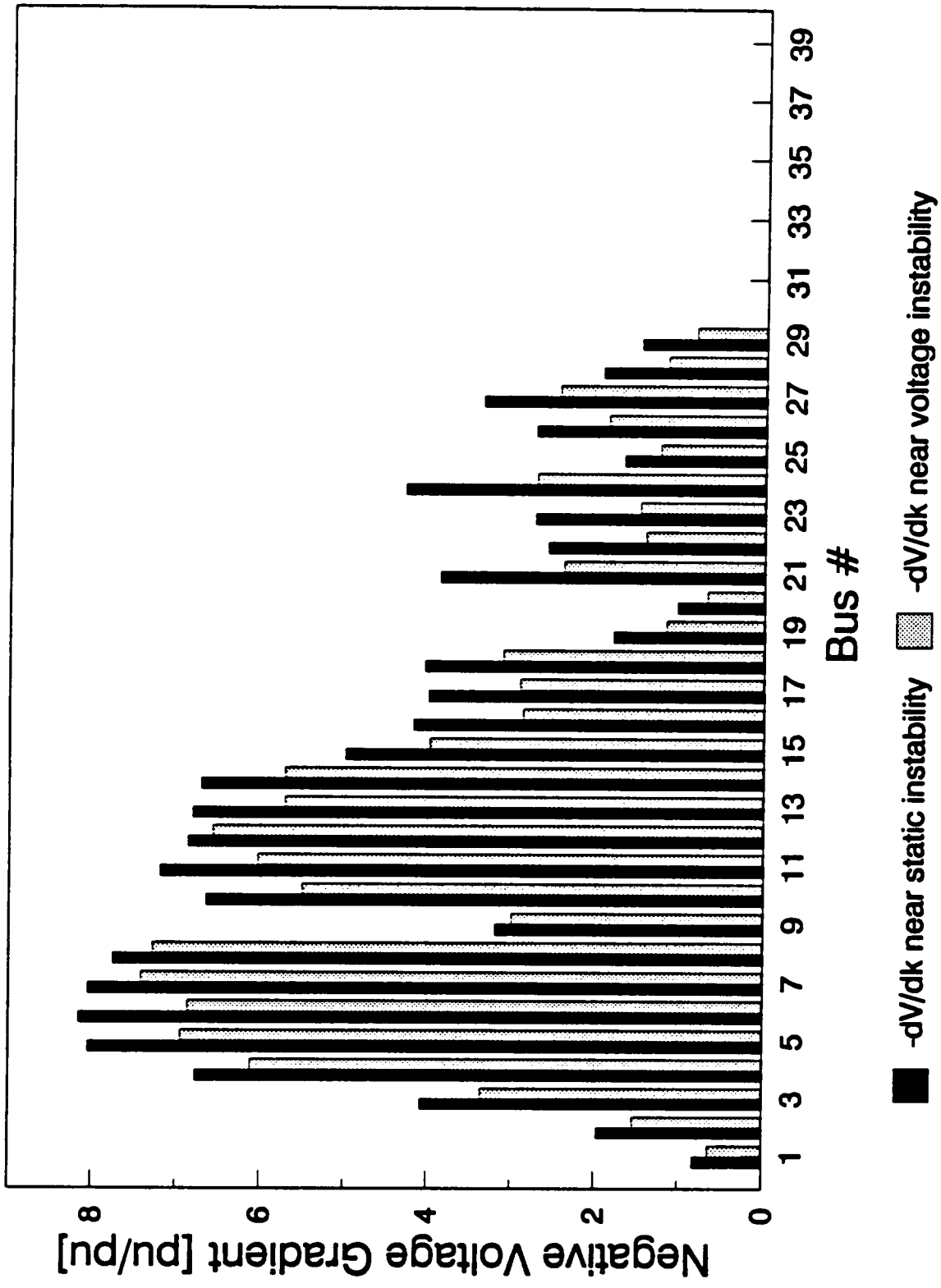

Figure 14. Voltage gradients near stability boundary.

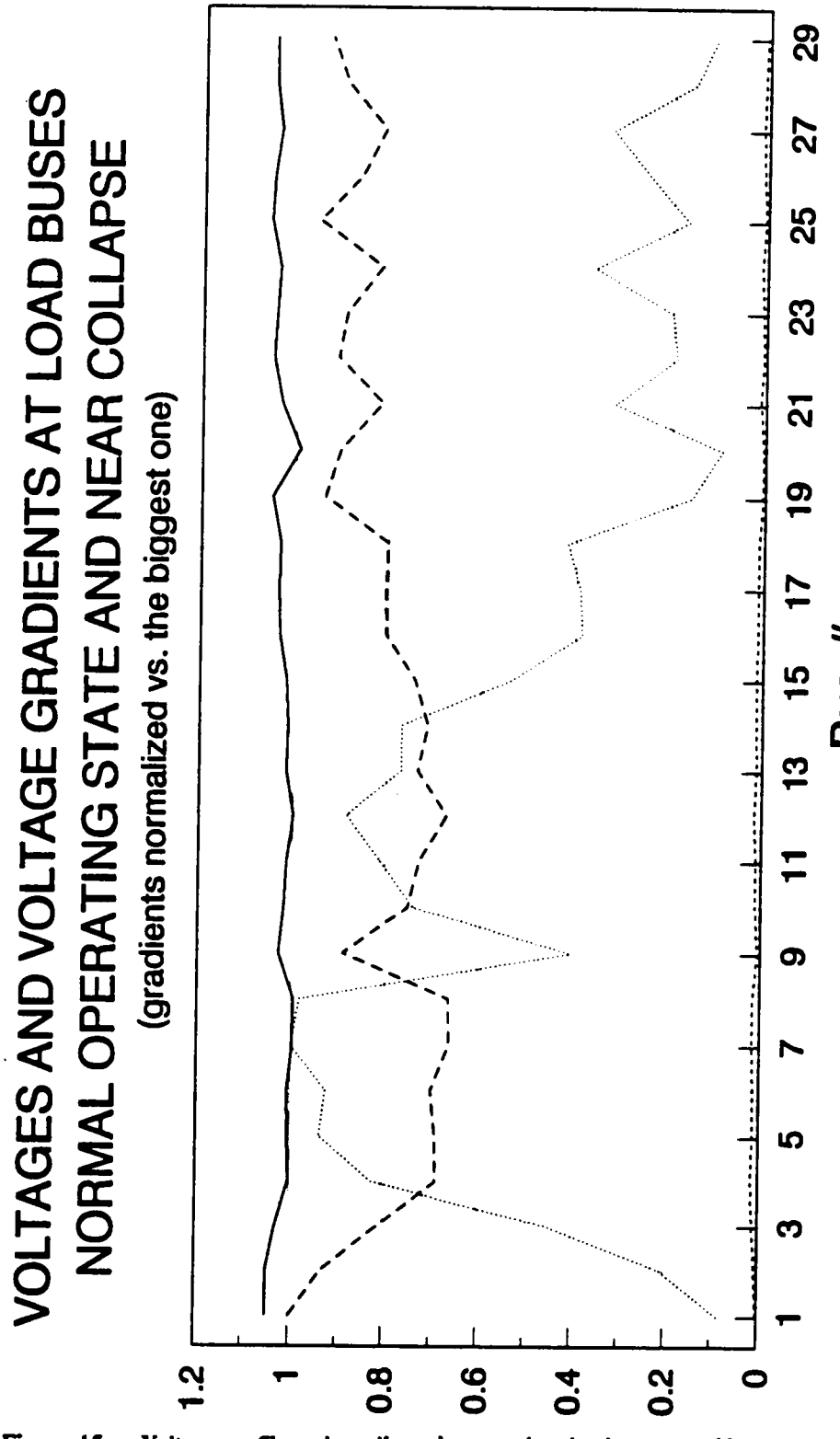

Figure 15. Voltage profile and gradients in normal and voltage unstable case.

the application of the ramp change of the load factor to the power system whose loads were modeled as constant complex power with small random fluctuations. Varying the directions of approach to stability boundary by changing matrices K_1, K_2, K_3, the validity of the voltage collapse condition (3.4.14) was checked and voltage profiles investigated for different loading patterns. This approach serves as a proposal for a realistic voltage collapse model in power systems and was used to extract some useful information about monitoring of voltage stability in power systems.

Figure 16 shows three scenarios of voltage instability based on the step change of load factor:

$$k(t) = k(t_0) + \Delta k\, h(t - t_0) \tag{3.6.1}$$

i) In the first case, step change started from the value $k(t_0) = 2.23345$ which corresponds to the last converged load flow situation calculated (Figure 12). The step $\Delta k = 0.0005$ was chosen to leave the final value of the load factor below bifurcation value.

ii) In the second scenario, the step change of the load factor was $\Delta k = 0.0015$, bringing the system above the bifurcation level. It should be noted that the exact bifurcation value could not be estimated with a very high accuracy through trend analysis of the steady state minimum sigular values of Jacobian, because of their rapid descent to zero as the load factor increase brings the Jacobian close to

singularity. It required some experimentation before proper values for Δk were found.

iii)In the third case, the same scenario was used with the application of the step change which brings the load factor above bifurcation level, but the load factor was brought back to initial level after 1 second.

$$k(t) = k(t_0) + \Delta k[h(t - t_1) - h(t - t_2)] \tag{3.6.2}$$

This case was simulated to investigate possibilities for some kind of stability preserving control in the system when voltage instability is incipient.

Figure 17 shows the voltage response at test system's load buses after application of scenario (i). A very large swing of bus voltages is noticable, especially in the group of buses with lowest voltages and highest voltage sensitivities (as confirmed by the results of steady state analysis in Figure 15). The voltages slowly recovered into a steady state after over 5 seconds and the system stabilized in a new steady state, closer to stability boundary. This was an interesting experiment, because it shows how intensive is the voltage response of the system near voltage stability boundary (load change of only 0.05% produced voltage drops of over 3% in magnitude). It also shows that various load buses in the system have very different sensitivities to load factor disturbances. The voltage at bus 1 did not practically change at all throughout the transient, while a group of critically affected buses (notably buses 4,7,8, and 12) underwent an intensive transient before settling in a new steady state. It is also worth noting that using dynamic simulation

in this case, it was possible to calculate a stable equilibrium point closer to the voltage instability than any state calculable by the application of the Newton Raphson algorithm used for steady state simulations.

Figure 18 shows the system load bus voltage response after application of scenario (ii). After initial voltage drop following the step change of the load factor, voltages were descending very slowly (voltage dropped 3% over a 5 second period at the most affected bus 7). About 5 seconds after the change of load factor, voltages started to drop very suddenly, causing the systemwide voltage collapse. It can be seen again that not all the buses have had the same intensity of response to the disturbance, but the most critical were again the buses in the heavily loaded group (4-8 and 11-15). Although the severity of the voltage collapse was strongest at those buses, the trend of very high negative voltage gradients is present at all the load buses in the system causing simultaneous collapse on all of them. The simulation could not be pursued until the voltages reached zero values, because Jacobian J_r used for dynamic simulations became near singular , causing divergence of the modified load flow and preventing further simulation. It is clear, however, that the voltage response trends are directed toward systemwide collapse. The dynamics of this voltage collapse model complies very well with the observations of the actual collapse cases. The blackout was preceded by a long period of 'hesitation' characteristic for saddle node bifurcations and its occurrence was sudden and disastrous for power system operation.

Figure 19 shows the simulation of the scenario (iii) during which the system was subjected to the same conditions as in the scenario (ii) for 1 second and the load factor was brought back to its initial value after that. The system voltage response (after the system was brought back to initial loading conditions) quickly recovered and the system settled in a stable steady state equal to initial conditions. This behavior persisted when the time of application of the second step was varied along voltage collapse descent interval. After some time, however, the system was not able to recover and collapsed even if the load factor was reduced to the level lower then the initial one. That critical time approximately corresponds to one third of the system descent time into collapse. It is important to note that even when the system is descending into collapse, load reduction may preserve the stability if it is accomplished within reasonable time. One second is enough time for modern monitoring systems to produce voltage instability alarms, although it would be possible to get early alarms much before the system actually goes unstable, by analyzing steady state results as the states approach the stability boundary.

Figure 20 shows the changes of the minimum eigenvalues of the Jacobian J_r which corresponds to equations g_p , g_q in the equation (3.3.4) shown for the three cases discussed above. The patterns of change of minimum eigenvalues ressemble the voltage changes on the most affected load buses. In the voltage collapse case produced by scenario (ii), the simulation was possible until the minimum eigenvalue of J_r reached values very near zero, suggesting matrix singularity within the precision of computation. The initial minimum singular values after

application of the load step change were of the order of 0.7 (for a 39-bus system the size of J_r is 78×78 . The final values before the divergence of the modified load flow were of the order of 0.05 with a noticable trend toward zero. Therefore, the system descent into collapse after the static bifurcation was continued until the singularity of J_r was reached. Voltage collapse simulation was possible until the system lost causality, as defined in the analysis of (3.4.8).

Figure 21 shows the voltage responses at two most vulnerable load buses (7 and 8) after application of scenario (ii) with various intensities of the Δk . The first simulation (1) corresponds to the situation shown in Figure 18, while two others were produced by increasing the step change by a small amount (10^{-6}) . Such a small change of system conditions produced very different times of descent into collapse, although the system trajectories were virtually identical for over 50% of the time of descent. This sensitivity of the system to parameter changes (shown in (3.4.14)) suggests that the alarms should better be available much before the system trajectory reaches the stability boundary, because very small changes of some loads would be enough to accelerate the descent into collapse very sharply. It is also noticable from Figure 21 that more intensive load increases are causing earlier descents into collapse.

In the second series of simulations, a system model was formed using the load model

$$\begin{aligned} P &= [k \times K_1 \times t + \beta \times N]P_0 \\ Q &= [k \times K_2 \times t + \beta \times N]Q_0 \end{aligned} \tag{3.6.2}$$

where

$$N = diag\{n_1, n_2, \ldots, n_m\} \tag{3.6.3}$$

and k, K_1, K_2, P_0, Q_0 are the same as defined in (3.5.2) and (3.5.3), while matrix N is a diagonal matrix whose nonzero elements are randomly generated (Gaussian) with zero mean and unit variance. Parameter β is the measure of randomness applied to the loads and it was kept at the level of 0.1% for our simulations. Since k represents the slope in (3.6.3), load factor is continously increasing and is corrupted with a small amount of Gaussian noise. The slope chosen for the ramp increase of k was 0.1% per second, or 6% per minute, which is a realistic model of the patterns of load increase like the one that preceeded voltage collapse in Japan described in the previous chapter. The pattern of total system loading for $K_1 = K_2 = I$ is shown in Figure 22.

Figure 23 shows various directions of approach to stability boundary, defined as a set of states having singular Jacobians. The plane of the Figure 22 symbolically represents the hyperspace of the system states reduced to two dimensions. Crossing zones of constant minimum eigenvalues, or minimum singular values on a path towards instability may be considered as a measure of the proximity to the boundary. From many possible directions (the one labeled (3) at Figure 23 was shown to induce loss of steady state stability in previous analysis), three were chosen for approach to voltage stability boundary:

i) The first loading pattern is the one when both active and reactive powers of all the loads are proportionaly increased ($K_1 = K_2 = I$) . It may be called the pattern of variable load factor and causes the system to approach the stability boundary at the same point where it was crossed in the scenario shown in Figure 18, but the approach is accomplished in a continous change of load factor (parameter λ) instead of a step change. It is labeled (2) on Figure 23. Since the scenario in Figure 18 shows that it is leading to voltage collapse, this case will certainly end in some kind of voltage instability;

ii) Second loading pattern corresponds to the case when active powers of the loads are left unchanged, but the reactive powers are increased with the load factor k ($K_1 = 0$, $K_2 = i$) . It is labeled (1) on Figure 23. Since many of the discussions about voltage collapse emphasized the important role that the reactive power plays in voltage instability situations, the initial idea was to approach the stability boundary by increasing VAR consumption in the system. The steady state analysis confirmed that such a loading pattern indeed produces voltage instability;

iii) The third loading pattern represents the increase of the reactive powers on the most vulnerable load buses only. Buses 4, 7, 8 and 12 were chosen and scenario defined by $K_1 = 0$, $k_{24} = k_{27} = k_{28} = k_{2,12} = 1$; $k_{2,i} = 0$, $i \neq 4,7,8,12$. This scenario also produces voltage instability.

Figure 24 shows voltage profiles on load buses obtained from the last converged load flows before stability boundary was reached for scenarios (i), (ii), (iii). Scenario (i) produced a critical value of the load factor $k = 2.23345$. The voltage profile is the most uniform of the three shown, although the voltages on critical buses are as low as 0.65 pu. Voltage profile for scenario (ii) is shown in the middle row on Figure 24. It was reached for $k = 4.670$ and is characterized by even lower voltage levels at those buses which were labeled critical in previous discussion. Scenario (iii) is represented by the voltage profile in the third row (Figure 24) reached for $k = 5.180$. Predictably, voltages at buses whose reactive power was increased have the lowest voltages (below 0.5 pu). This does not represent a realistic scenario for an actual power system, but was investigated as an extreme case. The dynamic simulations produced voltage collapse in all three simulated scenarios. There were no qualitative differences between the results obtained in those scenarios and mostly the figures corresponding to scenario (i) will be presented here.

Figure 25 represents voltages at 10 most critical load buses of the test system (4-8 and 11-15). The increase of system loading by 0.1% per second produced an average voltage drop of 0.2% per second for critical buses (except for bus 15). After the bifurcation level was exceeded, voltages started to drop much faster, bringing the system into complete collapse after about 15 seconds from the beginning of the simulation. The changes of phase angles corresponding to the same load buses are shown in Figure 26. The quadratic pattern of phase angle trajectories is due to the lack of modeling of generation control of the mechanical shaft powers,

which is deccelerating generators as the loads are increasing. Phase angles are shown without any reference angle, since the equations for all 10 generators were used for simulations. That is the reason why they seem to be changing quite fast while the relative angles between them remain almost constant until the moment when final instability occurs. At that point, angles cluster in two groups: those which correspond to buses 5,6,11,12,13 and 14 tend to slow down deccceleration while those corresponding to buses 4,7,8 and 15 tend to continue deccelerating. This angular instability is not nearly as pronounced as the voltage instability shown in Figure 25.

Figure 27 shows the change of the minimum singular value of the Jacobian matrix J_r used for simulations of scenario (i) presented on Figures 25 and 26. Starting from the value of 0.93, it decreases slowly at an almost linear rate (by 0.3 [sec^{-1}] while load is increasing at 0.1% per second) until the final instability, when it starts changing very abruptly and reaches values as low as 0.1 before the simulation algorithm started to diverge and system blacked out in total voltage collapse. This supports the idea to use the indication of near singularity of the Jacobian as an alarm for voltage instability. One important distinction needs to be made, however: for calculation of the bifurcation point, the full system Jacobian corresponding to $[f_p\, g_p\, g_q]^T$ needs to be evaluated, while the reduced Jacobian J_r is the one whose singularity coincides with the final collapse. Although J_r is smaller and easier to handle, the evaluation of the full J should produce the warning early enough to be a timely alarm for some kind of system control of the loading. Therefore, minimum singular value of J is an indicator of

voltage stability margin which is not difficult to calculate (the inverse power method may be used to calculate the minimum singular value in short enough time to make it feasible for a real-time monitoring. The algorithm would be easy to implement since the singular values are all real and nonnegative and as the system is approaching the stability boundary, one, or more of the singular values would start to decrese toward zero, thus providing an easy initial guess for efficient iteration, while in the real-time environment the results of the previous calculation may provide the best initial condition for iterative calculation of the next one.

Another important indication may be obtained by monitoring reactive power outputs of the system generators. Figure 28 shows the reactive powers generated by all 10 generators and reactive power generated by generator 2 (the one which is supplying the most reactive power) during the voltage collapse simulation (Figures 25-27). It is noticable that voltage collapse coincides with precipitous rise in the reactive power generation. Monitoring sudden increase of generated reactive powers can provide an alarm for incipient voltage instability, but without a definite threshold, or criterion of instability. It should therefore be used with caution and with some other criterion (such as the minimum singular value of Jacobian J). In our simulations, generators were modeled without hard limits on the reactive power generation. It would be more realistic to model them as P-V buses until the reactive power limits are reached and to convert them into P-Q buses afterwards. However, it would present some difficulty for dynamic simulation algorithm since it would change the order of the system whenever some of

the generators change mode. A steady state simulation was performed, however, with reactive power limits imposed on generators and reactive power generation analyzed vs. the load factor k in the proportional loading scenario ($K_1 = K_2 = K_3 = I$) . The stability boundary was reached at a lower load factor level $k = 1.636$ (Figure 29) because of the fact that as many as five generators were in the constant reactive power mode at that point (generator data are given in Apendix A). The reactive power generation and limits are important factors in the assessment of voltage stability margins and should be combined with minimum singular values in providing a reliable alarm. Monitoring and control aspects of their applications will be analyzed in the following chapters.

Figures 30, 31 and 32 are illustration of the voltage collapse induced by step change of load factor applied to reactive power requirements only. While Figure 30 does not show major voltage drops all the way to the collapse, zooming into the response of load buses 12, 8, 7 and 4 (Figure 31) and bus 12 only (Figure 32) provides more detail about the dynamics of the pre-collapse load bus voltages.

Figures 33 and 34 provide similar information about voltage dynamics for various step changes of the load factor (different by 10^{-6} similar to Figure 21 but with the assumed loading of reactive powers only). Figures 30-34 suggest that the system voltage behavior is qualitatively invariant with respect to the change of the loading pattern, although quantitiative response differences do exist.

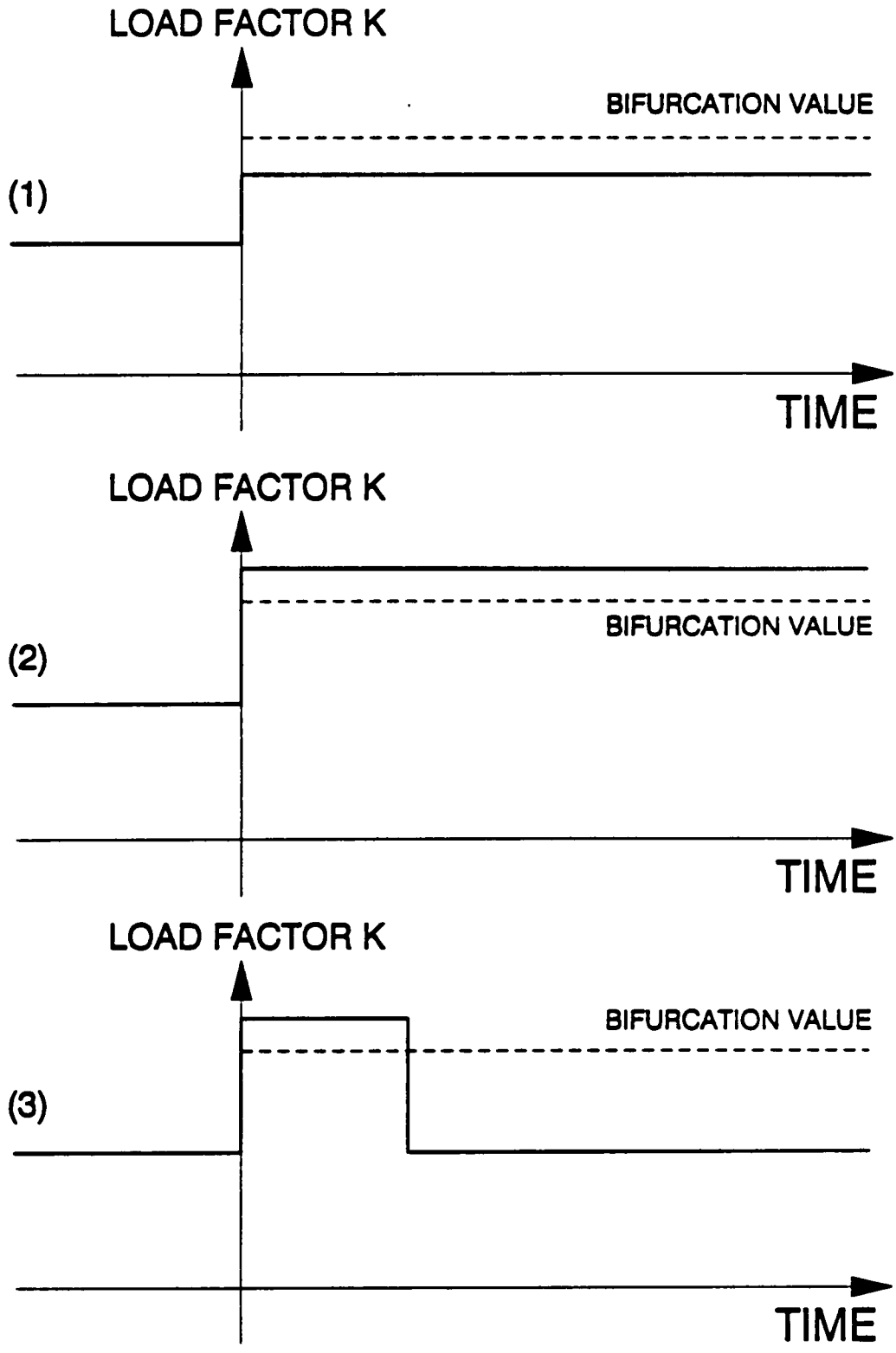

Figure 16. Load factor patterns for step change simulations.

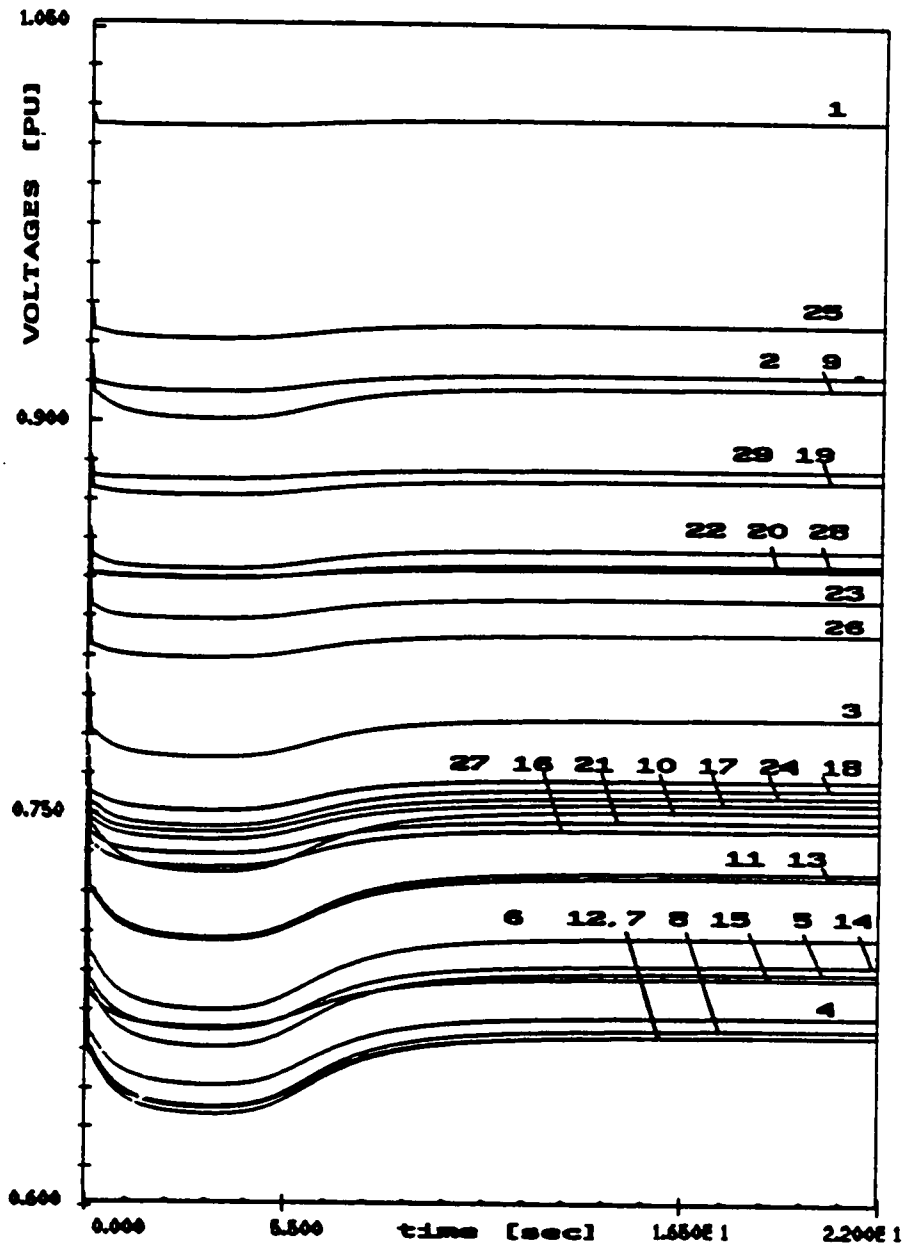

Figure 17. Voltage profile corresponding to Figure 16 (1).

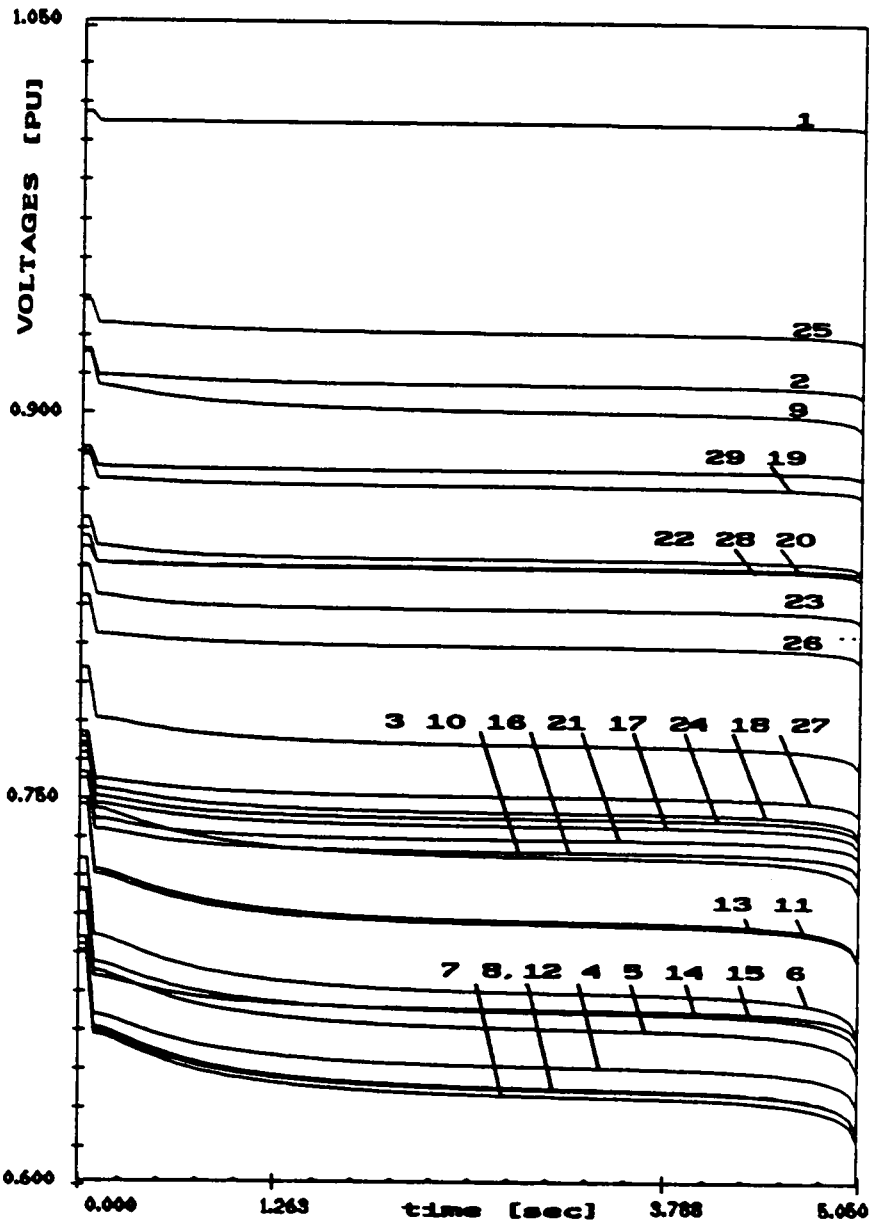

Figure 18. Voltage profile corresponding to Figure 16 (2).

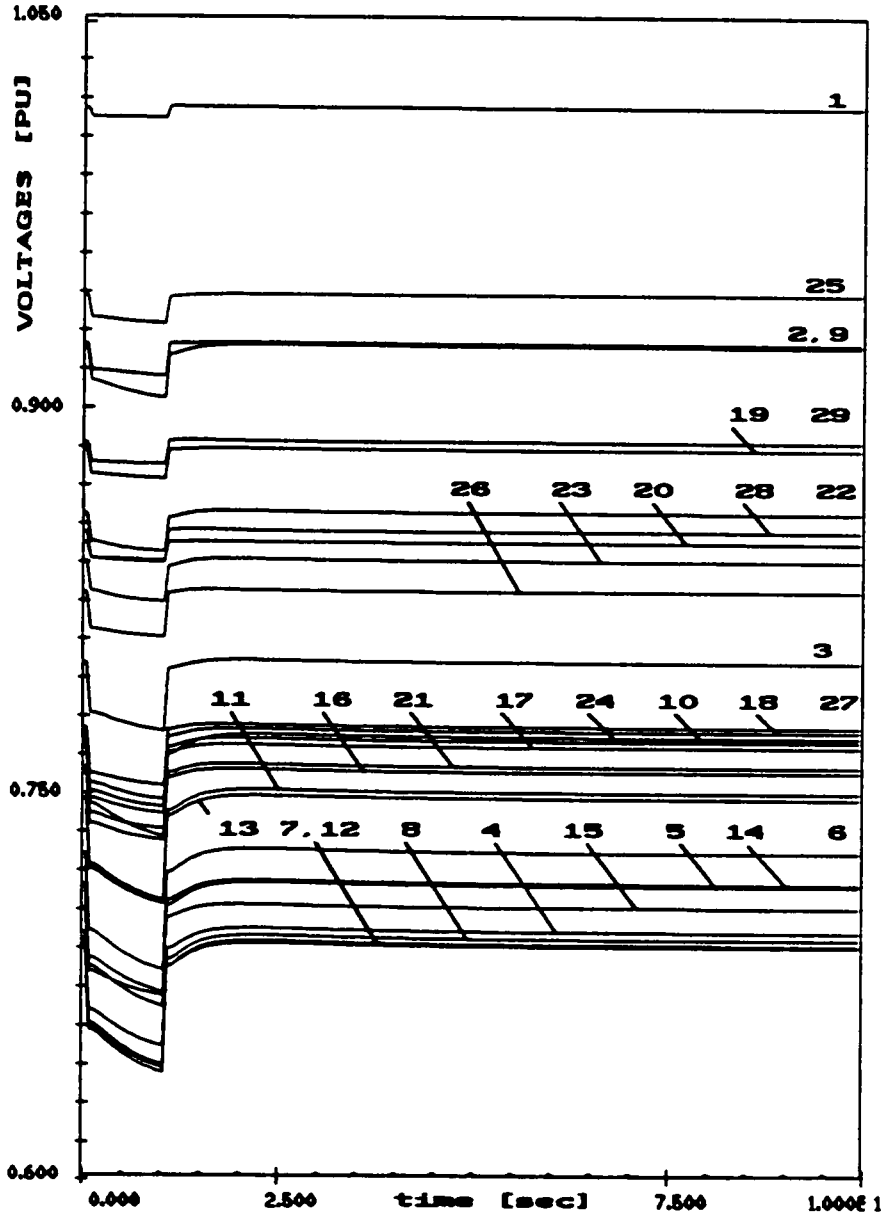

Figure 19. Voltage profile corresponding to Figure 16 (3).

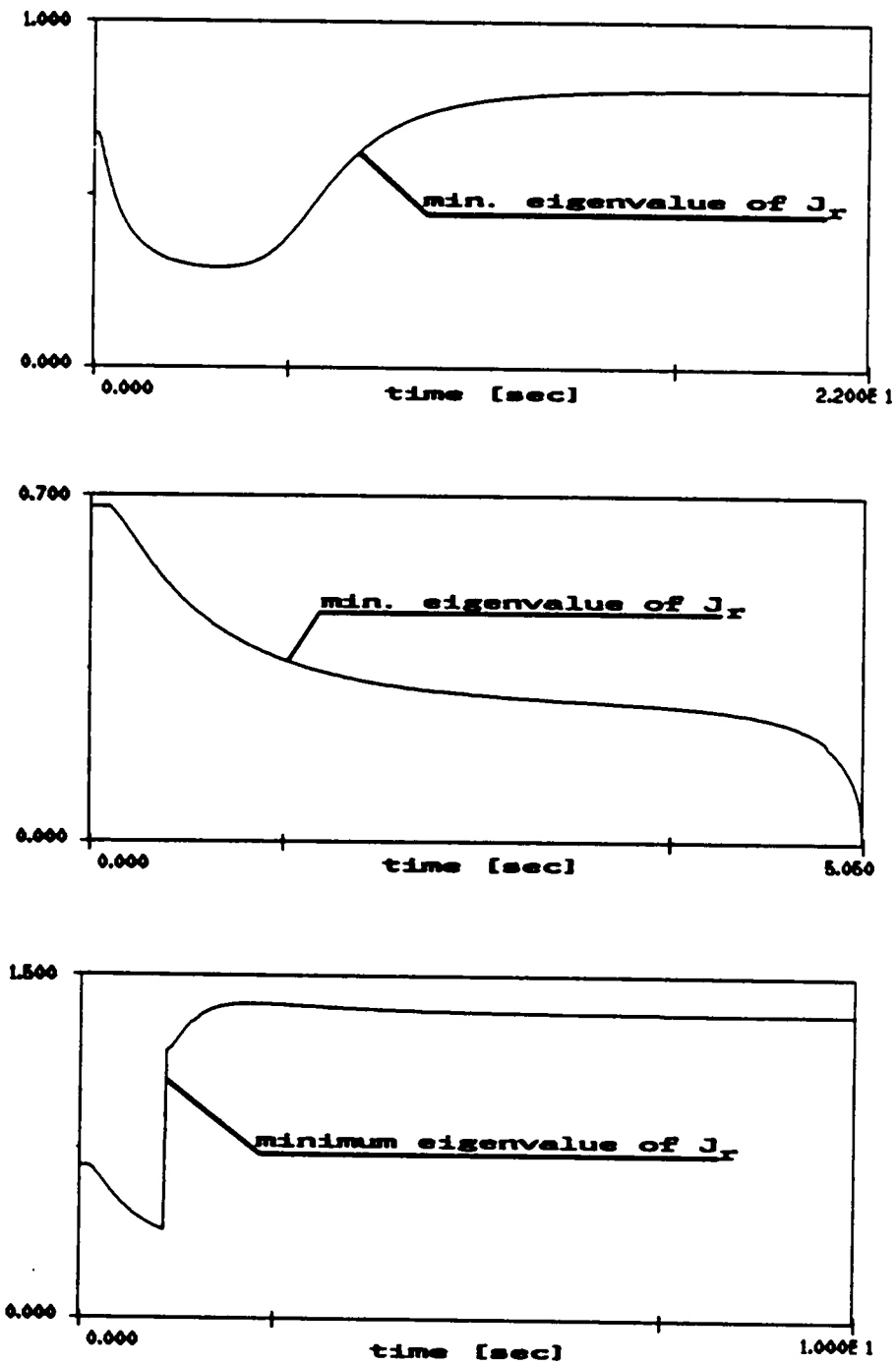

Figure 20. Minimum eigenvalues of Jacobian for Figures 17,18,19.

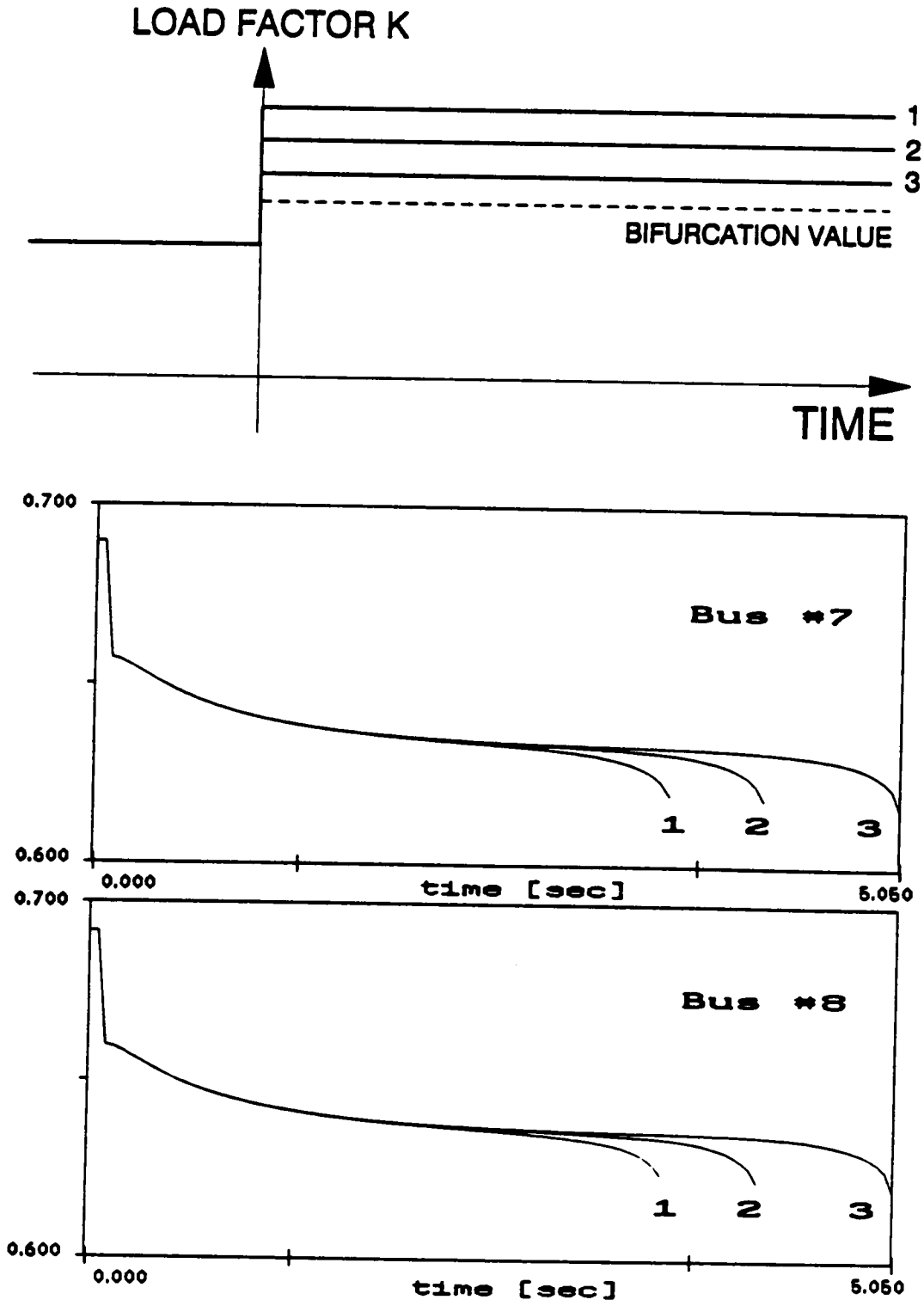

Figure 21. Voltage response for various step changes of load factor.

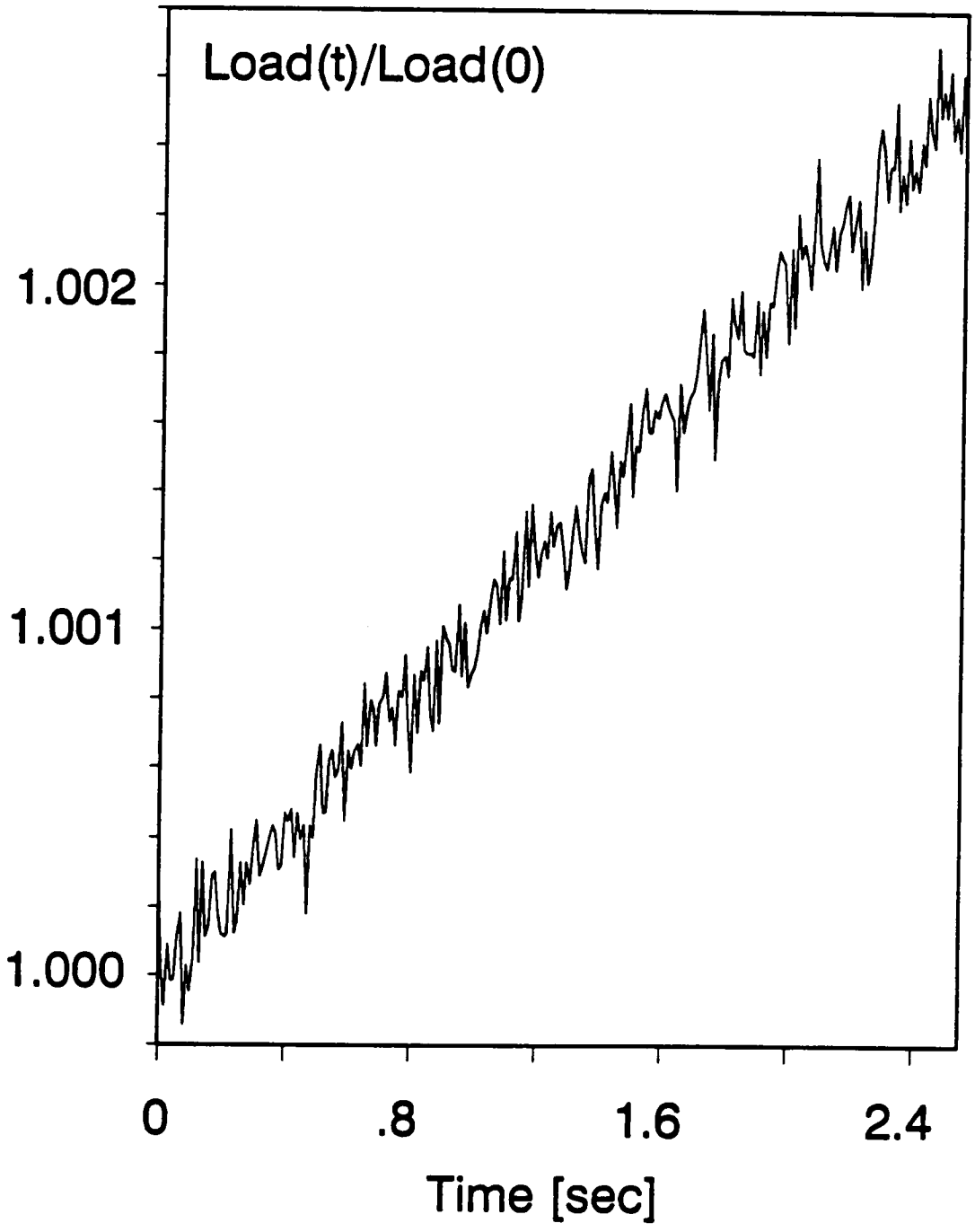

Figure 22. System loading pattern for ramp loading.

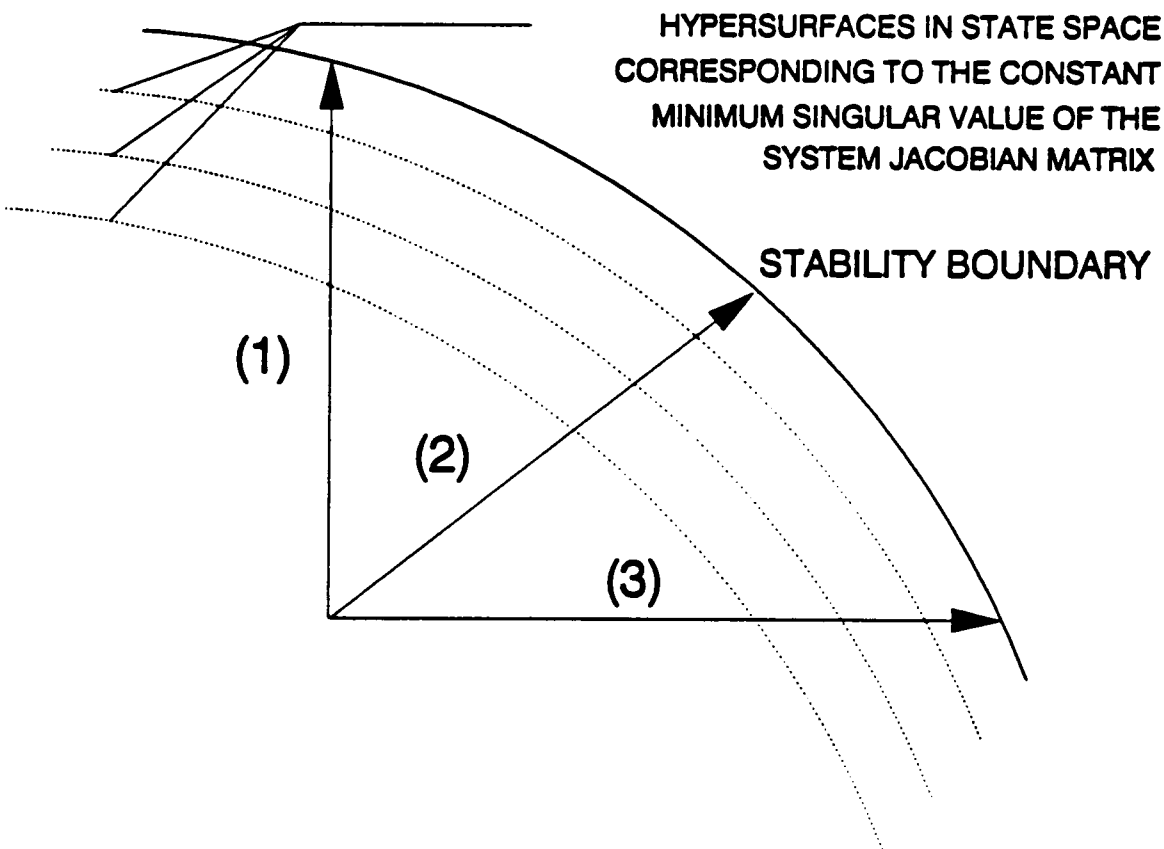

Figure 23. Directions of approach to stability boundary.

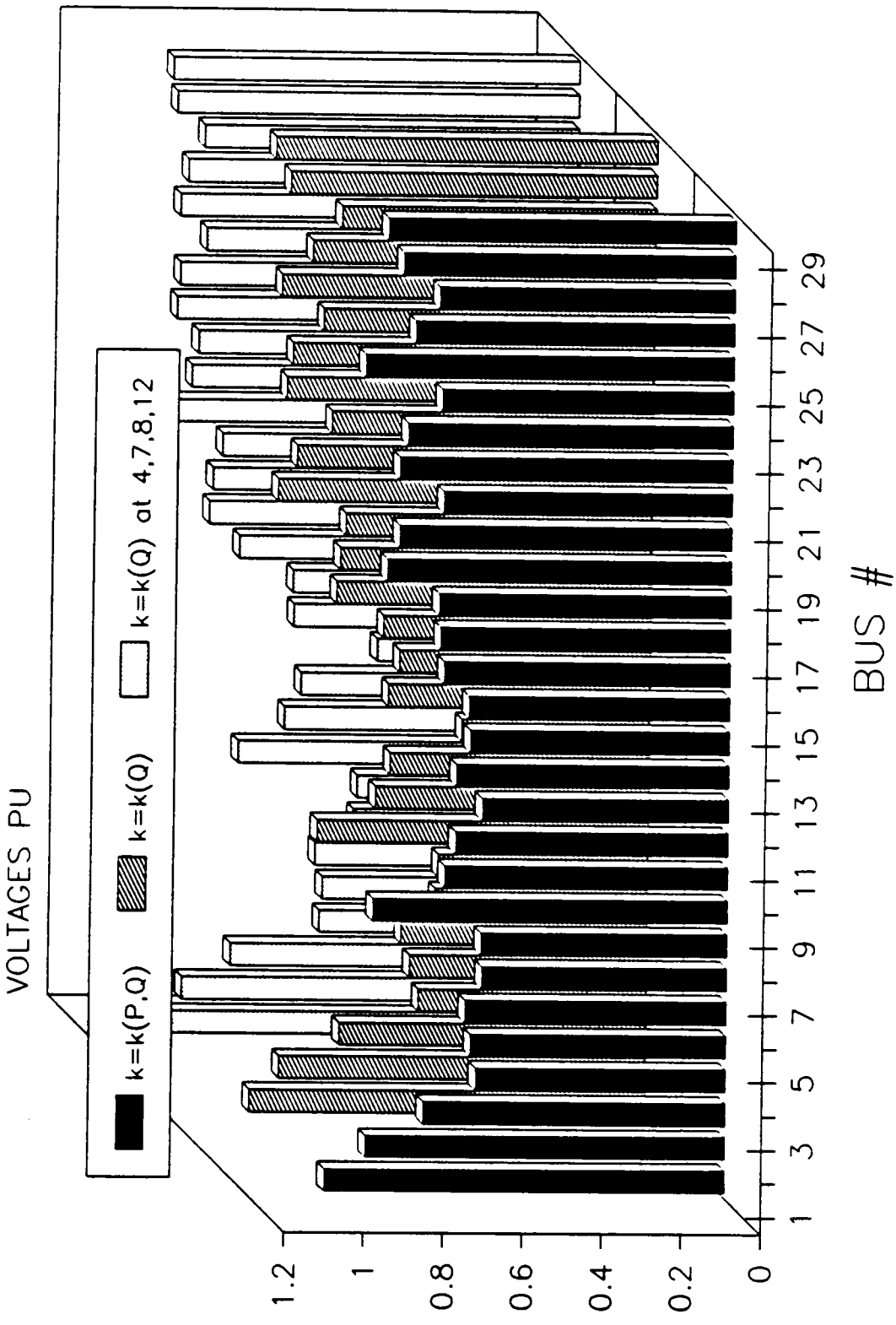

Figure 24. Voltage profiles at stability boundary (scenarios i, ii, iii).

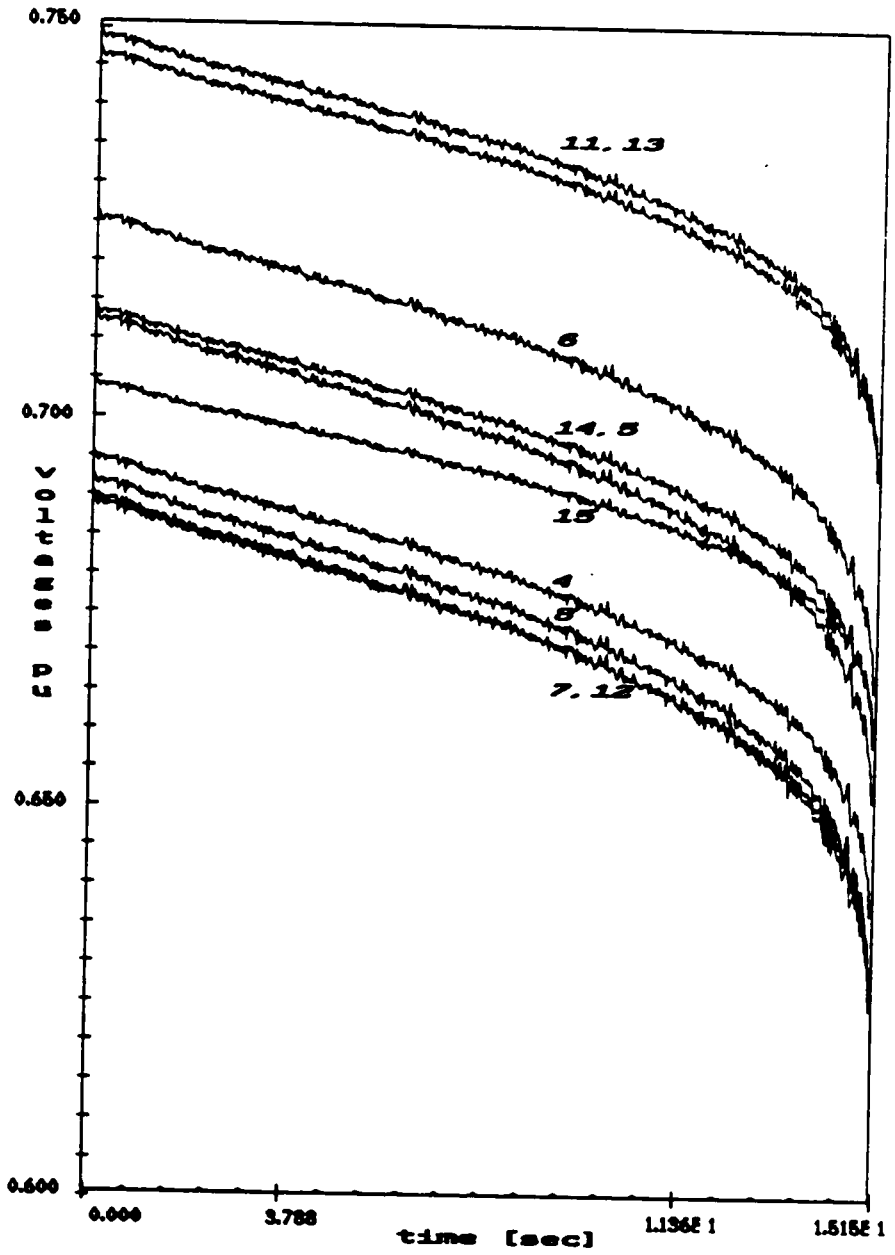

Figure 25. Voltage collapse at 10 most critical buses (scenario i).

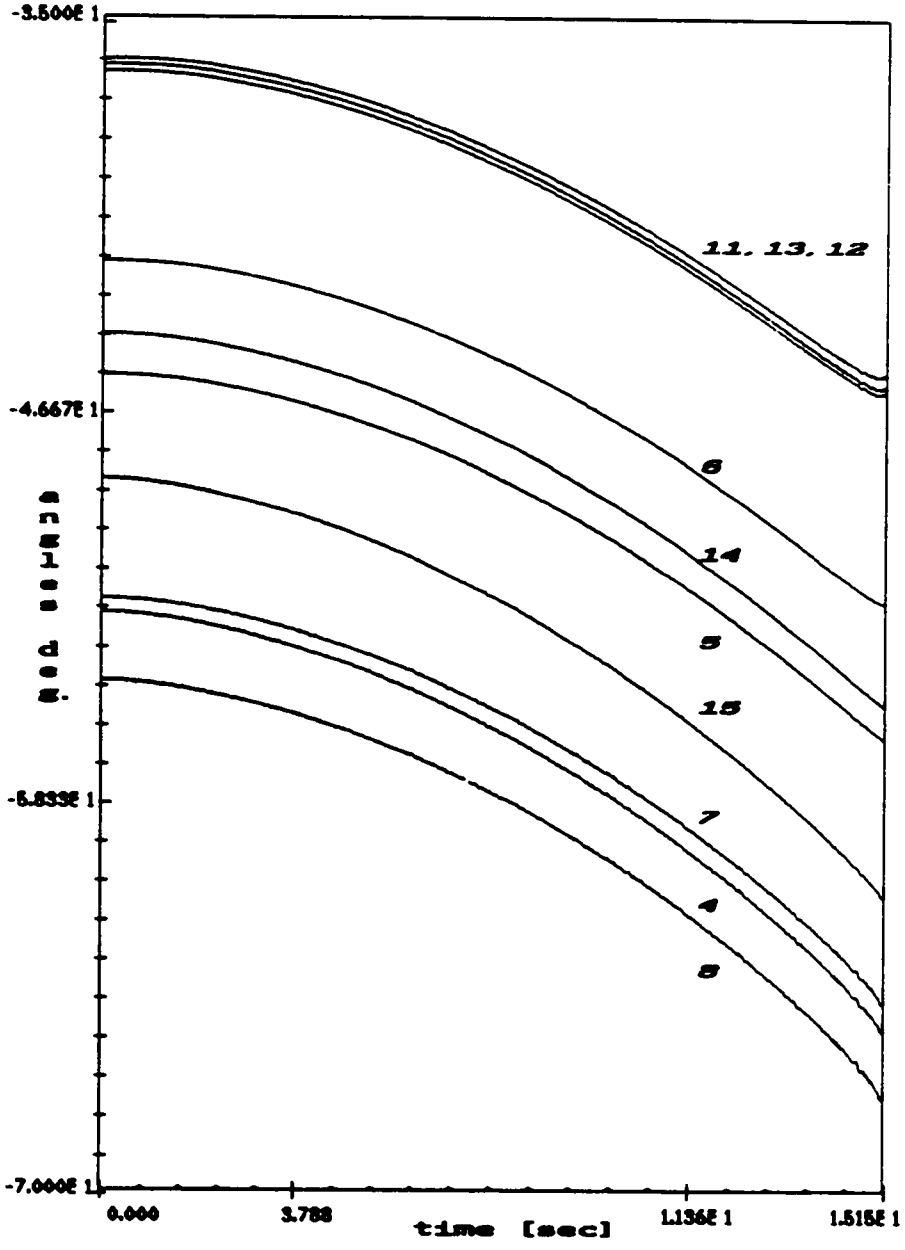

Figure 26. Phase angle trajectories corresponding to collapse in Figure 25.

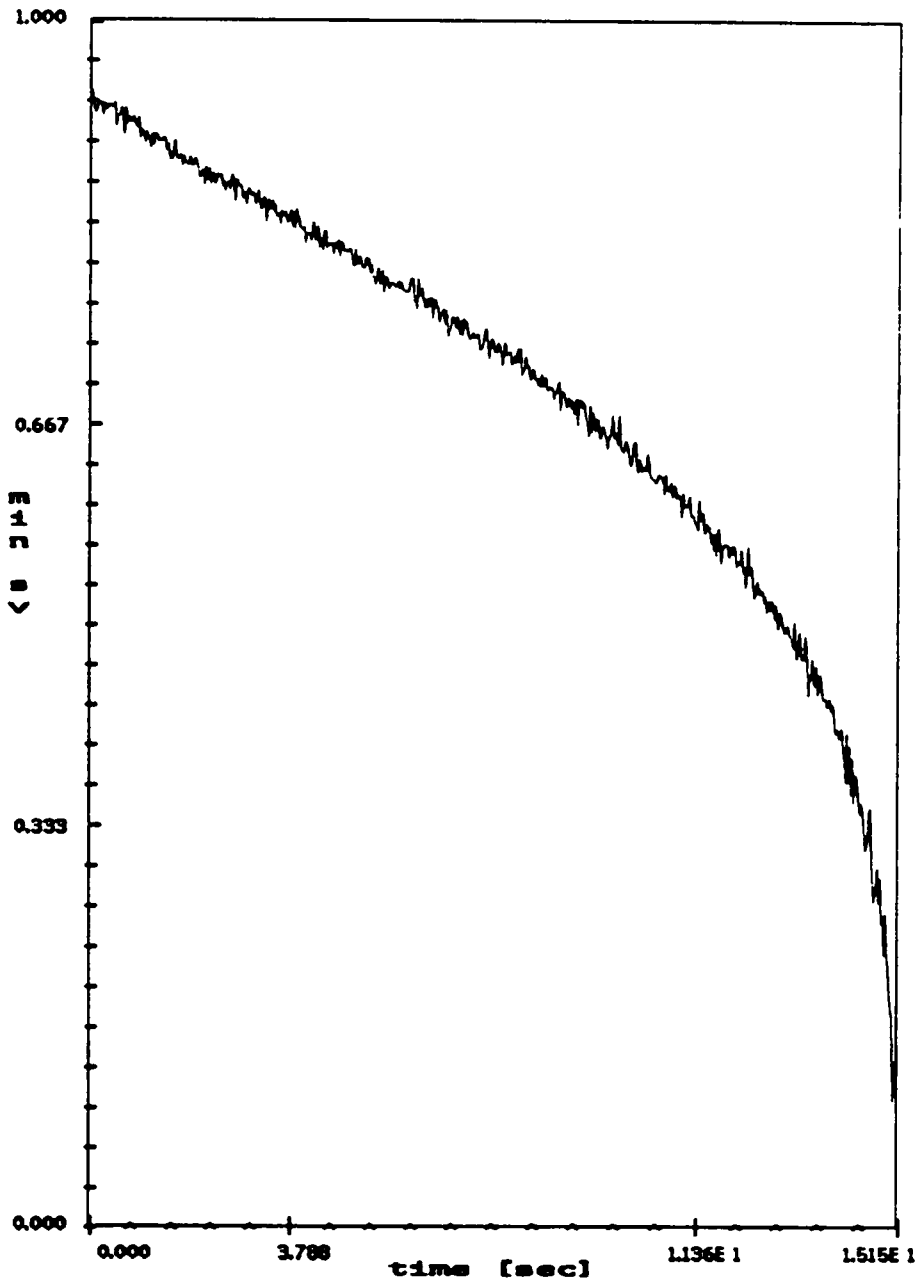

Figure 27. Minimum singular values of Jacobian for collapse in Figure 25.

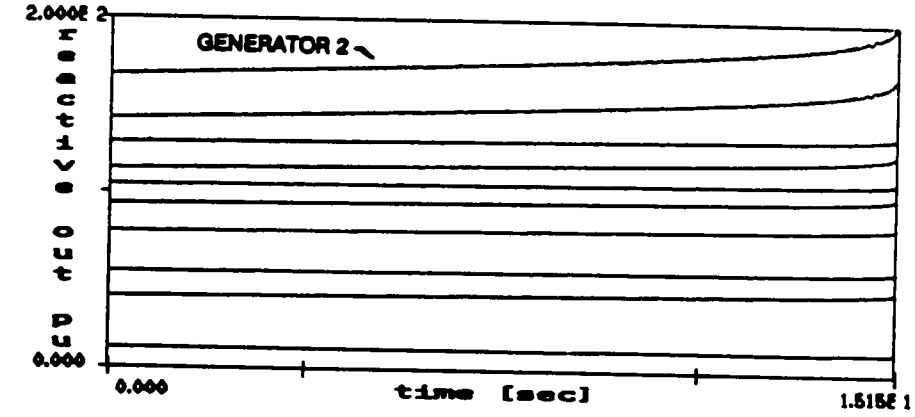

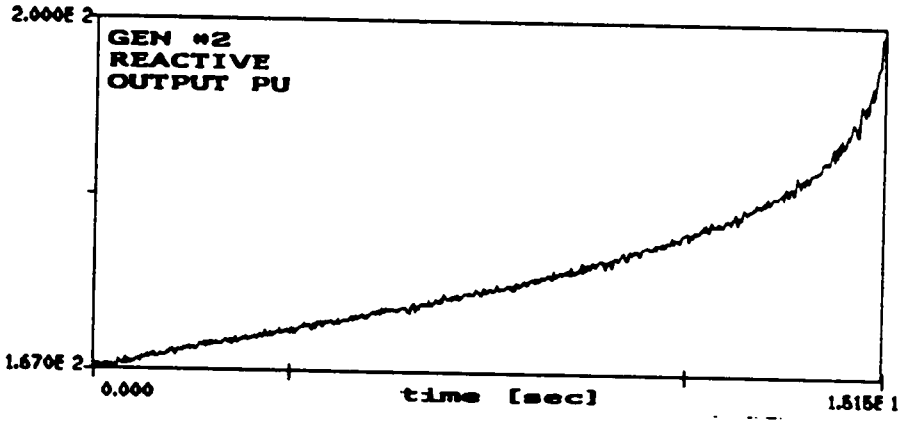

Figure 28. Reactive power generation corresponding to collapse in Figure 25.

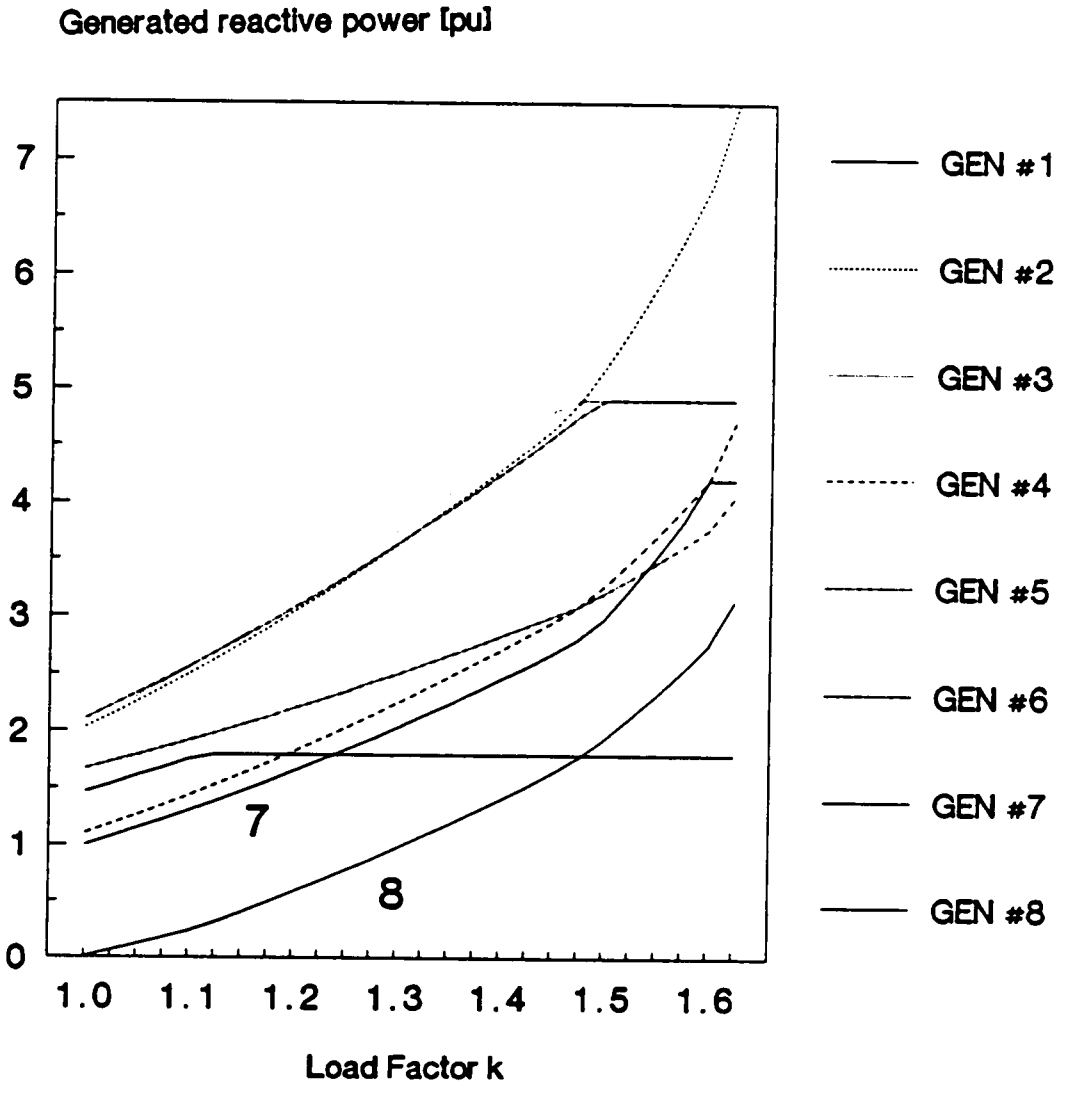

Figure 29. Reactive power generation when generation limits are observed.

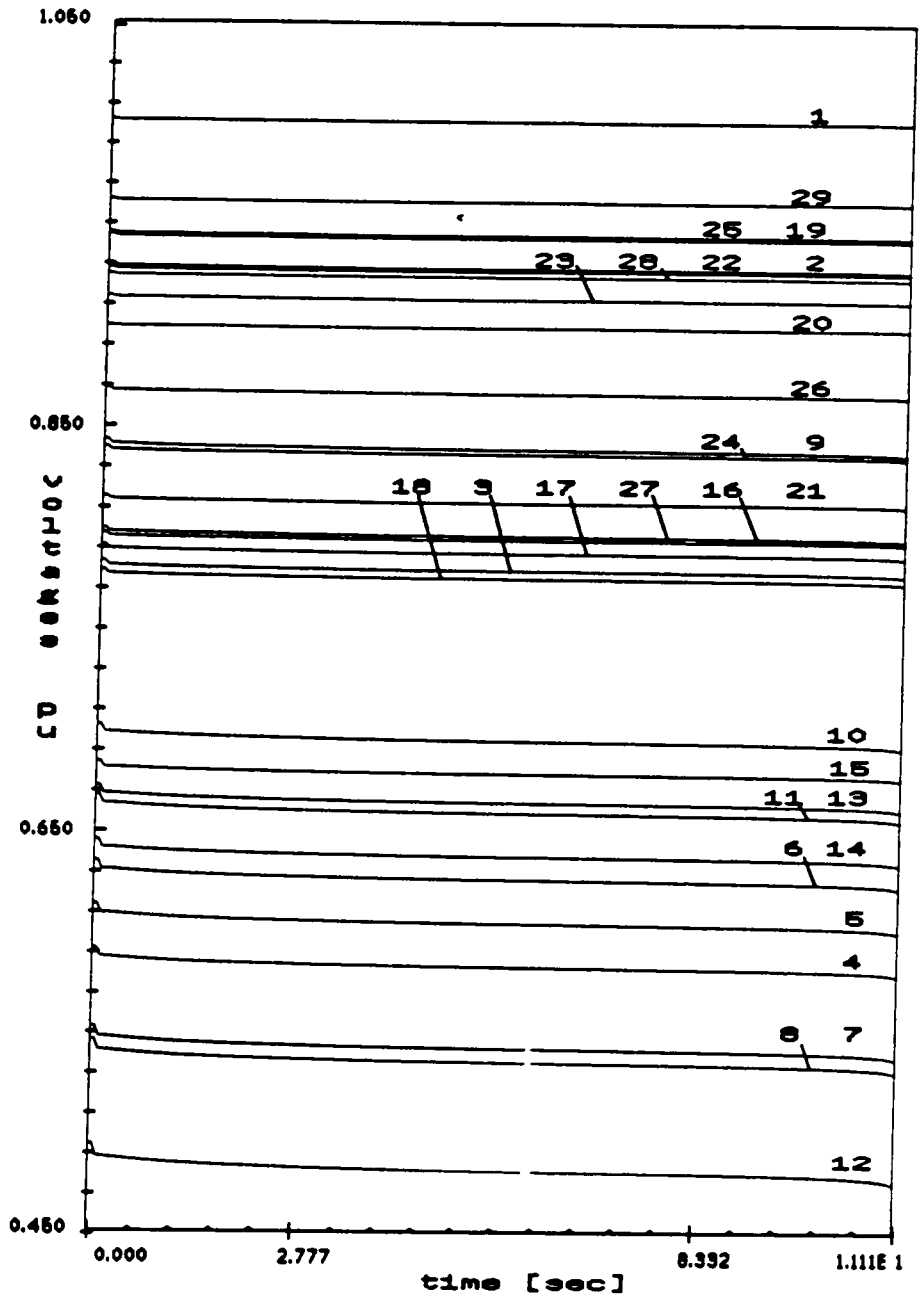

Figure 30. Voltage collapse due to step change of k applied to reactive powers only.

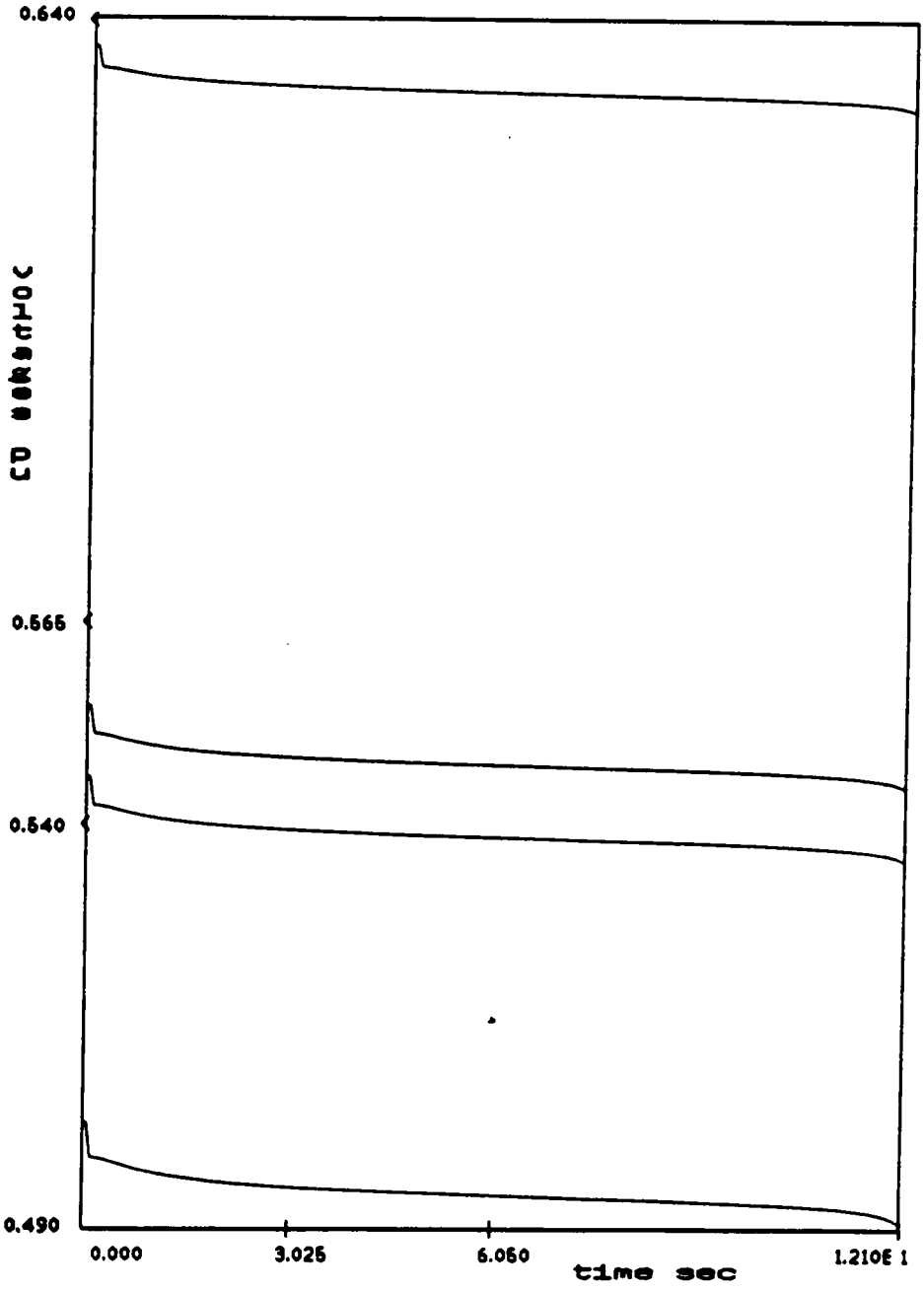

Figure 31. Voltage response of buses 12,8,7,4 for collapse in Figure 30.

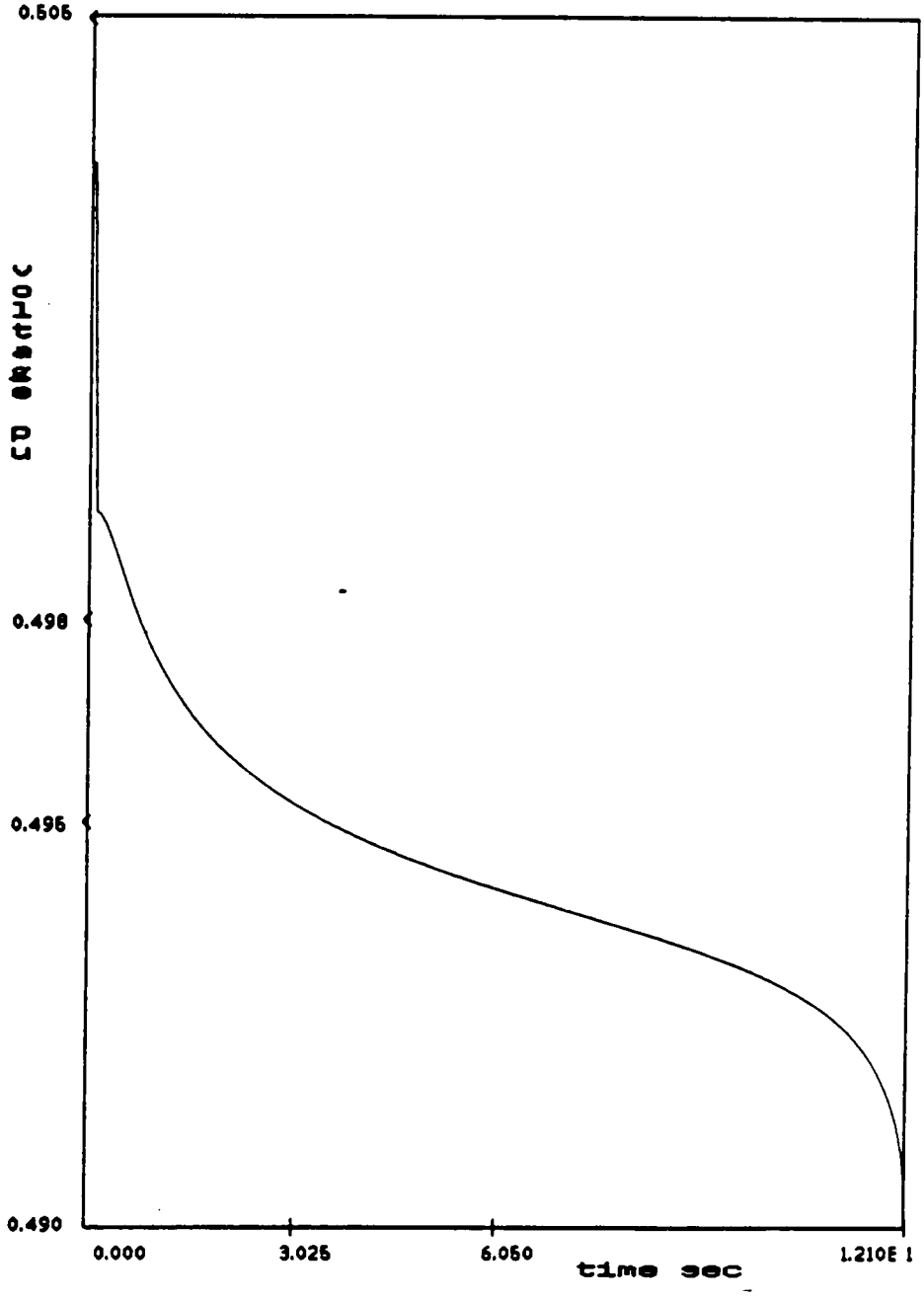

Figure 32. Bus 12 voltage response for collapse in Figure 30.

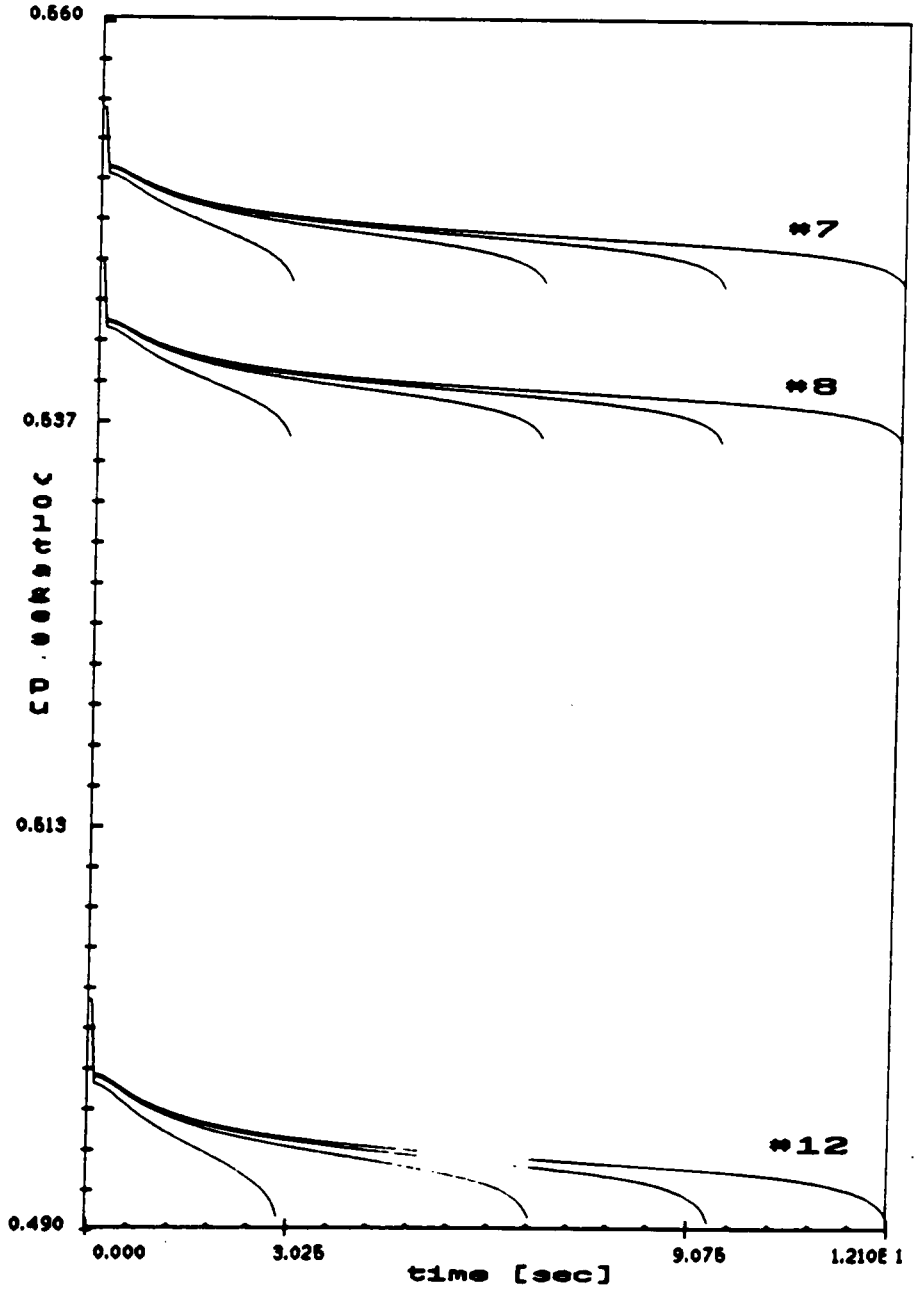

Figure 33. Voltage response for various step changes of k applied to reactive powers only.

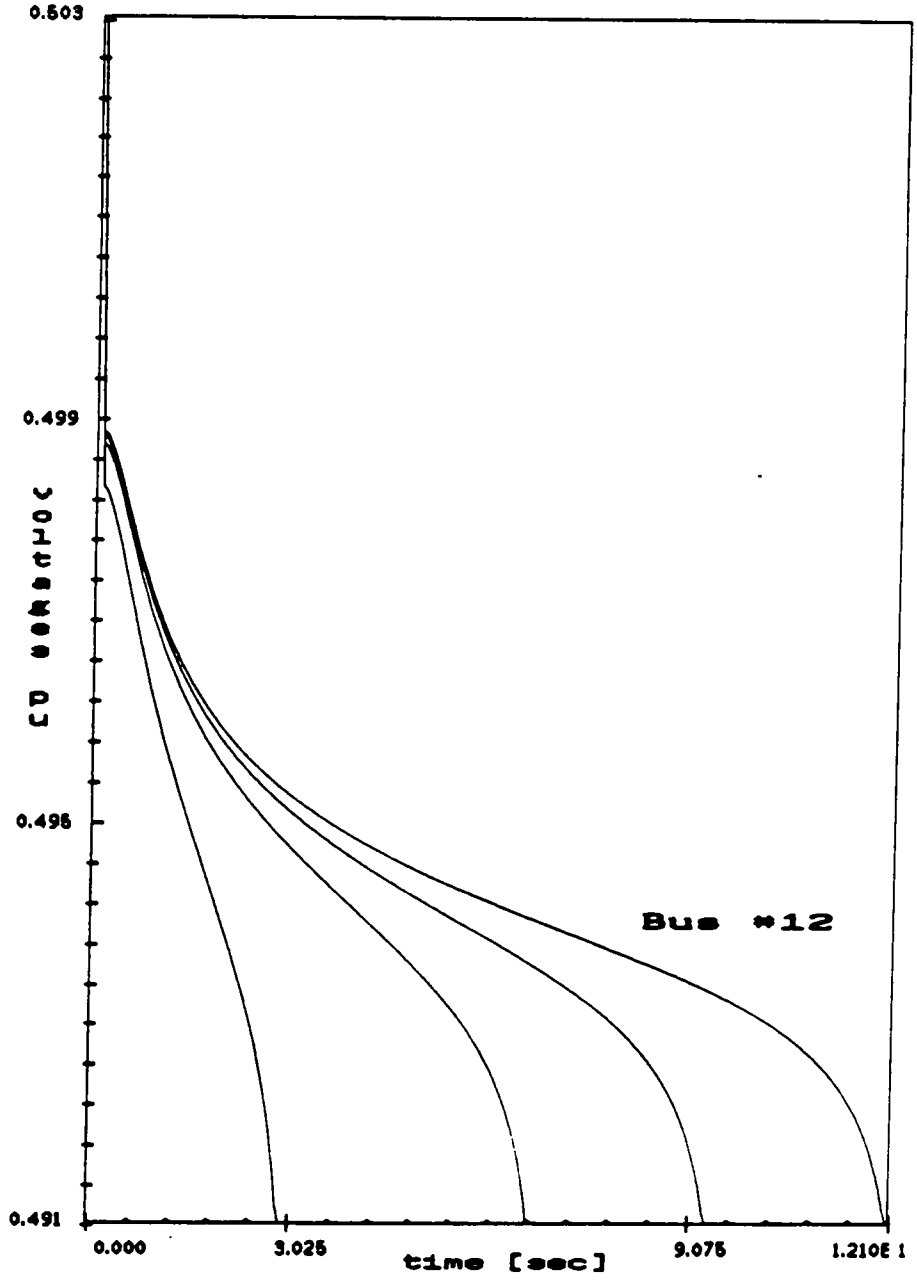

Figure 34. Bus 12 voltage response for collapses shown in Figure 33.

3.7 Conclusions

The 39-bus, 10-generator power system model with constant complex power loads was subjected to a series of simulations with different patterns of increasing loading. That brought their operating points close to stability boundaries represented as saddle node bifurcations of the system dynamic models represented by generator swing equations coupled with algebaric equations of the power balance at load buses. Saddle node bifurcations were reached by increasing the system loading through one parameter (load factor) changes. Conditions for the type of instability were investigated by analyzing the conditioning of the load flow Jacobian and its submatrices [40]. An algorithm was proposed for dynamic simulation of the voltage instablity by applying step, or ramp changes of parameter (load factor) to a selected set of loads and bring the system across the bifurcation value of the parameter. The system trajectory on a center manifold produced voltage collapse in all simulated cases. Simulations were possible until the near loss of system causality, where the collapse has already happened, although voltage profiles could not be tracked until they reach zero values. If the terminal value of the load factor were a bifurcation value, the system trajectory would be on a center manifold. Since in all the simulations the bifurcation values were not exactly known, system trajectories cannot be considered to be along center manifolds, although they are in the neighborhood (values of parameter are very close to the bifurcation value). A proposed scenarios of voltage collapse based on continuously increasing loading was simulated and minimum singular values of the

Jacobian and generated reactive powers proposed as indicators of proximity to voltage collapse. Their application will be discussed in more detail later in the text.

Chapter 4. Voltage Stability Monitoring: Phasor Measurements

4.1 Introduction

The voltage collapse simulation model established in the previous chapter can be used as a tool for development of monitoring techniques. Before an attempt is made to define a voltage stability monitoring system, a class of instabilities to be monitored should be defined. As was shown in Chapter 2, voltage instabilities may occur in a system with, or without sudden changes of network topology (line outages, loss of generation etc.) When voltage instability is triggered, or accompanied by topological changes, it is also likely that some transients would occur in short time intervals characteristic of the transient stability problems. Very sophisticated monitoring systems of today's technology may be hard pressed to track the system trajectories during transients of such a short duration. If, how-

ever, voltage instability is due to changes of power system parameters (loading) without topological changes in the network, or if the topological changes cause the system to settle in steady states which are dangerously close to voltage or steady state stability boundary, modern real-time monitoring systems can be designed to detect such states and set alarms and/or trigger systemwide control actions.

The purpose of this chapter is to propose an efficient use of one such monitoring system, real-time phasor measurement system which is currently being developed at Virginia Tech. The system is modular and distributed around a host computer, which may be chosen as a workstation, or a minicomputer, depending upon the size of the network. Each measurement site consists of the measurement microcomputer based on a fast 32-bit microprocessor with a coprocessor. The measurement microcomputer may be connected to a personal computer, or graphics terminal to allow local display of measurement data, if this is desired. It can also be connected to the host computer through a fast serial communication channel. The synchronization is achieved with GPS satellite receivers which provide the triggering pulses for data acquisition with an accuracy of 100 nanoseconds. Since GPS time dissemination service was recently made available to non-military users nationwide, synchronization problems, which are very important in phase angle measurements, were resolved by using their time pulses. Even if a deterioration of accuracy of one order of magnitude exists due to propagation of GPS signals through antenna cables, the accuracy of measurements (1 microsecond) corre-

sponds to the accuracy of phase angles to within 0.0216 degrees for a 60 Hz wave, which is more than enough for power system state monitoring.

Figure 35 symbolically shows the disposition of the phasor measurement system in a small 3 bus network. Figure 36 shows the structure of the measurement computer. Up to 16 analog signals (voltages and/or currents) may be brought to the signal conditioner, which transforms them to voltage signals with a $\pm 10V$ range and the output of the sample and hold circuits is directly connected to the A/D board which is one of the three modules of the measurement computer linked by a VME bus (A/D, CPU and communication boards). A/D board accepts 720 Hz pulses from the GPS satellite receiver and triggers A/D conversions on all input channels in sequence. Conversions are interrupt driven and as soon as one is completed, an interrupt service routine places the result in CPU memory. When all the conversions in the scan are completed, the CPU performs Discrete Fourier Transform calculation on the waveforms stored in memory (time window is equal to one cycle, or 12 data samples per signal). The final result is the positive sequence voltage, or current phasor. Tables of phasors associated with exact time stamps are stored in CPU RAM (1 MB) and sent to the host computer on request. They are also periodically sent to the local display (personal computer) to update its graphic presentation of the measured phasor several times per second. The exact time stamp is sent from GPS receiver to the communication module via serial communication channel and further to the CPU via VME bus. The CPU is connected via two serial communication channels to the debug terminal and another computer with permanent magnetic storage medium

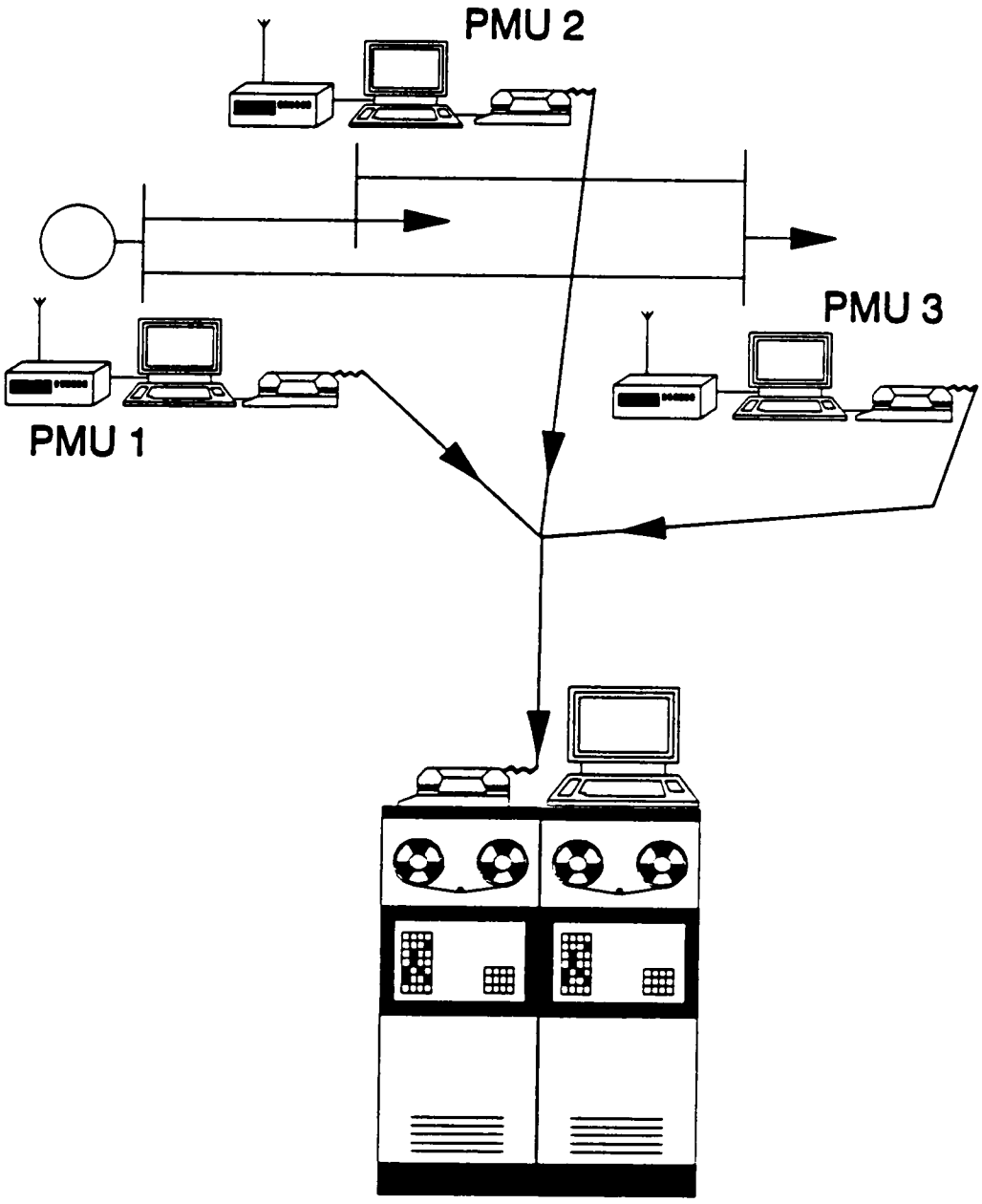

Figure 35. Phasor measurement system.

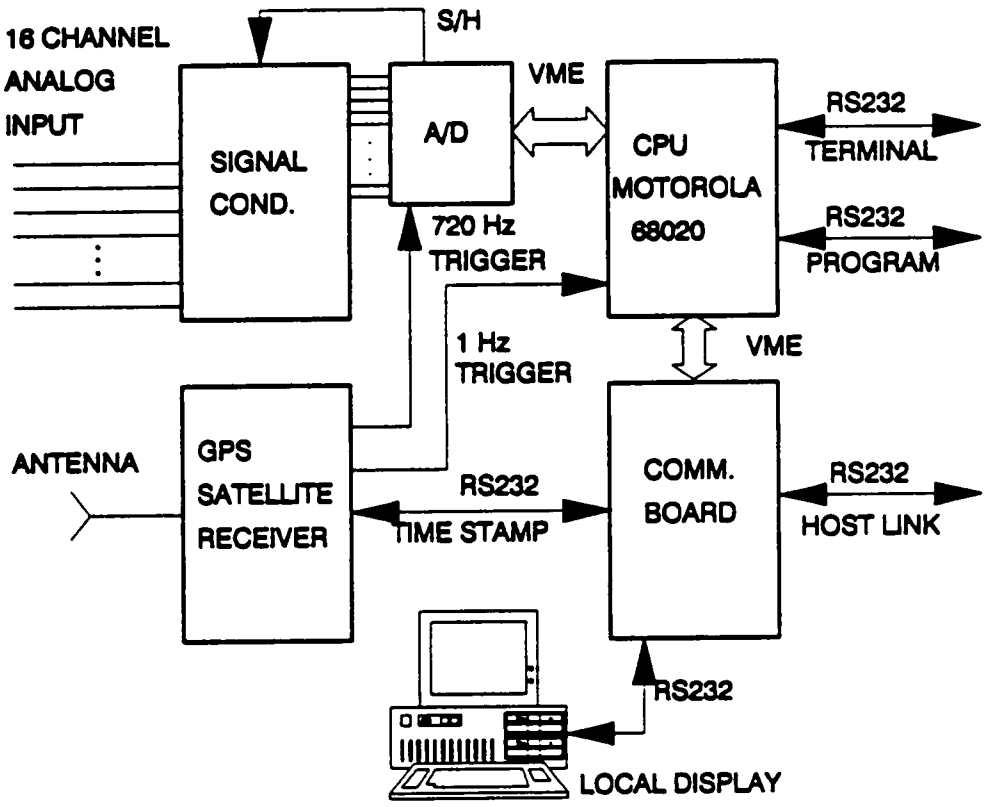

Figure 36. Functional diagram of the measurement microcomputer.

and cross- assembler for code development. These two communication links are not necessary when the system is installed in the field and no further changes of code are required. The communication module is connected with the remote host computer through a high speed serial communication channel, through which the host computer may initiate a number of actions in the measurement computer and receive data from it. The CPU has less then 1400 microseconds to perform A/D conversions, DFT, check for any alarms caused by sudden changes of the system state and handle the communication. Those tasks are arranged in multiple priorities whose execution is governed by the occurrence of the appropriate interrupt requests to the CPU. As a by-product of the phasor calculation, the system also calculates local network frequency and the rate of change of frequency and stores them in tables along with the phasors.

The host computer collects data from all the measurement sites. When the set of phasors is known from all the system buses, the host has complete information about the system state. Since the state is locally updated at the rate of 720 Hz, that is the theoretical upper limit for the rate of updates of system state at the host computer. The constraint is the speed of serial communication channels and finite time that measurement CPUs have available for communication with host (using recent 20 MHz microprocessors, the time allocated for communication is approximately 65 percent of the total time, i.e. in every second, 0.65 seconds are spent on the communication with the local display computer and the host). At 9600 baud rate of the host communication channel, the updates of system state are possible approximately every five cycles (83.3 miliseconds). Considering that

host computer has a very intensive communication burden collecting data from all measurement sites, the actual state processing rate may be even lower. Depending on the speed of the host and the processing task that it is supposed to accomplish in addition to communication with remote measurement computers, one can assess a realistic rate for periodical state and monitoring function updates that the host will perform.

The discussion in the previous chapter of the voltage instability phenomena resulted in proposition to use minimum singular value of the system Jacobian matrix and generated reactive powers as indicators of the stability margin. Since only one, the minimum singular value, is needed, it is not necessary to perform the whole singular value decomposition to obtain that information. Some of the simpler iterative numerical techniques, such as the inverse power method [179], may be used instead. This is even more so because the results of the calculations of the previous state are likely to be close to the updates (if the system does not experience topological changes). The calculation of the generated reactive powers is even more straightforward since it involves just the simple manipulation of the voltage and current phasors received from generator terminal buses. It is not unreasonable to predict that a medium sized workstation would handle the task of system state updates in a fraction of a second (0.1 to 1 second) when processing the data of the system similar to the 39-bus system used for simulations in the previous chapter. For larger systems, higher capacity host computers should be used and coupling with data concentrators would be advisable to relieve part of the communication burden from a host. There is an incentive, however, to reduce

the number of measurements acquired by the host and process the update based on incomplete system state data. The idea is based on the assumption that it is possible to identify groups of load buses in the system which are coherent with respect to voltage dynamics. If such groups exist, it would be possible to acquire measurements from a smaller number of representative members of the group and estimate the information about the rest of the group from acquired data. This chapter contains proposals for a criterion which may be used to find coherent groups of load buses (clusters) and an algorithm for determination of clusters based on the known coherency criterion. The theoretical framework will be illustrated by a number of examples obtained by simulation on the same 39-bus system model used for the simulations of voltage instability.

4.2 Clustering of load buses in power systems

The power system model of equation (3.4.8) is used in this discussion, where nonlinear power balance equations are defined as in (3.3.6). The linearization of the system $F = [f_p\ g_p\ g_q]^T$ around an equilibrium point gives

$$\begin{bmatrix} D_\delta f_p & D_\theta f_p & D_V f_p \\ D_\delta g_p & D_\theta g_p & D_V g_p \\ D_\delta g_q & D_\theta g_q & D_V g_q \end{bmatrix} \begin{bmatrix} d\delta \\ d\theta \\ dV \end{bmatrix} = \begin{bmatrix} J_1 & J_2 \\ J_3 & J_4 \end{bmatrix} \begin{bmatrix} d\xi \\ dV \end{bmatrix} \tag{4.2.1}$$

where $d\xi = [d\delta\ d\theta]^T$ is the vector of generator and load bus phase angles as in (3.4.12- 13). The condition for voltage instability is

$$\det\{J\} = \det\{J_1\}\ \det\{J_4 - J_3 J_1^{-1} J_2\} = 0 \tag{4.2.2}$$

The proximity of the system state to voltage instability may be assessed by tracking minimum singular values of J_1 and J and checking that none of them is singular. The singularity of J while J_1 is nonsingular is a condition for voltage instability type of static bifurcation. Obviously, to be able to recalculate Jacobian matrix fast, we need updated values for $[\delta\ \theta\ V\ E]^T$ as fast as possible (E is a vector of voltage magnitudes at generator terminal buses). We will investigate the possibility to acquire $[\delta\ \hat{\theta}\ \hat{V}\ E]^T$ where $\hat{\delta} \subset \delta$ and $\hat{V} \subset V$ and to attempt to reconstruct Jacobian from that partial information.

Let the set

$$W = \{1\ ,2\ ,\ldots\ ,m\} \tag{4.2.3}$$

be a set of load buses of the power system. A coherency relation C in the set W is defined as

$$C = \{(i,j) \mid \mu(i,j,\delta,\theta,V,E,\lambda) \leq \varepsilon\} \tag{4.2.4}$$

The function μ: $W^2 \times R^{2(n+m)+p} \rightarrow R^k$ is the criterion function, while $\varepsilon \in R^k$ is a set of prespecified thresholds. Function μ should be understood as a numeric relationship between load buses i and j which determines the existence of coherency

whenever vector valued function μ assumes values smaller than predefined set of thresholds ε. Function μ is symmetric

$$(\forall i \in W)(\forall j \in W) \Rightarrow \mu(i,j,\delta,\theta,V,\lambda) = \mu(j,i,\delta,\theta,V,\lambda) \qquad (4.2.4a)$$

Although very broadly defined in (4.2.4), coherency relation allows us to construct the coherency graph as ordered couple $G^1 = (C,W)$. Coherency graph G^1 is undirected and not necessarily connected on the set of load buses. Its form depends on the choice of the coherency relation (function μ). We can establish, however, the algorithm for determination of coherent clusters of load buses based on any assumed coherency relation C.

i) Initialize the counter $i := 1$

$$\begin{aligned} W &= W_1 \\ C &= C_1 \\ G^1 &= (W_1, C_1) \end{aligned} \qquad (4.2.5)$$

Increment the counter $i := i + 1$.

ii) Find the graph

$$G^i = (W_i, C_i) \subset G^1 - \bigcup_{k=2}^{i-1} G^k \qquad (4.2.6)$$

where

$$W_i \subset W - \bigcup_{k=1}^{i-1} W_k$$
$$C_i \subset C - \bigcup_{k=1}^{i-1} C_k \qquad (4.2.7)$$

such that G^i is the largest complete graph (clique) contained in

$$G_0^i = G^1 - \bigcup_{k=2}^{i-1} G^k \qquad (4.2.8)$$

Therefore, graph G^i has the property

$$(\forall i \in \{2,3, \ldots\})(\forall j \in W_i)(\forall k \in W_i) \Rightarrow (j,k) \in C_i \qquad (4.2.9)$$

iii) If the graph $G_o^{i+1} \neq \emptyset$, go to step (ii); else: stop.

If the algorithm was stopped after q steps, then the sets W_i , $i = 2,\ldots,q$

$$W_2 \cup W_3 \cup \cdots \cup W_q = \bigcup_{k=2}^{q} W_k = W_1 \qquad (4.2.10)$$

represent coherent clusters in W_1 . The clique problem is well known in graph theory [176]. It is NP-complete, which translates into being solvable in time polynomial to the size of the problem on a nondeterministic computer. Additional information about Turing model may be found in [176], where this problem is

analyzed. As far as voltage stability monitoring application is concerned, the inefficiency of the known clique algorithms does not represent a major obstacle, for cluster determination is accomplished off-line without concerns about computation time. It should be noted, however, that step (ii) of the algorithm can only be done by exhaustive search, which can be time consuming for the large scale systems (there are C_k^n subsets of cardinality k to be checked in a system with n nodes in a search for the clique of the order k . Some guidelines for practical faster computations are presented later in the text. Figure 37 shows a graph with 20 nodes subjected to a clustering process. The cliques 1 , 2 , ... , 5 are found in respective order of their numbers and are shown within areas closed by dashed lines. Thicker branches represent intracluster coherent pairs while thinner ones represent intercluster coherent pairs of nodes.

Once the clusters W_2 , ... , W_q are determined, a measurement system is formed by choosing one representative measurement from each cluster

$$j_2 \in W_2 \ , \ \dots \ , \ j_q \in W_q \tag{4.2.11}$$

The choice of locations j_2 , ... , j_q is arbitrary and depends on the desired application. For the purposes of voltage stability monitoring, it is good to choose the representative measurement so that it produces the least error in assessment of the proximity indicators, or at least that the error produced be conservative. However, such an effect cannot be guaranteed, since the sensitivities of the minimum singular values of Jacobian vs. errors in state vector are not easily calcula-

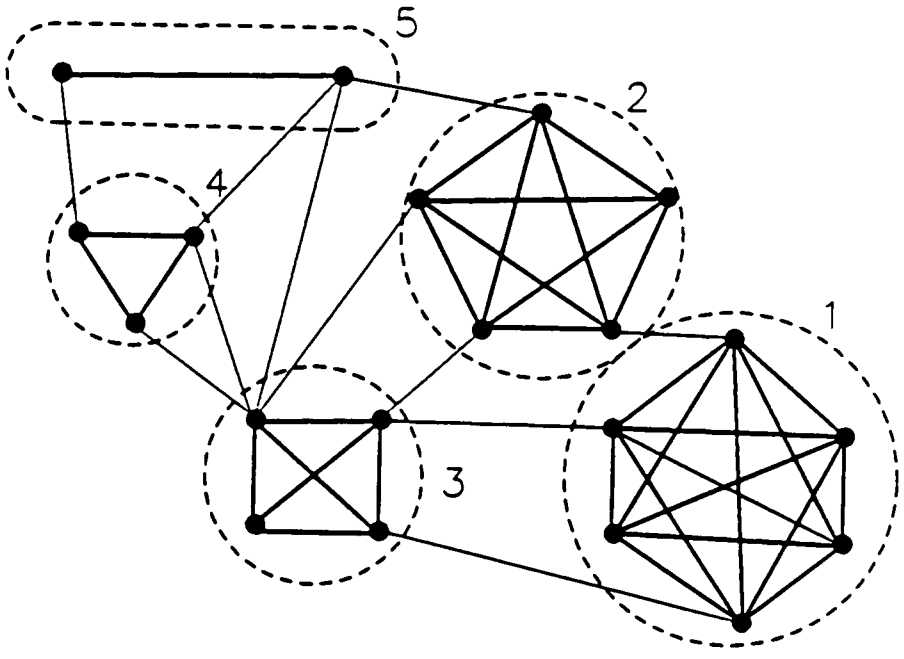

Figure 37. An example of clustering on a graph with 20 nodes.

ble. One intuitively good choice is to take as representative measurements those buses which have the largest voltage sensitivities with respect to uniform loading of the system. Such loading was shown to induce voltage instability in the system and those buses whose voltages are falling at a faster rate are vulnerable points in the system. When measurement sites are known, the measurement system is complete and the approximate state vector may be calculated with the assumption

$$(\forall k \in \{2,3,\ldots,q\})(\forall i \in W_k)(\forall j \in W_k) \Rightarrow (V_i \angle \theta_i = V_j \angle \theta_j) \qquad (4.2.12)$$

that all the voltage phasors in one measurement cluster are equal. This assumption may at first appear gross, but is indeed bounded by the choice of the coherency relation. If very tight tolerances are required, the threshold vector ε in (4.2.4) will be chosen close to zero vector and effects of the errors will be reduced. The choices of coherency criteria will be discussed later.

The assumption (4.2.12) produces an error in assessment of the state vector

$$\hat{x} = \begin{bmatrix} \delta \\ \hat{\theta} \\ \hat{V} \\ E \end{bmatrix} = \begin{bmatrix} \delta \\ \theta \\ V \\ E \end{bmatrix} + \begin{bmatrix} 0 \\ \Delta\varepsilon_1 \\ \Delta\varepsilon_2 \\ 0 \end{bmatrix} = x + \Delta x \qquad (4.2.13)$$

The error is due to the fact that $2(n+m)$ measurements from n generator and m load buses are approximated from $2(n+q-1) \leq 2(n+m)$ measurements ob-

tained from all the generator buses and representative measurements from clusters. Vectors $\Delta\varepsilon_1$ and $\Delta\varepsilon_2$ have zero components only at $q-1$ elements corresponding to representative measurements of $q-1$ clusters. The Jacobian matrix may be linearized around its correct value for a given state x

$$J(\hat{x}) = J(x) + D_\delta J\,\Delta\varepsilon_1 + D_\theta J\,\Delta\varepsilon_2 \tag{4.2.14}$$

The upper bound on the norm of error of $J(\hat{x})$ can be established as

$$\|J(x) - J(\hat{x})\| \leq \|D_\delta J\|\,\|\Delta\varepsilon_1\| + \|D_V J\|\,\|\Delta\varepsilon_2\| \tag{4.2.15}$$

where $D_\delta J$ and $D_V J$ represent the sensitivity arrays of the Jacobian with respect to changes of δ and θ . An upper bound norm may be established which would estimate the error of the approximation, but such a calculation would be of limited use in the critical region where the system Jacobians are near singular, and that is exactly where we are mostly concerned about the performance of the monitoring algorithm. It is much more useful to assess the accuracy of the approximation using numerical simulations of the system operating states near the stability boundary.

For such an analysis, concrete coherency criteria are needed. Two of them, which represent the initial effort to quantify coherency properties of the power system load buses, will be presented in the following text.

4.2.1 Coherency Criterion 1: Sensitivity Analysis

Let us assume that the power system is in a steady state defined by $[\delta\ \theta\ V\ E]^T$ with a Jacobian matrix $J = J(\delta, \theta, V, E)$. The vector of phase angles is $[\Delta\xi] = [\Delta\delta\ \Delta\theta]^T$. If the system state changes due to the change of one, or more of the loads, the relationship between the changing system state elements and change of loading can be expressed using the inverse of Jacobian

$$\begin{bmatrix} \Delta\delta \\ \Delta\theta \\ \Delta V \end{bmatrix} = \begin{bmatrix} \partial\delta/\partial P_g & \partial\delta/\partial P_l & \partial\delta/\partial Q_l \\ \partial\theta/\partial P_g & \partial\theta/\partial P_l & \partial\theta/\partial Q_l \\ \partial V/\partial P_g & \partial V/\partial P_l & \partial V/\partial Q_l \end{bmatrix} \begin{bmatrix} \Delta P_g \\ \Delta P_l \\ \Delta Q_l \end{bmatrix} \tag{4.2.16}$$

or

$$\begin{bmatrix} \Delta\xi \\ \Delta V \end{bmatrix} = \begin{bmatrix} A_1 & A_2 \\ B_1 & B_2 \end{bmatrix} \begin{bmatrix} \Delta P \\ \Delta Q \end{bmatrix} = \begin{bmatrix} A \\ B \end{bmatrix} [\Delta\psi] \tag{4.2.17}$$

Vectors P_g, P_l and Q_l represent generator active powers and load active and reactive powers respectively. Vector $\Delta P = [\Delta P_g\ \Delta P_l]^T$ represents the disturbance of the active powers. Matrix B is the sensitivity matrix of voltage magnitudes at load buses with respect to any changes of loading and/or redistribution of generation. Let r_i be $i-th$ row of the matrix B . The coherency condition may be defined as follows

$$(\forall k \in \{2,3,\ldots,q\})(\forall i \in W_k)(\forall j \in W_k)(\forall \Delta\psi \in B(\rho)) => \\ => (\|\Delta V_i - \Delta V_j\| < \varepsilon) \tag{4.2.18}$$

where $B(\rho) \subset R^{n+2m}$ represents the sphere with diameter ρ and center in $[\delta\ \theta\ V\ E]^T$. The claim expressed in (4.2.18) is that for a class of bounded disturbances $\Delta\psi$ around the operating point, the voltage changes within clusters should remain bounded. This is equivalent to the claim

$$0 \leq \| (r_i - r_j)\Delta\psi \| \leq \varepsilon \tag{4.2.19}$$

The last result is satisfied if $r_i - r_j$ is othogonal to $\Delta\psi$, which clearly is not possible for all $\Delta\psi$ within $B(\rho)$. If, however, r_i and r_j are close to being equal in the space spanned by rows of B, then (4.2.19) will be always satisfied. Obviously, we cannot expect them to be equal because the inverse of Jacobian would be singular in that case. We can formulate the coherency requirement as a condition for vectors r_i and r_j to have angular differences and magnitudes within prespecified tolerance limits

$$\mu(i,j) = \mu(j,i) = \begin{bmatrix} \mu_1 \\ \mu_2 \end{bmatrix} = \begin{bmatrix} 1 - \dfrac{< r_i, r_j >}{\|r_i\| \, \|r_j\|} \\ \|r_i - r_j\| \end{bmatrix} \leq \begin{bmatrix} \varepsilon_1 \\ \varepsilon_2 \end{bmatrix} = \varepsilon \tag{4.2.20}$$

where $< r_i, r_j >$ is the vector inner product in R^{n+2m}. The coherency graph may then be formed using (4.2.3-4). The coherency criterion (4.2.20) is established using sensitivity analysis in only one operating state. One might wonder whether such a loose condition may preserve enough accuracy throughout the system

loading patterns to stability boundary. It appears that although the power system is nonlinear, coherency relationship among load buses is well preserved as the system loading level increases and its Jacobian matrix becomes closer to singular (its rows become more parallel). The simulation results which will be presented in the next section will confirm this.

Another concern may be the preservation of the coherency under a certain class of contingencies (i.e. line outages). The condition (4.2.20) does not guarantee coherency to any system whose topology is different from the studied one. That requires a number of coherency relations $C^1, C^2, \ldots, C^p$ to be established using (4.2.20) for different network topologies representing different contingencies in the system which we want to incorporate into our study. The resulting coherency relation should then be the intersection of the coherency relations corresponding to cases $1,2,\ldots,p$

$$C = C^1 \cap C^2 \cap \cdots \cap C^p = \bigcap_{k=1}^{p} C^k \tag{4.2.21}$$

Subsequent calculations for cluster determination are the same as for the case when only one operating state (or network topology) is considered. It is to be expected, however, that a restrictive condition such as (4.2.21) would significantly reduce the size of clusters and diminish the effects of clustering. A coherency measure which falls between contradictory requirements for reduction of the

number of measurements and accuracy of the monitoring functions should be reached by compromise in every particular application case.

4.2.2 Coherency Criterion 2: Dynamic Analysis

Another approach to definition of the coherency may be by using simulation data of power system time response to a disturbance. Disturbance is again modeled as a change of loading. Let us assume that the system loads are modeled as constant complex power loads corrupted with a small amount of Gaussian noise

$$\begin{aligned} P_i &= P_{i0}[1 + \beta N(0,1)] \\ Q_i &= Q_{i0}[1 + \beta N(0,1)] \end{aligned} \tag{4.2.22}$$

Generator active power outputs are constant. Constant β , which is a multiplier for Gaussian noise with zero mean and unit standard deviation, is chosen to be relatively small (of the order of 0.1 %) . If the system is then subjected to a dynamic simulation using the algorithm shown in previous chapter for voltage stability simulations, the voltage time responses on load buses (sampled at equal time intervals Δt over N sampling intervals) may be represented as vectors

$$V'_i = [V_i(\Delta t)\ V_i(2\Delta t) \ldots V_i(N\Delta t)]^T \tag{4.2.23}$$

from which a vector of voltage response deviations from its average value over the same interval may be derived as

$$V_i = V'_i - \hat{V}_i = \\ = [V_i(\Delta t) - \hat{V}^i \ \ldots \ V(N\Delta t) - \hat{V}^i]^T \tag{4.2.24}$$

where

$$\hat{V}^i = \sum_{i=1}^{N} \frac{V_i(i\Delta t)}{N} \qquad \hat{V}_i = [\hat{V}^i \ldots \hat{V}^i]^T \tag{4.2.25}$$

The typical output of such a simulation is shown in Figure 38.

The coherency between time responses V_i may be established by analyzing the following relationship between them

$$\mu = \frac{\| V_i - V_j \|}{\| V_i \| \| V_j \|} \leq \varepsilon \tag{4.2.26}$$

If the amount of Gaussian noise added to the loads, and the threshold ε are varying, a number of coherency relations may be established resulting in a range of coherent groups, from trivial clusters (one node in each) to impractically big clusters whose application would not give satisfactory results in monitoring. The choices which can be used in practice are presented in the next section.

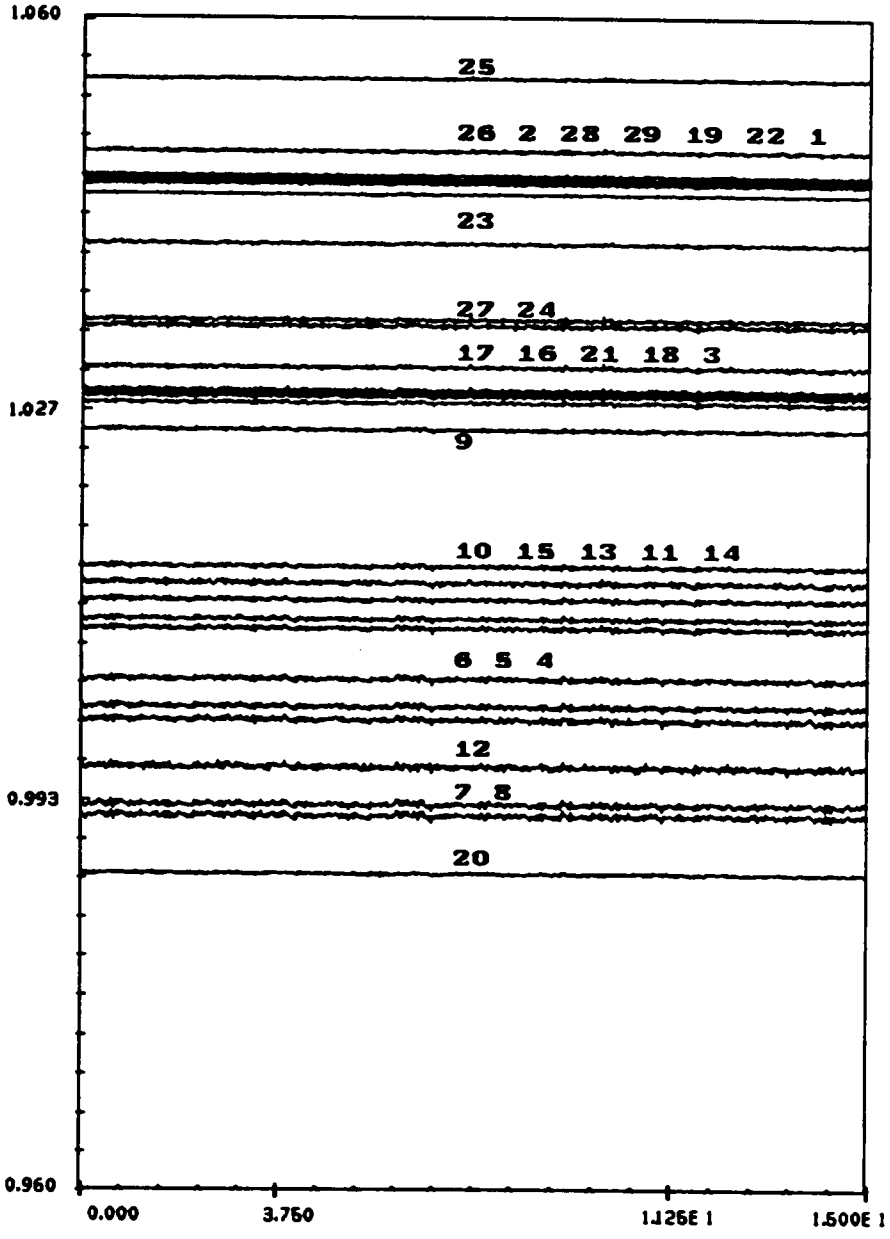

Figure 38. Voltage response on load buses with 0.1% noise on system loads.

4.2.3 Guidelines for Application

When the above described algorithm is applied to a particular power system, some caution should be exercised to avoid the possibility that calculated clusters become too small, or too big, resulting in the loss of monitoring effectiveness, or accuracy respectively. Some trial and error is necessary to establish the necessary and sufficient degree of coupling between load buses which would provide satisfactory execution of the monitoring function(s). Some shortcuts and hints may prove valuable in reducing the computation time needed to calculate clusters which may be substantial in cases of larger power systems.

When using the cohernecy criterion 1, it is useful to represent both coherency criteria (μ_1 and μ_2 from (4.2.20)) by square matrices. Before applying thresholds, coherency related parameters may be arranged as follows

$$M_1 = \begin{bmatrix} \mu_1(1,1) & \mu_1(2,1) & \dots & \mu_1(m,1) \\ \mu_1(2,1) & \mu_1(2,2) & \dots & \mu_1(m,2) \\ \dots & \dots & \dots & \dots \\ \mu_1(m,1) & \mu_1(m,1) & \dots & \mu_1(m,m) \end{bmatrix} \tag{4.2.27}$$

$$M_2 = \begin{bmatrix} \mu_2(1,1) & \mu_2(2,1) & \dots & \mu_2(m,1) \\ \mu_2(2,1) & \mu_2(2,2) & \dots & \mu_2(m,2) \\ \dots & \dots & \dots & \dots \\ \mu_2(m,1) & \mu_2(m,1) & \dots & \mu_2(m,m) \end{bmatrix} \tag{4.2.28}$$

For the purposes of our calculation, only upper, or lower triangular parts of matrices M_1 and M_2 need to be considered because of the symmetry of μ . Figure 39 shows matrix M_1 for the 39-bus power system from Figure 5. Matrices shown correspond to four different load factors (3.5.2) and their integer elements m_{ij} should be interpreted as follows (r_i and r_j are rows of matrix B in (4.2.17))

$$m_{ij} = k \ <=> \ \frac{k}{10} \leq \frac{< r_i, r_j >}{\|r_i\| \, \|r_j\|} < \frac{k+1}{10} \qquad (4.2.29)$$

It can be noticed how the degree of angular coupling expressed by $\mu_1(\,)$ is increasing as the loading level increases. Figure 39 gives indication of the values of ε_1 that could be used with criterion 1. Similar analysis can be done on matrices M_2 to check the magnitudes of rows of B in (4.2.17). Results suggest that the magnitudes are less sensitive to changes of loading than angular coupling, but they require looser tolerance conditions due to large magnitude differences between individual rows. It is reasonable from the above to attempt to construct the coherency relation by linearization in the normal operating state, where the degree of angular coupling among rows of B is the smallest and to perform simulations on clusters obtained that way with various loading patterns which move the system close to voltage stability boundary and various tolerance levels ε . To determine coherency relation from M_1 and M_2 when tolerances ε_1 and ε_2 are known, matrices $\hat{M}_1 = [\hat{m}^1_{i,j}]_{m,m}$ and $\hat{M}_2 = [\hat{m}^2_{i,j}]_{m,m}$ may be constructed

$$\hat{m}^k_{i,j} = \left\{ \begin{array}{l} 1 \ , \ if \ \mu_k(i,j) < \varepsilon_1 \\ \\ 0 \ , \ if \ \mu_k(i,j) \geq \varepsilon_1 \end{array} \right\} \ k = 1,2 \qquad (4.2.30)$$

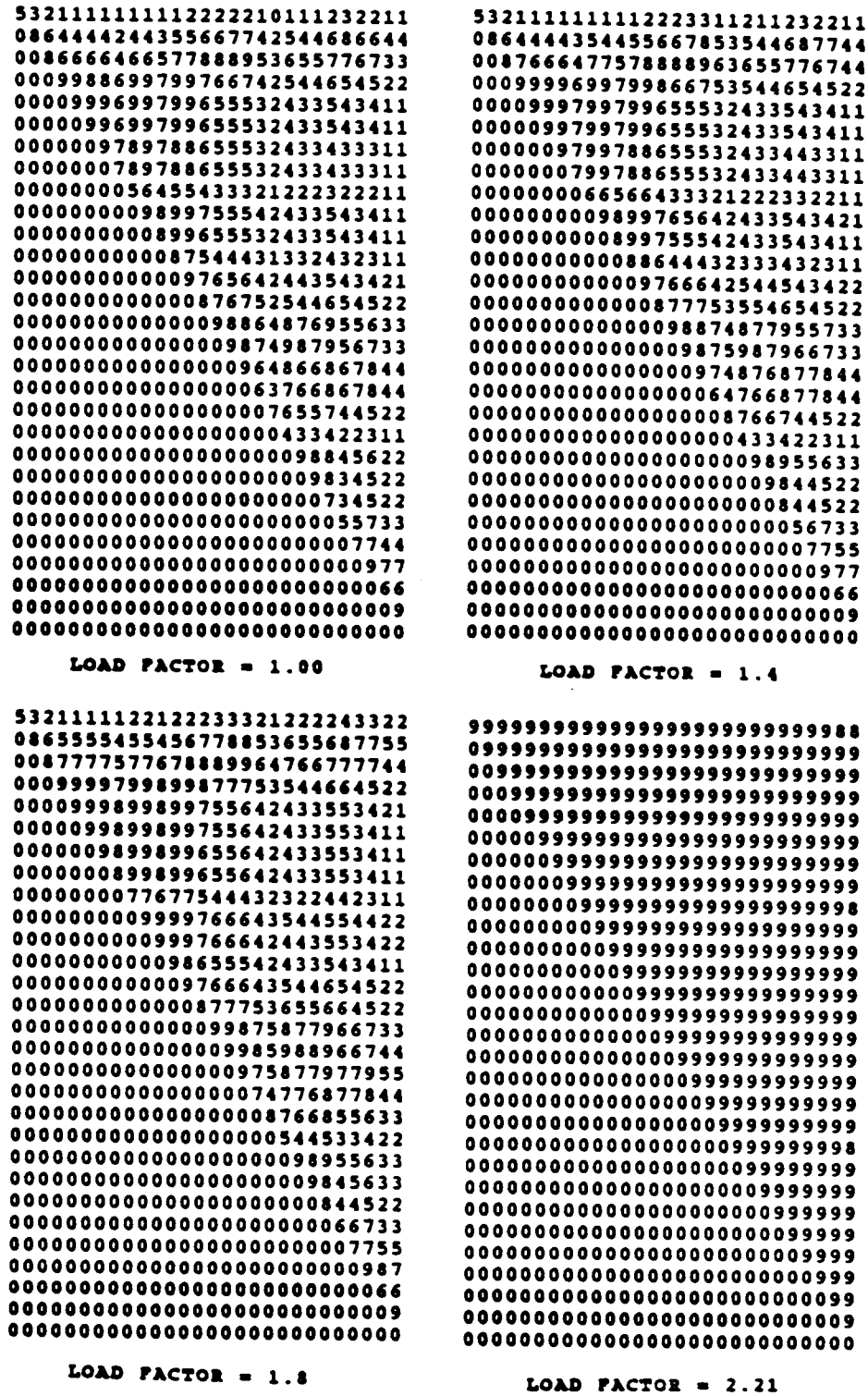

Figure 39. Coherency matrices for system from Figure 5 (M_1) .

The analysis of

$$M = [\hat{m}^1_{i,j} \wedge \hat{m}^2_{i,j}]_{m,m} = [m_{i,j}]_{m,m} \tag{4.2.31}$$

where $\wedge$ is the logical 'and' operator (applied to every pair of matrix elements separately), will determine the final coherency relation M . Matrix M has a property that its element $m_{i,j}$ is equal to 1, if and only if buses i and j are coherent with respect to μ and ε . The number of nonzero entries in the i-th row represents the number of buses that bus i is coherent with. Obviously, for clique of the order k to exist, there must be at least k rows (columns) with at least k nonzero entries and if k_{max} is the maximum number of nonzero entries in any row, or column of M then there are no cliques of the order greater then k_{max} . The clustering proces may be visualized as a sequence of simultaneous interchanges of rows and corresponding columns (rows i and j and columns i and j interchange places in one step) in order to transform matrix M into the most block diagonal form possible. At the end, the nonzero blocks on the main diagonal of M represent clusters while nonzero entries outside those blocks represent intercluster coherency links which are disregarded. If a case is encountered when calculated clusters contain nodes which are not physically connected in the system, then such clusters should be split into smaller ones which do not have such a property. If the coherency criterion is properly designed, such situations are not likely to occur.

4.3 Simulation Results

A brief overview of simulation results will be presented in this section. Several clustering cases were investigated and their performance with respect to the calculation of approximate minimum singular value of Jacobian investigated.

Figure 40 shows the clusters calculated on a 39-bus test system using coherency criterion 1 with tolerance levels

$$\begin{bmatrix} \varepsilon_1 \\ \varepsilon_2 \end{bmatrix} = \begin{bmatrix} 0.05 \\ 0.25 \end{bmatrix} \tag{4.3.1}$$

Those values mean that normalized vector inner products in the space spanned by rows of matrix B (4.2.17) should exceed 0.95 if calculated between two members of any cluster, while simultaneously their magnitudes should not be different by more then 0.25. In three-dimensional space, the angular tolerance would correspond to the angle of 18.2 degrees. Such constraints have produced 5 nontrivial clusters (with more than one node in each) with a reduction of the number of measurements of 8 (out of 39), or savings of over 20% in the installation costs of the monitoring system. Similarely, Figures 41 and 42 show clusters obtained for tolerances

$$\begin{bmatrix} \varepsilon_1 \\ \varepsilon_2 \end{bmatrix} = \begin{bmatrix} 0.12 \\ 0.25 \end{bmatrix} \tag{4.3.2}$$

and

$$\begin{bmatrix} \varepsilon_1 \\ \varepsilon_2 \end{bmatrix} = \begin{bmatrix} 0.20 \\ 0.25 \end{bmatrix} \tag{4.3.3}$$

respectively, which correspond to normalized inner products of 0.88 (28.4 degrees in three-dimensional space) and 0.80 (36.9 degrees in three-dimensional space) while magnitude tolerance is kept constant at 0.25. The reduction of the number of measurements obtained in cases (4.3.2) and (4.3.3) is 12 and 16 out of 39, which represents installation cost savings of 31% (41% for (4.3.3)). Figure 43 shows the minimum singular values of exact Jacobian obtained by full phasor measurement set, and approximate Jacobians obtained with reduced measurement sets with representative measurements in each cluster placed at the nodes having highest voltage sensitivities. The uniform loading pattern (3.5.2) was used to move the system close to stability boundary where voltage instability was proven to exist using dynamic simulations. It is remarkable how close are approximate and exact minimum singular values are in case (4.3.1) where 20% of the measurements are approximated. Even in cases (4.3.2) and (4.3.3) where 31% and 41% of the measurements were approximated, results obtained are very satisfactory. The final determination of the extent of measurement reduction would be made by a compromise between available resources and desired accuracy in every particular application case.

Figure 44 shows the clustering algorithm performance in the same circumstances as in Figure 43, except that minimum eigenvalues were calculated instead of

minimum singular values of Jacobian. The curves obtained show very similar patterns and even better matching in the critical zone when Jacobians are near singular. The reason for it is that eigenvalues are not constrained to be positive and change sign when Jacobian becomes singular. Those eigenvalues shown negative in Figure 44 correspond to approximate Jacobians since such cases could not produce convergent load flows in the case of exact Jacobian. The disadvantage of using eigenvalues as stability margin indicators is, among other things, that in certain cases they may be complex numbers and more difficult to calculate in a real-time environment.

Figure 45 shows the result of the clustering process when all possible line outages (except those which would also represent generator outages) were taken into account using the above described variation of coherency criterion 1 (4.2.21). The tolerances used were $\varepsilon_1 = \varepsilon_2 = 0.25$. Only one cluster was obtained as a result of that calculation with a reduction of only three measurements (7.7%). This result shows another important property of the 39-bus test system: the same load buses which were found among the most vulnerable in all simulated voltage instability cases were also found to be the most voltage coherent. Their voltage coherency persists under almost all possible changes of network topology at the same loading level.

Figure 46 shows the dependence of accurate and approximate minimum singular values of Jacobian for uniform loading (3.5.2). As expected from the situation when just a few measurements are missing, the agreement between the calculated

values is remarkable: of the order of a few percent throughout the loading range. Figure 47 represents the same monitoring situation for a different loading pattern (only reactive power requirements are increasing proportionnally with the value of the load factor). That loading pattern was also shown to induce voltage instability in previous simulations. Once again, the agreement between the exact and approximate minimum singular values is very good. This suggests that the loading pattern does not influence significantly the performance of the algorithm.

Figures 48, 49 and 50 represent the same clustering situation under uniform loading and the system subjected to outages of lines between buses 4 and 5, 13 and 14; and 4 and 14 respectively. In all three cases the differences between exact and approximate values are very small.

Figure 51 shows the clusters of the 39-bus system calculated for all the possible line outages except six (lines (4,5), (4,14), (6,11), (10,11), (10,13) and (13,14)). It should be noted that line (6,11) is actually a transformer. One (but larger) cluster was obtained with a reduction of 8 measurements (20%) using the tolerance $\varepsilon_1 = \varepsilon_2 = 0.30$. Figure 52 shows the relationship between exact and approximate singular values of Jacobian for such a case.

Figure 53 shows the clusters and algorithm performance under unifrom loading using the criterion 2 with the tolerance level $\varepsilon = 0.15$. There are 4 clusters and a reduction of 12 measurements (31%) is achieved. Minimum singular values are very close to each other throughout the loading range. Figure 54 shows the algo-

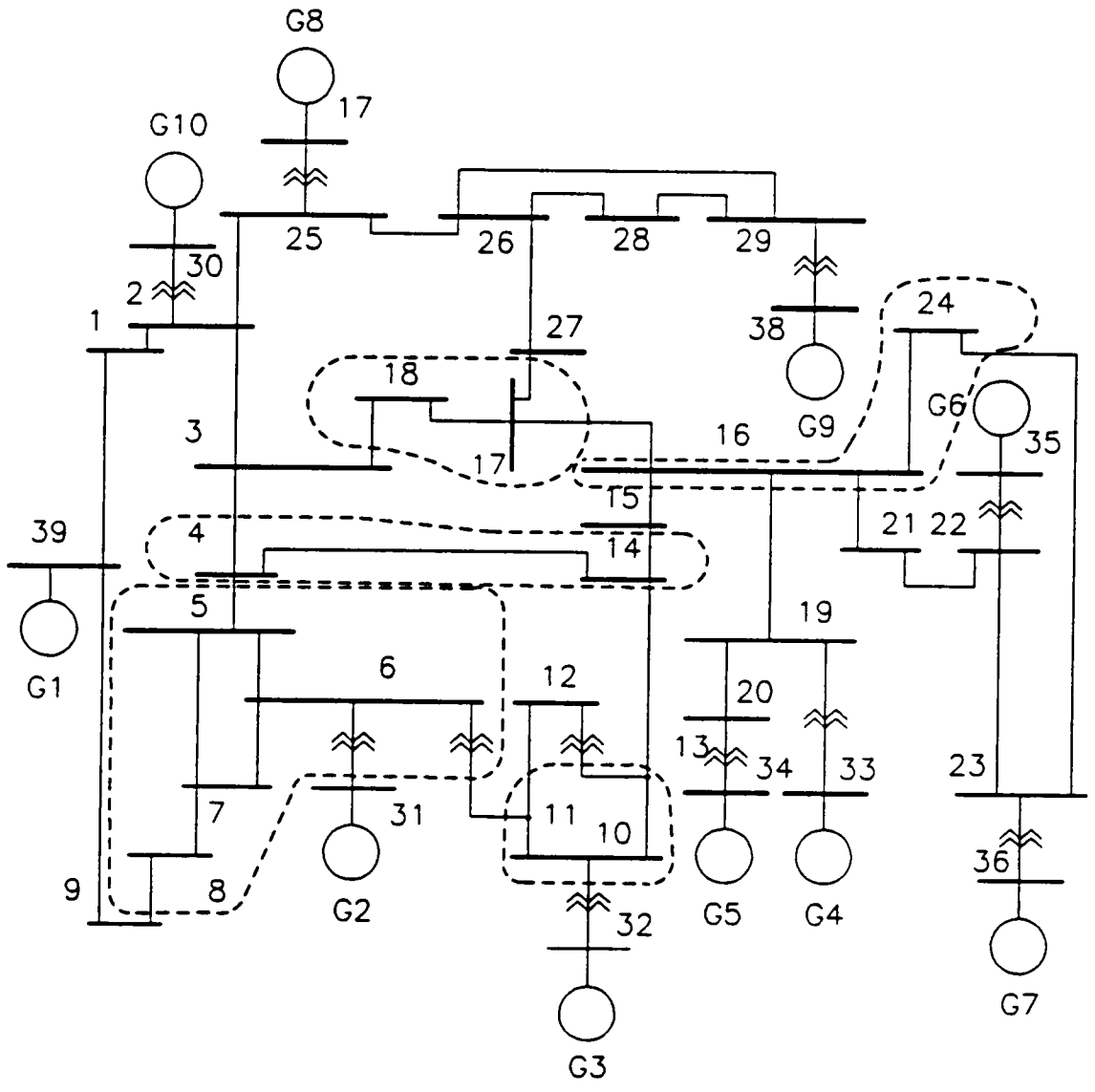

Figure 40. **Clustering using criterion 1:** $\varepsilon_1 = 0.05, \varepsilon_2 = 0.25$.

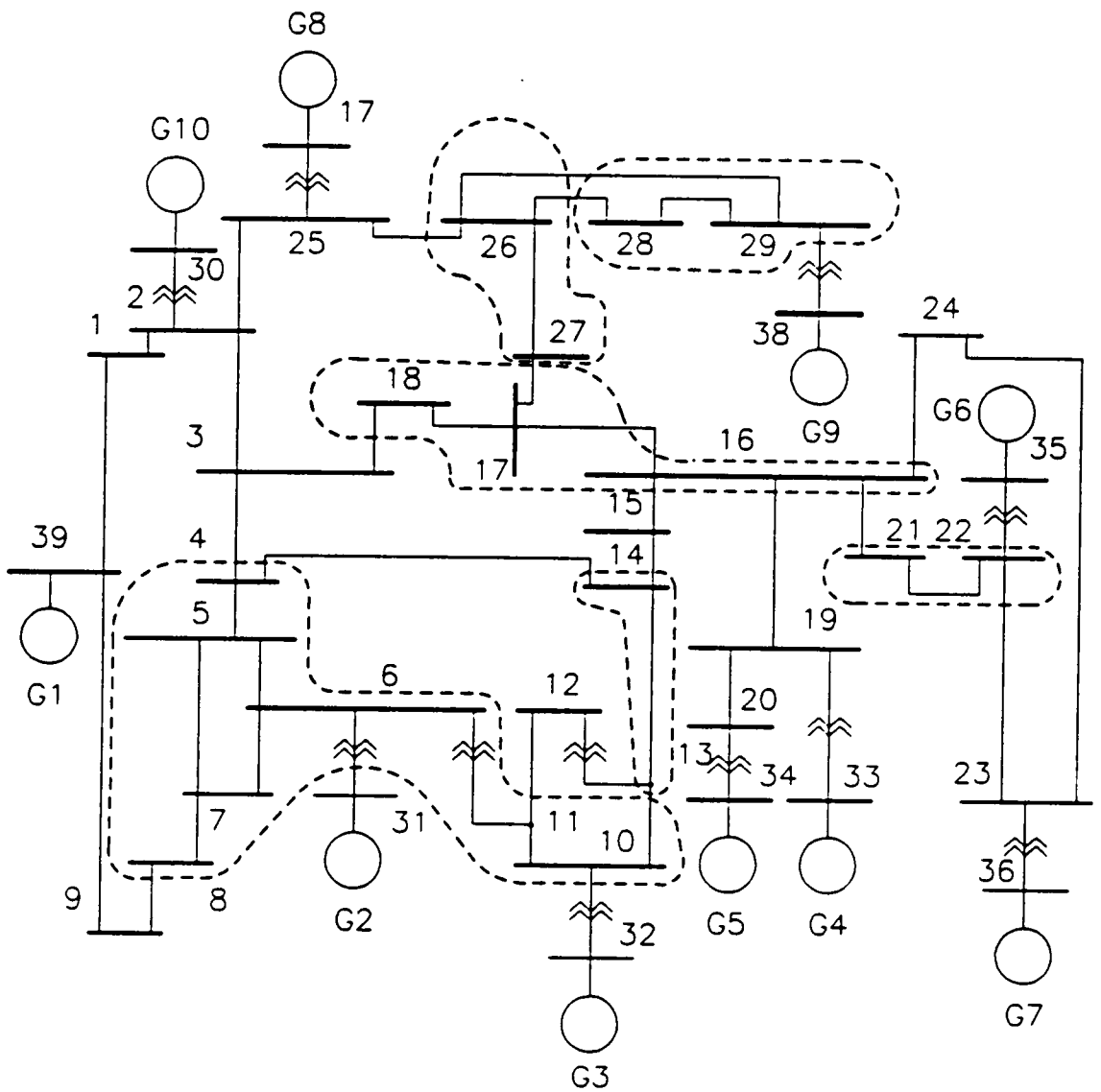

Figure 41. **Clustering using criterion 1:** $\varepsilon_1 = 0.12, \varepsilon_2 = 0.25$.

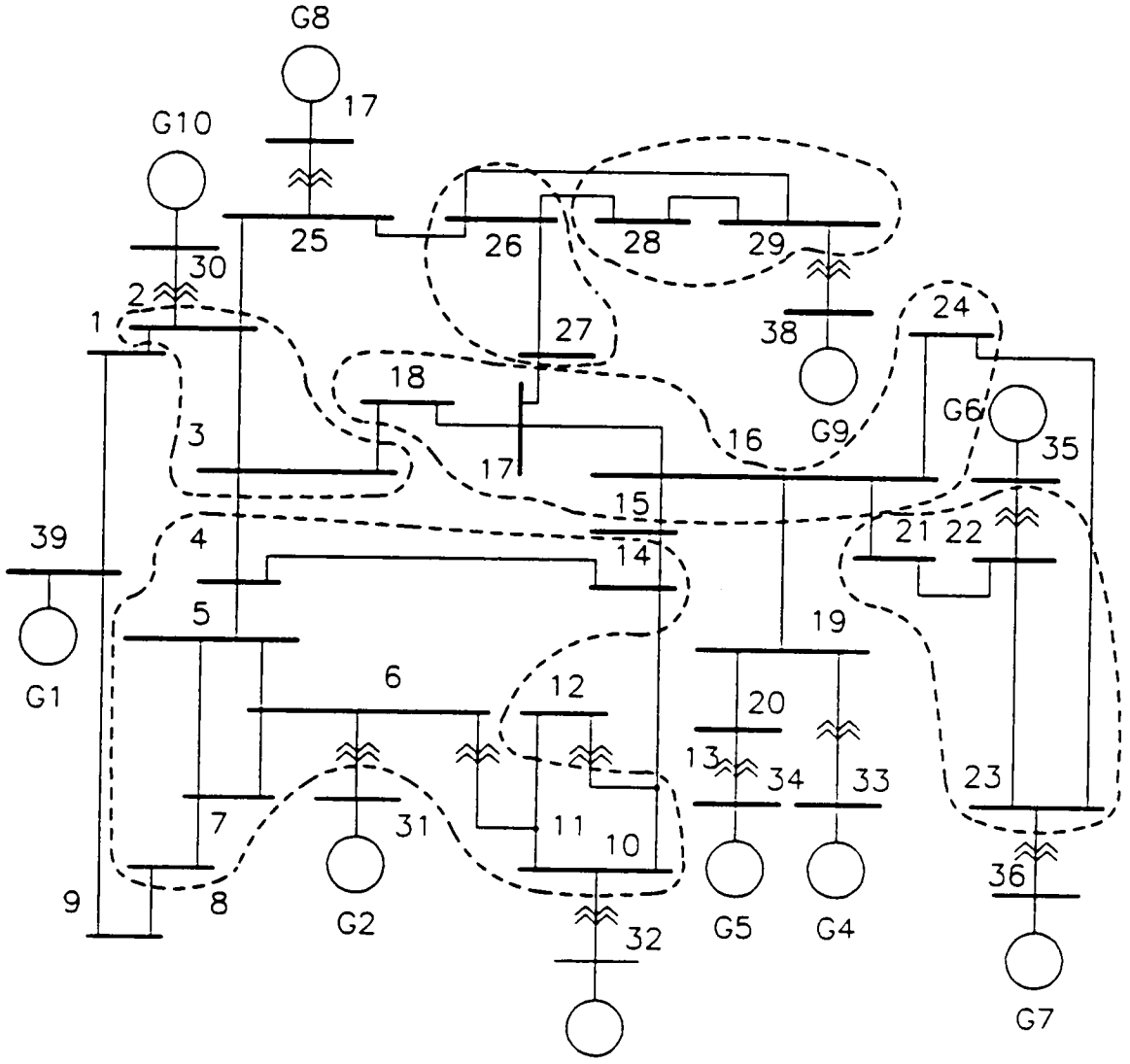

Figure 42. **Clustering using criterion 1:** $\varepsilon_1 = 0.20, \varepsilon_2 = 0.25$.

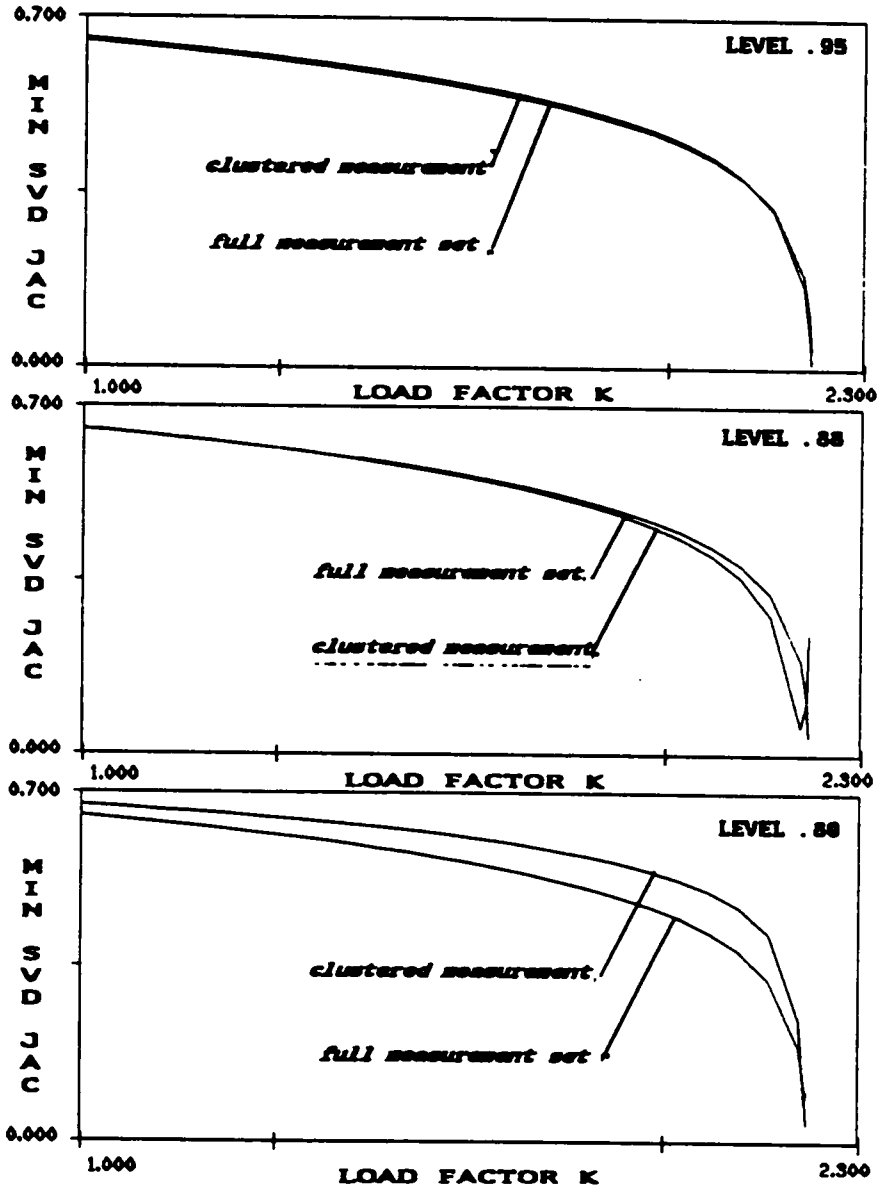

Figure 43. Algorithm performance for clusters in Figures 40–42 and uniform loading.

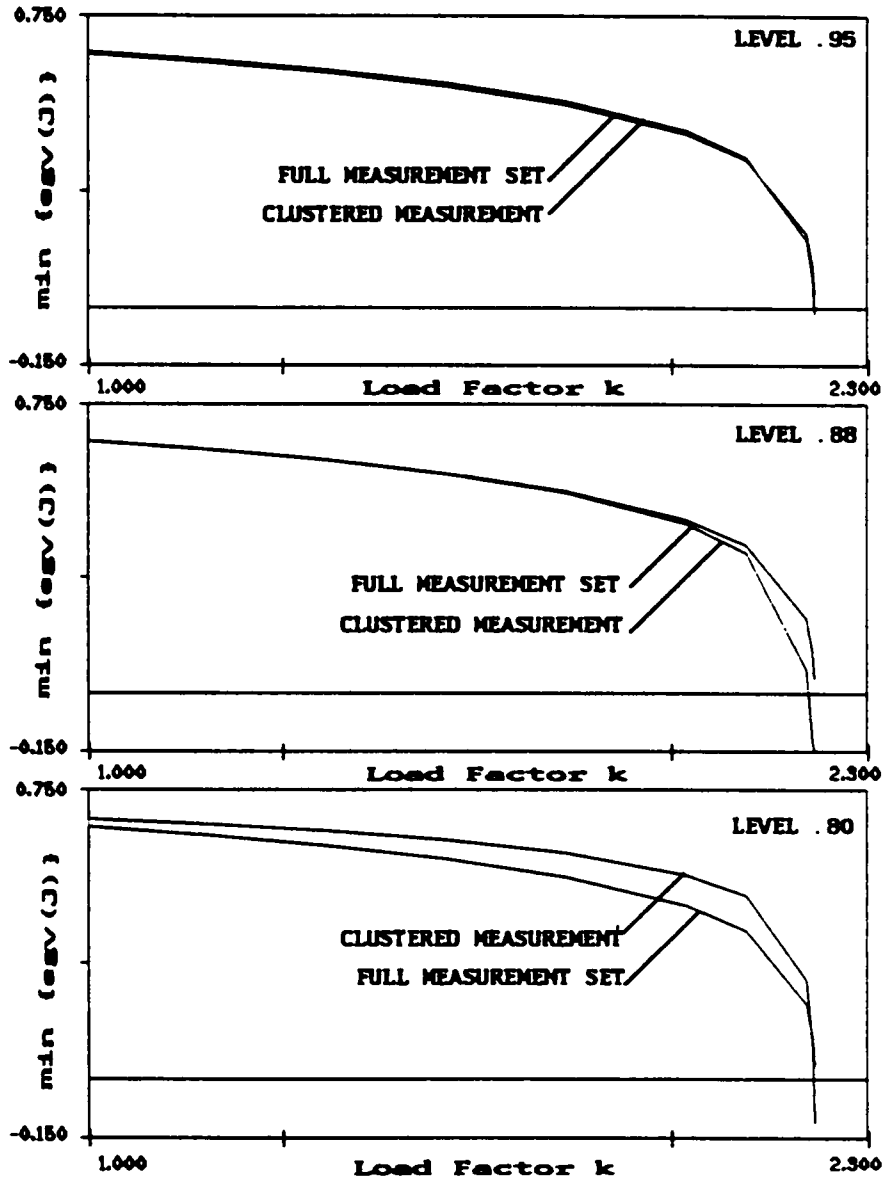

Figure 44. Algorithm performance as in Figure 43 when minimum eigenvalues are monitored.

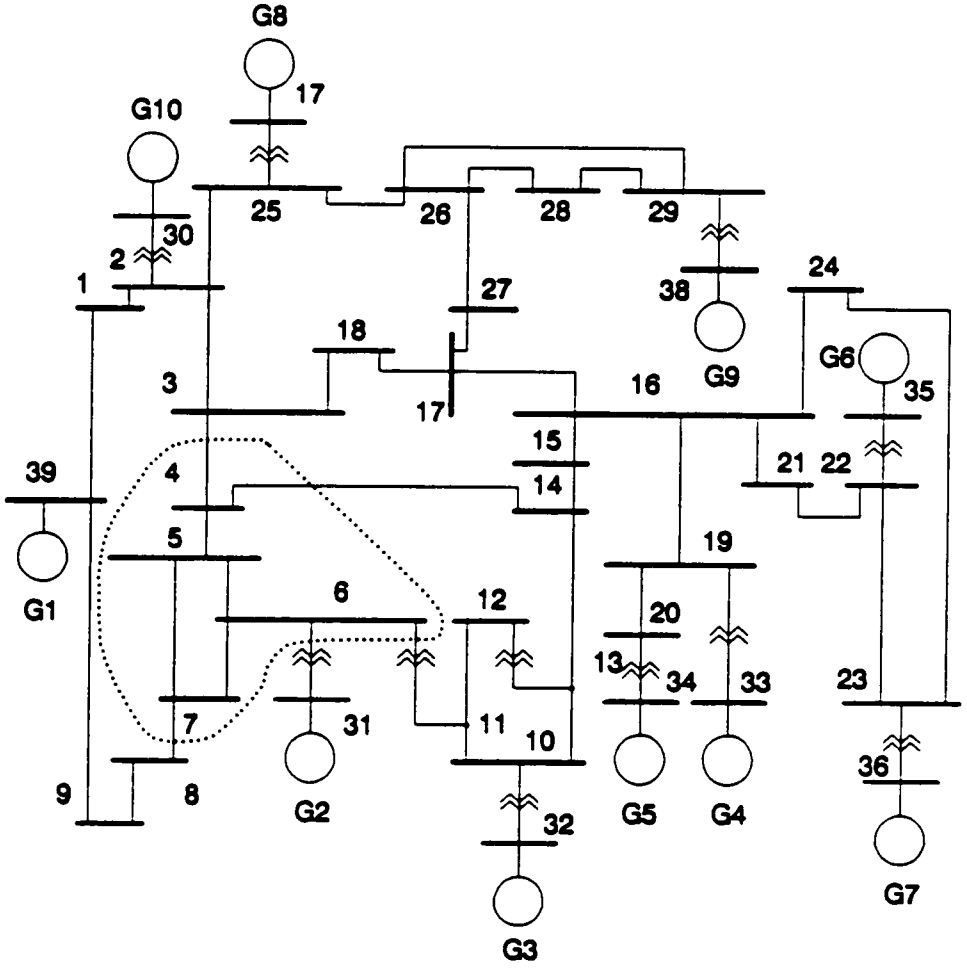

Figure 45. Clusters when effects of all line outages are considered.

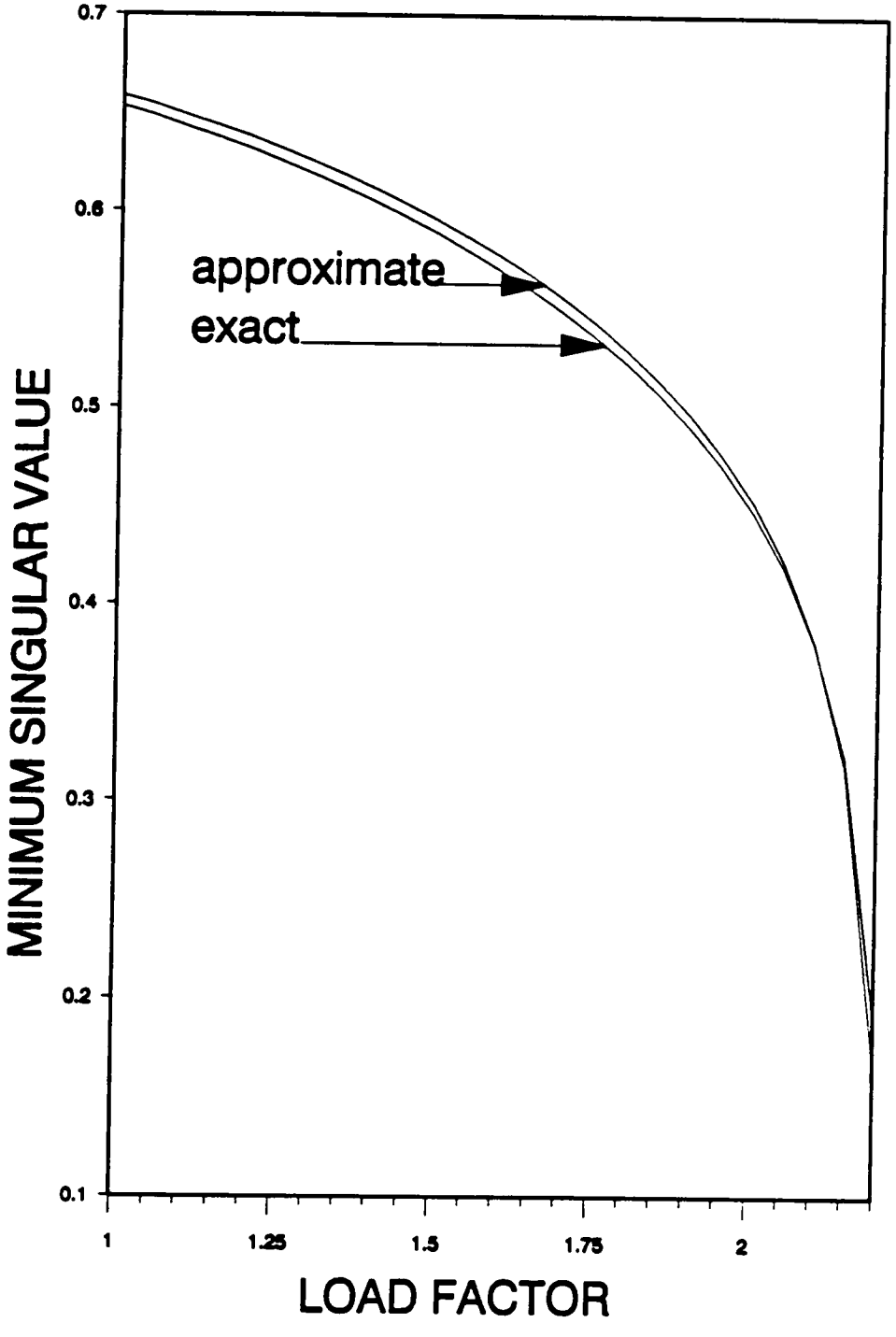

Figure 46. Algorithm performance for clustering shown in Figure 45.

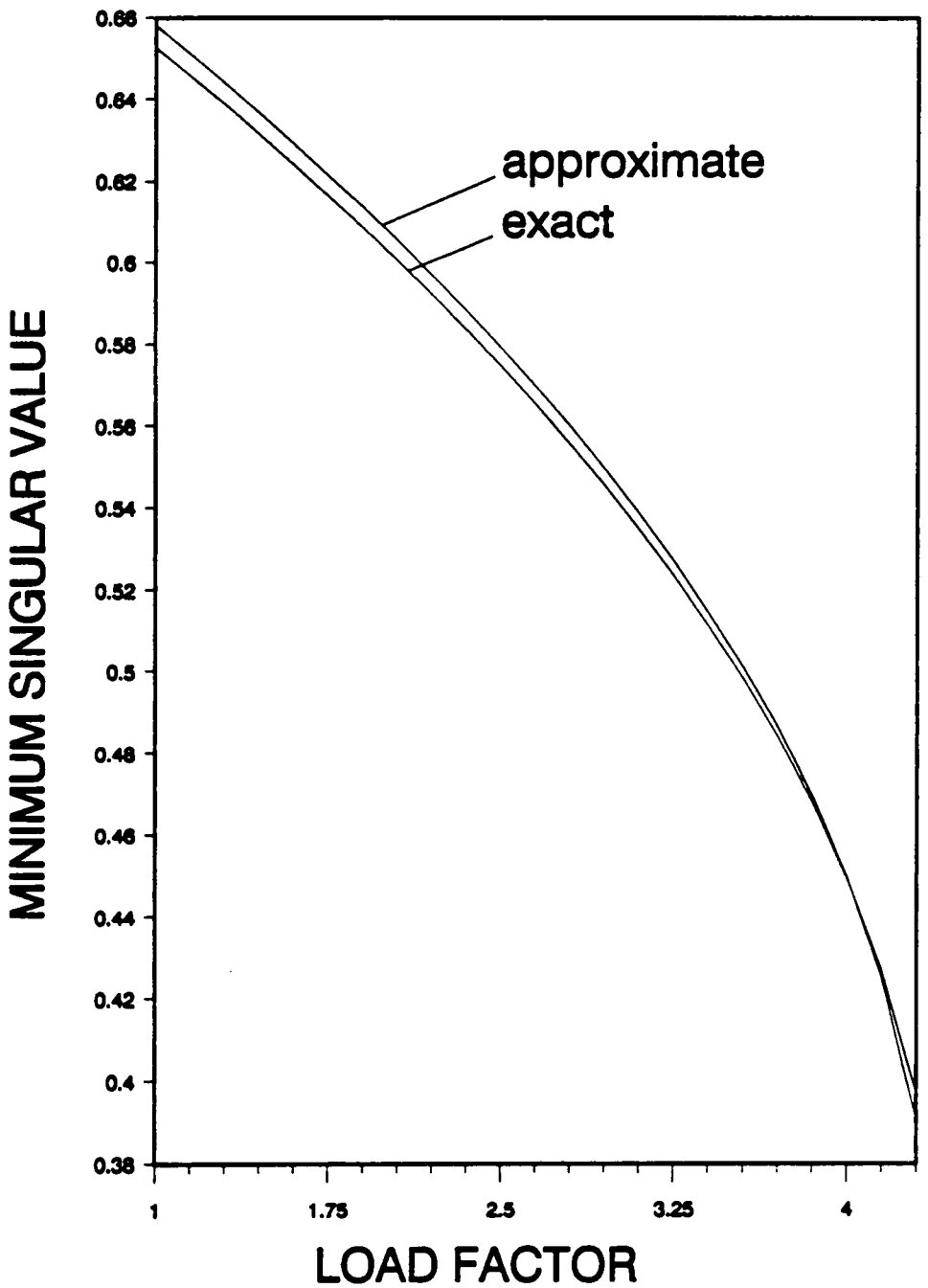

Figure 47. Algorithm performance for clustering shown in Figure 45 and reactive loading of the system.

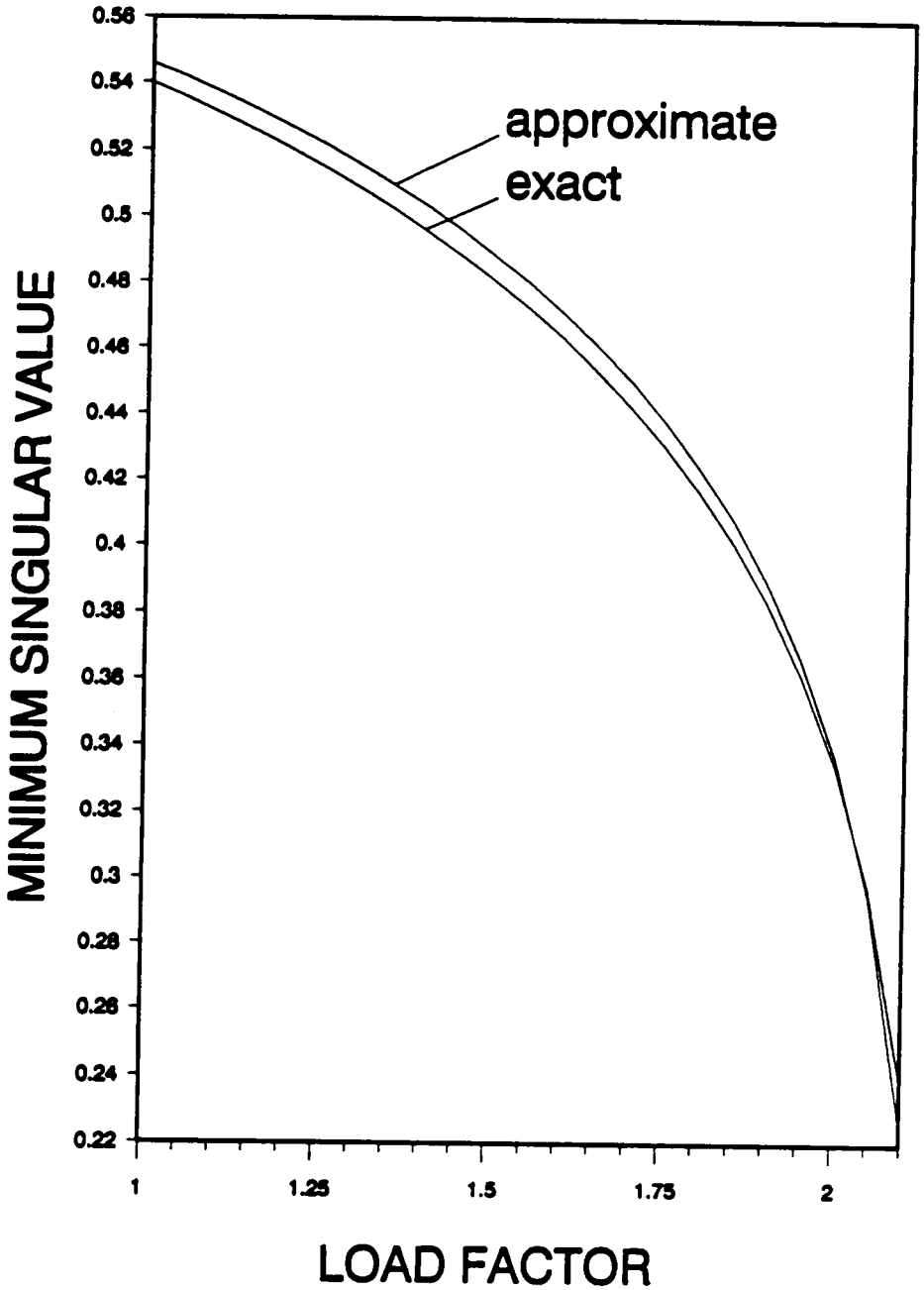

Figure 48. Algorithm performance for clustering shown in Figure 45 and line (4,5) outage.

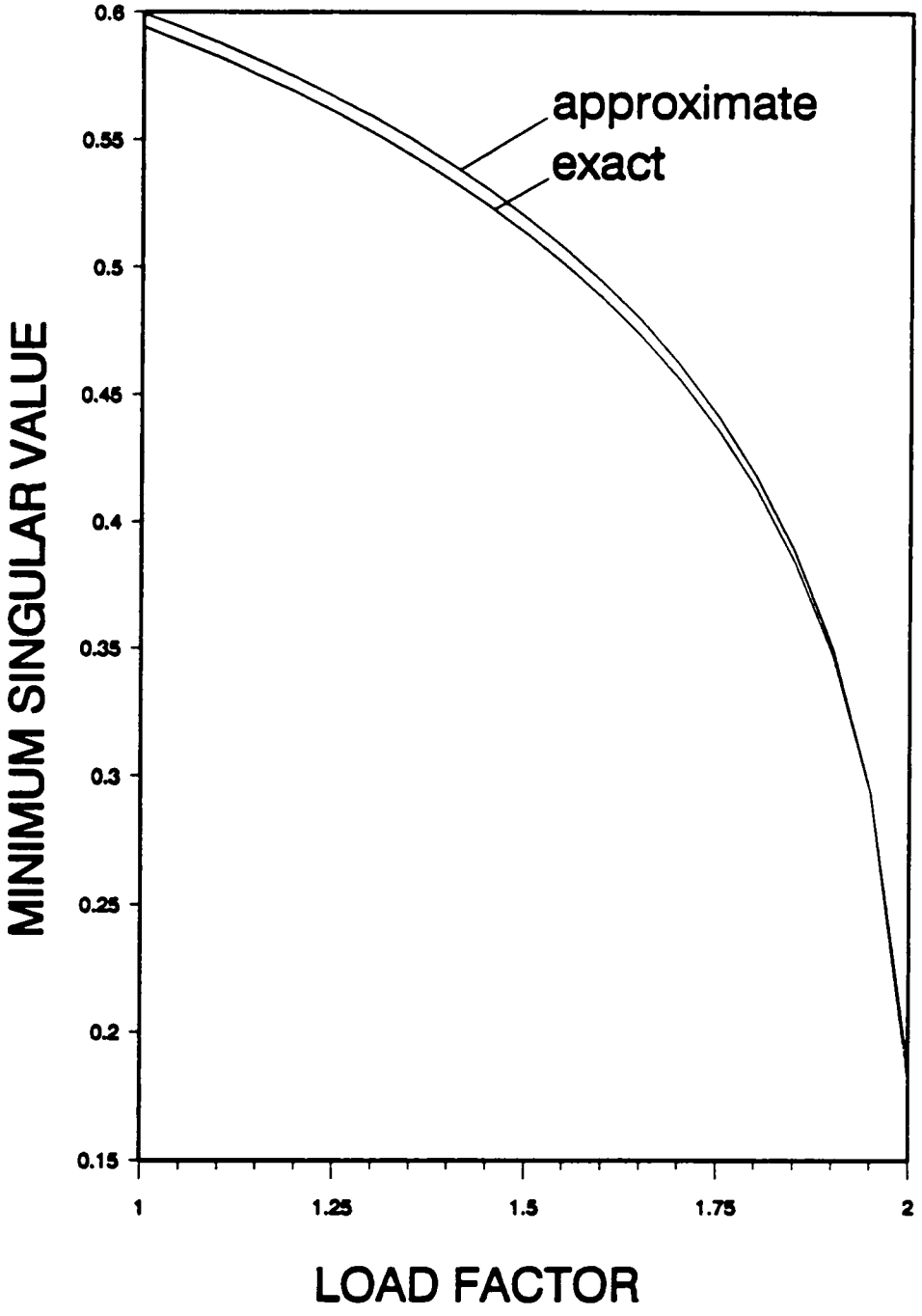

Figure 49. Algorithm performance for clustering shown in Figure 45 and line (13,14) outage.

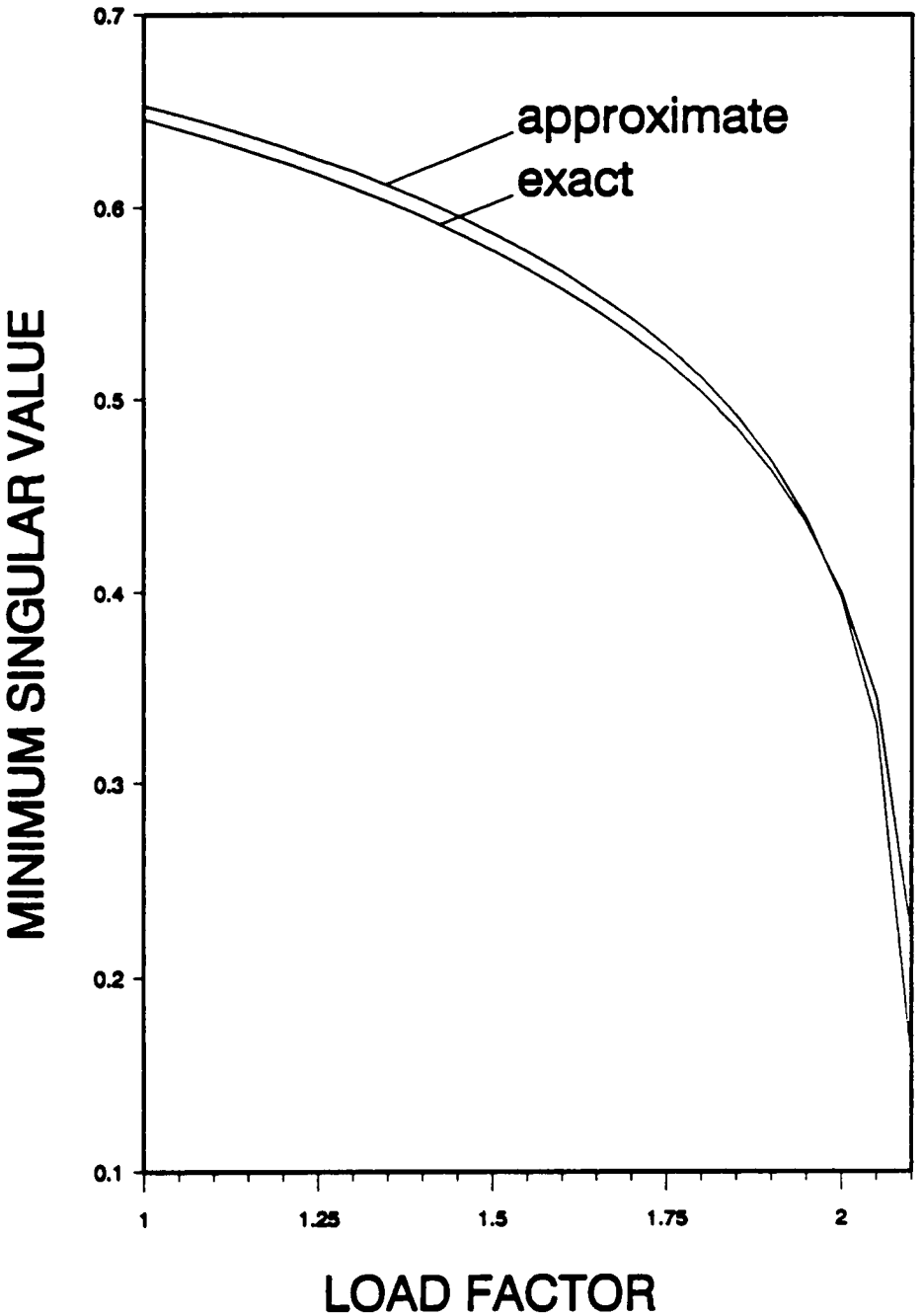

Figure 50. Algorithm performance for clustering shown in Figure 45 and line (4,14) outage.

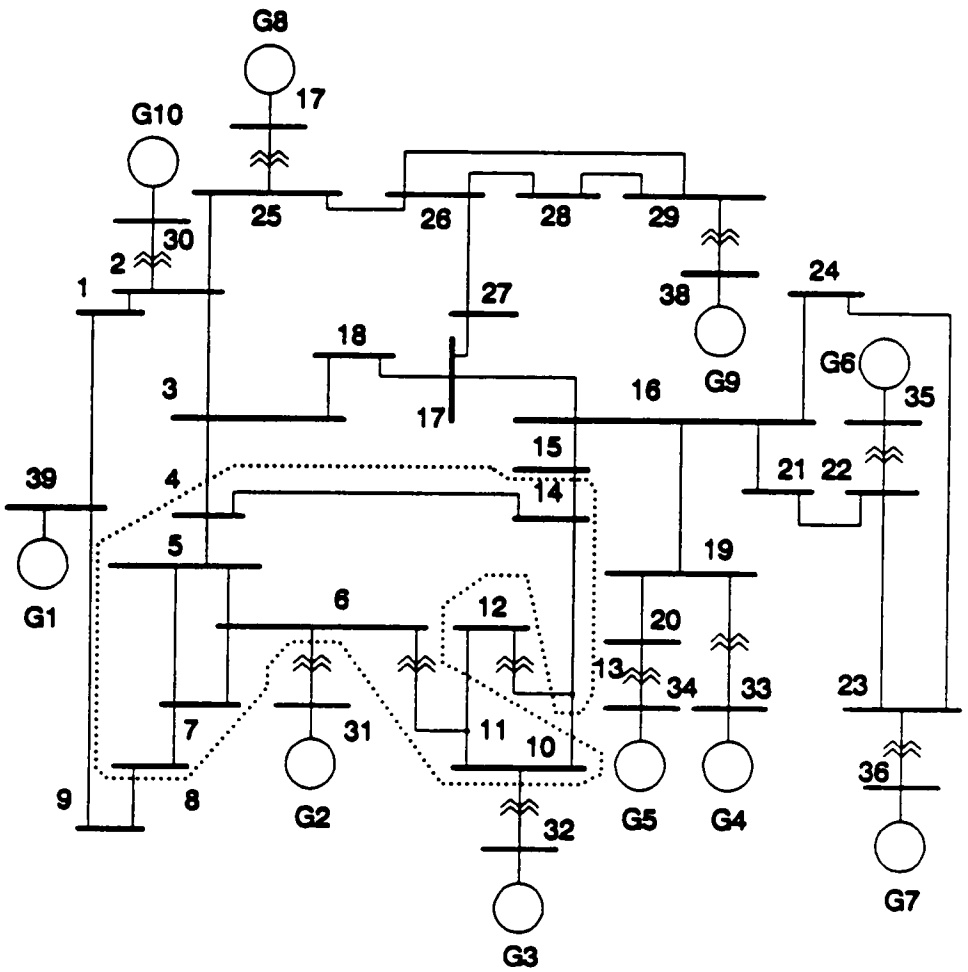

Figure 51. Clusters when all but six contingencies are accounted for (see text).

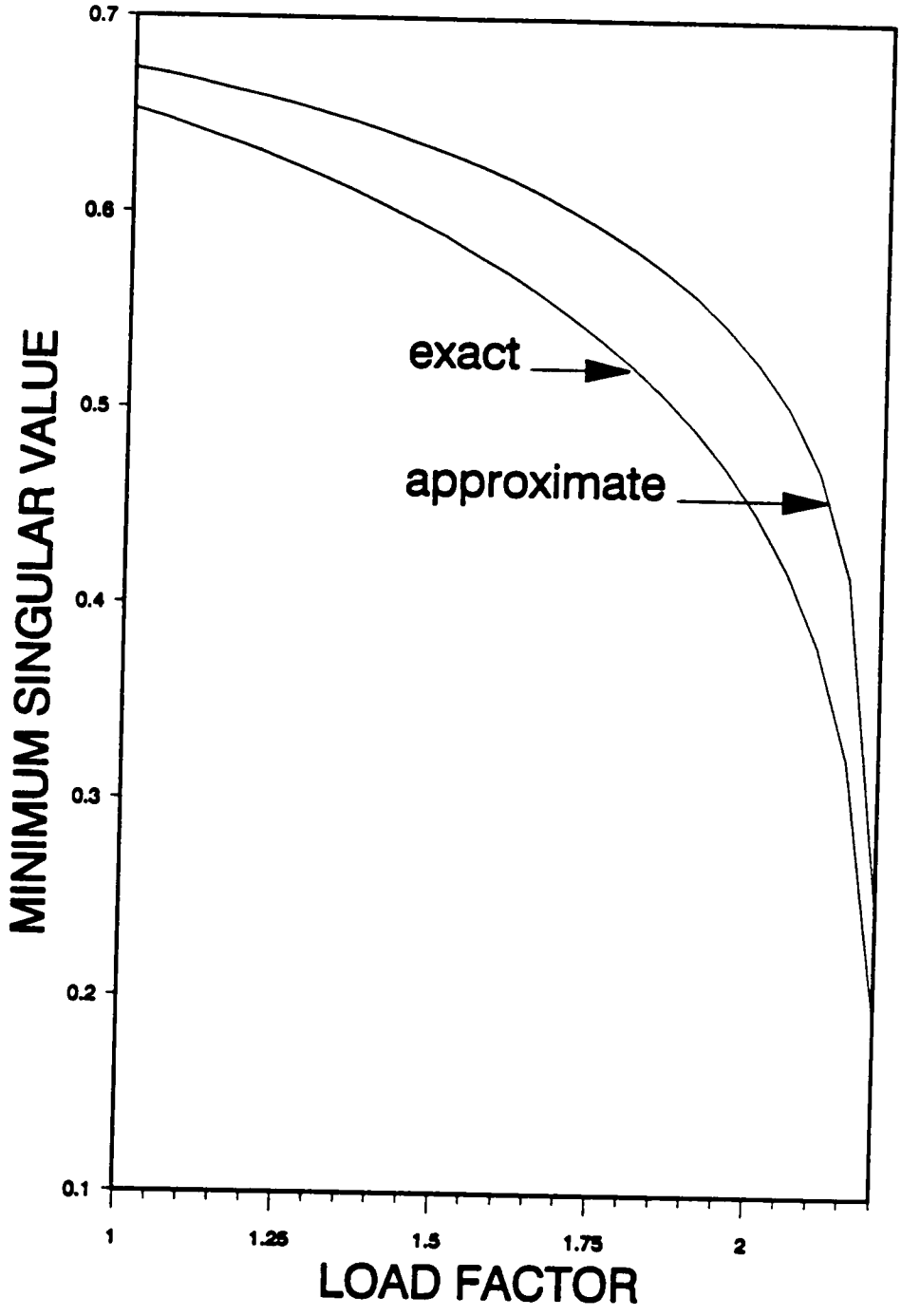

Figure 52. Algorithm performance for the clustering in Figure 51.

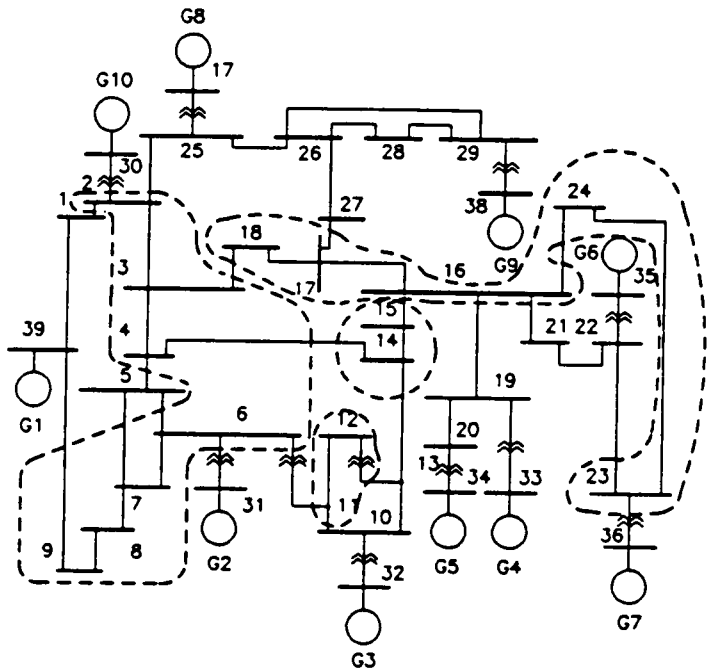

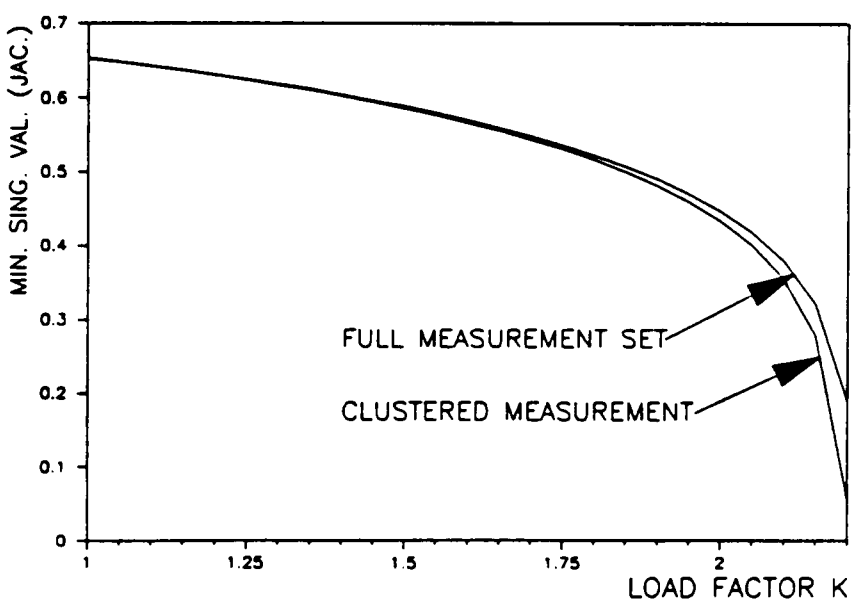

Figure 53. Clustering using criterion 2: $\varepsilon = 0.15$.

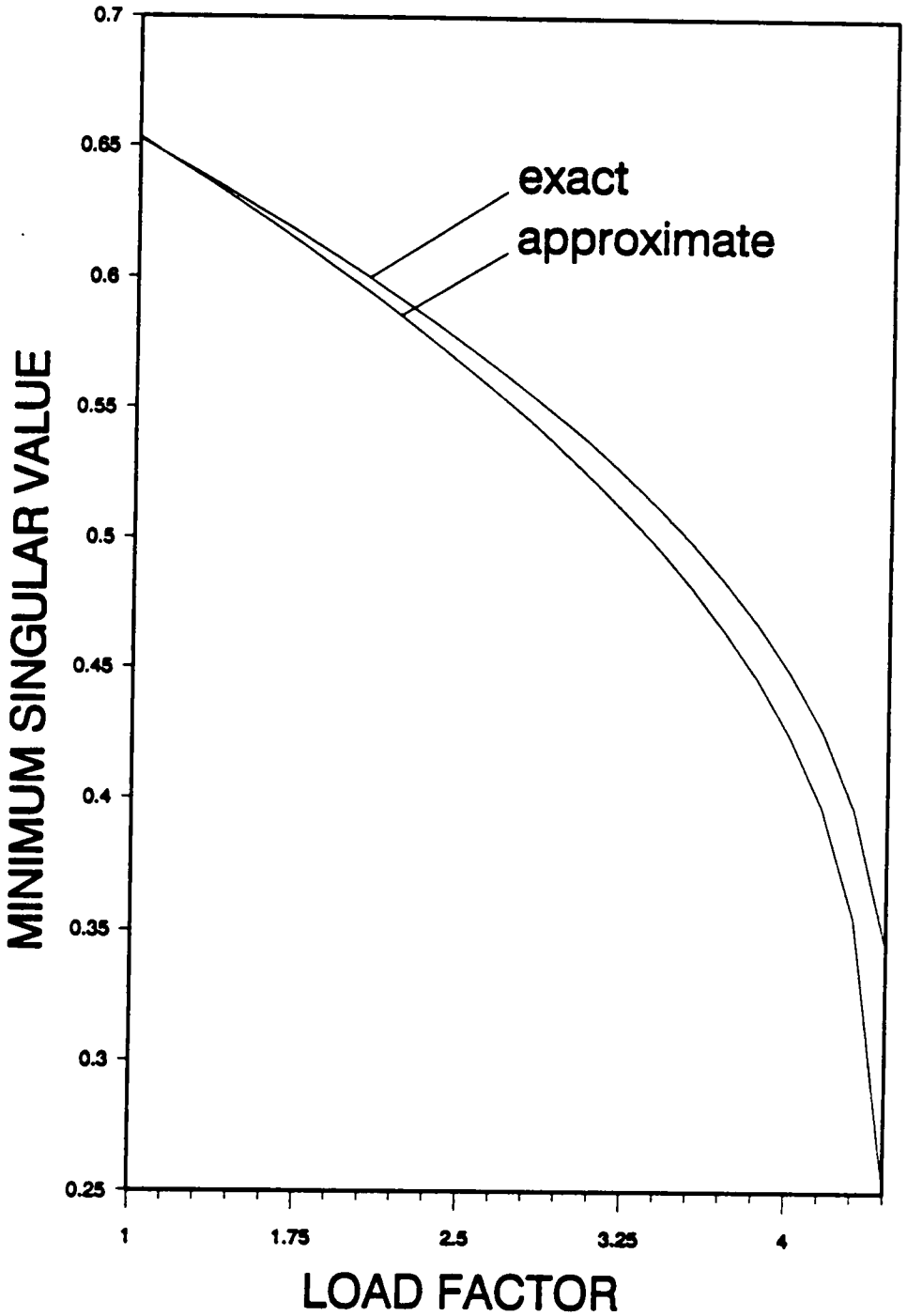

Figure 54. Algorithnm performance for clustering in Figure 53 and reactive loading of the system.

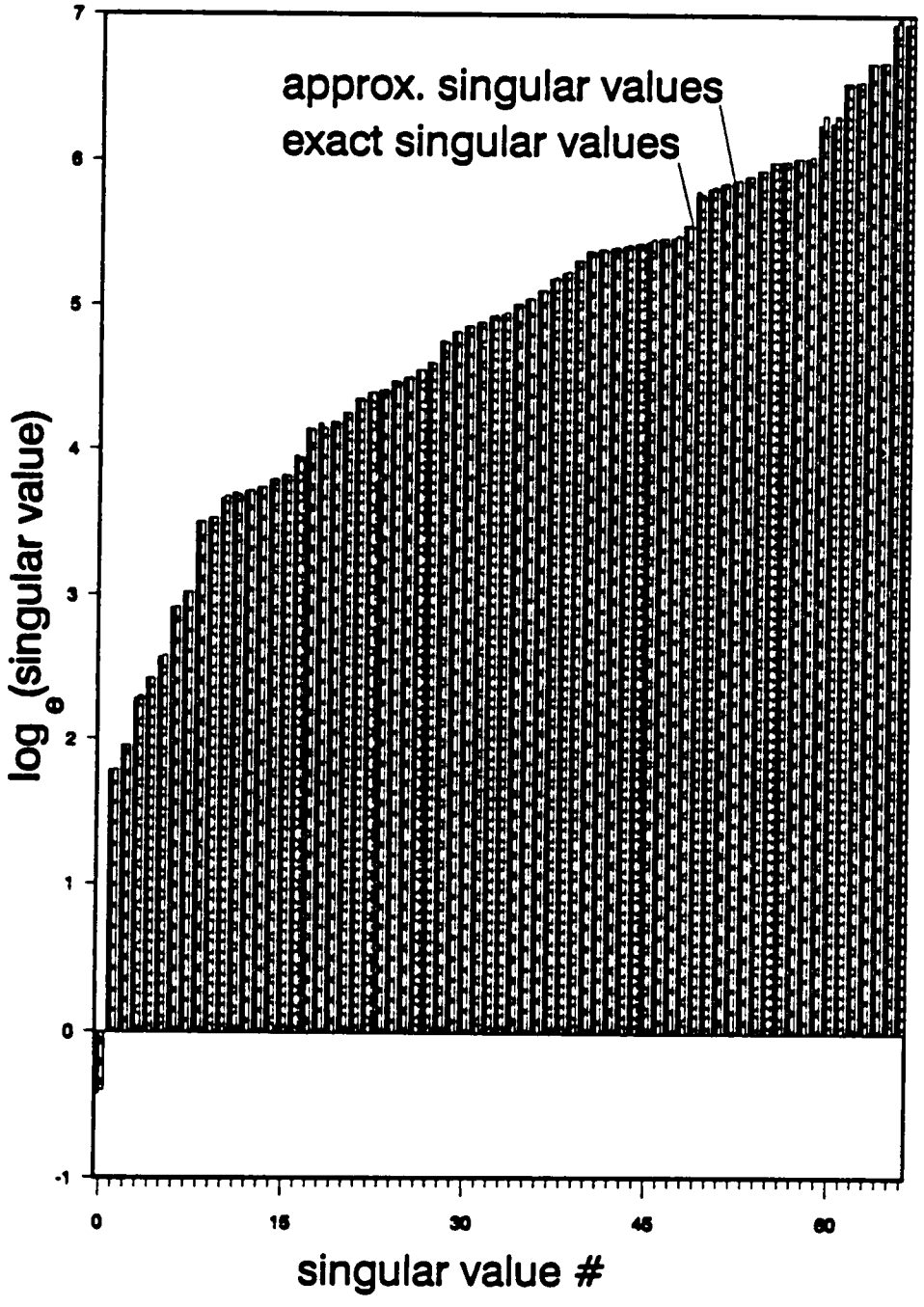

Figure 55. Complete exact and approximate SVD of Jacobian using clusters in Figure 53.

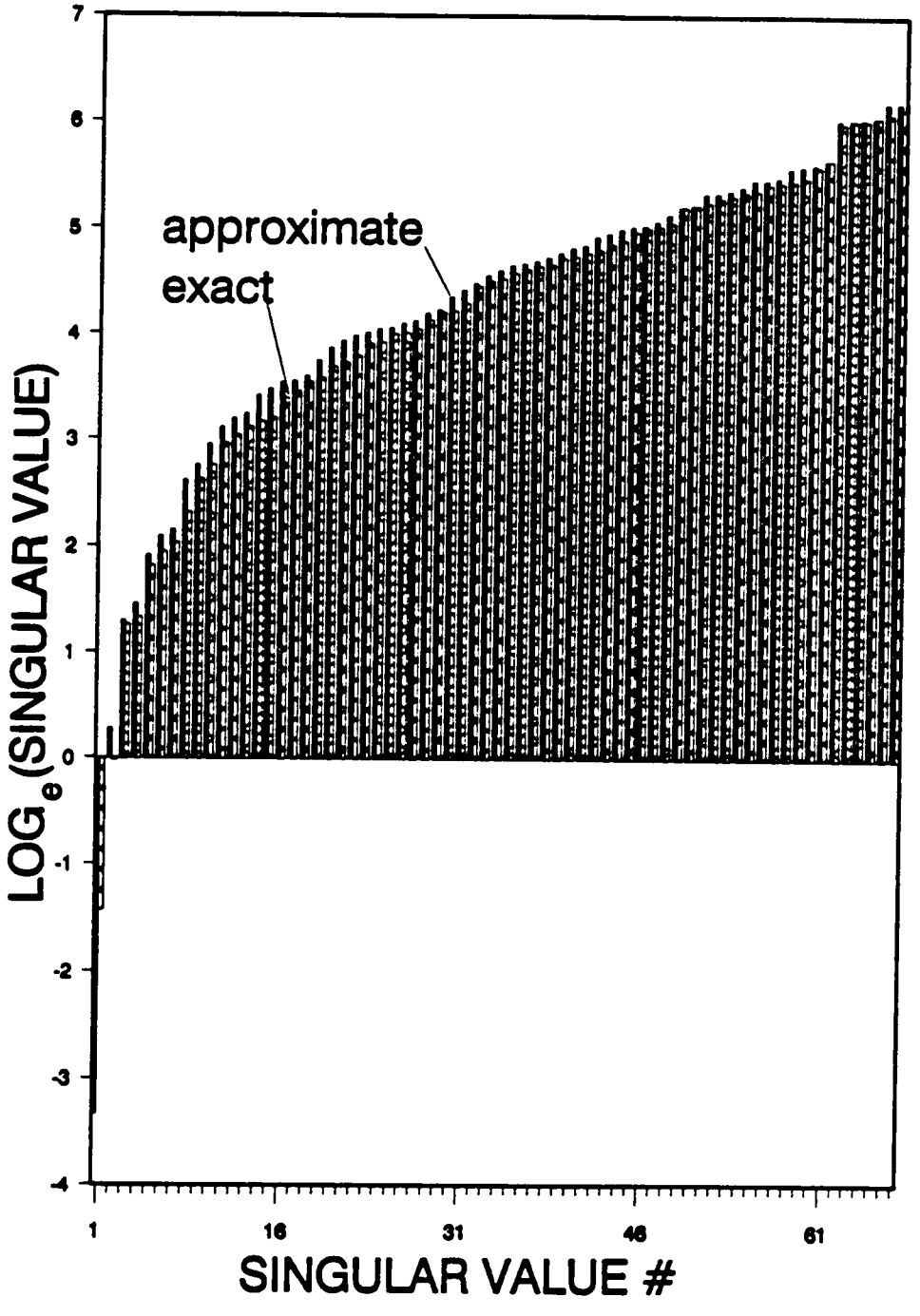

Figure 56. Complete SVD of Jacobian at voltage stability boundary using clusters in Figure 53.

rithm performance for the loading by increasing reactive power requirements only. Finally, Figures 55 and 56 represent the results of complete singular value decomposition of the load flow Jacobian (67×67) in a normal operating state (Figure 55) and close to voltage stability boundary reached by uniform loading (Figure 56). Natural logarithms of singular values are represented instead of singular values themselves for easier detection of relative differences. While singular values in the normal operating regime are almost identical, differences are still very small near voltage stability boundary. This means that the clustering algorithm does not only preserve the near singularity information, but the whole spectrum of system Jacobian, which suggests that it may be a good candidate for a number of other monitoring functions as well.

4.4 Conclusions

An investigation into uses of direct state vector measurements in power system resulted in the study of the possibilities to reduce the number of measurements of elements of the state vector. Such an approach is based on the assumption that some of the measured phasors are highly coherent with respect to voltage dynamics when the system loading changes, and moves the system towards the voltage stability boundary.

An algorithm was presented which determines the coherent clusters of load buses in a power system based on an arbitrary criterion function. The algorithm is described in the framework of graph theory and the analysis is completed with two proposed coherency criteria.

The effects of clustering using both criteria were tested by calculation of the indicators of proximity to voltage instability (minimum singular values of Jacobian). Very good agreement was obtained between the results based on accurate and approximate measurements of the state vector. Further research is neessary to study alternative choices for criteria functions and the effects they might have on the algorithms for monitoring and control of voltage stability with real-time measurement systems.

The design of coherency criteria may be extended to incorporate the effects of different loading patterns and/or topological changes in the network. An attempt to account for a variety of topological changes and still preserve the accuracy of the algorithm leads to deterioration of the efficiency of the objective of the algorithm (the reduction of the number of measurements). A compromise needs to be found in such cases. The algorithm which would create a solution could easily be formalized as a certain type of objective function to be optimized.

The applicability of the clustering algorithm is not limited to monitoring of voltage stability. It would lend itself well to many monitoring and control functions based on phasor measurements in power systems, assuming an appropriate choice

of coherency criteria is made. The advances in computer hardware and software will futher extend the range of its applications.

Chapter 5. Voltage Stability Emergency Control

5.1 Introduction

The work presented in previous chapters was mainly concentrated on determination of conditions characteristic for voltage instability in power systems and design of an effective monitoring strategy which would be able to produce an early alarm when such conditions are detected in the system. Tracking of both minimum singular values of the load flow Jacobian matrix and generated reactive powers were recommended as monitoring algorithm. Effects of clustering of the load buses were analyzed with respect to the accuracy of calculated proximity indicators and acquisition of reduced system state vector (subset of the set of system phasors) was found to be a feasible and accurate monitoring strategy. A logical next step in such an analysis is the issue of a control strategy in case of an emergency created by triggering of alarms.

As pointed out previously, types of voltage instabilities studied here are associated with dynamics in time intervals of the order of several seconds to several minutes. The reason for such a distinction is that currently available computer hardware is not able to process system data and devise control strategies within times typically associated with transient instabilities. It would take more time to predict the evolution of the system state than the time within which the transient took place. The monitoring scheme proposed in Chapter 4 is built under assumption that system state acquisition and processing times are of the order of 1 second. Introduction of a control function would make the processing times even longer and realistic time intervals between systemwide control decisions are likely to be of the order of a few seconds.

Figure 57 shows the symbolic diagram of an integrated monitoring and control system based on real-time phasor measurements. White arrows represent the communication channels along which the system state update is being sent to the central processing computer every 83.3 milliseconds. The central computer contains all the necessary information about system parameters (line and transformer impedances, transformers tap positions and breaker positions (network topology). If some of these parameters change, it occurs at a relatively low rate and the system does not need to burden the fast communication with phasor measurement microcomputers to obtain it. Black arrows represent slow communication input to the host computer, which provides the update of network topology related parameters. Gray arrows represent control communication channels that connect the host with substations where the phasor measurement units are

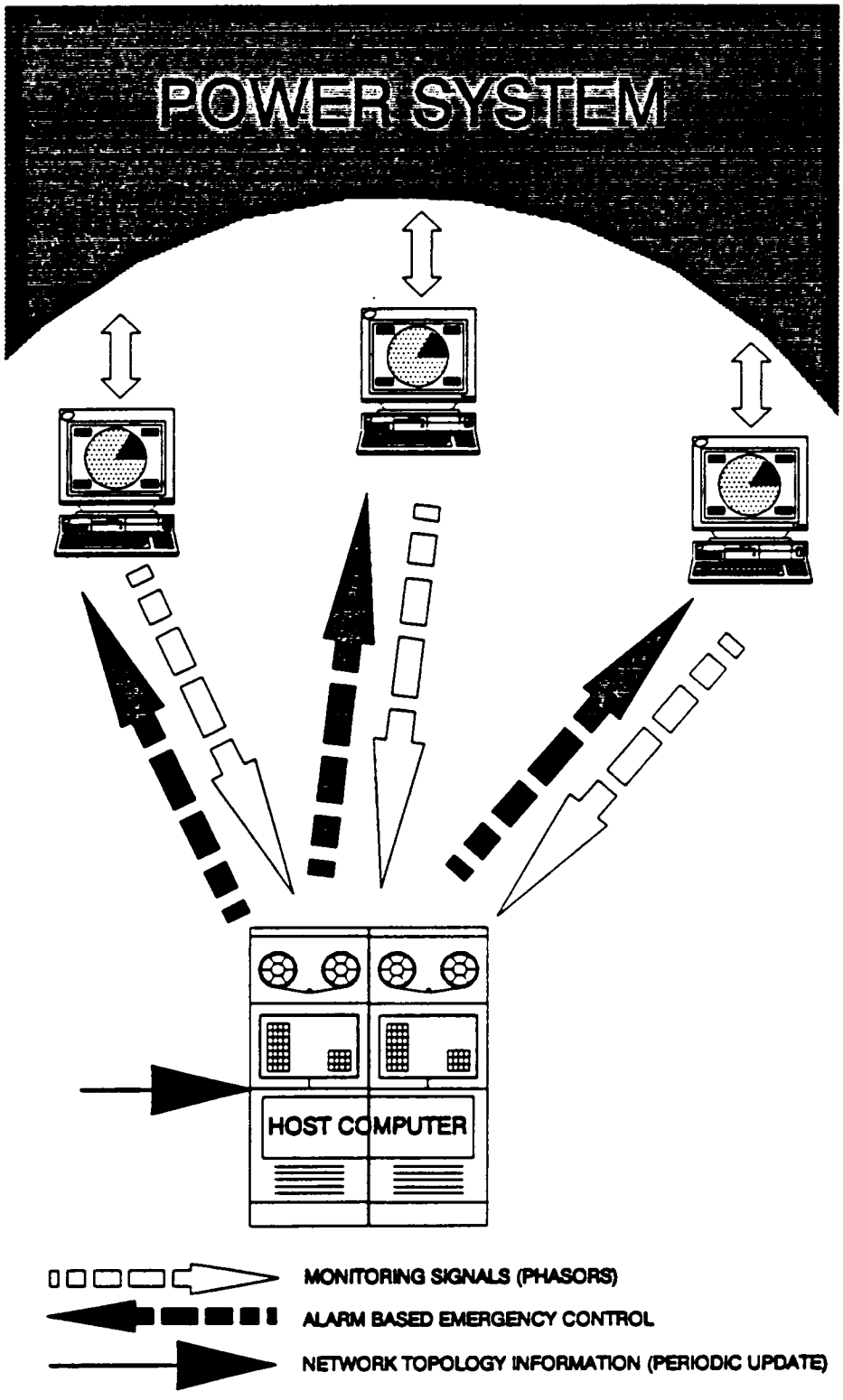

Figure 57. Monitoring and control scheme based on phasor measurements.

placed. Given assumptions about the dynamics and nature of voltage instability, there are not many choices for control. Operating time intervals of tap changers are of the order of 5-100 seconds and their action is very limited: if loads connected to tap changing transformers are stiff, tap changing action may only provide some reduction in transmission losses by increasing the voltage at the primary side, provided that loads are not completely insensitive to changes of voltage levels within their operating range. Generator controls may increase the active and reactive power generation to meet the load demand, but such an action is automated and does not require processing of the system state. There may be an important stabilizing effect in redistribution of the generation, but the parameters of redistribution would require the host to calculate an appropriately formulated optimal load flow in real- time, which would optimize voltage proximity indicators within other operating constraints. This is an interesting topic for research in its own right, but presently available computer hardware and optimal load flow algorithms do not allow such an implementation in time intervals of our concern. Redistribution of the generation qualifies as a longer term stabilizing control action of the system. The only remaining tools are reactive compensation (which is the topic of next chapter) and some form of load shedding, which may provide the necessary improvement of stability margin and bring the system back into secure operating region. In order to be effective, load shedding needs to be done on as small part of the system as possible (preferably excluding consumers which require high reliability of service). The analysis in the following text is concentrated on detection of the minimum set of loads to be affected by the sta-

bilizing control action based on the effects of the proposed control on proximity indicators.

5.2 Sensitivity Analysis of Proximity Indicators

Let us consider the power system model (3.3.4) which is assumed to be in a quasi-steady state. The system trajectory (δ, θ, V, λ) is slowly approaching voltage stability boundary due to small changes in parameter vector λ (which contains network transmission line parameters, tap changer positions, active and reactive load requirements etc.). The most likely source of loss of stability margin is the increase of total loading level in the system. However, there may exist other sources (i.e. line outages) which can change the network topology and move the system from the stable state into another one which may be characterized by a lower stability margin, measured by the minimum singular value of the system Jacobian and reactive power generation of the system. How the changes of system load at particular locations affect proximity indicators will be investigated in this section. That information may than be used to reduce, or eliminate those loads which have the most pronounced effect on deterioration of values of proximity indicators.

5.2.1 Sensitivity analysis of minimum singular values of Jacobian

Let the system (3.3.4) be in a stable equilibrium $(\delta_0, \theta_0, V_0, \lambda_0)$ for which a minimum singular value

$$\sigma^0_{\min}\{J(\delta_0, \theta_0, V_0, \lambda_0)\} \; < \; \sigma^{crit}_{\min} \tag{5.2.1}$$

was determined to be below certain prespecified level $\sigma^{crit}_{\min}$, which is considered a threshold for a control action. Since $\delta \in R^n$, $\theta \in R^m$, $V \in R^m$ and $\lambda \in R^p$, minimum singular value of Jacobian may be considered a smooth function of λ

$$\sigma_{\min}: \quad R^{n+2m+p} \rightarrow R^+ \cup \{0\} \tag{5.2.2}$$

because singular values are nonnegative. It is also a well known fact from perturbation theory [178] that the eigenvalues of a matrix depend continously on the elements of matrix. A possibility needs to be investigated of a change of λ such that the new value of $\sigma_{\min}$ is outside critical zone. In other words, we are looking for $\Delta\lambda \in R^p$ such that

$$\begin{aligned} \sigma_{\min}(\lambda_0 + \Delta\lambda) \quad &> \quad \sigma_{\min}(\lambda_0) \\ \sigma_{\min}(\lambda_0 + \Delta\lambda) \quad &\notin \quad [0, \sigma^{crit}_{\min}] \end{aligned} \tag{5.2.3}$$

Parameter vector $\lambda = [\lambda_1, \ldots, \lambda_p]^T$ may be partitionned into three parts: two which correspond to active and reactive load requirements $P = [P_1, \ldots, P_m]^T$, $Q = [Q_1, \ldots, Q_m]^T$ and one which contains the rest of parameters $\Lambda = [\lambda_{2m+1}, \ldots, \lambda_p]^T$.

$$\lambda = [P \mid Q \mid \Lambda] \tag{5.2.4}$$

The control action may be accomplished through changes in P and Q. Therefore, the form of desired change of parameter (system loading) is

$$\Delta\lambda = [\Delta P \mid \Delta Q \mid 0]^T \tag{5.2.5}$$

such that as many elements of ΔP and ΔQ as possible are unchanged (because the least number of loads should be affected). Also, if $i-th$ element of ΔP is nonzero, $i-th$ element of ΔQ should also be nonzero (load shedding affects both active and reactive parts of load at one location). Function $\sigma_{\min}$ may be locally developed around λ_0 into first order Taylor series

$$\sigma_{\min}(\lambda + \Delta\lambda) = \sigma_{\min}(\lambda) + \sum_{i=1}^{p} \frac{\partial \sigma_{\min}}{\partial \lambda_i} \Delta\lambda_i + O(\|\lambda\|^2) \tag{5.2.6}$$

Coefficients $\partial\sigma_{\min}/\partial\lambda_i$ represent participation factors of parameter $\lambda_i \in \lambda$ to the overall change of $\sigma_{\min}$ due to the change of λ. Only the first $2m$ participation factors

$$\begin{aligned} SP &= \left\{ \frac{\partial \sigma_{\min}}{\partial P_1}, \ldots, \frac{\partial \sigma_{\min}}{\partial P_m} \right\} \\ SQ &= \left\{ \frac{\partial \sigma_{\min}}{\partial Q_1}, \ldots, \frac{\partial \sigma_{\min}}{\partial Q_m} \right\} \end{aligned} \tag{5.2.7}$$

are interesting for our study. The critical load (i) of the system (3.3.4) in the state $(\delta_0, \theta_0, V_0, \lambda_0)$ is the one with a property

$$\left|\frac{\partial\sigma_{\min}}{\partial P_i}\right| P_i + \left|\frac{\partial\sigma_{\min}}{\partial Q_i}\right| Q_i > \left|\frac{\partial\sigma_{\min}}{\partial P_j}\right| P_j + \left|\frac{\partial\sigma_{\min}}{\partial Q_j}\right| Q_j \qquad (5.2.8)$$
$$\forall j \neq i, \quad j \in \{1,\ldots,m\} = W$$

The above condition states that shedding of load i will have larger impact on $\sigma_{\min}$ than any other load of the system. Critical load is the first candidate for load shedding. However, if critical load requires high reliability of supply, the set of loads may be reordered in decreasing order of combined participation factors for active and reactive power $W_0 = (i_1, \ldots, i_m)$

$$\begin{aligned} &\left|\frac{\partial\sigma_{\min}}{\partial P_{i_1}}\right| P_{i_1} + \left|\frac{\partial\sigma_{\min}}{\partial Q_{i_1}}\right| Q_{i_1} > \quad \ldots \\ &\ldots \quad > \left|\frac{\partial\sigma_{\min}}{\partial P_{i_m}}\right| P_{i_m} + \left|\frac{\partial\sigma_{\min}}{\partial Q_{i_m}}\right| Q_{i_m} \end{aligned} \qquad (5.2.9)$$

For an improvement of $\Delta\sigma$ of the minimum singular value of Jacobian, the first k loads from the ordered m-tuple W_0 (or the first k loads from that set which do not require high reliability of service) need to be eliminated from the system. Number k is chosen in such a way that

$$\sum_{j=1}^{k} \frac{\partial\sigma_{\min}}{\partial P_{i_j}} P_{i_j} + \frac{\partial\sigma_{\min}}{\partial Q_{i_j}} Q_{i_j} > \Delta\sigma_{\min} \qquad (5.2.10)$$

is satisfied. Figure 58 shows symbolically the two-dimensional equivalent of a stability region with zones of constant minimum singular values of Jacobian marked by dashed lines.

The grey zone next to stability boundary represents system states such that $\sigma_{min} \in [0\,,\ \sigma_{min}^{crit}]$. If the system trajectory (dashed arrow) cross into the zone of $\sigma_{min} < \sigma_{min}^{crit}$, an alarm is triggered, the sensitivities $\frac{\partial \sigma_{min}}{\partial P_i}$ and $\frac{\partial \sigma_{min}}{\partial Q_i}$ calculated and set of loads targeted for shedding. The result of such a control action is the return of system trajectory into the security region, where longer term control may be applied to redistribute generation, provide more generation from interties with neighboring systems and reconnect loads which were subjected to shedding in as short a time as possible. The application of (5.2.10) does not guarantee that the final value of σ_{min} after load shedding would become

$$\sigma_{min}^{new} = \sigma_{min}^{old} + \Delta\sigma \qquad (5.2.11)$$

Minimum singular value has a high negative slope and the pronounced nonlinearity with respect to changes in loading in vicinity of the stability boundary (region of near singularity of the system Jacobian - Figure 59). The sensitivity analysis is based on linearization and the desired 'unloading' of the system corresponds to the backward trajectory along the slope of tangent to σ_{min} in $(\delta_0, \theta_0, V_0, \lambda_0)$. It may therefore be necessary to perform additional load shedding after the initial one to obtain the desired level of improvement. An initial shedding of one, or two critical loads may be the best strategy, followed by addi-

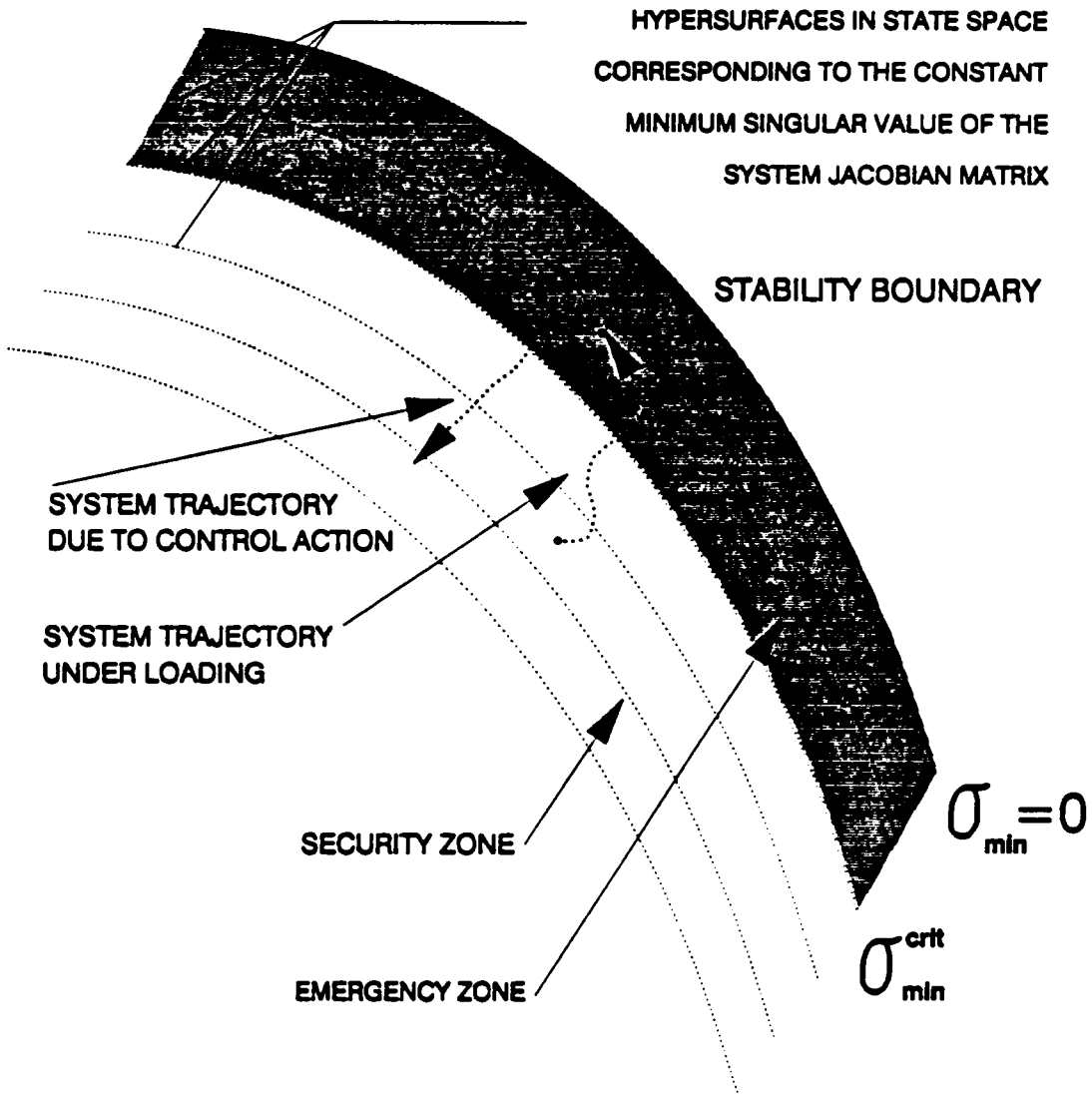

Figure 58. System trajectory during emergency control

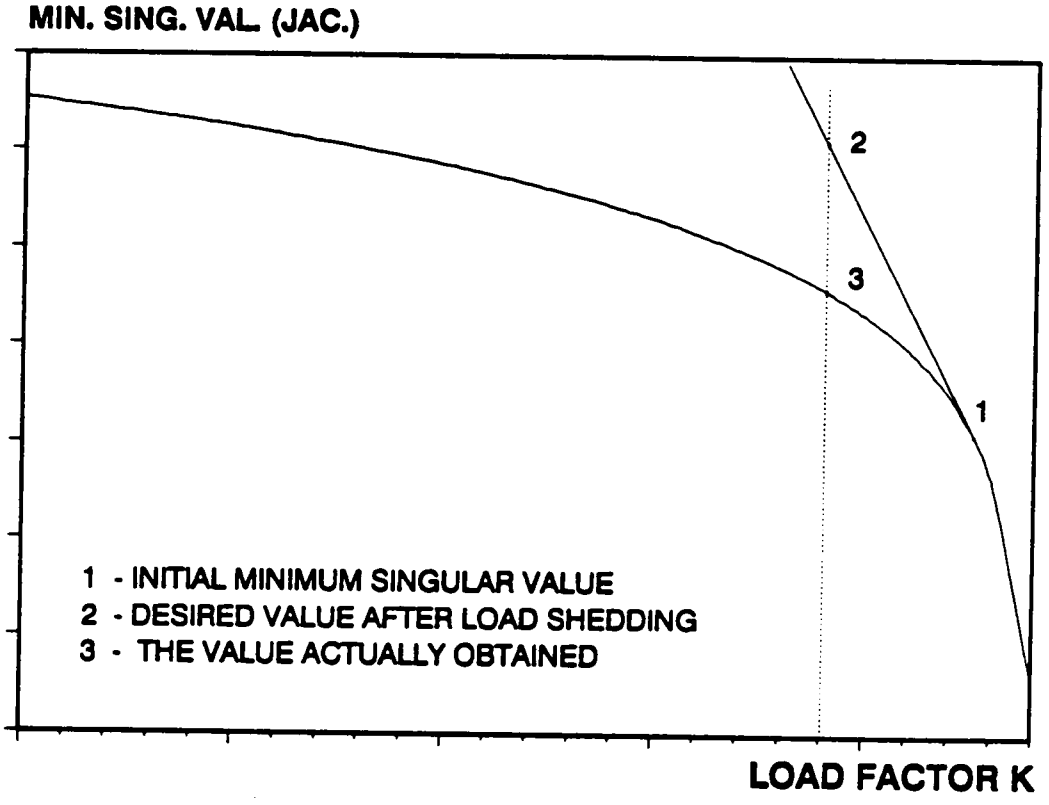

Figure 59. Effect of nonlinearity on estimation of the effects of load shedding.

tional shedding if necessary. There are several reasons against sheddding too many loads simultaneously: caution should be exercised with respect to transient system dynamics during load shedding. Also, sudden unloading of large portion of the system load may actually deteriorate the performance index σ_{min} due to necessity to reduce and redistribute generation in accordance with new system conditions.

Another important issue is the one of choosing a proper value for the threshold σ_{min}^{crit} . There are no rules other than heuristic ones for such a choice. The general shape of $\sigma(k)$ is shown in Figure 60. Loading level k in the above context represents a typical loading pattern which is particular for a given system and can be modeled from historical system loading data; k is the measure of loading level

$$k = \frac{|S|}{|S_0|} \tag{5.2.12}$$

where S_0 is the total loading in normal operating state while S is loading which corresponds to any other operating state. Typical dependence of σ_{min} is almost linear for a relatively wide range of loading levels. When those levels are exceeded, the slope of that curve becomes much steeper. If sensitivities $\partial\sigma_{min}/\partial k$ are determined by simulation in normal operating state and very near bifurcation, the dependence $\sigma_{min}(k)$ may be approximated by the two tangents to the curve in those two operating points (Figure 60). The intersection of two tangents may be an appropriate choice for critical loading level k_{crit} . The minimum singular value that corresponds to k_{crit} may be adopted as σ_{min}^{crit} .

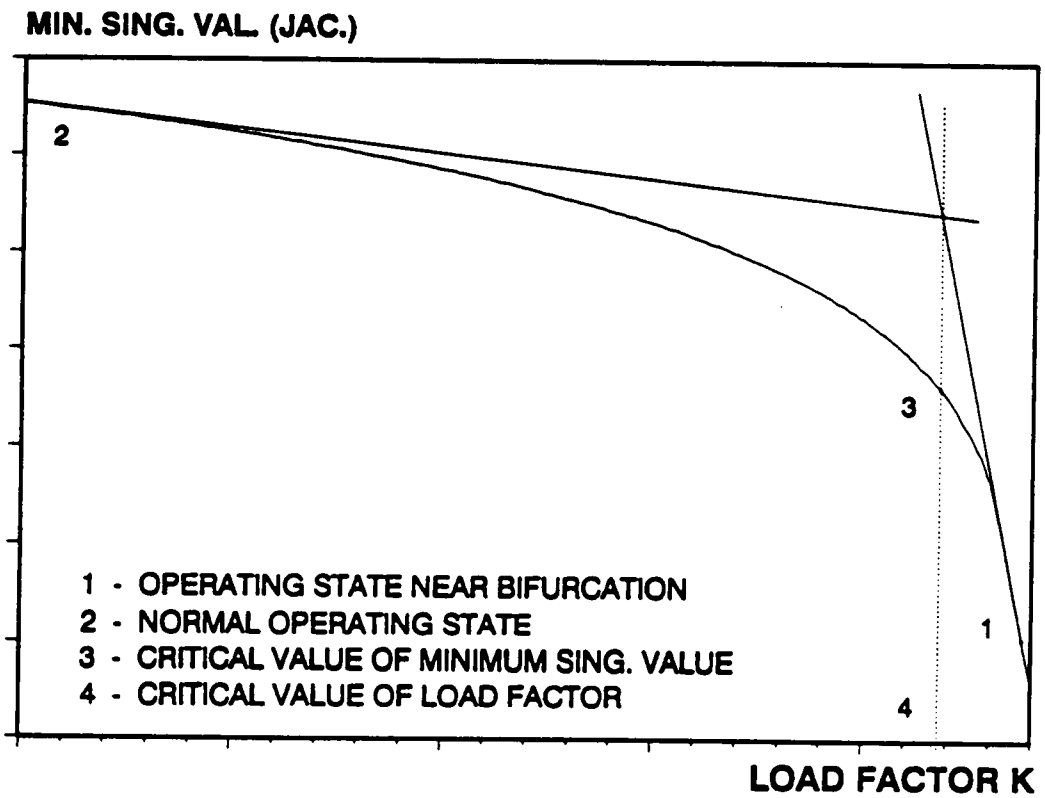

Figure 60. Determination of the critical value of a proximity indicator.

For three trajectories to the stability boundary (uniform loading of both active and reactive parts of loads without constraints in Q_g, uniform loading of reactive parts of the loads without constraints in Q_g, and uniform loading of both active and reactive parts of the loads with constraints in Q_g) the following values of thresholds were calculated respectively:

i) Uniform PQ loading, no constraints: $K_{crit} = 0.9936 k_{\max}^{crit} = 2.1988$ and the corresponding Jacobian index $\sigma_{\min}^{crit} = 0.2009$.

ii) Uniform Q loading, no constraints: $K_{crit} = 0.9965 k_{\max}^{crit} = 4.5491$ and the corresponding Jacobian index $\sigma_{\min}^{crit} = 0.2230$.

iii) Uniform PQ loading, Q_g constrained: $K_{crit} = 0.9902 k_{\max}^{crit} = 1.6207$ and the corresponding Jacobian index $\sigma_{\min}^{crit} = 0.5124$.

Practical determination of the load participation factors $\partial\sigma_{\min}/\partial P_i$ and $\partial\sigma_{\min}/\partial Q_i$ may be accomplished after acquisition of the state and parameter vector $(\delta_0, \theta_0, V_0, \lambda_0)$. The following algorithm may be used

1) Form the system Jacobian matrix $J(\delta_0, \theta_0, V_0, \lambda_0)$ and calculate its minimum sigular value $\sigma_{\min}$. Initialize the counter $i := 1$.

2) Assume a small increase of the active part of load i

$$P'_i = P_i + \Delta P \tag{5.2.13}$$

and calculate the new system state which corresponds to it. Knowing $(\delta_0, \theta_0, V_0, \lambda_0)$ as initial condition, one iteration of the Newton method would be enough to provide results. In general, any of the iterative load flow solution techniques would converge very fast. Using perturbed Jacobian corresponding to the new state, calculate σ_{min} that corresponds to it. Power method may be used to get σ_{min} very fast.

3) Repeat step (2) using perturbation

$$Q'_i = Q_i + \Delta Q \tag{5.2.14}$$

of the reactive part of load i.

4) Increment counter $i := i + 1$. If $i < m$ go to step (2). Else: calculate load participation factors

$$\begin{aligned} \frac{\partial \sigma_{min}}{\partial P_i} &\simeq \frac{\sigma'_{min} - \sigma_{min}}{\Delta P_i} \\ \frac{\partial \sigma_{min}}{\partial Q_i} &\simeq \frac{\sigma''_{min} - \sigma_{min}}{\Delta P_i} \end{aligned} \tag{5.2.15}$$

5) Apply the algorithm (5.2.10) to determine a set of candidates for load shedding.

As one can note from the above, this algorithm represents a heavy computational burden for the central processing computer, although it is simplified as much as possible. Conclusion can be drawn that it may be better to rely on some other

method for real -time identification of critical loads. The logical alternative to the algorithm presented is the second voltage collapse proximity indicator proposed in this text, generated reactive power.

5.2.2 Sensitivity analysis of generated reactive powers

The previously proposed algorithm may easily be modified and simplified by doing a sensitivity analysis of generated reactive powers instead of minimum singular values of the Jacobian for selection of the candidates for load shedding:

1) Form the Jacobian $J(\delta_0, \theta_0, V_0, \lambda_0)$ from acquired data and calculate the generated reactive powers

$$Q_{gi} = Im\{V_{gi} I_{gi}^{\times}\} \tag{5.2.16}$$

from acquired data (both voltage and current phasors are obtained from measurement units placed at generator terminal buses). Initialize counter $i := 1$.

2) Assume a small increase of load i (5.2.13) and calculate load flow which corresponds to it as well as generated reactive powers. Given the set of system voltage phasors $V_i \angle \xi_i$, generated reactive power is

$$Q'_{gi} = V_i \sum_{j=1}^{n+m} V_j [G_{ij} \sin \xi_{ij} - B_{ij} \cos \xi_{ij}] \tag{5.2.17}$$

where $\xi_{ij} = \xi_i - \xi_j$ and G_{ij}, B_{ij} are transmission line admittance and susceptance.

3) Repeat step (2) for a small increase of the reactive portion of load i (5.2.14) and calculate Q_{gi}.

4) Increment counter. If $i < m$ go to step (2); else: calculate sensitivities of reactive powers Q_{gi} as

$$\begin{aligned} \frac{\partial Q_{gi}}{\partial P_i} &= \frac{Q_{gi} - Q'_{gi}}{\Delta P_i} \\ \frac{\partial Q_{gi}}{\partial Q_i} &= \frac{Q_{gi} - Q''_{gi}}{\Delta Q_i} \end{aligned} \tag{5.2.18}$$

5) Determine the critical load j which has the property

$$\Delta Q_j > \Delta Q_k, \quad \forall k \in \{1,2,\ldots,m\} - \{j\} \tag{5.2.19}$$

where

$$\Delta Q_j = \frac{\partial Q_{gi}}{\partial P_j} P_j + \frac{\partial Q_{gi}}{\partial Q_j} Q_j \tag{5.2.20}$$

and generator i is assumed to be critical (to have the highest generation of reactive power). When critical load is eliminated, next candidate for load shedding is the critical load of the remaining set of loads.

This algorithm is computationally much more effective than the previous one presented. It requires $2m$ iterations of the Newton load flow to produce disturbed system states and some simple arithmetic to calculate generated reactive powers and load participation factors. The disadvantage of this method is that it cannot provide a clear quantitative measure of the improvement of stability margin as the method based on minimum singular values of Jacobian does. However, the close correlation between the decrease of the minimum singular value of Jacobian and generated reactive power guarantees that load shedding would move the system state away from stability boundary by an amount which is not easy to quantify in terms other than reactive powers. If the improvement obtained by load shedding is not enough, subsequent load sheddings after reevaluation of the system state would eventually bring the system back into secure operating region (criterion for transition is again $\sigma_{\min} > \sigma_{\min}^{crit}$).

Another simplification of the algorithm for identification of critical loads is possible. It is based on the inversion of Jacobian J calculated from the acquired system state data

$$J^{-1}(\delta_0, \theta_0, V_0, \lambda_0) = \begin{bmatrix} \frac{\partial \delta}{\partial P_g} & \frac{\partial \delta}{\partial P_l} & \frac{\partial \delta}{\partial Q_l} \\ \frac{\partial \theta}{\partial P_g} & \frac{\partial \theta}{\partial P_l} & \frac{\partial \theta}{\partial Q_l} \\ \frac{\partial V}{\partial P_g} & \frac{\partial V}{\partial P_l} & \frac{\partial V}{\partial Q_l} \end{bmatrix} \qquad (5.2.21)$$

where P_g, P_l and Q_l represent vectors of generated active powers, active and reactive load requirements. The sensitivity matrix of the generated reactive powers (5.2.17) vs. the vector of variable state elements $x = (\delta, \theta, V)$ is

$$J_g = \left[\frac{\partial Q_g}{\partial x} \right] = \begin{bmatrix} \frac{\partial Q_{g1}}{\partial \delta} & \frac{\partial Q_{g1}}{\partial \theta} & \frac{\partial Q_{g1}}{\partial V} \\ \cdots & \cdots & \cdots \\ \frac{\partial Q_{gn}}{\partial \delta} & \frac{\partial Q_{gn}}{\partial \theta} & \frac{\partial Q_{gn}}{\partial V} \end{bmatrix} \tag{5.2.22}$$

The relationship between changes of reactive generation and changes of loading and active generation may be expressed as

$$\Delta Q_{gi} = \left[\frac{\partial Q_{gi}}{\partial \delta} \right] \left[\frac{\partial \delta}{\partial P_g} \right] \Delta P_g + \left[\frac{\partial Q_{gi}}{\partial \theta} \right] \left[\frac{\partial \theta}{\partial P_l} \right] \Delta P_l + + \left[\frac{\partial Q_{gi}}{\partial V} \right] \left[\frac{\partial V}{\partial Q_l} \right] \Delta Q_l \tag{5.2.23a}$$

$$\begin{bmatrix} \Delta Q_{g1} \\ \cdots \\ \Delta Q_{gn} \end{bmatrix} = \begin{bmatrix} \frac{\partial Q_{g1}}{\partial \delta} & \frac{\partial Q_{g1}}{\partial \theta} & \frac{\partial Q_{g1}}{\partial V} \\ \cdots & \cdots & \cdots \\ \frac{\partial Q_{gn}}{\partial \delta} & \frac{\partial Q_{gn}}{\partial \theta} & \frac{\partial Q_{gn}}{\partial V} \end{bmatrix} \begin{bmatrix} \frac{\partial \delta}{\partial P_g} & \frac{\partial \delta}{\partial P_l} & \frac{\partial \delta}{\partial Q_l} \\ \frac{\partial \theta}{\partial P_g} & \frac{\partial \theta}{\partial P_l} & \frac{\partial \theta}{\partial Q_l} \\ \frac{\partial V}{\partial P_g} & \frac{\partial V}{\partial P_l} & \frac{\partial V}{\partial Q_l} \end{bmatrix} \begin{bmatrix} \Delta P_g \\ \Delta P_l \\ \Delta Q_l \end{bmatrix} \tag{5.2.23b}$$

$$[\Delta Q_g] = J_g J^{-1} [\Delta \psi] = S [\Delta \psi] \tag{5.2.23c}$$

where $\Delta\psi = [\Delta P_g \ \Delta P_l \ \Delta Q_l]^T$. The rows r_i of the sensitivity matrix $S = [r_1 \ r_2 \ \dots \ r_n]^T$ represent sets of load and active generation participation factors $\partial Q_{gi}/\partial P_{gj}$, $\partial Q_{gi}/\partial P_{lj}$ and $\partial Q_{gi}/\partial Q_{lj}$, on which a load shedding candidate selection (5.3.19) may be applied. This algorithm requires just one matrix inversion and one matrix multiplication and is very suitable for real-time processing. Disadvantage of the Jacobian is that the inverse of Jacobian is a full (non-sparse) matrix, which may require large storage capacity, but the savings in computation time would more than offset the loss in computer storage. If total generated reactive power is adopted as a voltage collapse proximity indicator rather than reactive power generated by critical machine, the algorithm may be made faster. Total generated reactive power is

$$Q_g^t = \sum_{i=1}^{n} Q_{gi} = \sum_{i=1}^{n} \sum_{j=1}^{n+m} V_i V_j [G_{ij} \sin \xi_{ij} - B_{ij} \cos \xi_{ij}] \qquad (5.2.24)$$

and its sensitivity matrix with respect to variable elements of the state vector $x = (\delta, \theta, V)$ is

$$J_g^t = \left[\frac{\partial Q_g^t}{\partial x} \right] = \left[\frac{\partial Q_g^t}{\partial \delta} \quad \frac{\partial Q_g^t}{\partial \theta} \quad \frac{\partial Q_g^t}{\partial V} \right] \qquad (5.2.25)$$

The sensitivity of Q_g^t vs. $[P_g \ P_l \ Q_l]^T$ is

$$[\Delta Q_g^t] = \begin{bmatrix} \frac{\partial Q_g^t}{\partial \delta} & \frac{\partial Q_g^t}{\partial \theta} & \frac{\partial Q_g^t}{\partial V} \end{bmatrix} \begin{bmatrix} \frac{\partial \delta}{\partial P_g} & \frac{\partial \delta}{\partial P_l} & \frac{\partial \delta}{\partial Q_l} \\ \frac{\partial \theta}{\partial P_g} & \frac{\partial \theta}{\partial P_l} & \frac{\partial \theta}{\partial Q_l} \\ \frac{\partial V}{\partial P_g} & \frac{\partial V}{\partial P_l} & \frac{\partial V}{\partial Q_l} \end{bmatrix} \begin{bmatrix} \Delta P_g \\ \Delta P_l \\ \Delta Q_l \end{bmatrix} \quad (5.2.26a)$$

$$[\Delta Q_g^t] = J_g^t J^{-1} = S' \quad (5.2.26b)$$

Matrix S' has just one row which consists of active generation and load participation factors

$$S' = \begin{bmatrix} \frac{\partial Q_g^t}{\partial P_{g1}} & \cdots & \frac{\partial Q_g^t}{\partial P_{gn}} & \frac{\partial Q_g^t}{\partial P_{l1}} & \cdots & \frac{\partial Q_g^t}{\partial P_{lm}} & \frac{\partial Q_g^t}{\partial Q_{l1}} & \cdots & \frac{\partial Q_g^t}{\partial Q_{lm}} \end{bmatrix} \quad (5.2.27)$$

from which the set of candidates for load shedding may be selected by forming the load influence factors

$$\Delta Q_i = \frac{\partial Q_g^t}{\partial P_i} \Delta P_i + \frac{\partial Q_g^t}{\partial Q_i} \Delta Q_i \quad (5.2.28)$$

and extract the critical load i having maximum ΔQ_i , or k loads i_1 , ... , i_k (which have maximum sum of ΔQ_i among all loads) such that

$$\Delta Q' = \sum_{j=1}^{k} \Delta Q_{i_j} > \Delta Q^{spec} \tag{5.2.29}$$

the reduction of the reactive generation is greater than the specified quantity ΔQ^{spec} . That does not guarantee that the final value of the Q_g^t will be

$$Q_g^{t'} = Q_g^t - \Delta Q^{spec} \tag{5.2.30}$$

because of the system nonlinearity, but such a load shedding guarantees an improvement of stability margin ($\sigma_{\min}$) if the amount of disconnected load is not excessive to the extent of requiring redistribution of generation.

5.2.3 Selective load shedding

The load control which is to be applied in cases of detected voltage instabilities needs to be very fast and with controlled effects. In extreme circumstances, simple shedding of the whole parts of network identified as main candidates for load shedding is the only solution. It is possible, however, to investigate some forms of load control which may prove useful in power systems with proven record of voltage unstable operation due to heavy loading. One such possibility is direct load control which can be accomplished through communication between control center and individual customers. If such a control were available in the voltage collapse case in Japan in 1987 [131], it could at least be attempted to reduce the

loading level in the system after all the static compensation was switched on and was not enough to prevent further deterioration of the voltage profile in 500 kV network.

Among load control techniques, direct load control is very attractive because it represents the potential to control the system loading level much before it reaches dangerous zone. A typical configuration consists of the master controller placed in the control center and a large number of individual controllers placed in customers' residences. Controllers may act on one, or more types of loads (i.e. different types of appliances) and have different control cycles for them based on loading profile of the system. One controller is capable of controlling several types of loads and even operate independently from the master controller, which does not need to provide the synchronization signal after controller is set up by a master controller. The smoothness of control is accomplished through division of a big group of customers into large number of small blocks, controlled asynchronously. An important task which smart controllers could perform is the acquisition of historical trends of loading within their zones of control. That function may be very useful for master controllers, which could than formulate control strategies based on fresh statistical system loading data and effectively avoid overloading system conditions (voltage collapse in Japan was mainly caused by uncontrolled loading of the system by the air conditionning equipment with a very stiff voltage characteristic).

A typical communication system between the master controller and individual controllers is established by VHF/FM radio channels operating at High Band (144 to 174 MHz). This choice of frequency is popular because it allows very economic design of the receivers. As pointed out in [133], there were 225 programs of direct load control in the US in 1986. Out of them, 155 programs were using VHF/FM radio communication. Out of 2.5 million controlled load points, 79% were communicating with master controllers through VHF/FM.

Possible strategy which could be used for direct load control in the systems operating near voltage stability limit could incorporate sensitivity analysis of voltage collapse proximity indicators and emphasize shedding of loads in zones which are identified as critical for voltage stability. If such a control were not enough to provide a safe stability margin, the extent of shedding may be intensified by the master controller up to the full shedding of some zones. The analysis presented in this chapter was done with the intent to promote direct load control as a routine way to control voltage stability based on real- time phasor measurements.Effects of static compensation will be investigated in the next chapter.

5.3 Simulations and Comments

The algorithms presented in the previous section will be briefly illustrated by examples and simulations done on a 39-bus test system in critically stable operating regions near voltage stability boundary.

Figure 61 represents sensitivities of the minimum singular value of load flow Jacobian matrix with respect to active and reactive parts of the individual loads. The system state in which the sensitivity is investigated is obtained by proportional increase of both active and reactive parts of loads through multiplier k (phasor diagram of that state is given in Figure 12 and that state was used as initial system state for dynamic simulation of voltage collapse shown in Figures 18 and 25). It is noticable that sensitivities of the minimum singular value vs. active portions of loads is bigger than sensitivities vs. reactive portions for almost all loads. Sensitivities are expressed in unitless form [pu/pu] which represents an equivalent change of minimum singular value per unit change of loads. Figure 62 shows cumulative sensitivities vs. individual loads (both active and reactive parts). It is relatively easy to visually detect the zone of high sensitivity (loads 4 through 8). The following list represents the set of candidates for load shedding based on the sensitivity analysis of minimum singular value of Jacobian and their share in the total sum of participation factors vs. all loads:

Load: 8, participation: 6.75%

Loads: 8,7, participation: 13.28%

Loads: 8,7,4, participation: 19.06%

Loads: 8,7,4,5, participation: 24.44%

Loads: 8,7,4,5,6, participation: 29.36%

It can be noted that nonzero sensitivities are associated with some zero loads (loads 5 and 6 are zero loads). The interpretation of this observation is simply that any changes (increases) of loading at those buses would have a pronounced effect on the changes of the minimum singular value of Jacobian, but those buses obviously cannot be considered for load shedding.

Figures 63 and 64 show the voltage profile of the test system without any load shedding, after elimination of the most critical load (8), and after elimination of loads (8,7). The shedding of load 8 produces a substantial improvement of voltage profile (from 0.7 pu up to 0.9 pu on the most heavily loaded buses). The improvement of voltage profile after subsequent shedding of load 7 is nowhere near the extent of improvement of the shedding of load 8 alone, which suggests that the optimal emergency control consists of shedding load 8. Figure 64 represents voltage profile for the three cases explained above, but with voltage buses ordered by increasing magnitude for each particular case. It shows more obviously the change of voltage profile after load shedding. In terms of the values of proximity indicator σ_{min} , a case without shedding has $\sigma_{min} = 0.07065$ with a condition

number of Jacobian of 70631.02 . Shedding of load 8 alone improves it to $\sigma^{8}_{min} = 0.57817$ with much better condition number 1474.91 , while additional shedding of load 7 makes $\sigma^{8,7}_{min} = 0.59388$ with condition number 1513.01 . The increase of the condition number in this last case suggests that redistribution of generation is needed for system to settle in optimal conditions for that level of loading.

Figures 65 and 66 show the sensitivity analysis of minimum singular value in the case when loading was accomplished through increase of reactive power requirements only. This case was also shown to induce voltage collapse (Figures 30-33). Load participation factors are much more concentrated in the region of loads 4-8 with the addition of load 12, which is the critical load for this loading situation. Participation factors of reactive portions of loads are much bigger in this case than participation factors of the active portions. Critical loads and their share of the total sum of participation factors are

Load: 12, participation: 7.72%

Loads: 12,8, participation: 15.24%

Loads: 12,8,7, participation: 22.36%

Loads: 12,8,7,4, participation: 28.21%

Loads: 12,8,7,4,5, participation: 33.53%

The effect of shedding load 12 alone and loads 12 and 8 is shown in Figures 67 and 68. The case when no shedding is done corresponds to $\sigma_{min} = 0.12879$ and condition number of Jacobian 3343.74 . Shedding of load 12 produces $\sigma_{min}^{12} = 0.44067$ and condition number 1367.98 . After additional shedding of load 8, $\sigma_{min}^{12,8} = 0.56959$ and condition number 1482.43 . It should be noted that load 12 is $S_{12} = 0.085 + j4.017$ while load 8 is $S_8 = 5.220 + j8.062$, yet elimination of load 12 produces more improvement in the voltage profile (Figure 68) than elimination of load 8.

Figures 69 and 70 show the sensitivities of the minimum singular value vs. loads in the normal operating regime. Although the sensitivities are typically two hundred times smaller than those near stability boundary, their relative values indicate that the largest sensitivities are associated with loads which were found to be critical in voltage unstable cases. This observation suggests that early applications of the sensitivity test, when the system is still far from the stability boundary, may as well be used to intensify direct load control of critical loads during loading and prevent occurrence of critical conditions and crossing of the system state into the emergency zone where complete load shedding is required.

Sensitivity tests of generated reactive powers of critical generators as well as total system reactive generation give almost the same sets of critical loads as the ones performed on the minimum singular values of Jacobian. Figures 71, 72 and 73 show the reactive powers generated by all 10 generators of the test system for the first studied case (uniform loading of both active and reactive parts of all loads),

second case (uniform loading of reactive parts of loads only) and the case when loading was uniform on both active and reactive loads, but reactive generation was constrained on some generators (case whose development was shown in Figure 29). The substantial reduction of reactive generation is noticeable, particularely on machines 2 and 3, which are critical in both unconstrained cases, while only machine 2 is critical in the case when reactive generation constraints are observed, since five of the other generators have reached limits (generators 1,3,4,6,7). The load bus voltage profile for the third case is shown in Figure 74, with voltage profile after elimination of loads 8 and both 8 and 7, which were again found to be critical in this case.

Normalized load participation factors for the total reactive generation in the range of load factors (uniform loading of active and reactive portions of loads) are shown in Figure 75 for four of the most critical loads (8,7,4 and 9). Normalized load factors represent the share of absolute load factors in the total sum of load factors. It can be noticed that active load participation factors are uniformly increasing with the loading level while the share of reactive load factors is uniformly decreasing with loading and changes trend just before the critical level. Figure 76 shows cumulative effect of normalized load factors for the four critical loads and cumulative effect of active and reactive normalized sensitivities. Combined cumulative effect of normalized load factors shows a tendency to rise near collapse (this can be interpreted as a tendency that the critical loads become more critical as the system is approaching bifurcation). This property is shown with more detail in Figure 77, where normalized reactive load sensitivity factors are

shown for a range of load factors very near bifurcation. The share of those four reactive loads in the total sum of sensitivity factors is increasing very sharply as the system is approaching bifurcation. This observation and the results of previous analyses indicate that one load region of the test system studied is very vulnerable to the increase of loading. That region is lightly shaded in Figure 78. There is also a grup of generators which is the most sensitive to increase of loading, shown dark shaded in Figure 78. Even before the critical conditions are encountered in the system, those regions may be determined by simulation and their situation taken care of in the planning stage (increasing active and reactive generation capacity, if possible and provide an effective load control in the critical load regions).

5.4 Conclusions

A sensitivity analysis of the minimum singular values of Jacobian was used to determine critical sets of loads, defined as those loads whose changes have the most profound effect on the changes of minimum singular value of load flow Jacobian. An algorithm was used which numerically determines the load participation factors and selection of the most critical loads made by selection of those loads which have the largest participation factors.

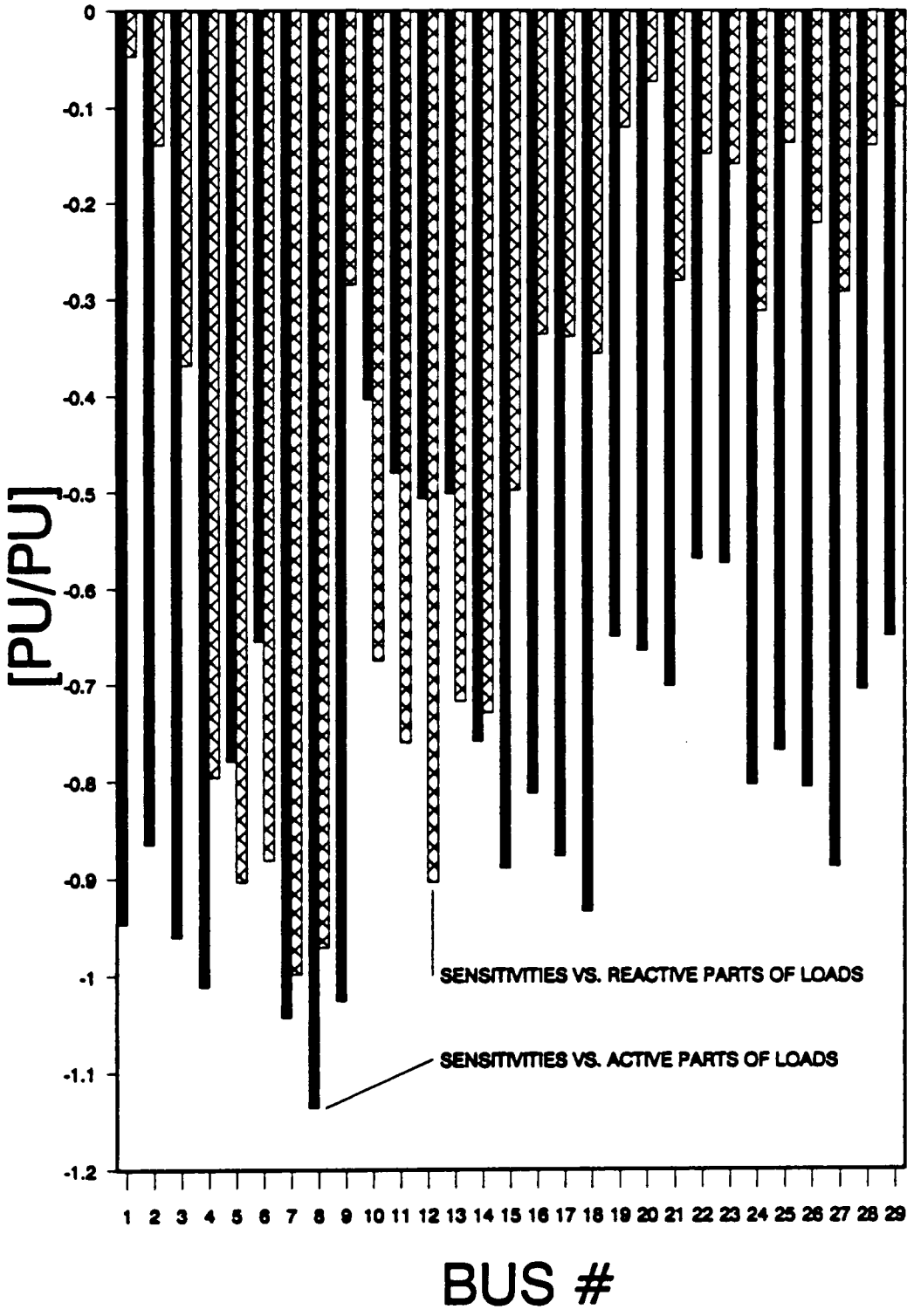

Figure 61. Load participation factors vs. minimum singular value (PQ loading).

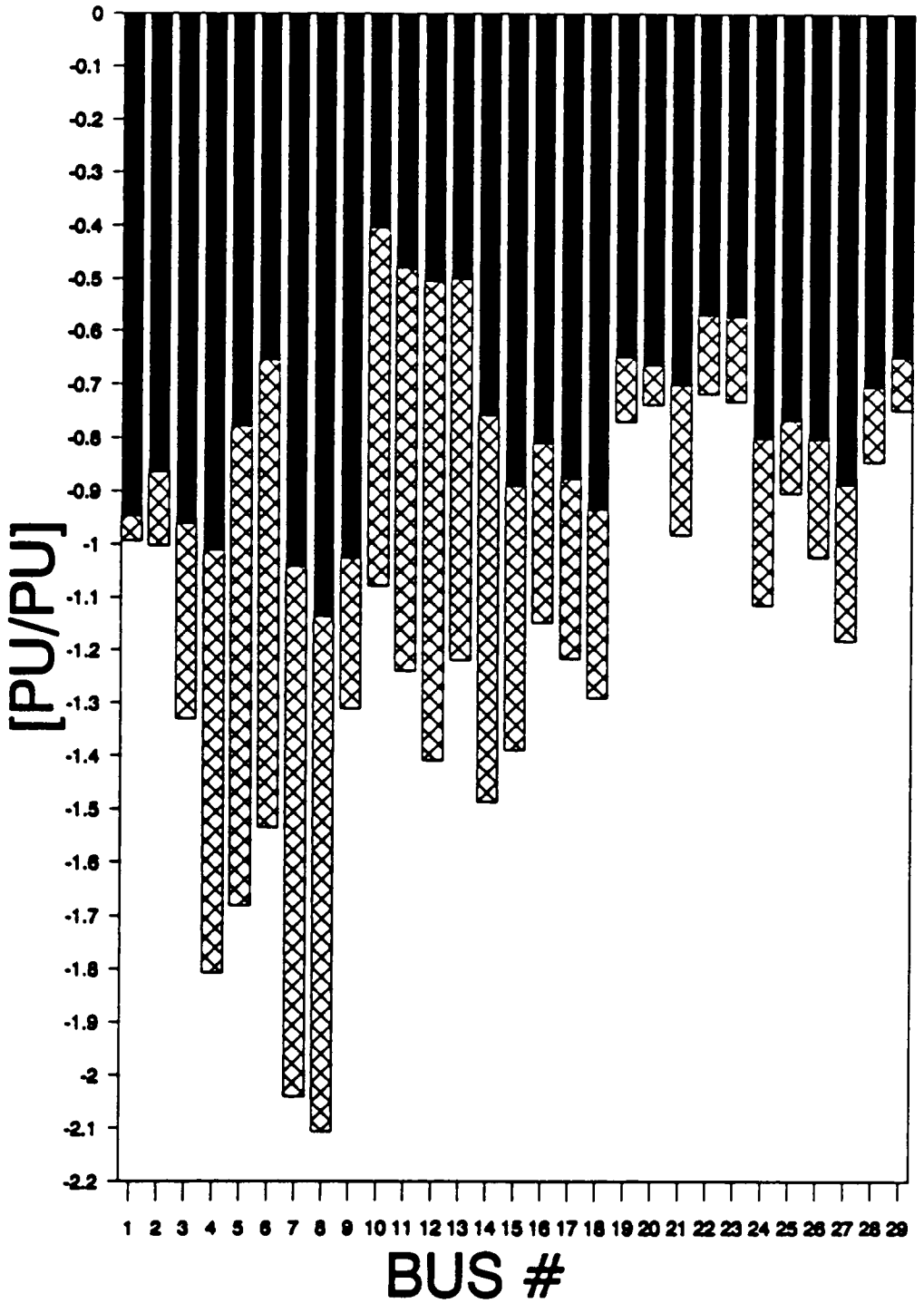

Figure 62. Cumulative load participation factors corresponding to Figure 61.

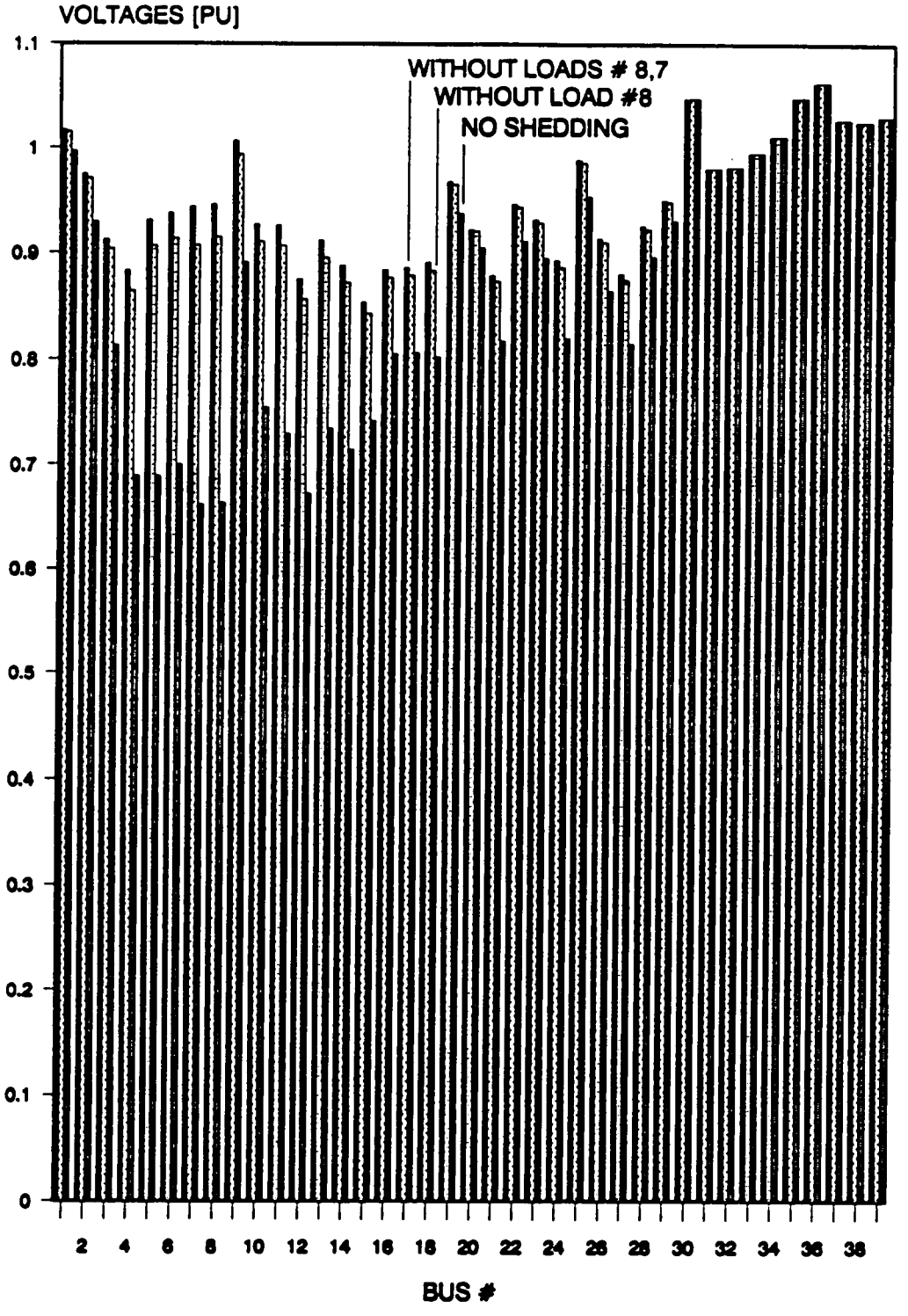

Figure 63. Voltage profile before and after load shedding (PQ loading).

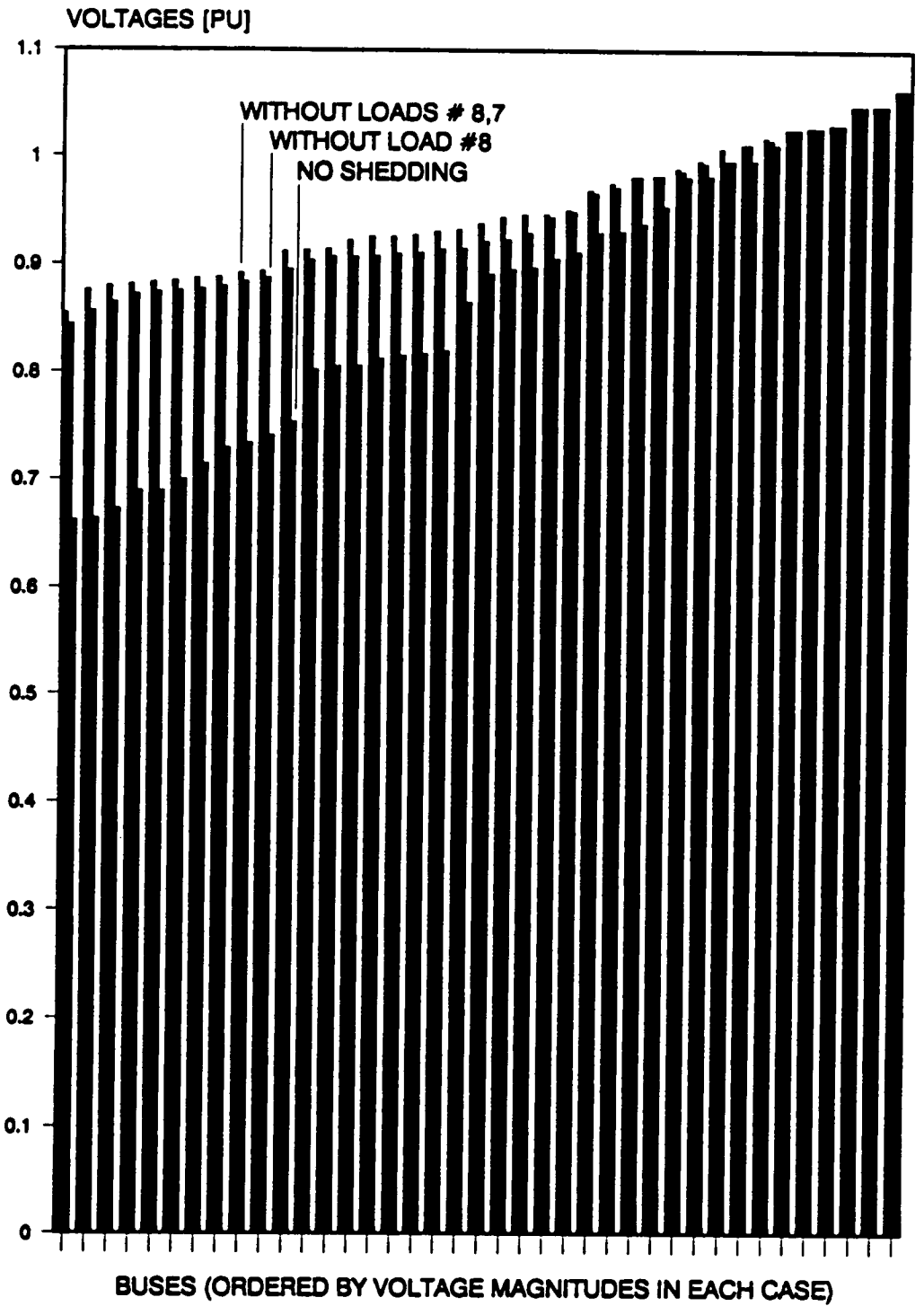

Figure 64. Voltage profile of Figure 63 with voltage magnitudes ordered.

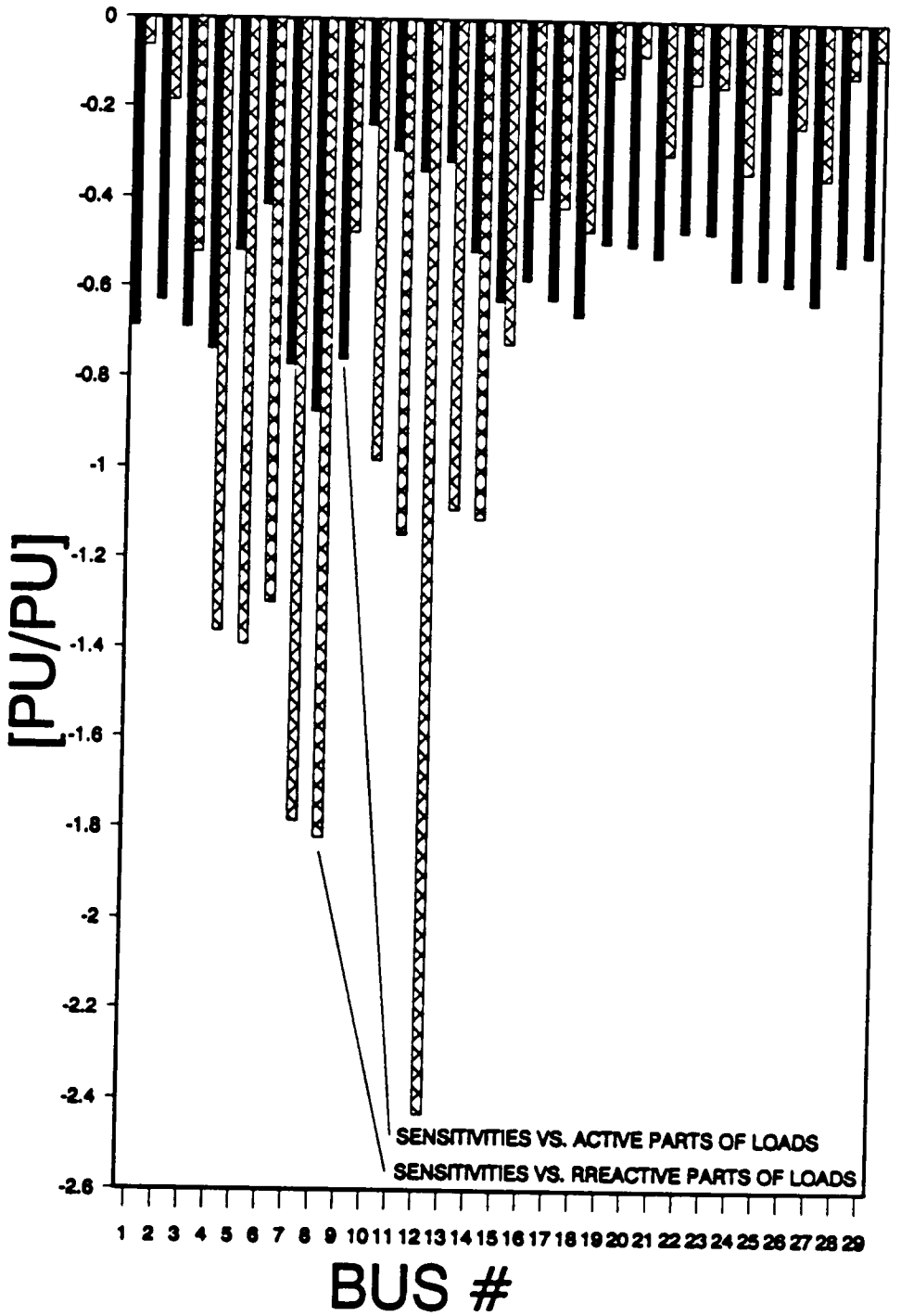

Figure 65. Load participation factors vs. minimum singular value (Q loading).

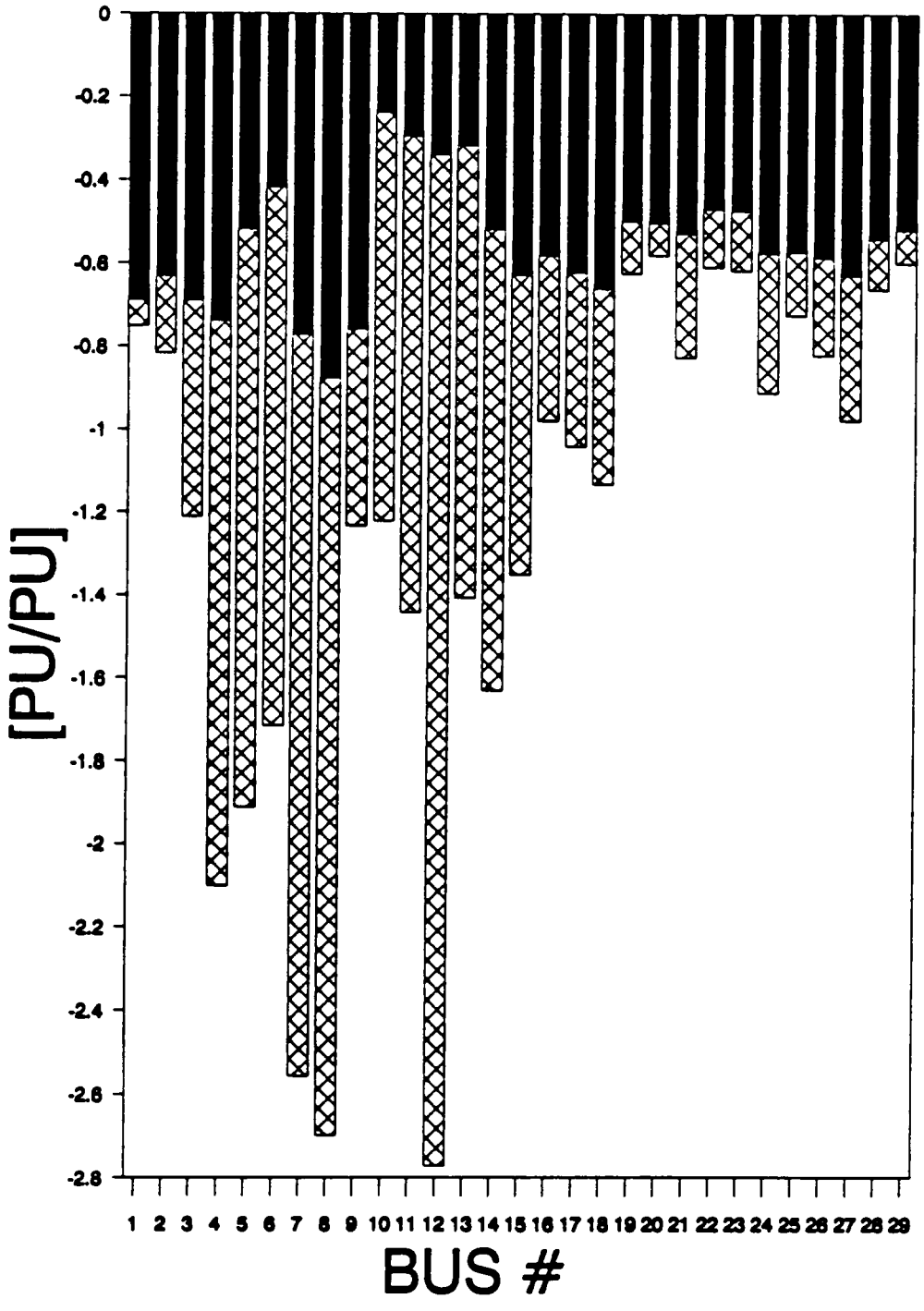

Figure 66. Cumulative load participation factors corresponding to Figure 65.

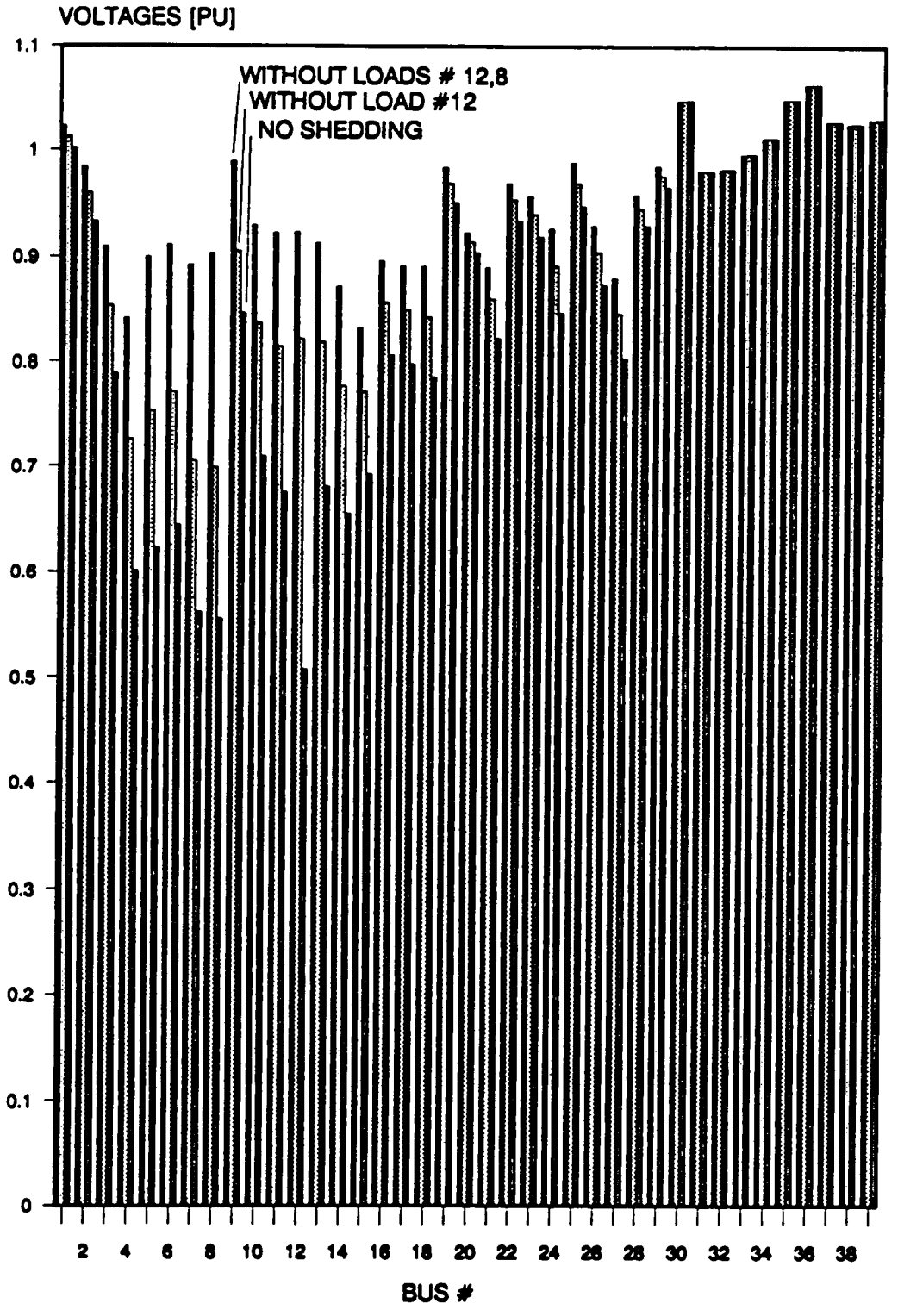

Figure 67. Voltage profile before and after load shedding (Q loading).

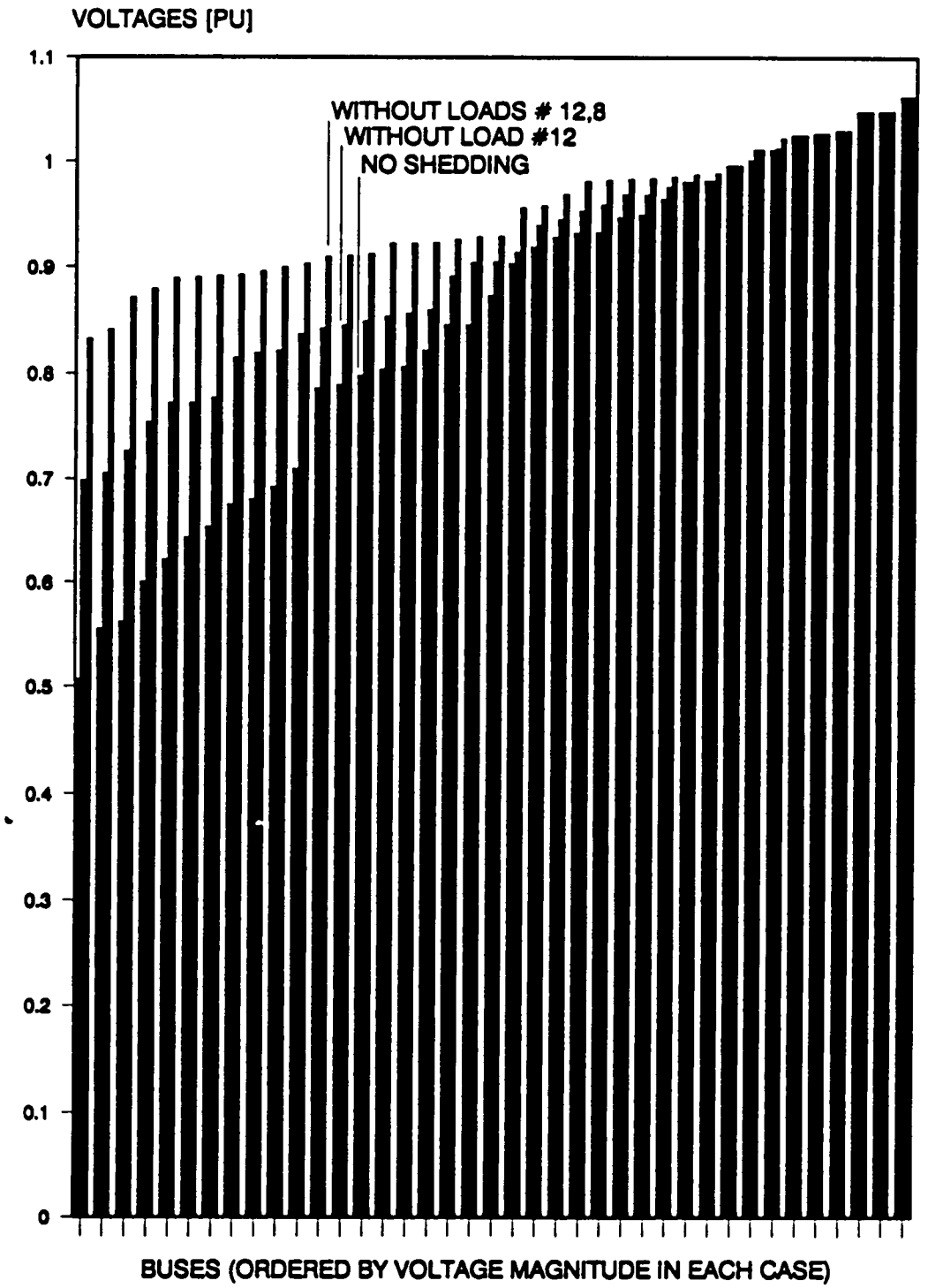

Figure 68. Voltage profile of Figure 67 with voltage magnitudes ordered.

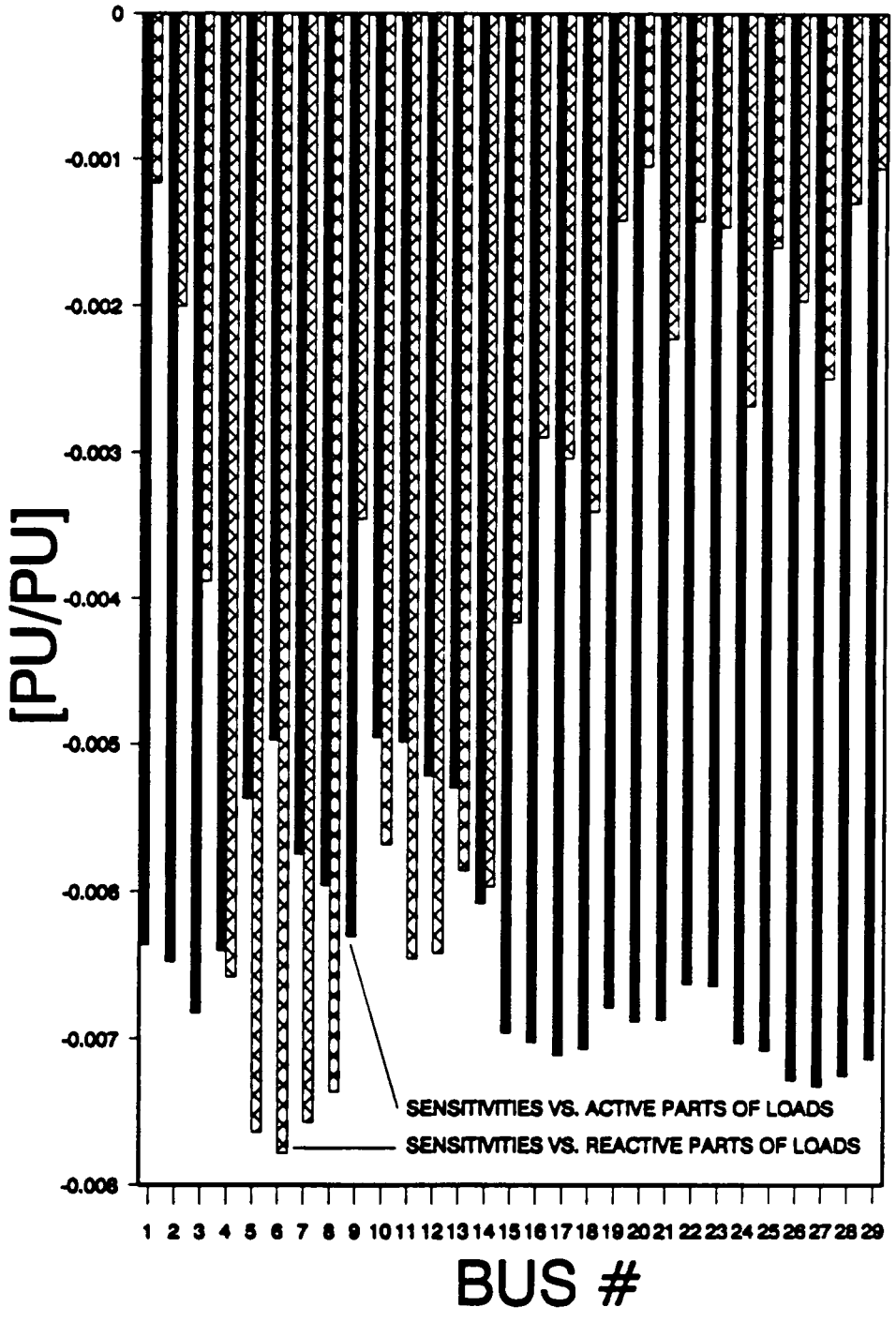

Figure 69. **Load participation factors vs. min. singular value in normal state.**

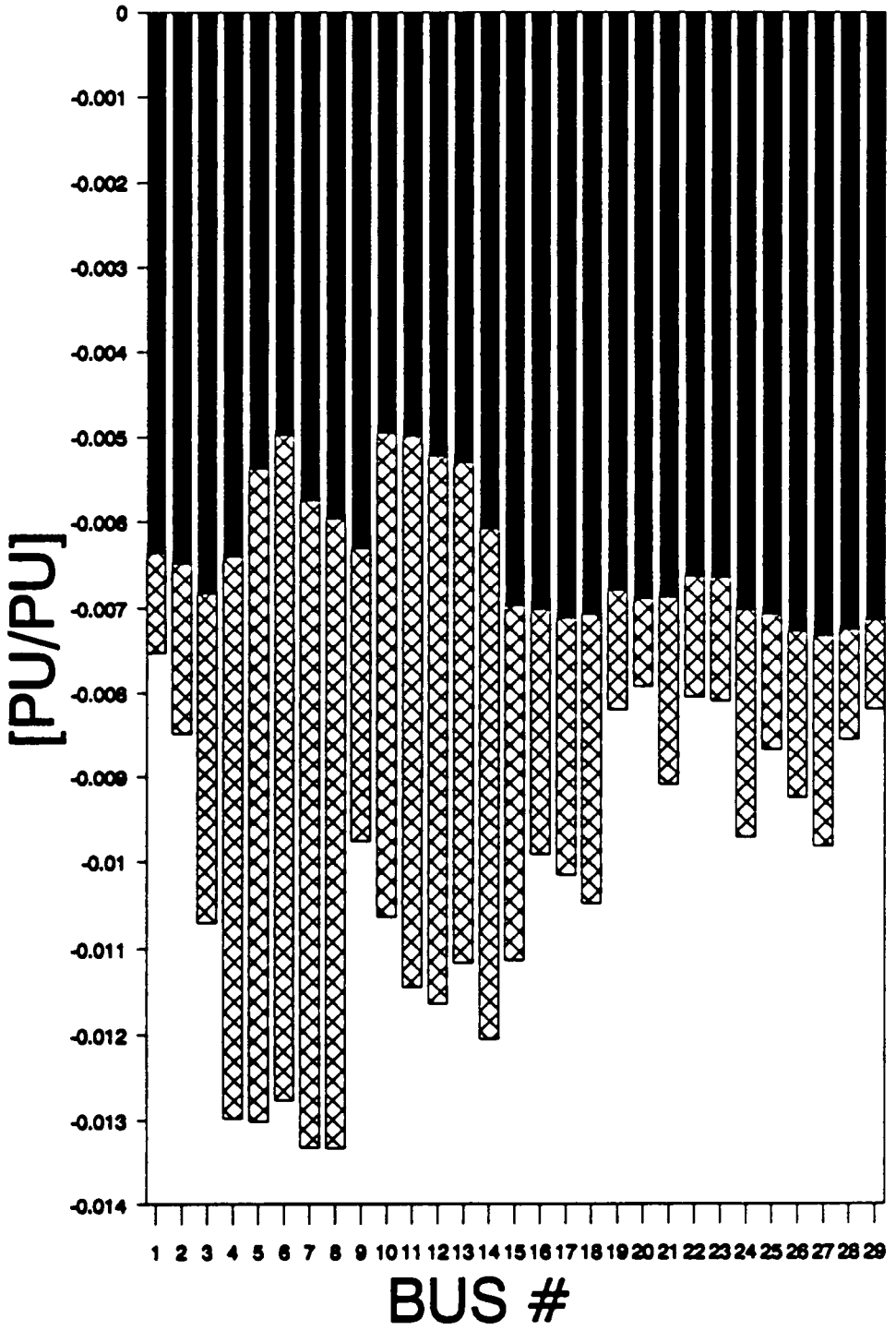

Figure 70. Cumulative load participation factors corresponding to Figure 69.

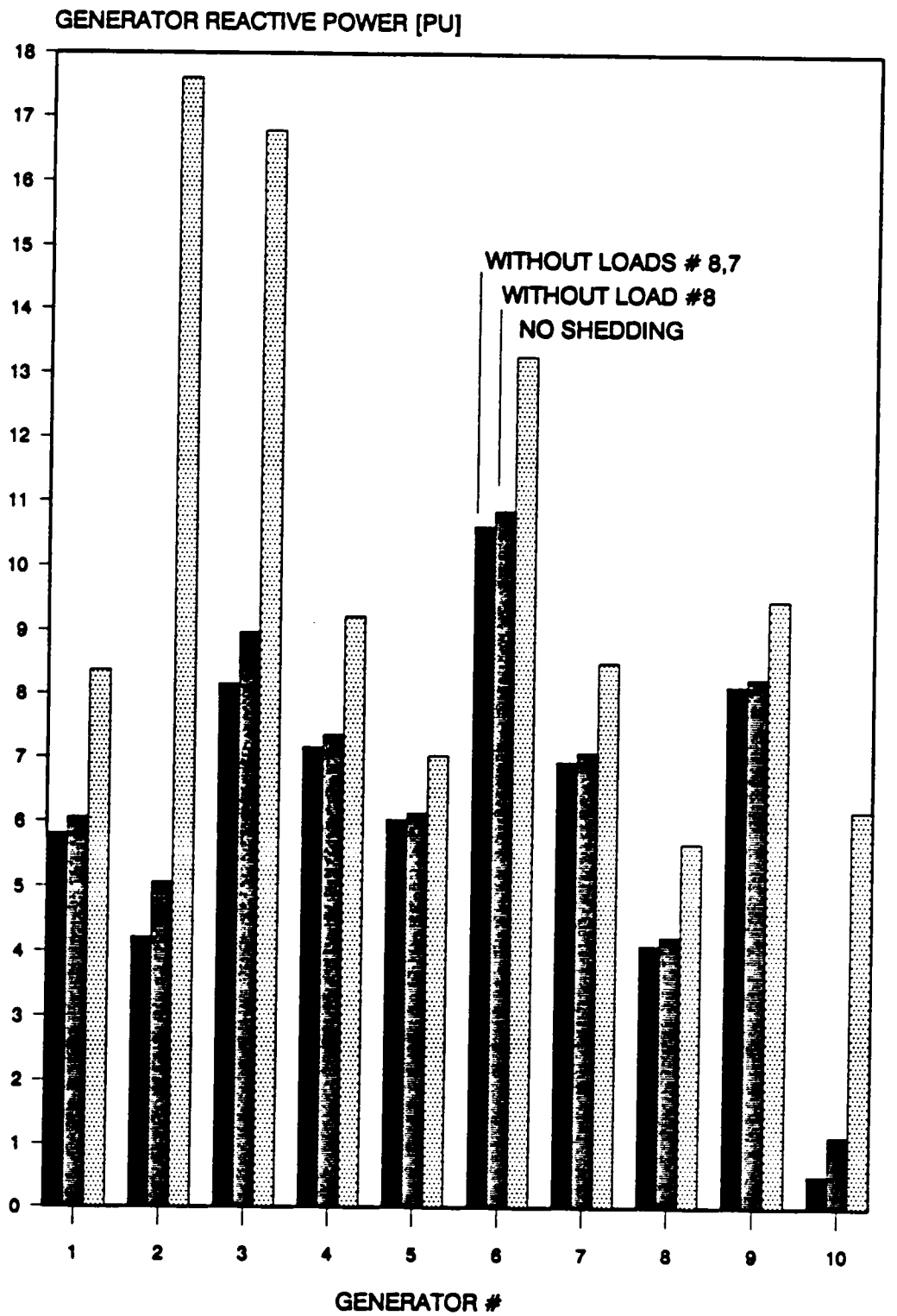

Figure 71. Reactive generation for critical state and load shedding (PQ loading).

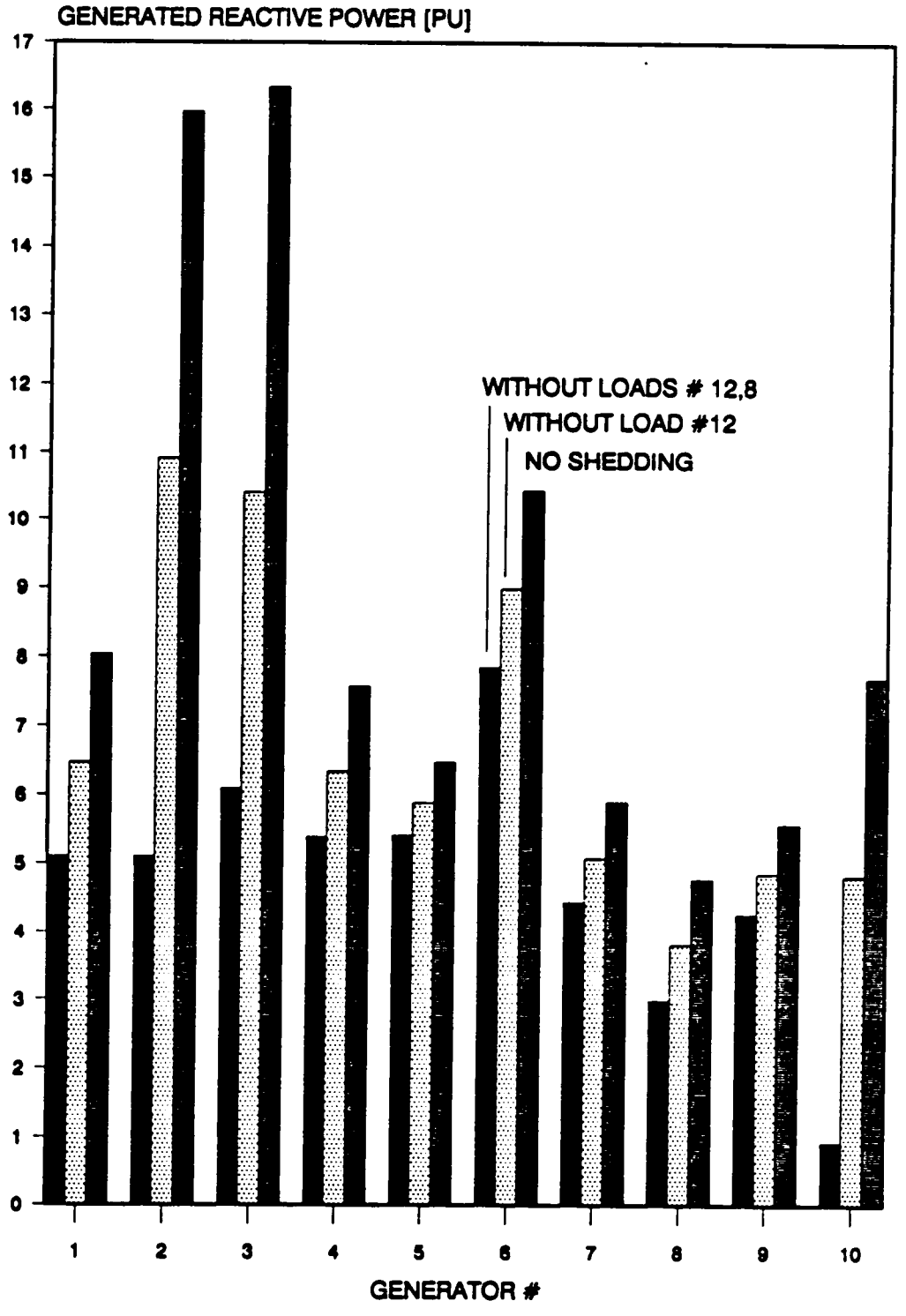

Figure 72. Reactive generation for critical state and load shedding (Q loading).

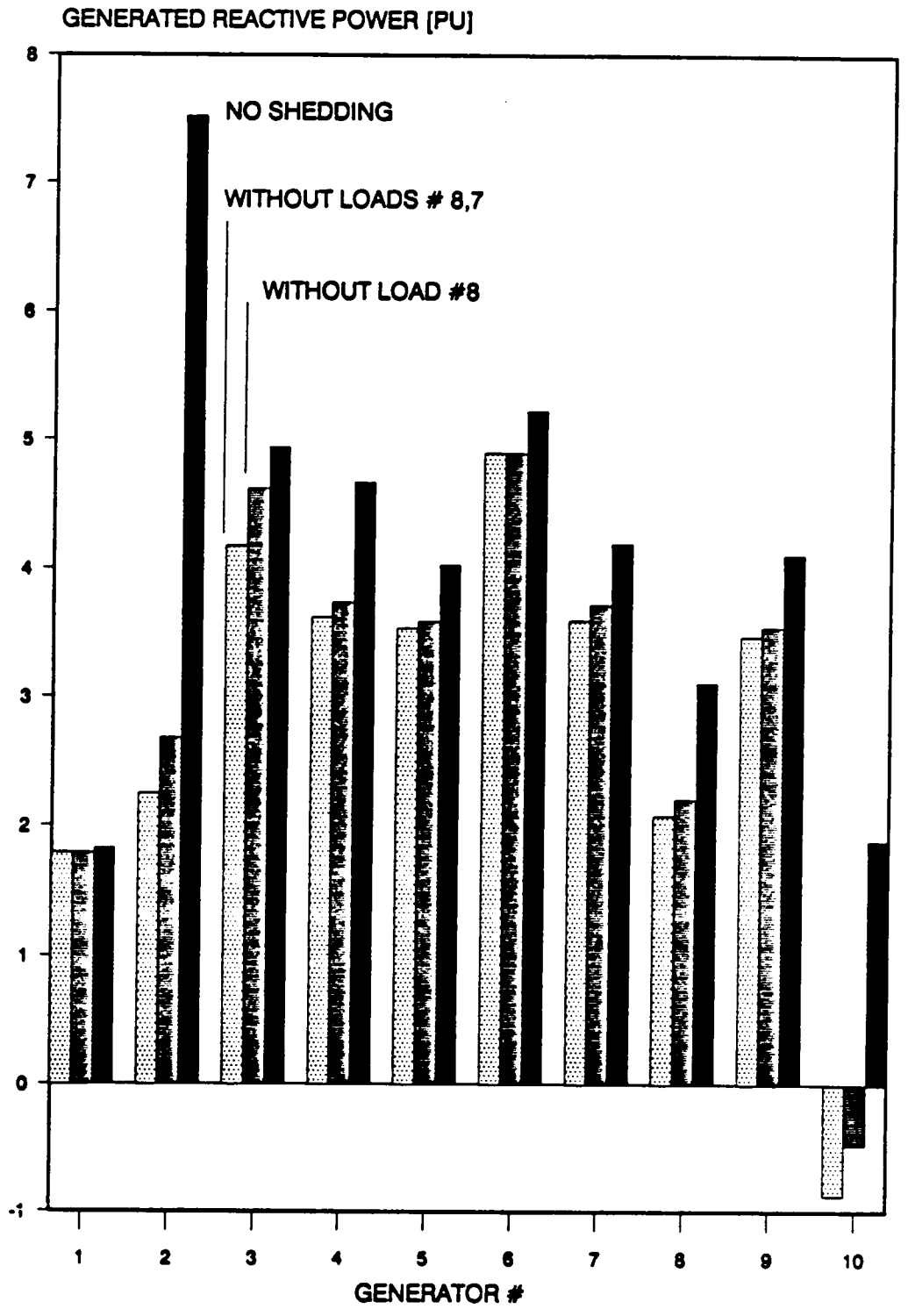

Figure 73. Reactive generation for critical state and load shedding (PQ constrained loading).

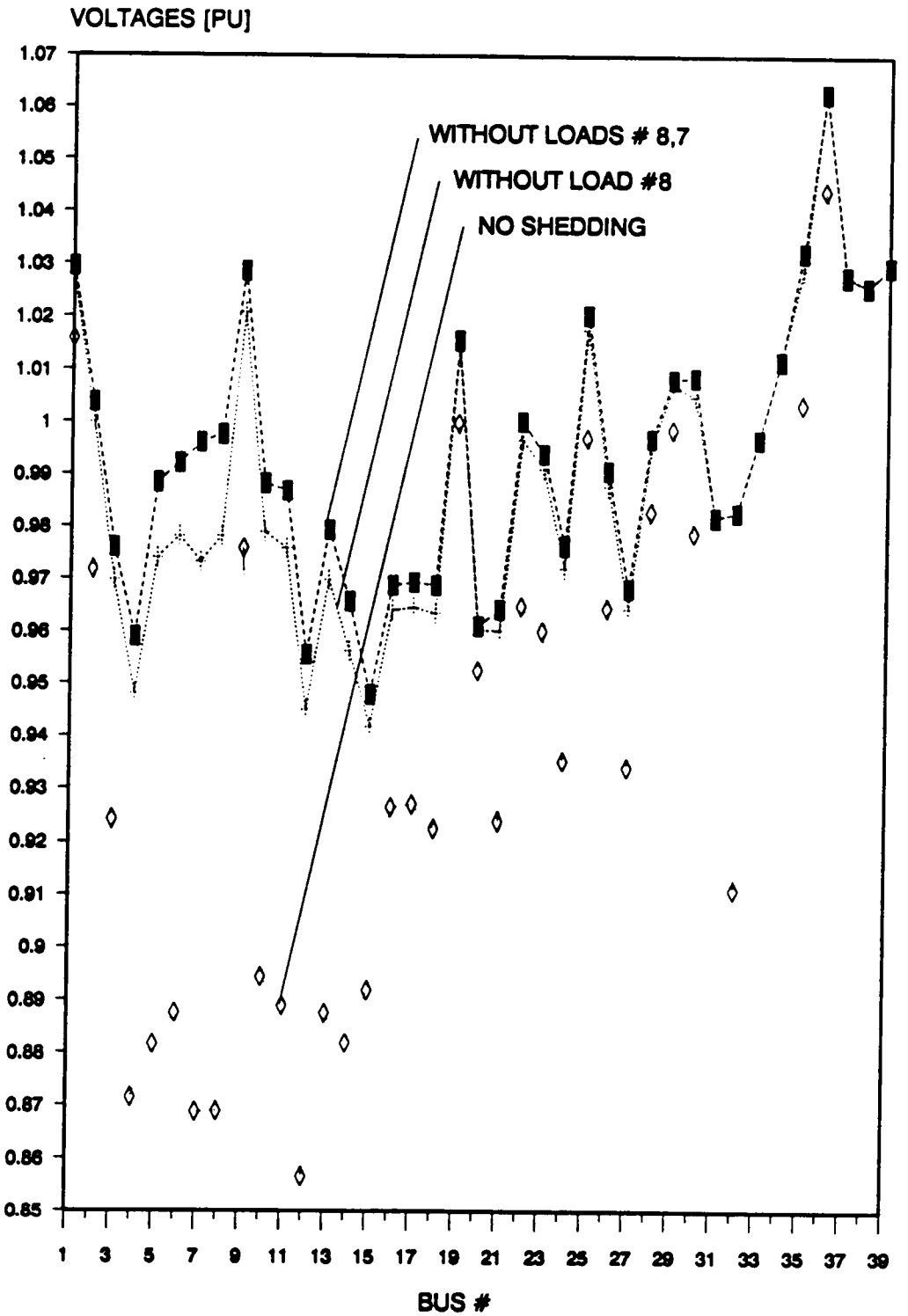

Figure 74. Voltage profiles for critical case and load shedding with PQ constrained loading.

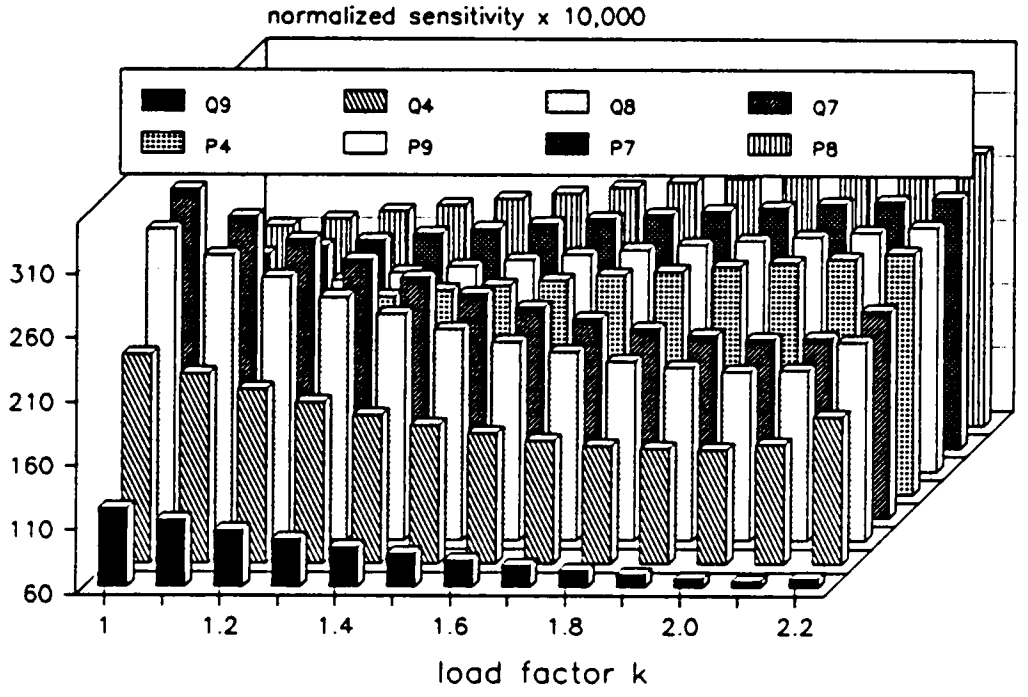

Figure 75. Critical load participation factors vs. total system reactive generation.

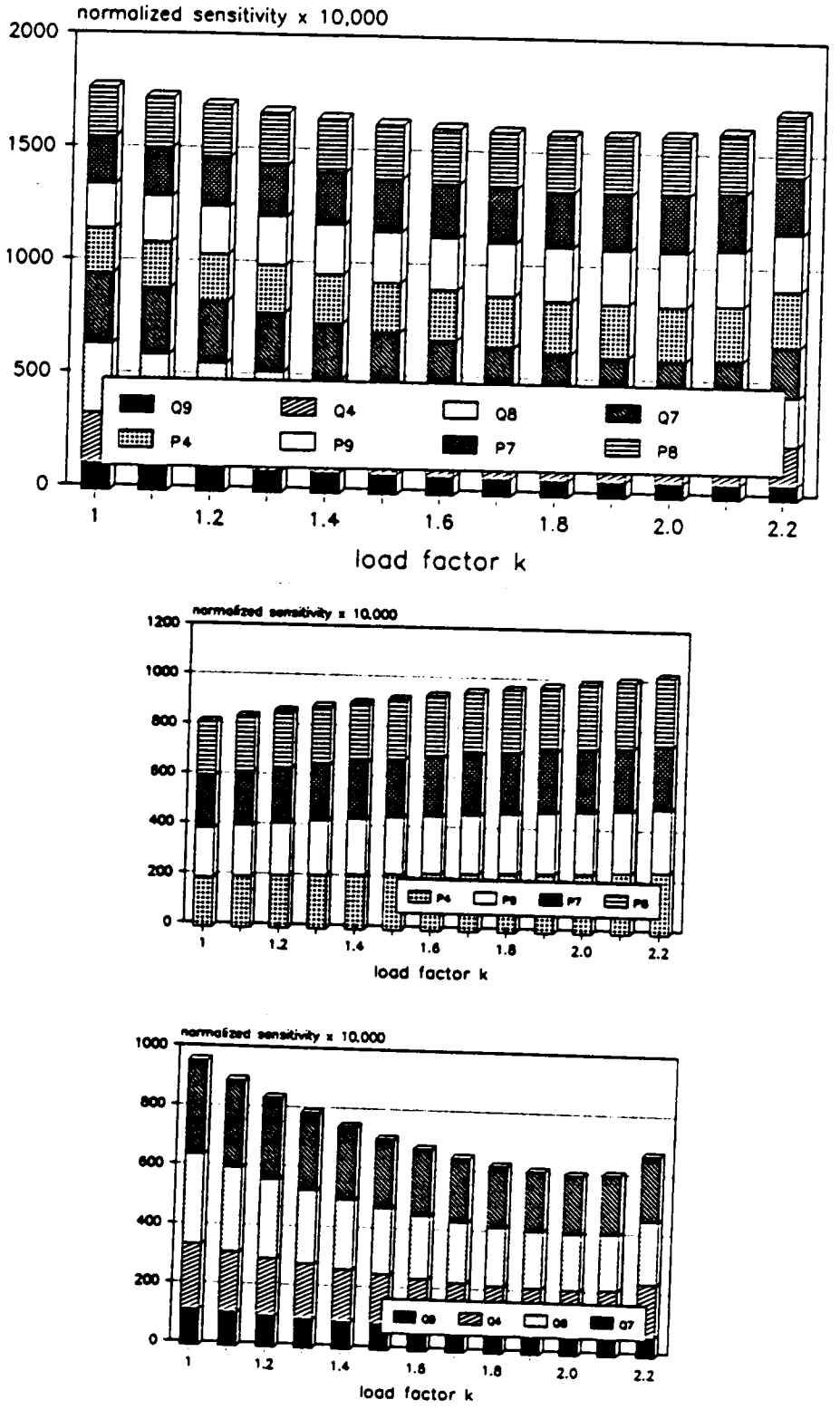

Figure 76. Cumulative critical load participation factors vs. total reactive generation.

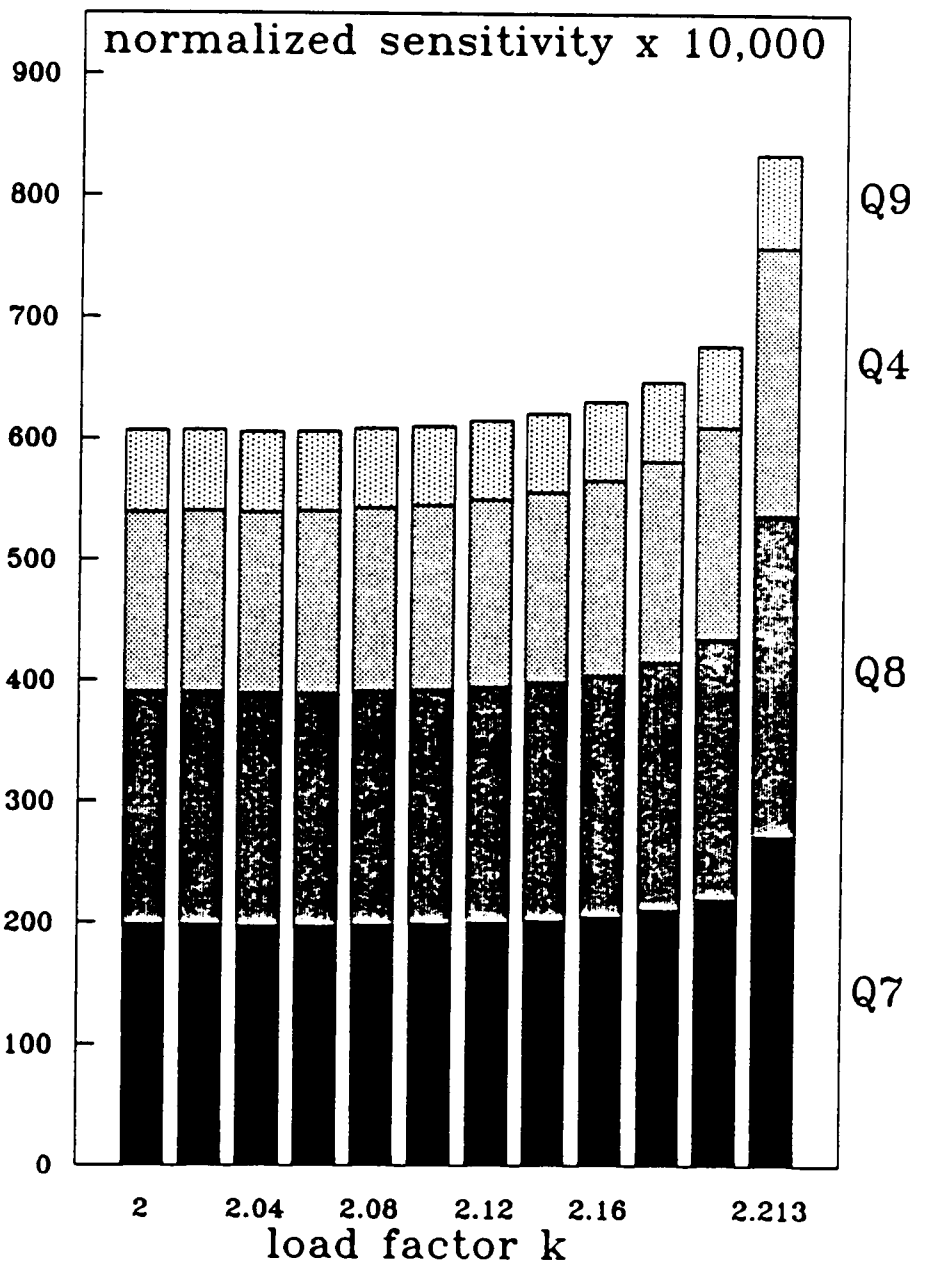

Figure 77. Reactive critical load participation factors near stability boundary.

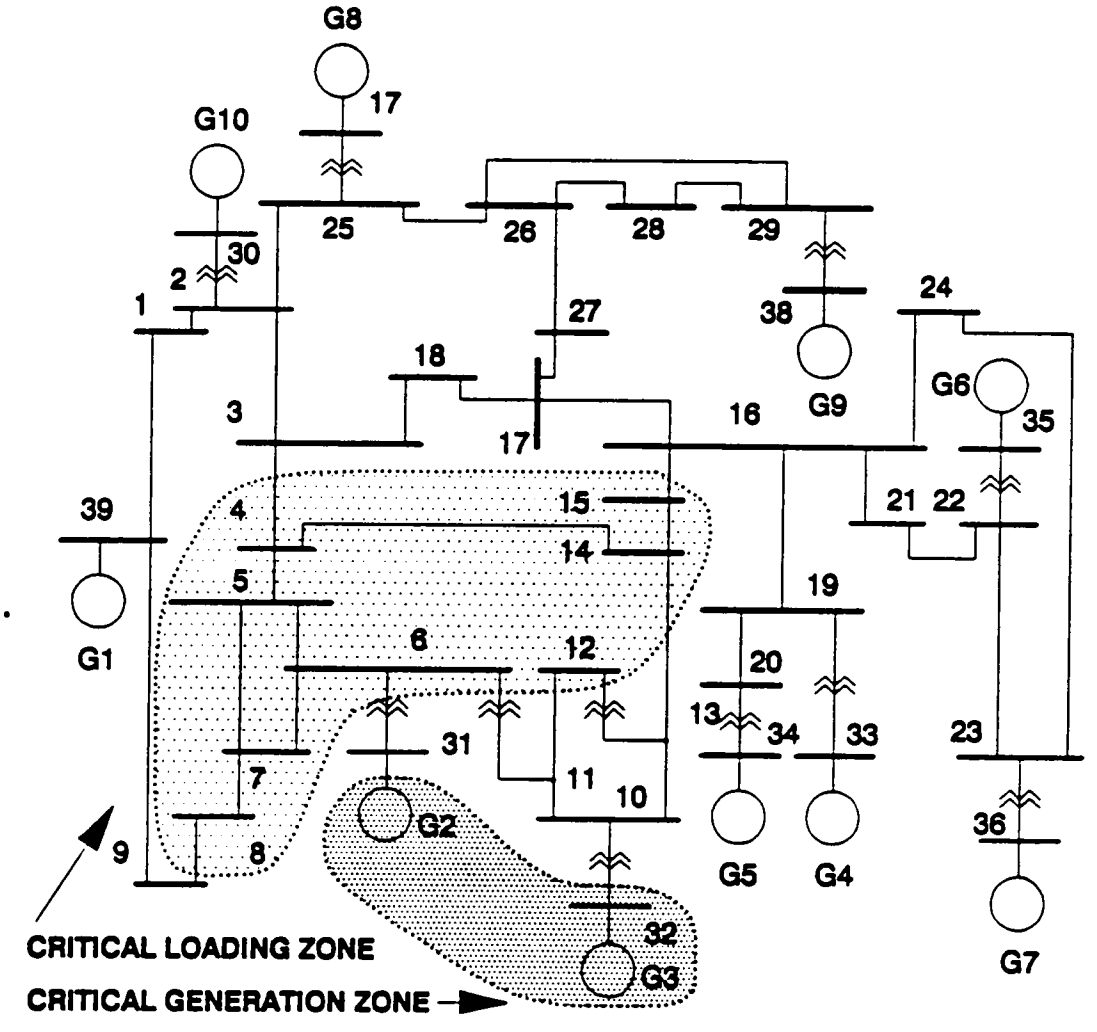

Figure 78. Test system with critical loading and critical generation zones.

Similar numerical sensitivity analysis was performed on the reactive powers generated by critical machines (those generators whose reactive outputs are the largest) and choice of critical loads accomplished by selection of those loads whose participation factors were the largest. Simulation results have proved that both methods are good and give identical results for all practical purposes, since the shedding of too many loads is not advised as an emergency control. If local generation (i.e. alternative energy sources) is available, it would reduce voltage stability problems in the system.

The objective to produce the algorithm for identification of critical loads which would not bear a heavy computational burden for real-time applications lead to proposal of two more procedures, both based on calculation of sensitivity matrix of generated reactive powers (total generated reactive power in the system) with respect to changes of loads. This was accomplished by multiplying the Jacobian of the system of equations which define the reactive power generation (total reactive power generated in the system) with the inverse of Jacobian in a given operating state. The state is proposed to be acquired by a fast real-time phasor measurement system. The calculation of the sensitivity matrix does not require more than one matrix inversion and one matrix multiplication, which makes it appropriate for real-time operation.

The results obtained by simulations are encouraging and suggest that further research in the application of the proposed algorithms in large scale systems would be useful.

Chapter 6. Voltage Stability and Static Compensation

6.1 Introduction

When conditions are detected which indicate that power system is approaching voltage instability, a control action must be applied to move the system state away from stability boundary. An emergency control based on identification and shedding of critical loads was proposed and investigated in previous chapter. The possibilities for control are not limited to remote load control or (more drastic) complete load shedding on buses where voltage collapse proximity indicators are most sensitive. It was established earlier (Figures 28 and 29) that voltage collapse is accompanied by a precipitous rise of reactive power generation. It is interesting to investigate the effects which var compensation may have on voltage stability boundary, because such compensation, if available, would allow the system to

return to secure operating region by moving the stability boundary away rather than moving its state from the boundary by restricting the load level.

In general, var compensation encompasses various types of compensation divided into two main groups: static var compensation and rotating var compensation. Rotating var compensators are synchronous condensers and all var generators which have rotating parts. Static var compensators are characterized by a lack of moving parts in generators of reactive power. General types of static var compensators are: i) Mechanically switched capacitors and reactors (which allow discrete active control); ii) Saturated reactors (which allow continous inherent control); iii) Thyristor controlled reactors (which allow continous active control); iv) Thyristor switched capacitors and reactors (which allow discrete active control).

Modeling of static compensation is relatively simple and in most cases it is sufficient to create networks of switches, capacitors and reactors. It can easily be incorporated into power system models for both static and dynamic analyses.

Various applications include voltage control, load balancing, increasing power transfer capacity, increasing transient stability margin, damping of power oscillations, subsynchronous resonances etc. Our primary concern is the application of SVC to extend the voltage stability margin. The appropriate type of var compensators for that purpose are static var compensators (mechanically, or

thyristor switched capacitor banks). One typical installation is shown in Figure 79.

Since capacitors are normally built for operating voltages under 50 kV, capacitor banks are usually connected to HV and EHV networks through transformers. They can be modeled as linear elements generating active losses of the order of $1 - 5$ percent of their var rating. Their response times are of the order of 0.1 s. The effect of inclusion of capacitor banks in power systems may be modeled as an addition of a certain amount of shunt capacitance to compensated load buses in load flow studies, when their control is discrete. If they are controlled continously, or quasi-continously, then their action may be regarded as tranformation of $P - Q$ buses into $P - V$ buses for a certain range of generated reactive powers which correspond to the minimum and maximum amount of compensation.

The objective of our study is to investigate:

i) The choice of optimal locations for SVC.

ii) The amount of compensation needed for certain displacement of stability boundary.

Since this study does not take into account the other possible SVC functions in power system, it should be regarded as analysis of one aspect of SVC application and not as a recommendation for design of an integrated SVC control system.

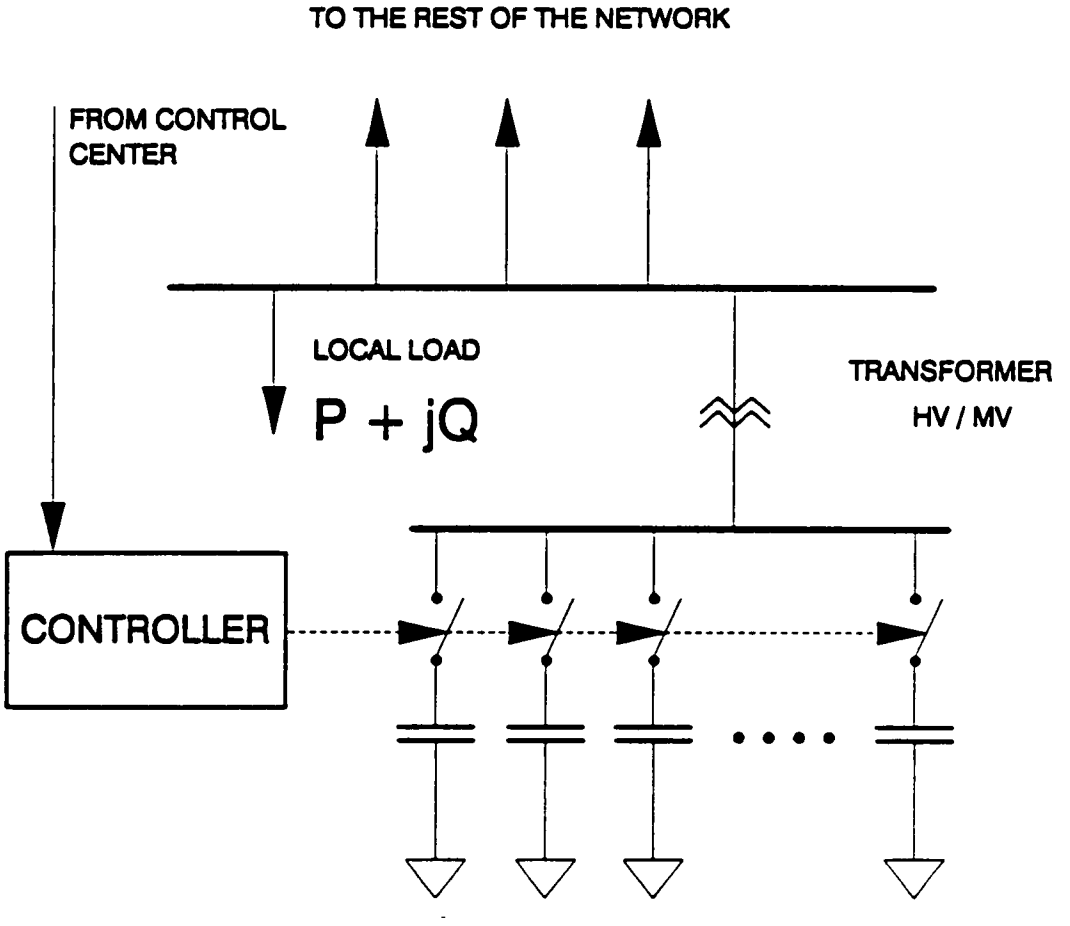

Figure 79. Static var compensation on a load bus.

We assume that a certain amount of static compensation is available at certain locations (whose convenient choice we investigate) and we would like to know how far can we extend the stability boundary by applying all the SVC available at those locations. Defined this way, the objective of our study does not require the continous adjustment of SVC and it can therefore be modeled as shunt capacitance at load buses which retain their constant $P-Q$ property. If central processing computer (which collects on-line phasor measurements data from local microcomputers) has communication links to controllers which regulate the SVC action, then SVC may be integrated into a systemwide centralized voltage stability control system.

6.2 *Sensitivity Analysis of Proximity Indicators*

Let us consider a simple power system model which consists of a generator and a constant P-Q load connected by a transmission line of reactance X . Let V_s be the sending end voltage and V_r the voltage at the receiving end of the line. Let the quantity ξ represent the phase angle difference across the transmission line and $S = P(1 + jk)$ the power consumed at the receiving end. Simple manipulation with the expressions for active and reactive power transfer

$$\begin{aligned} P &= \frac{V_s V_r}{X} \sin \xi \\ Q &= \frac{V_s V_r}{X} \cos \xi - \frac{V_r}{X} \end{aligned} \tag{6.2.1}$$

provide the analytical expressions for high and low voltage solutions with respect to the value of the consumed active power P

$$V_r^h = \sqrt{\frac{V_s^2}{2} - kPX + \sqrt{\frac{V_s^4}{4} - PX(PX - kV_s^2)}}$$
$$V_r^l = \sqrt{\frac{V_s^2}{2} - kPX - \sqrt{\frac{V_s^4}{4} - PX(PX - kV_s^2)}} \qquad (6.2.2)$$

Figures 80 and 81 show dependence of high and low voltage solutions for various values of P with k taken as parameter through which the power factor is changed. Numerical values used in this example are $V_s = 1.0\ pu$ and $X = 0.4\ pu$. The points of maximum power transfer are those where high and low voltage solutions are equal, i.e.

$$\frac{V_s^4}{4} - PX(PX - kV_s^2) = 0 \qquad (6.2.3)$$

Depending on the power factor of the load, maximum power transfer capability is changing between 0.55 pu (for $k = 1.0$) to 1.25 pu (for $k = 0.0$) and above 1.90 pu (for $k = -0.45$). It is interesting to note that capacitive loads (obtained for negative values of k) produce a voltage rise at the receiving end for a wide range of loading levels. That may lead into unjustified belief that the system is becoming more stable while it is in fact approaching bifurcation which may occur at very high level of the receiving end voltage (over 0.9 pu in some cases).

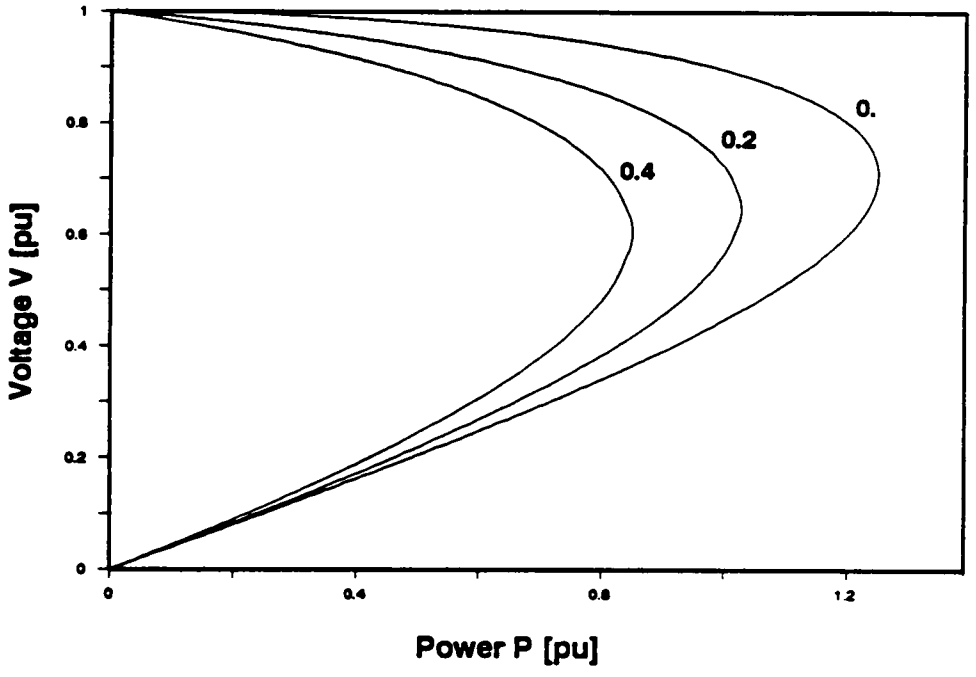

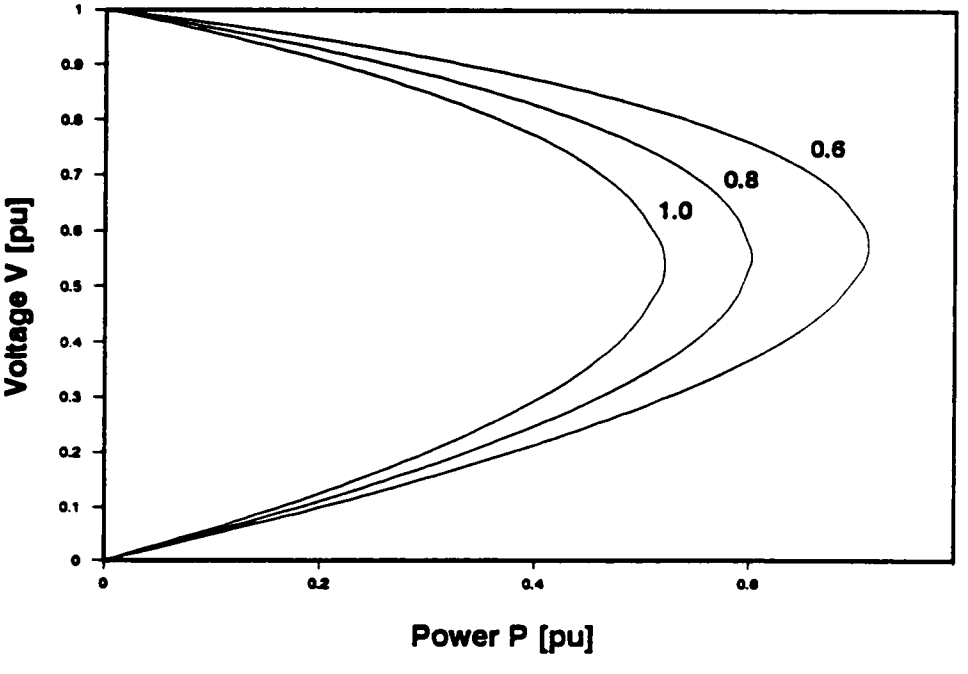

Figure 80. P-V relationship for inductive loads.

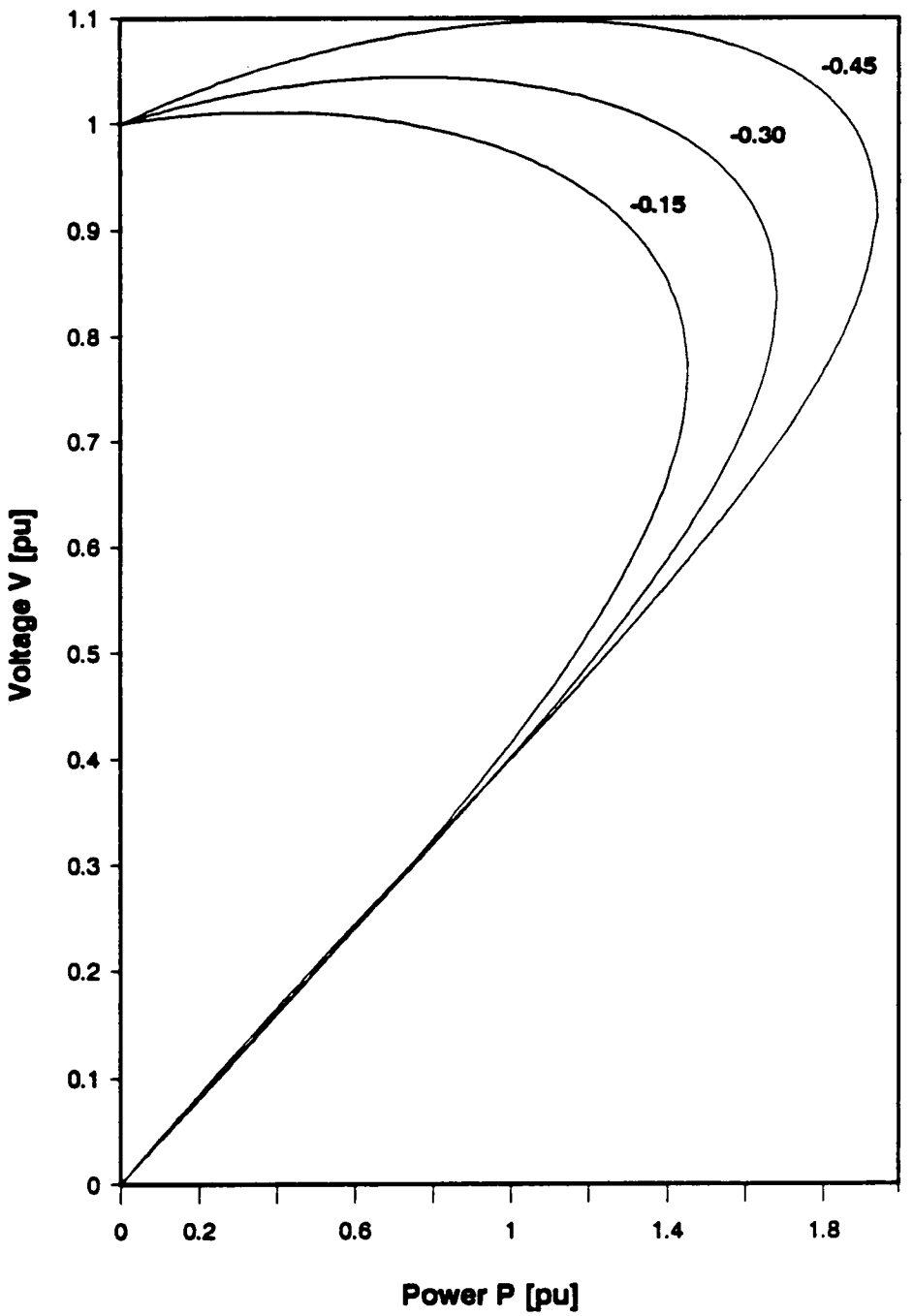

Figure 81. P-V relationship for capacitive loads.

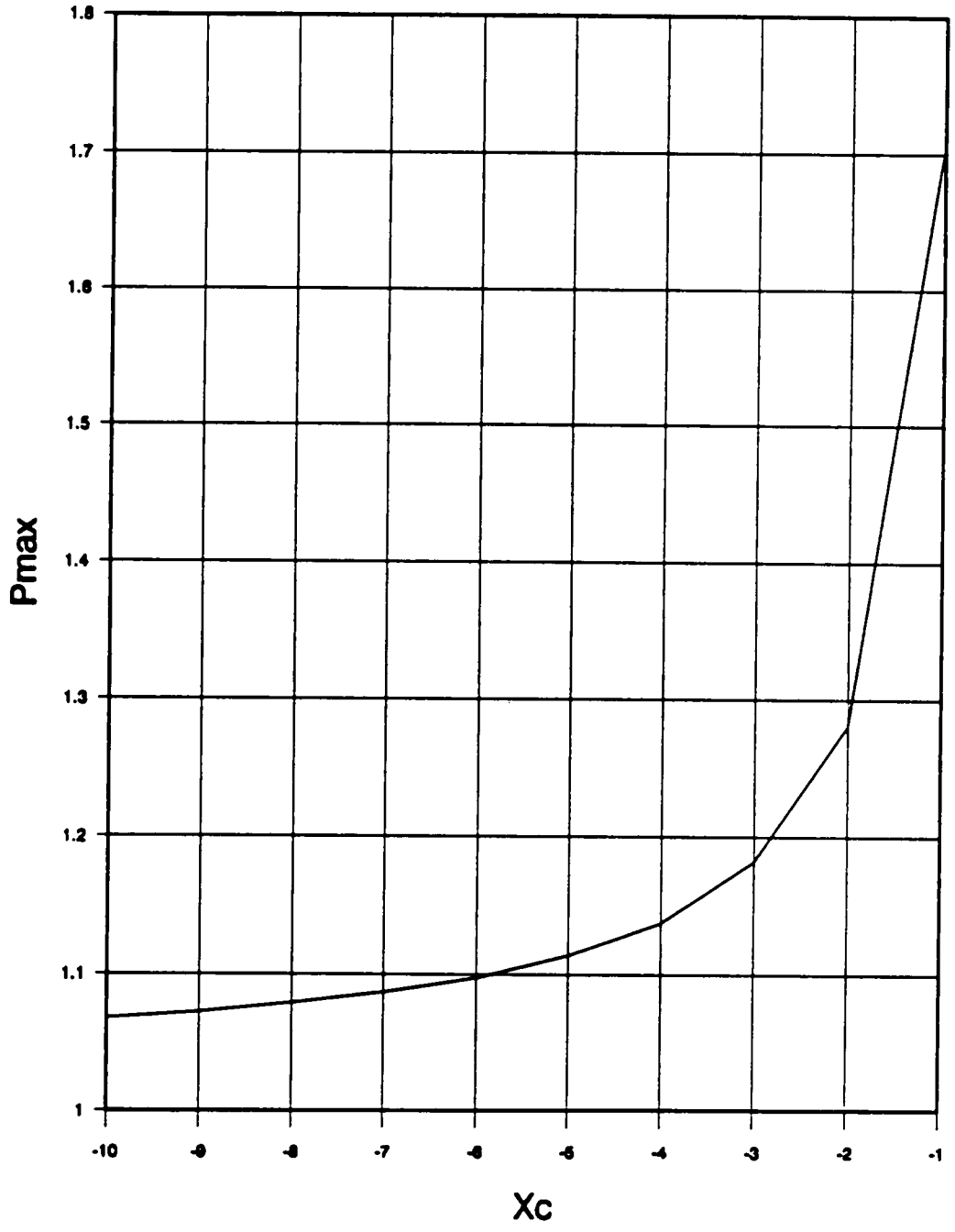

Figure 82. Critical loading vs. static compensation.

Figures 80 and 81 represent loading with constant power factor. When shunt capacitor is connected to the load, it is not a source of constant reactive power because the reactive power it generates depends on the square of the voltage it is connected to. If $k = 0.2$ is assumed in the previous example and an additional shunt capacitor connected in parallel with the load, dependence of the maximum power transfer on the value of shunt compensation reactance X_c is shown in Figure 82. Large negative amounts of X_c correspond to small shunt compensation while smaller negative amounts of X_c represent more substantial compensation. It can be noted from Figure 82 that the increase of maximum power transfer for a range of shunt reactances $X_c \in (-\infty, -0.4]$ is less than 0.1 *pu* but it starts to increase rapidly as larger amounts of shunt compensation become available. For $X_c \in [-0.4, -1.0]$ maximum power transfer climbs by 0.56 *pu* (from 1.14 *pu* to 1.70 *pu*).

Another numerical example which will be presented is based on two generator, one load power system model used in [40]. Generators are producing P_1 and P_2 and have terminal voltage phasors $V_0 \angle \delta_1$ and $V_0 \angle \delta_2$. Both generators are connected to the load which consumes $P_3 + jQ_3$ through two lossless transmission lines of equal reactances X . Voltage phasor at the load bus is $V_1 \angle \delta_3$ and the shunt capacitor of susceptance B is connected in parallel with the load. The following notation and parameters are used in [40]

$$
\begin{aligned}
V_0 &= 1.0 \\
X &= 1.0 \\
\Delta P &= P_2 - P_1 \\
\theta &= \delta_2 - \delta_1 \\
\phi &= \delta_3 - \delta_1
\end{aligned}
\tag{6.2.4}
$$

to produce the voltage collapse bifurcation point

$$
x^0 = (\theta^0, \phi^0, V^0, \Delta P^0, P_3^0, B^0, Q_3^0) = (0, -\frac{\pi}{4}, \frac{1}{\sqrt{2}}, 0, -1, 0, 0) \tag{6.2.5}
$$

The local unfolding of the system model (elaborated in [40]) is given by the equation

$$
\gamma_0 = -\frac{B}{4} - \frac{\Delta P}{2} + \frac{P_3 + 1}{2} - \frac{Q_3}{2} - \frac{B^2}{16} = 0 \tag{6.2.6}
$$

around the bifurcation point x^0 . The sensitivity of the maximum power transfer at bifurcation x^0 with respect to shunt capacitance B is

$$
\begin{aligned}
\frac{\partial P_3}{\partial B} &= \frac{1}{2} + \frac{B}{4} \\
\frac{\partial P_3}{\partial B}\Big|_{x=x^0} &= \frac{1}{2}
\end{aligned}
\tag{6.2.7}
$$

which means that the maximum power transfer is increasing at half the rate of increase of shunt compensation at bifurcation point x^0 . Although this result was obtained by linearization, it suggests that the improvement of stability margin by

increasing shunt compensation would require substantial amounts of compensation.

Load flow equations for this example (taking into account notation and parameter values in (6.2.4)) are

$$\begin{aligned} -V_1 \sin(\theta - \phi) - V_1 \sin \phi &= 0 \\ V_1 \sin(\phi - \theta) + V_1 \sin \phi &= P_3 \\ -V_1 \cos(\phi - \theta) - V_1 \cos \phi &= (B-2)V_1^2 \end{aligned} \tag{6.2.8}$$

It can be solved for load voltage V_1 in terms of P_3 and B

$$V_1 = \sqrt{\frac{4 \pm \sqrt{16 - 4P_3^2(B-2)^2}}{2(B-2)^2}} \tag{6.2.9}$$

from which the bifurcation relationship

$$16 - 4P_3^2(B-2)^2 = 0 \tag{6.2.10}$$

gives the following relation between P_3 and B

$$|P_3| = \frac{2}{|B-2|} \tag{6.2.11}$$

which also gives $\partial P_3/\partial B = 1/2$ around $B = 0$ and shows that maximum power transfer would increase infinitely for $B = 2$ due to resonance between shunt capacitance and inductances of transmission lines. For more realistic values of $B \in [0,1]$, the maximum power transfer doubles (from 1 *pu* to 2 *pu*) but most

of the increase occurs for larger values of B (close to 1 pu). It should also be noted that the reactances of transmission lines are chosen very high in this example. If they were lower, the resonance point would be obtained for even higher values of B which are not typical in power systems.

The above examples are indicative of the performance that can be expected of shunt compensated systems in more complex power network topologies. However, algorithms and simulations are needed to verify those hypotheses.

The analytical approach for the shunt compensation problem is chosen to be similar to the one presented in previous chapter for identification of critical loads in critically stable system: sensitivity analysis of voltage collapse proximity indicators with respect to shunt capacitances at load buses and identification of load bus locations which are most influential in changing the values of proximity indicators near bifurcation points.

6.2.1 Sensitivity analysis of minimum singular value of Jacobian

Minimum singular value of the power flow Jacobian is one of the proposed proximity indicators. It can be used for sensitivity analysis whose objective is to determine the effects of shunt compensation on voltage stability margin. The variation of numerical technique described in section 5.2.1 may be used to assess the values of participation factors. One important difference is that sensitivities

of σ_{min} with respect to changes in active powers are no longer needed, because they do not play any role in estimating the system state when static compensation is applied. Let us assume that a set $B = \{B_1, \ldots, B_m\}$ of shunt capacitances is added to the system as var compensation (some of the values of B_i may be zero, indicating lack of var compensation at location i). The change of σ_{min} which would correspond to the change of the system state is (using linear approximation)

$$\Delta\sigma_{min} = \sum_{j=1}^{m} \frac{\partial\sigma_{min}}{\partial Q_j} \frac{\partial Q_j}{\partial B_j} B_j = \sum_{j=1}^{m} \frac{\partial\sigma_{min}}{\partial Q_j} V_j^2 B_j \qquad (6.2.12)$$

Real value of $\Delta\sigma_{min}$ would be somewhat different due to nonlinear relationship between σ_{min} and B_i , but we are mostly concerned with the sensitivities of σ_{min} with respect to various shunt compensation locations i

$$S_i = \frac{\partial\sigma_{min}}{\partial B_i} = V_i^2 \frac{\partial\sigma_{min}}{\partial Q_i} \qquad (6.2.13)$$

If sensitivities S_i were ordered in decreasing order

$$S = (S_{i_1}, \ldots, S_{i_m}) \qquad (6.2.14)$$

the ordered m-tuple

$$W_s = (i_1, i_2, \ldots, i_m) \qquad (6.2.15)$$

represents the permutation of the set of load bus numbers ordered in such a way that the first element represents the number of the bus which would affect most σ_{min} if static shunt compensation were placed on it, second element is the bus number of the second most suitable bus location for var compensation etc. When static var compensation is to be installed on a limited number of buses $k < m$, first k elements of W_s are the most suitable locations and their relative importance (and installed var compensation capacity) may be made proportional to relative values of their respective sensitivities.

The algorithm presented above is based on numerical calculation of sensitivities $\partial\sigma_{min}/\partial Q_i$ and further processing of obtained data to prioritize locations for static var compensation. If an algorithm were needed in real-time to assess the amount of compensation needed for certain displacement of stability boundary, it may be advantageous to use the sensitivity analysis of another voltage collapse proximity indicator: total generated reactive power.

6.2.2 Sensitivity analysis of generated reactive powers

The sensitivity analysis of

$$Q_g^t = \sum_{j=1}^{n} Q_{gi} \tag{6.2.16}$$

with respect to B_i , $i = 1,...,m$ has the advantage that it can be accomplished in a straightforward manner, without performing $m+1$ load flows to assess the sensitivities $\partial Q_g^t/\partial Q_j$ as it is the case when sensitivities $\partial \sigma_{min}/\partial Q_j$ are calculated.

For value of Q_g^t given by (5.2.24), Jacobian matrix J_g may be calculated as in (5.2.25) and sensitivities with respect to reactive powers of loads calculated by multiplying it with a corresponding submatrix of inverse of the load flow Jacobian J (see (5.2.26a))

$$[\Delta Q_g^t] = \begin{bmatrix} \frac{\partial Q_g^t}{\partial \delta} & \frac{\partial Q_g^t}{\partial \theta} & \frac{\partial Q_g^t}{\partial V} \end{bmatrix} \begin{bmatrix} \frac{\partial \delta}{\partial Q_l} \\ \frac{\partial \theta}{\partial Q_l} \\ \frac{\partial V}{\partial Q_l} \end{bmatrix} [\Delta Q_l] \qquad (6.2.17)$$

$$[\Delta Q_g^t] = S'[\Delta Q_l] = \sum_{j=1}^{m} \frac{\partial Q_g^t}{\partial Q_i} \Delta Q_{li} \qquad (6.2.18)$$

Sensitivities of total generated reactive power with respect to shunt susceptances may then be obtained as

$$S'' = \left[\frac{\partial Q_g^t}{\partial Q_{l1}} \frac{\partial Q_{l1}}{\partial B_1} \quad \cdots \quad \frac{\partial Q_g^t}{\partial Q_{lm}} \frac{\partial Q_{lm}}{\partial B_m} \right] \tag{6.2.19}$$

$$S'' = [s_1 \quad \cdots \quad s_m]$$

and linearized approximation for change of Q_g^t due to inclusion of shunt susceptances B_i , $i = 1,...,m$ in the network

$$\Delta Q_g^t = \sum_{j=1}^{m} s_j \Delta B_j \tag{6.2.20}$$

If sensitivities s_i were ordered in decreasing order $(s_1 , \ldots , s_m)$, the ordered m- tuple $(i_1 , \ldots , i_m)$ represents the list of most favorable locations for static compensation in decreasing order of importance while sensitivities s_i may be considered as relative weighting factors for determination of the installed capacities. If k locations are to be chosen for static var compensation using the above algorithm, they should be taken as first k elements from $(i_1 , \ldots , i_m)$ with installed capacities in proportion with their respective sensitivities

$$\max\{B_{i1}\} : \max\{B_{i2}\} : \ldots : \max\{B_{ik}\} = s_{i1} : s_{i2} : \ldots : s_{ik} \tag{6.2.21}$$

The simulation analyses in the next section with the application of static compensation designed using the above criteria will show what effect it has on the voltage stability boundary.

6.3 Simulations and Comments

The sensitivity analysis described in section 6.2.2 was performed on the 39-bus power system model for a number of critically stable situations.

Figure 83 shows the sensitivities of total generated reactive power Q_g^t with respect to shunt capacitances installed at load buses of the system for four load factors very close to stability boundary, which was approached by proportional progressive loading of both active and reactive parts of the loads. It can be noted that sensitivities of certain buses are rising sharply as stability boundary is being approached (those are the same buses which were identified as critical load buses in the previous chapter). Figure 84 represents similar situation for different loading levels close to stability boundary reached by progressive loading of reactive powers only. Once again, the critical load buses were found to be the most favorable locations for shunt compensation. In both cases (Figure 83 and 84) the generated reactive powers were not constrained.

Figure 85 shows the sensitivities of Q_g^t with respect to load bus shunt compensation when progressive loading was applied on both active and reactive powers, but with the additional assumption that generated reactive powers are limited on all generators. Although the sharp rise of sensitivities is noticable as in the two previous situations, different load buses are found to be convenient locations for static var compensation. It is not the cluster of buses (4-8) which is critical and

favored for var support placement, but another cluster of buses (21-24) with significantly higher sensitivities than the rest of the system. Almost identical conclusions are drawn from Figure 86, which represents sensitivities of $\sigma_{min}(J)$. It is not necessary to analyze separately the algorithms presented in sections 6.2.1 and 6.2.2 because they give almost identical results.

Figure 87 shows the changes of Q_{gen} and σ_{min} for shunt compensation $B_{23} \in [0.5, 5.0]$ at load bus 23 . Both voltage collapse proximity indicators are found to be the most sensitive to changes of shunt compensation at that load bus when var support is applied at system state corresponding to Figures 85 and 86. Generators 1,3 and 6 are operating in constant reactive power mode throughout that range. It can be seen from Figure 87 that all generated reactive powers are changing by relatively small amounts and almost linearly while σ_{min} is climbing by only 0.03 (from 0.52 to 0.55), although the amount of compensation installed at bus 23 changed from 50 MVAr to 500 MVAr (which is unrealistic). It indicates that even substantial amounts of reactive support installed at one location would not significantly improve the stability margin. A notable exception from overall trend is the reactive power change at generator 7 which is electrically and physically the closest to the var support location. The unloading of generator 7 is the main reason for improvement of stability index σ_{min} . The result of simulation shown in Figure 87 indicates that more substantial var support is needed for satisfactory improvement of stability index without load shedding.

Figure 88 shows three static compensation scenarios which were simulated on the same test system and starting from the same initial conditions. The first scenario is an extreme: it assumes that static compensation B_i , $i = 1,...,29$ is available at every load bus in the system and it is proportional to the sensitivities of Q_g^t with respect to relevant shunt susceptances. A compensation factor k_c is introduced such that

$$B_i(k_c) = K_c\, B_{i0} \ , \quad i = 1,...,m \tag{6.2.22}$$

where B_{i0} are chosen such that they are numerically equal to one tenth of respective calculated sensitivities with respect to Q_g^t . This choice is a convenience because most of the susceptances are between 0 and 1 for $k_c = 1$ when B_{i0} are chosen as described above.

The second scenario (Figure 88) represents the choice of static var compensation on 10 most sensitive locations only, with nominal values B_{i0} equal to values of the first scenario. The third scenario is a choice of only four var support locations corresponding to the most sensitive buses in three clusters of buses (4-8), (10-16) and (21-23) which have distinctly higher sensitivities than the other load buses in the system. Locations 4, 12, 15 and 23 were chosen for static compensation, again with nominal values B_{i0} equal to the values used for the same buses in the other two scenarios.

Figure 89 shows the load bus voltage profile for scenario 1 when compensation factor k_c is changed between 0 (no var support) to 1.8 (substantial support). The

voltages on many load buses climbed by over 20 percent through that range of k_c and voltage profile was significantly improved. Figure 90 shows generated reactive powers and minimum singular value of the load flow Jacobian for the change of k_c which corresponds to Figure 89. The increase of K_c from 0 to 0.2 was enough to bring σ_{min} from 0.25 to 0.55 while further increase to $k_c = 1.8$ was only able to improve σ_{min} to the value of 0.68 . In the same region $k_c \in [0,2]$ the decrease of reactive generation was more pronounced than for higher values of k_c . The explanation of this observation is that the initial condition for this simulation was very close to stability boundary and very small changes of system parameters (equivalent reactive powers consumed at load buses) are enough to produce significant relief. That does not mean, however, that the system would be secure with compensation factor of only 0.2 . A small increase of loading would bring it to the critically stable region once again. It is only at $k_c = 0.4$ that all but generator 1 are back into the P-V mode and some of them even start to consume reactive power (generators 3, 8 and 10) for $k_c = 1.8$.

Figures 91 and 92 show the effect of compensation using scenario 2 for a range of compensation factors k_c same as in the previous case. It is very interesting to note that using only 10 static var support locations (and smaller total installed capacity) the improvement obtained was almost identical to the results of simulations of scenario 1. Figure 93 shows one important difference, however: if progressive P-Q loading of the system is applied starting with various levels of compensation (expressed by value of k_c), the critical loading levels are increasing almost linearly with the increase of k_c , but with different slopes. For $k_c = 1$, sce-

nario 1 would give the critical load factor $k_{crit} = 1.93$ while scenario 2 would provide only $k_{crit} = 1.78$ compared to $k_{crit} = 1.636$ in case when no var support is available. It seems not only that the stability boundary is being displaced proportionally to the total amount of reactive support available, but it also increases almost linearly even when nonlinearities such as reactive generation limits are observed.

Finally, Figures 94 and 95 show the evolution of system voltage profile, reactive generation and minimum singular value of Jacobian when scenario 3 is applied through a wider range of compensation factors $k_c \in [0,4]$. While reactive generation is predictably higher than for scenarios 1 and 2, load bus voltages are somewhat lower and σ_{min} has slightly lower values in the plateau corresponding to $k_c \in [0.4, 4.0]$. It is obvoius that scenario 3 does provide satisfactory improvement of the stability indices for $k_c > 1$ by making the system small-disturbance stable, but does not improve the critical loading to more than $k_{crit} = 1.70$ compared to the uncompensated case, when $k_{crit} = 1.636$ (Figure 96, which also shows the total reactive power generation for various values of compensation factors). It can be noted that total generated reactive power and critical load factor depend almost linearly on the compensation factor k_c and can be correlated with each other, which is another confirmation that Q_g^i is a well chosen indicator of stability margin. The minimum singular value of Jacobian seems to perform worse in the situations where system nonlinearity is compounded with reactive generation constraints, but it remains an excellent index of local stability

properties (it should not be forgotten that σ_{min} was obtained from a linearized system).

6.4 Conclusions

An analysis was done by simulation on a 39-bus test power system of the effects that locations and amounts of static var compensation have on the stability margin of the system. Two previously proposed stability indices, minimum singular value of load flow Jacobian and total generated reactive power, were used as starting points for sensitivity analysis. A numerical differentiation algorithm was proposed for calculation of the sensitivities of σ_{min} with respect to shunt susceptances installed at different load bus locations. A simpler and computationally more effective algorithm was proposed for calculation of sensitivities of Q_g' with respect to var support locations. Since both algorithms produced almost identical results, a faster one (which corresponds to Q_g') is preferable for this application.

The choice of locations is made from the list of sensitivity factors arranged in decreasing order of their magnitudes. The installed compensation capacity is proposed to be proportional to the values of corresponding sensitivity factors for the chosen locations.

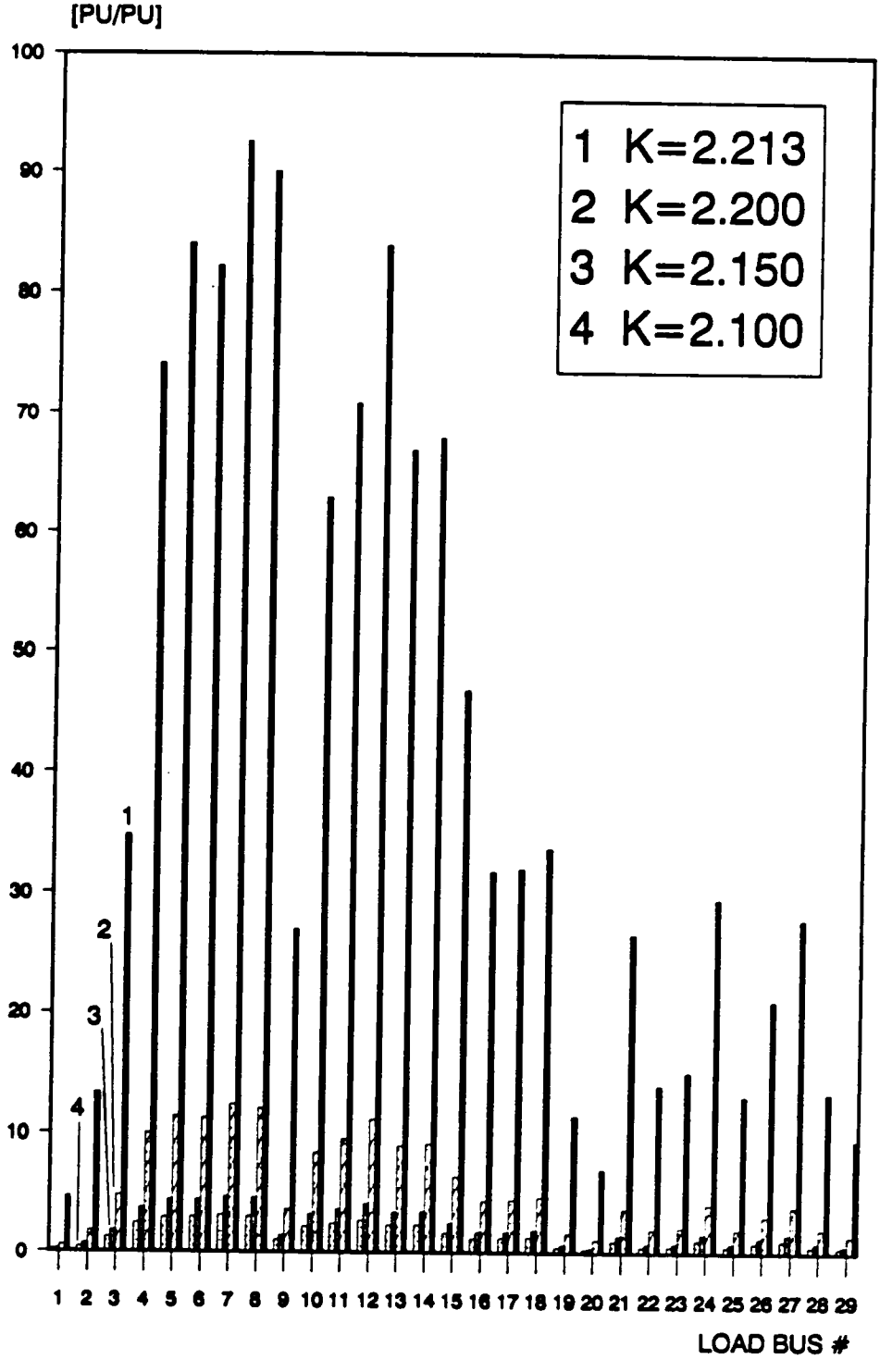

Figure 83. Sensitivity vs. shunt capacitance for PQ critical loading.

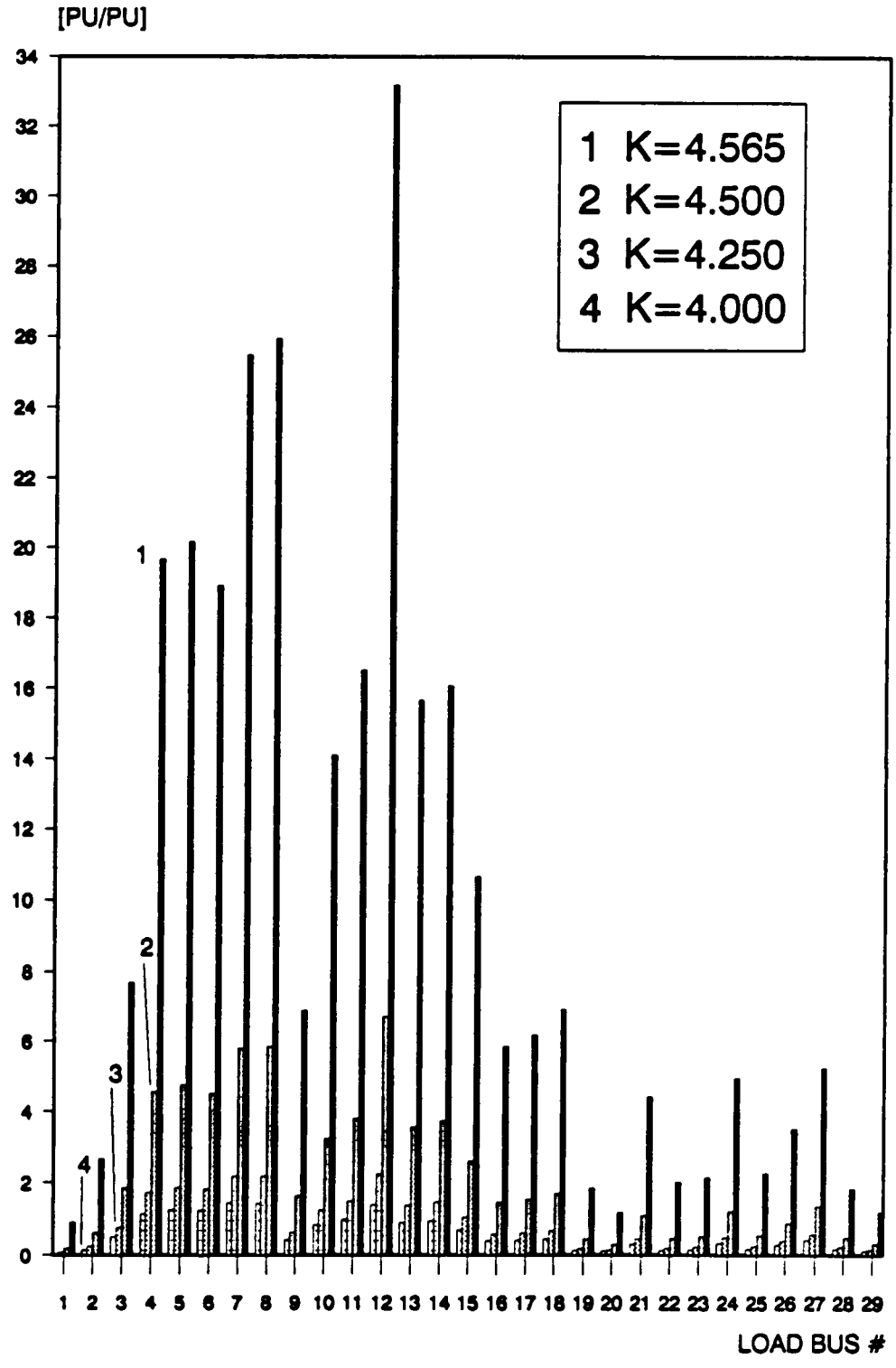

Figure 84. Sensitivity vs. shunt capacitance for Q critical loading.

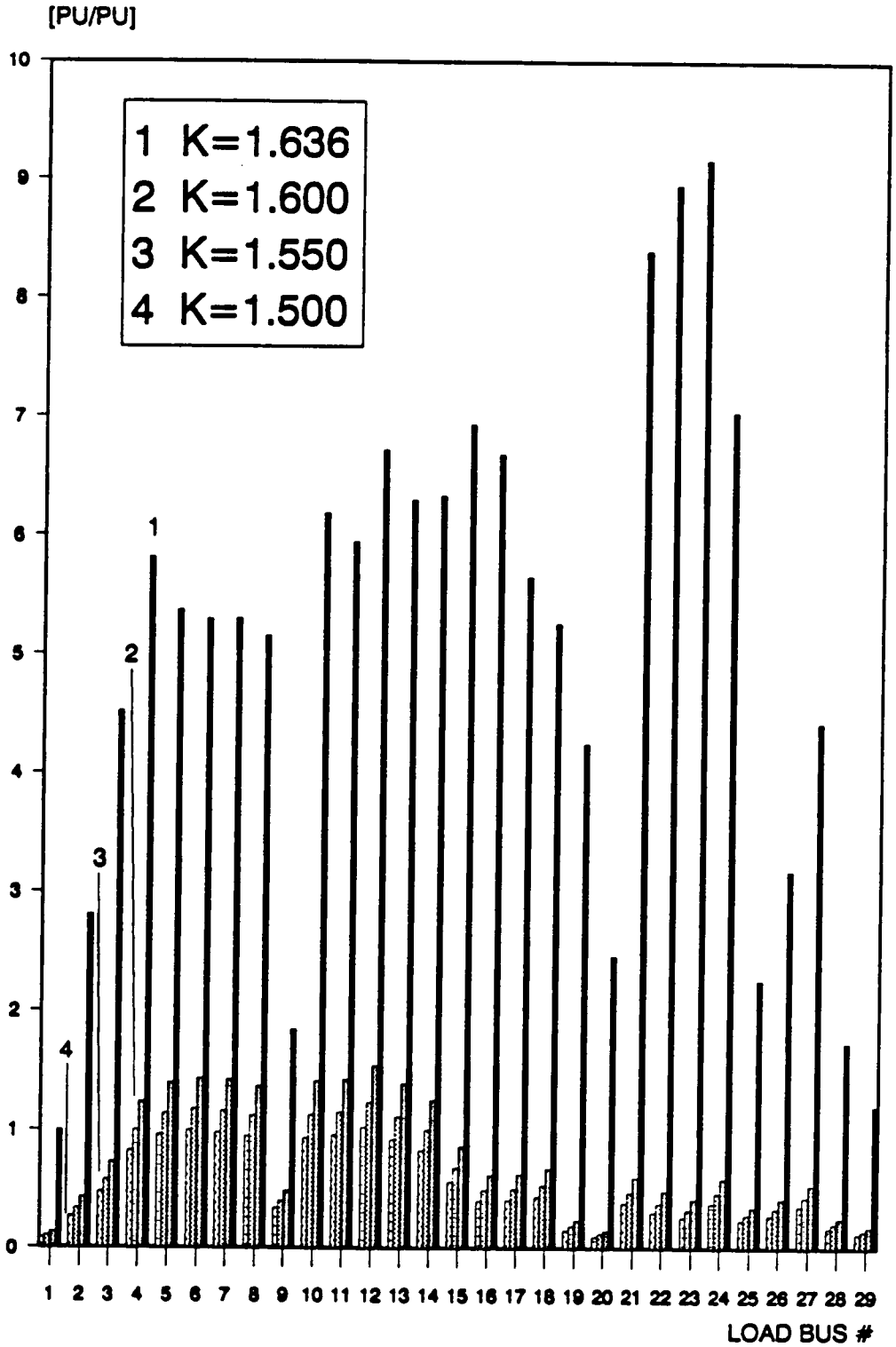

Figure 85. Sensitivity vs. shunt capacitance for Q constrained loading.

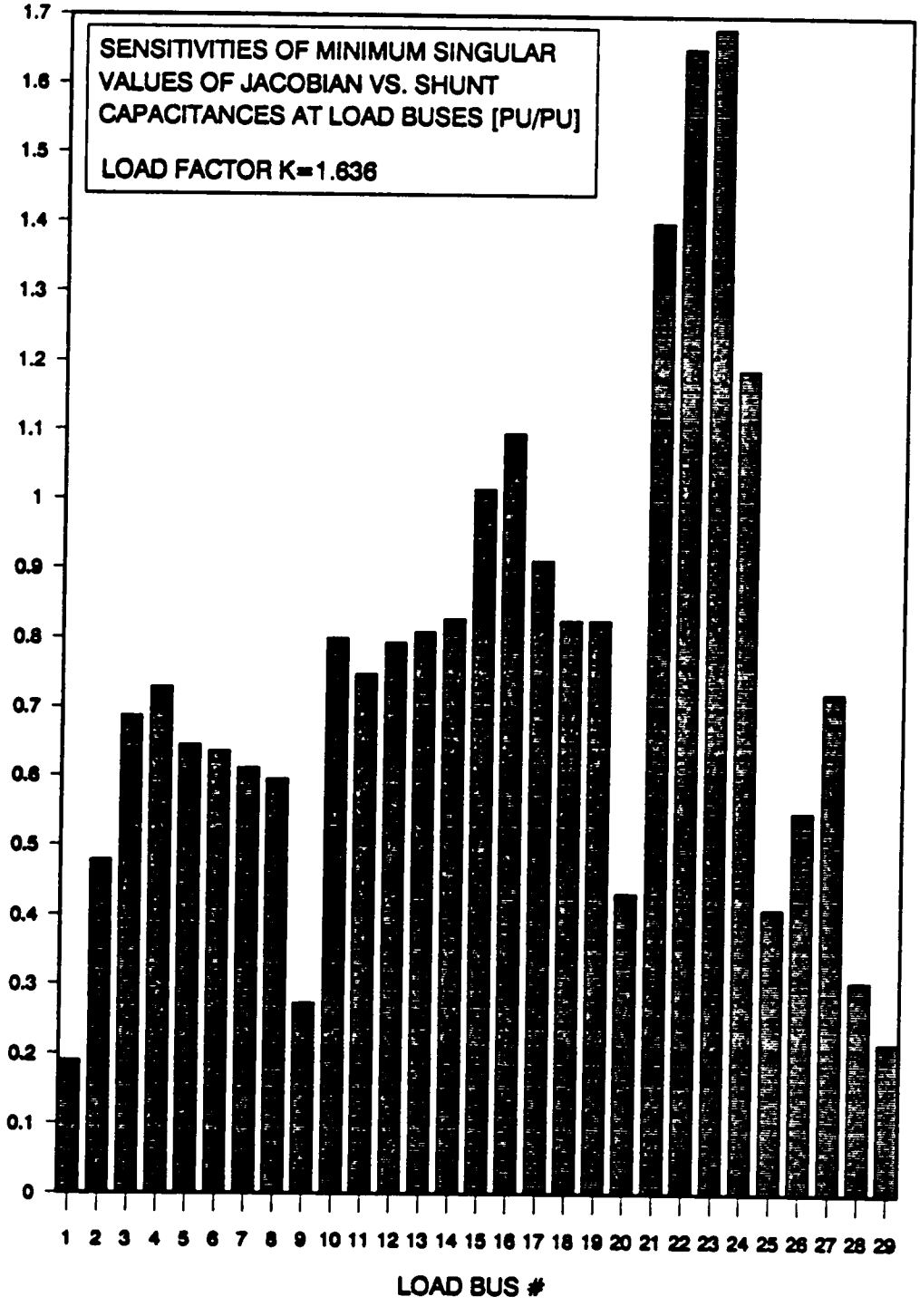

Figure 86. Sensitivities of minimum singular value for Q constrained loading.

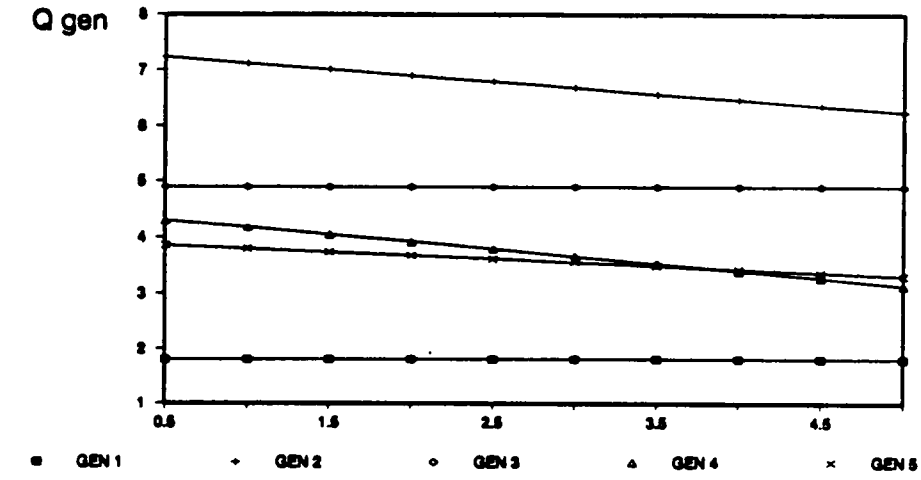

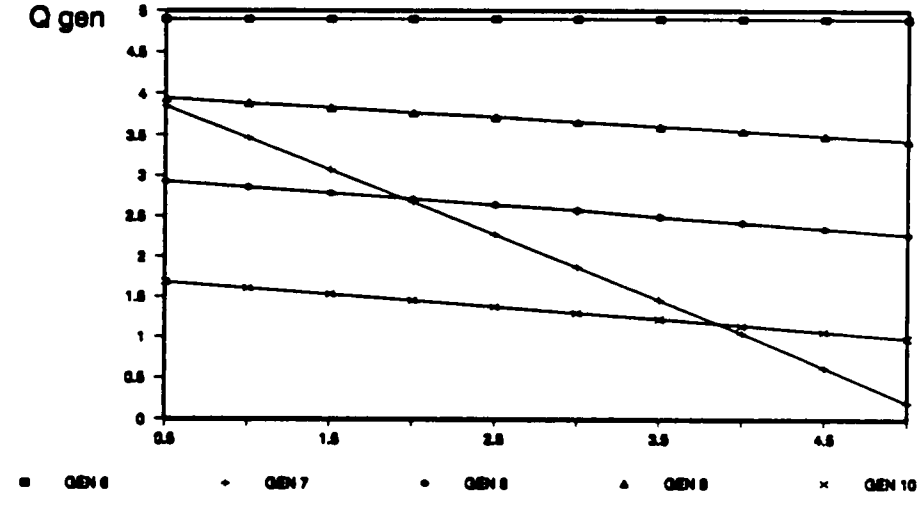

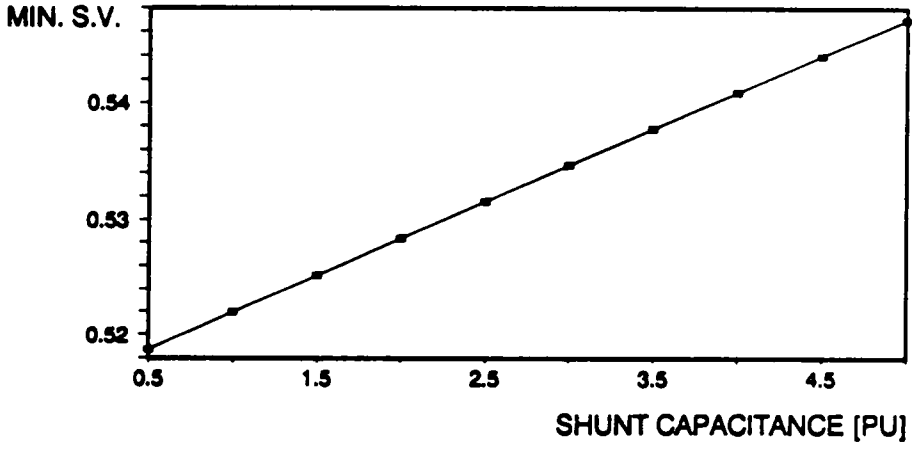

Figure 87. Stability indices for compensation at bus 23.

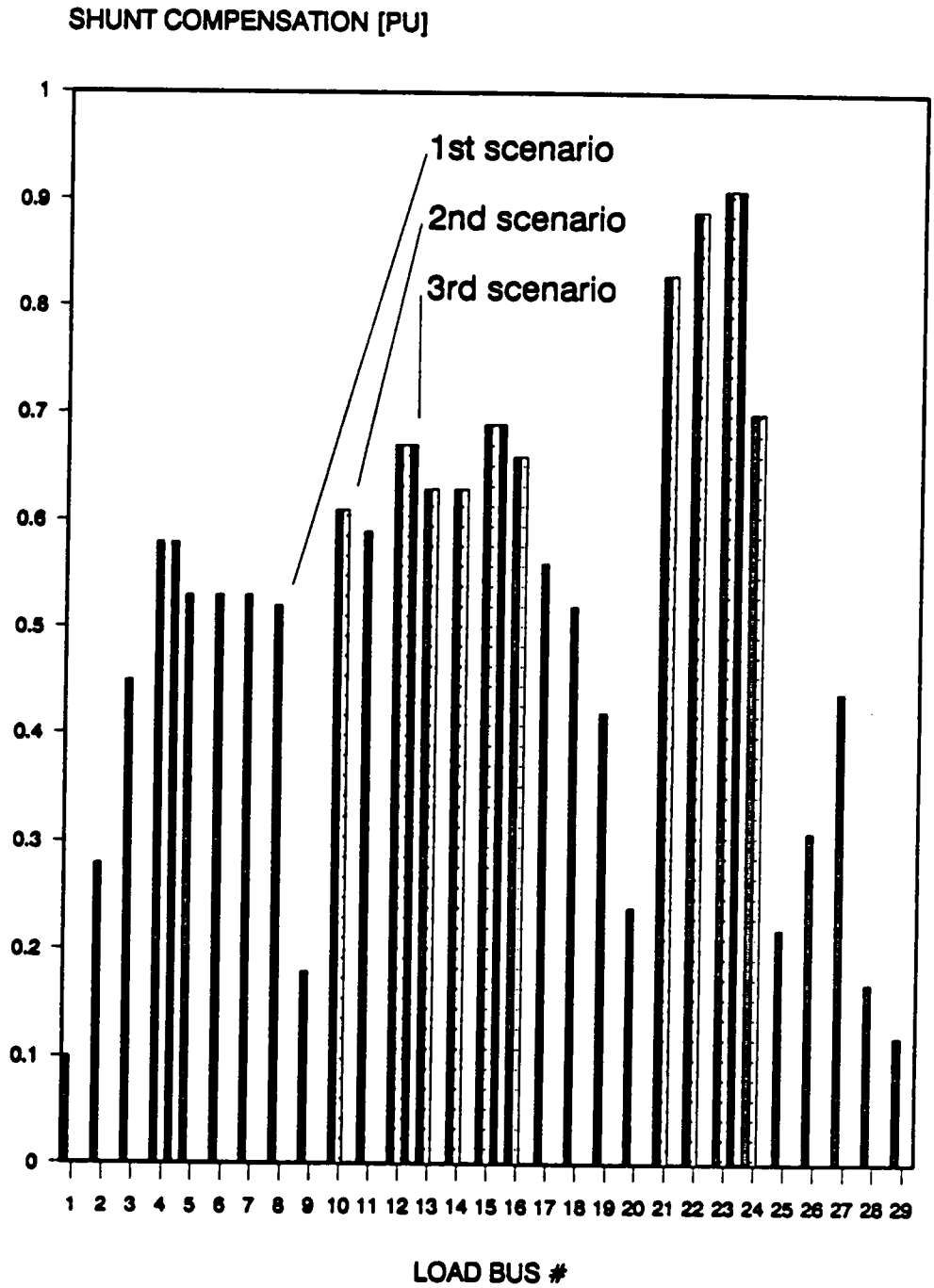

Figure 88. Three static compensation scenarios.

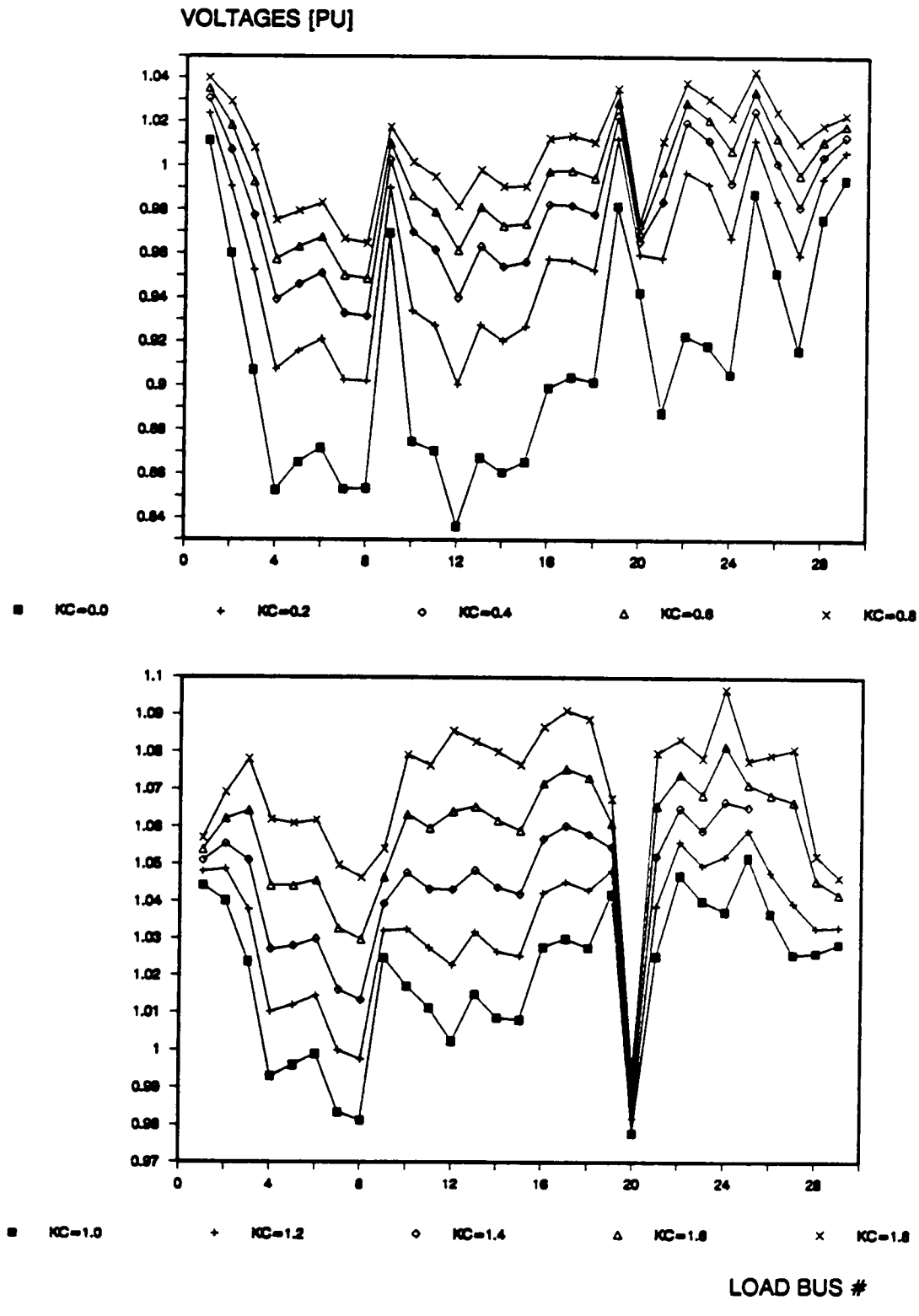

Figure 89. Scenario 1: load bus voltage profile.

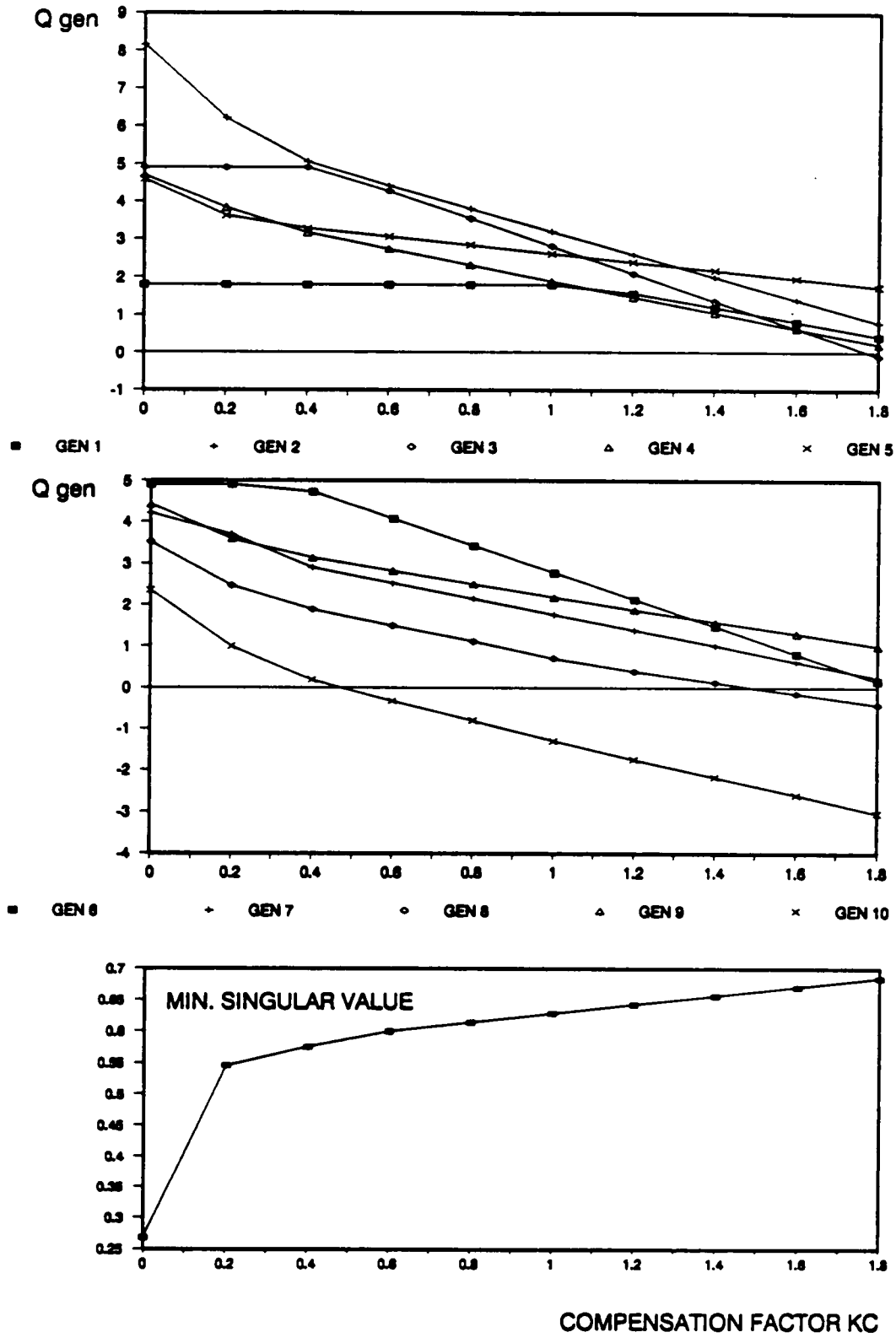

Figure 90. **Scenario 1: stability indices.**

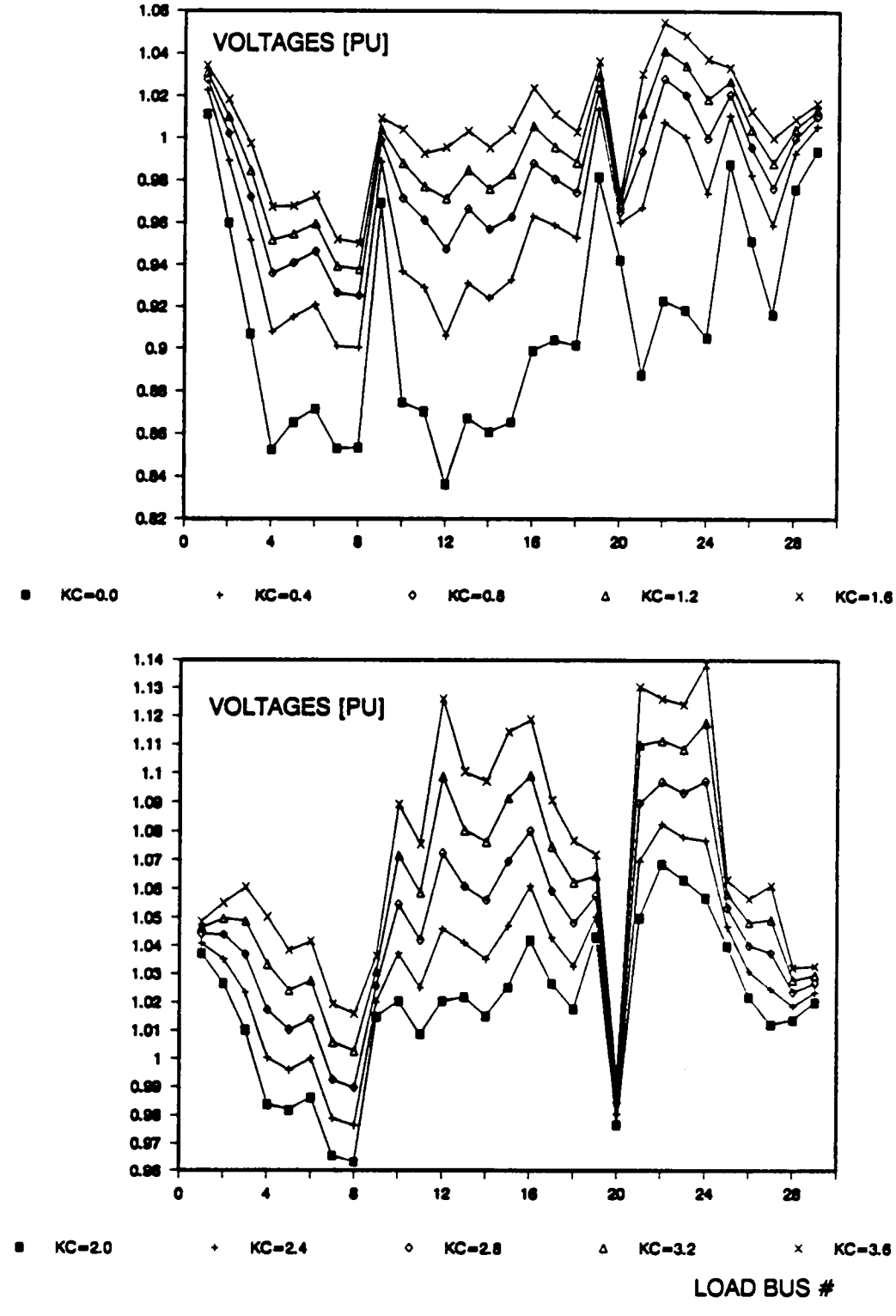

Figure 91. Scenario 2: load bus voltage profile.

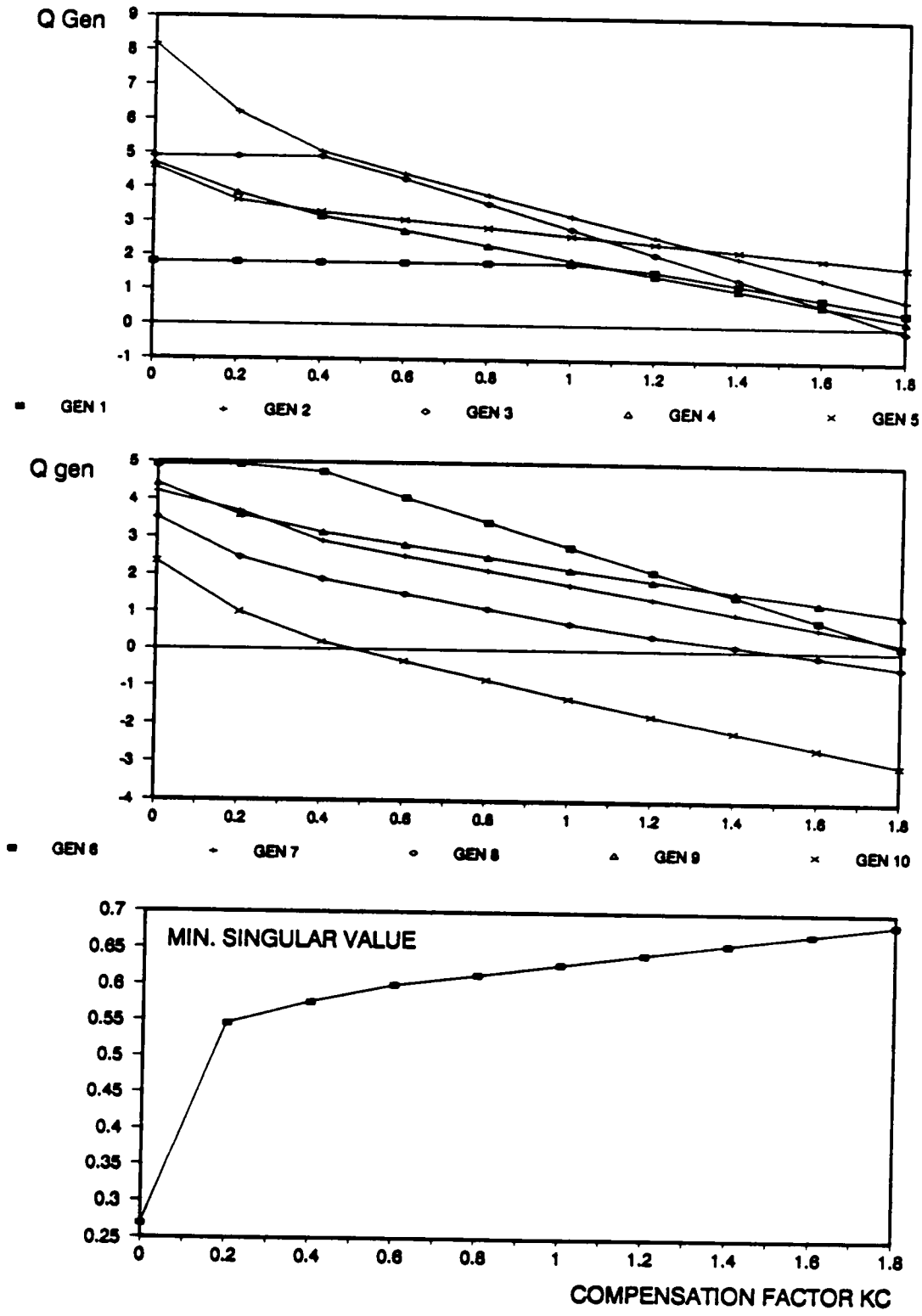

Figure 92. Scenario 2: stability indices.

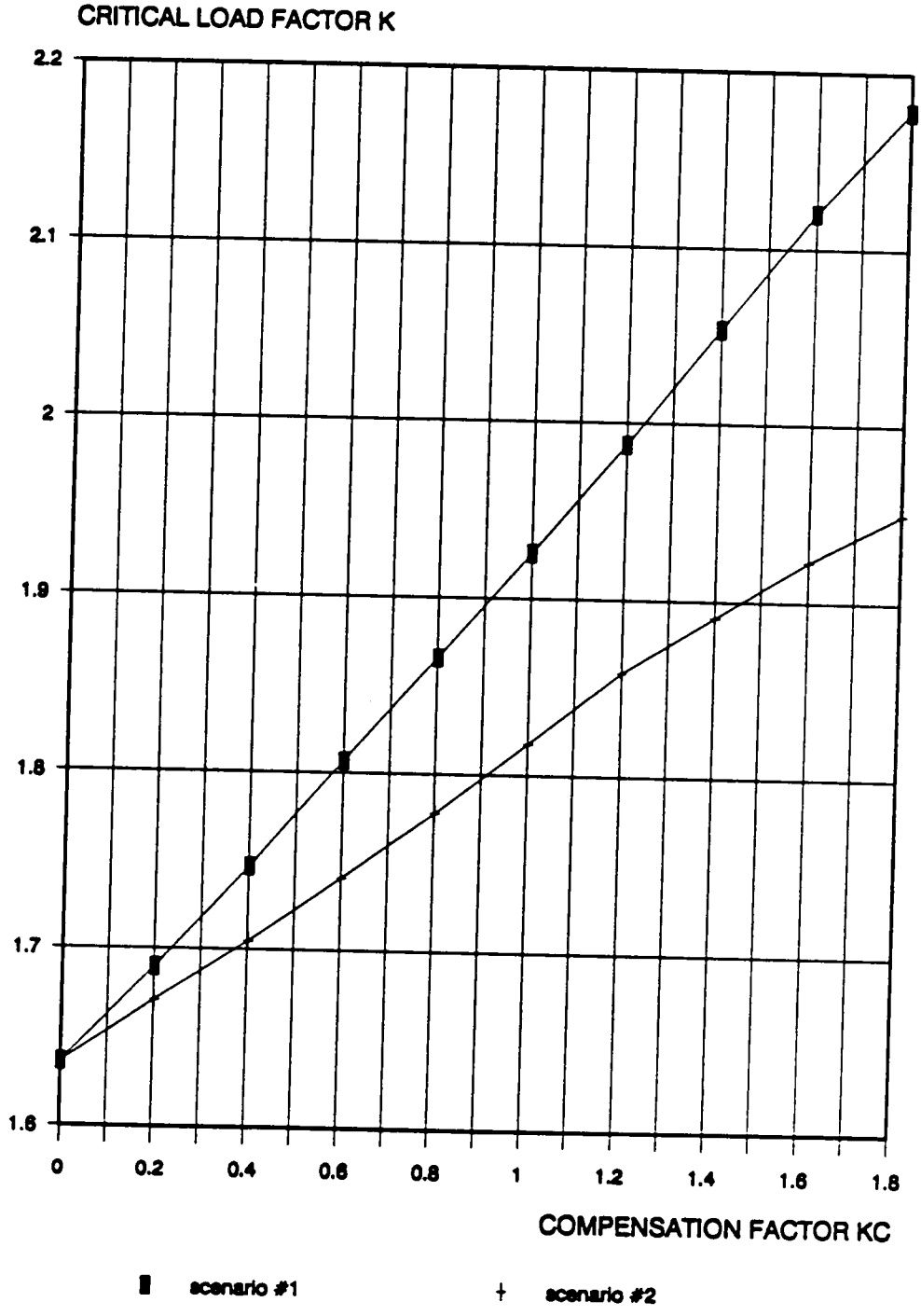

Figure 93. Scenarios 1 and 2: the margin of critical loading.

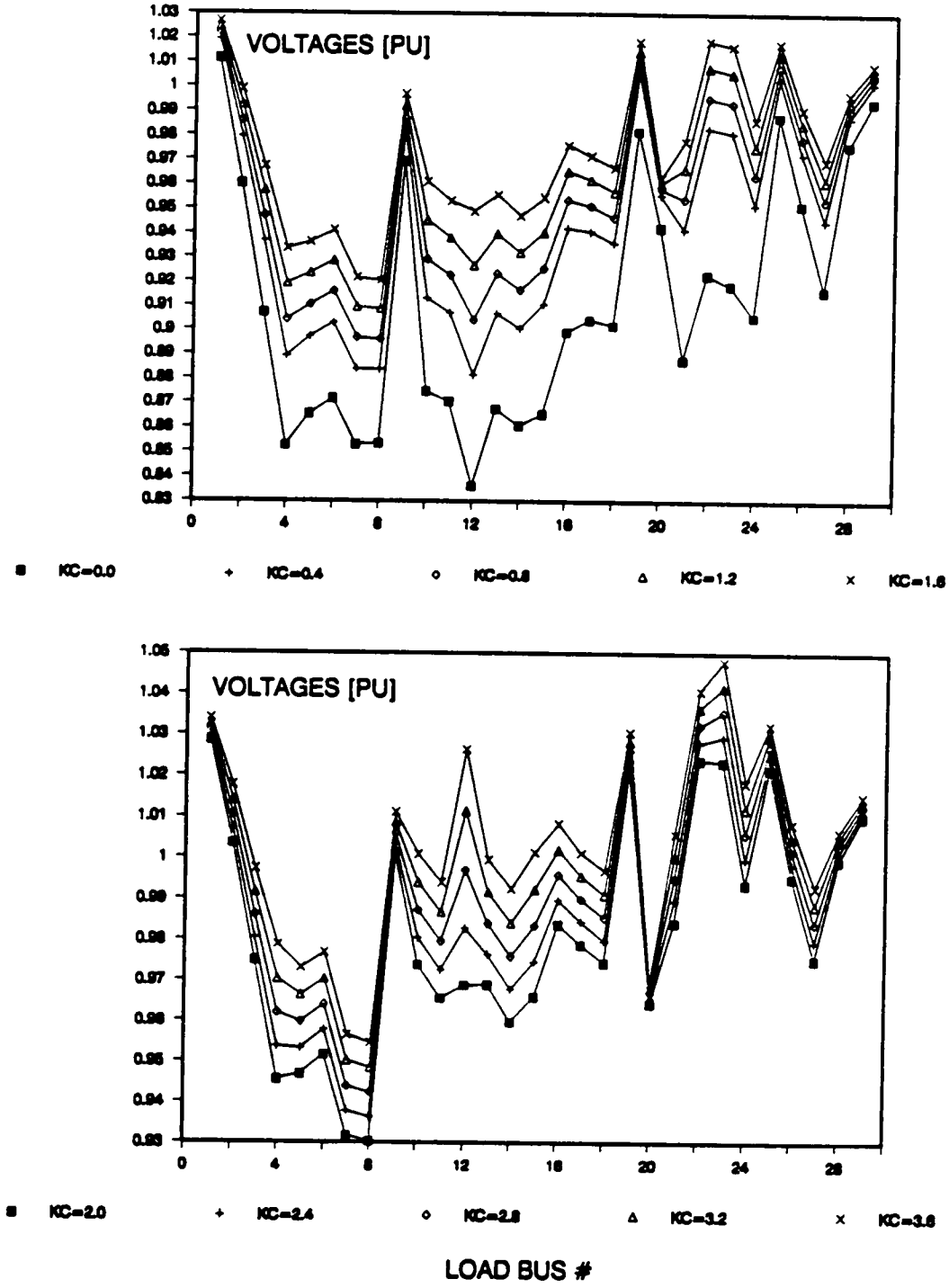

Figure 94. Scenario 3: voltage profile.

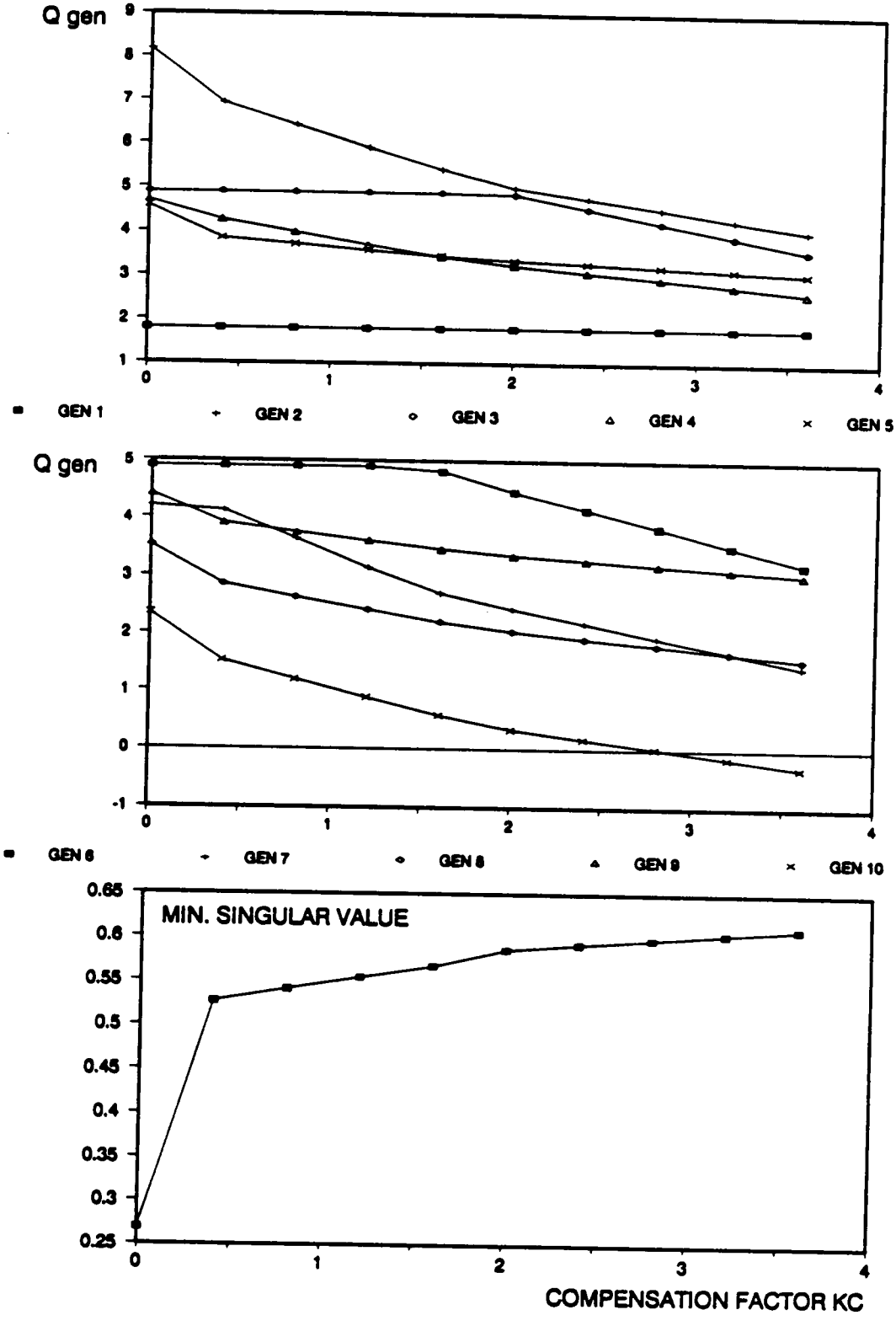

Figure 95. Scenario 3: stability indices.

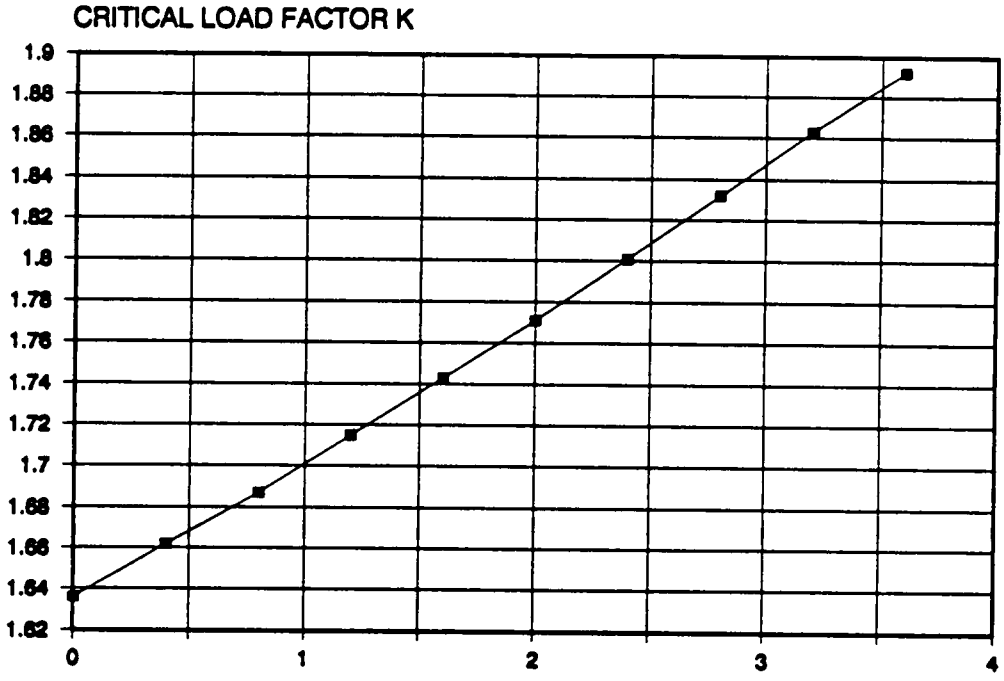

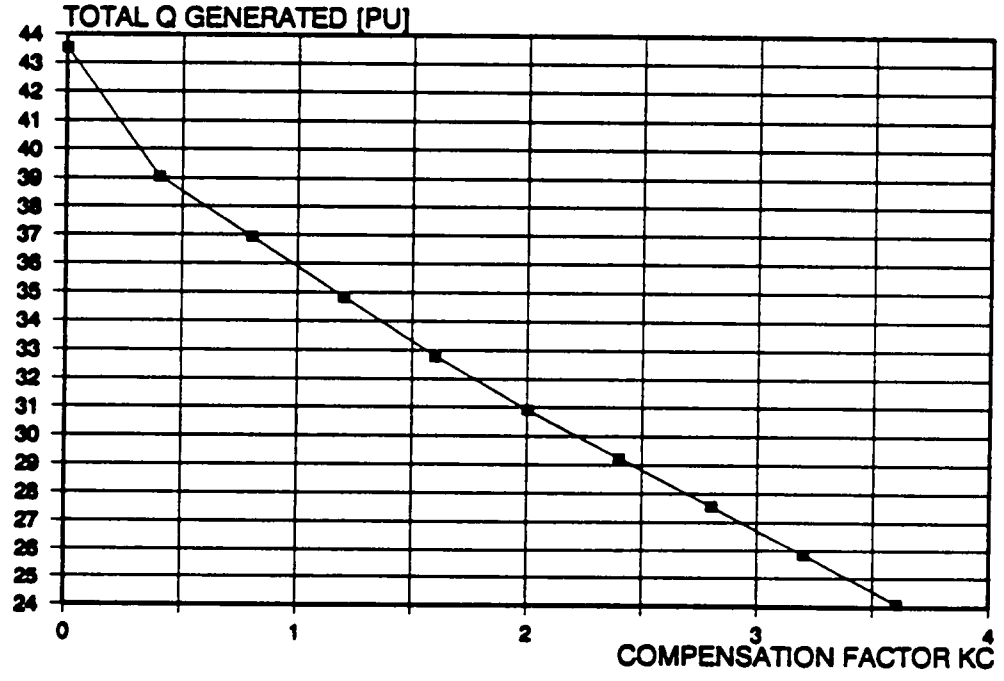

Figure 96. Scenario 3: margin of critical loading and total generated Q.

Three scenarios of static compensation were simulated on a 39-bus test system. The first one assumes a static var compensation system installed at every load bus in the system. The second one deals with the compensation system installed on 10 most sensitive load buses with the same amount of compensation they have in scenario 1. The third scenario represents the compensation on only 4 load buses chosen in three clusters of highly sensitive buses. In all three cases similar levels of compensation factor k_c produced surprisingly similar voltage profiles, but the stability margin (the margin of critical loading) was very different. It seems that the stability margin depends almost linearly on the total static compensation installed capacity and that smaller amounts of compensation (which can improve voltage profile to satisfactory level) are not enough to improve the stability margin as well. This observation also supports the claim that the phenomenon of voltage collapse is inherently linked with the balance of reactive powers in the system.

As a final conclusion, static compensation may be of limited help when voltage instabilities similar to the one described in [131] occur in power systems. Although it may provide some relief when the loading is high, only substantial amounts of reactive power injected by static compensation may significantly improve the stability margin. Most power systems do not have such a var support reserve and the best strategy for voltage collapse situations would be to include all the var support available when the loading is approaching critical levels, but to monitor stability indices $\sigma_{\min}$ and Q_c^i in real-time and resort to emergency load shedding if necessary to prevent total system blackout.

Chapter 7. Conclusions

Power system voltage instabilities in various forms have been observed in power systems of Western Europe, U.S.S.R., Japan and in U.S. Instabilities were often accompanied by heavy loading of the system with insufficient reactive power generation capability to maintain voltages. Many of the incidents ended in a systemwide voltage collapse on load buses. It seems likely that a number of voltage instability cases may be expected in the future without any human errors, or contingencies in the system, but rather due to the sharp increase of demand caused by changing weather conditions or some other significant event. Wheeling and the unpredictable patterns of power flows may also contribute to the reduction of stability margins. The main motivation for the work presented in this text was to complement numerous theoretical results published in the literature with some research directed toward development of practical applications which could be used to protect power systems from voltage instabilities. At this time, commercially available hardware is more than able to allow effective stability

monitoring of the slow voltage dynamics at the system level. Development of monitoring systems is a first step toward controlling voltage stability. Fast control applications are also needed as an extension of monitoring systems.

As a first step toward a better understanding of a class of voltage instabilities in power systems, a simulation model of voltage collapse was built on a 39-bus, 10-generator power system model with constant complex power loads. Voltage collapse was treated as a dynamic phenomenon whose development is caused by a slow change of system parameters (system loading) which brings the steady state operating points close to stability boundary represented as saddle node bifurcation of the system dynamic model (represented by generator swing equations coupled with algebaric equations of the power balance at load buses). Saddle node bifurcations were reached by increasing the system loading through one parameter (load factor) changes. Conditions for the type of instability were investigated by analyzing the conditioning of the load flow Jacobian and its submatrices [40]. An algorithm was proposed for dynamic simulation of the voltage instablity by applying step, or ramp changes of parameter (load factor) to a selected set of loads and by bringing the system across the bifurcation value of the parameter. The system trajectory on a center manifold produced voltage collapse in all simulated cases. Simulations were possible until the near loss of system causality, where the collapse has already happened, although voltage profiles could not be tracked until they reach zero values. If the terminal value of the load factor were a bifurcation value, the system trajectory would be on a center manifold. Since in all the simulations the bifurcation values were not exactly known,

system trajectories cannot be considered to be along center manifolds, although they are in the neighborhood (values of parameters are very close to the bifurcation value). The simulation results represent one contribution of this work, because they allow to track potential indicators of proximity to voltage instability which can be used for monitoring in actual power systems. The suitable indicators for real-time monitoring were found to be the minimum singular value of the power flow Jacobian matrix and generated reactive powers. A number of topics for further research emerges from the simulation results: the important issue of minimal power system model sufficient to capture relevant modes of voltage dynamics; the investigation of relationship between loss of causality in the system which was found to coincide with final collapse of voltages and the occurrence of impulse modes in power system dynamic response; and the effects of nonlinearities of load characteristics and dynamics of some types of loads (i.e. induction motors).

The analysis of requirements for design of a real-time monitoring system for voltage stability (based on phasor measurements and previously identified voltage collapse proximity indicators) resulted in the study of possibilities to reduce the number of measurements of elements of the state vector. Such an approach is based on the assumption that some of the measured phasors are highly coherent with respect to voltage dynamics when the system loading changes, and moves the system towards the voltage stability boundary. An algorithm was presented which determines the coherent clusters of load buses in a power system based on an arbitrary criterion function. The algorithm is described in the framework of

graph theory and the analysis is completed with two proposed coherency criteria. The effects of clustering using both criteria were tested by calculation of the indicators of proximity to voltage instability (minimum singular values of Jacobian). Very good agreement was obtained between the results based on accurate and approximate measurements of the state vector.

The design of coherency criteria may be extended to incorporate the effects of different loading patterns and/or topological changes in the network. An attempt to account for a variety of topological changes and still preserve the accuracy of the algorithm leads to deterioration of the efficiency of the objective of the algorithm (the reduction of the number of measurements). A compromise needs to be found in such cases. The algorithm which would create a solution could easily be formalized as a certain type of objective function to be optimized. The underlying idea behind the results presented in Chapter 4 is the concept of voltage coherency among groups of load buses in power systems. The possibilities for exploitation of that idea are hardly exhausted by the above application. It could be used in power system state estimation and design of monitoring and control systems with different design objectives. The open field for research is an investigation of coherency relationships which would capture dynamic behavior of voltages and be less sensitive to changes of system parameters.

The control aspects of voltage unstable situations in power systems were the subject of the last two chapters of this text. While indicators of proximity to voltage collapse are derived from the system state vector (acquired in real-time),

control should be directed toward changes of the parameters. System loading level was identified as one of the main causes for degradation of stability margin. The logical choice for control was to perform emergency load shedding which would instantaneously reduce loading level and improve stability indices. The objective of such an action is to affect the smallest part of the system, and sensitivity analysis of the minimum singular values of Jacobian was used to determine critical sets of loads, defined as subset of loads whose changes have the most pronounced effect on the changes of minimum singular value of load flow Jacobian. The objective to produce an algorithm for identification of critical loads which would not bear a heavy computational burden for real-time applications was accomplished by proposing two sensitivity based algorithms whose simplicity allows very fast calculation when the system state vector is known. This was accomplished by multiplying the Jacobian of the system of linearized equations for reactive power generation (total reactive power generated in the system) with the inverse of the load flow Jacobian. The state is assumed to be acquired by a fast real-time phasor measurement system. The calculation of the sensitivity matrix does not require more then inversion of one part of a load flow Jacobian and one matrix multiplication, which makes it very appropriate for real-time operation. The research of incorporation of sparsity techniques (for applications in large power systems) and fast optimal power flows for determination of power distribution under critical loading conditions are the topics of future research.

To investigate possible control actions which could make an emergency load shedding unnecessary, an analysis was done by simulation on a 39-bus test power system of the effects that locations and amounts of static var compensation have on the stability margin of the system. Two previously proposed stability indices, minimum singular value of load flow Jacobian and total generated reactive power, were used as starting points for sensitivity analysis. A numerical differentiation algorithm was proposed for calculation of the sensitivities of σ_{min} with respect to shunt susceptances installed at different load bus locations. A simpler and computationally more effective algorithm was proposed for calculation of sensitivities of total generated reactive power Q_t^t with respect to var support locations. Since both algorithms produced almost identical results, a faster one (which corresponds to Q_t^t) was found preferable for this application. The choice of locations is made from the list of sensitivity factors arranged in decreasing order. The installed compensation capacity is proposed to be proportional to the values of corresponding sensitivity factors for the chosen locations. Three scenarios of static compensation were simulated on a 39-bus test system in order to assess the effects of placement and amount of var support on stability boundary. It was established that the stability margin depends almost linearly on the total installed capacity of static compensation, and that smaller amounts of compensation (which can improve voltage profile to satisfactory level) are not enough to improve the stability margin satisfactorily. Static compensation was found to be of limited help when voltage instabilities similar to the one described in [131] occur in power systems. Although it may provide some improvement at high load-

ing levels, only substantial amounts of reactive power injected by static compensation may significantly improve the stability margin. Most power systems do not have such a var support reserve and it would be impractical to build it.

The feasibility of implementation of the analyses and algorithms presented in this text relies on development of a feasible integrated monitoring and control hardware for power system voltage stability. The phasor measurement system which was designed at Virginia Polytechnic Institute and State University during the past four years represents an ideal starting point for implementation of real-time monitoring and control procedures. It takes advantage of the best modular hardware components which are commercially available at this time and shows great promise for a number of future applications which require high rate of systemwide data acquisition at high accuracy. The improvement of the existing hardware which would take advantage of the superior performance of the next generation of microcomputers will represent a challenging research effort per se and will extend the feasibility of real-time power system monitoring and control beyond the current objective of controlling the slow dynamics.

Bibliography

1. C. Barbier, J. Barret, "An analysis of the phenomena of the voltage collapse on a transmission system" ; *Revue Generale d'Electricite* , 1980, pp.672-690.

2. J. Barret et al., "Power system voltage regulation" ; *RGE, Special Issue*, July 1980, pp.37-48.

3. Direction de la Production et du Transport d'EDF, "Les risques d'incident generalise de tension sur les reseaux de transport - analyse des phenomenes et recherche des remedes" ; *Doc.nr.D.63/563-A* .

4. J. Medanic, M. Ilic-Spong, J. Christensen, "Discrete models of ULTC transformers coordination" ; *Trans. IEEE PWRS-2*, No.4, Nov.1987, pp.873-882.

5. M. Ilic-Spong, J. Thorp, M. Spong, "Localized performance of decoupled Q-V network" ; *IEEE Trans. CAS*, Vol.CAS-33, No.3, March 1986, pp.316-322.

6. J. Thorp, M. Ilic-Spong, G. Varghese, "Optimal secondary voltage - var control using the pilot-point information structure" ; *Proc. 23th CDC*, Dec. 1984, pp. 462-466.

7. J. Thorp, M. Ilic-Spong, G. Varghese, "An optimal secondary voltage - var control technique" ; *IFAC Automatica*, Vol.22, No.2,1986, pp.217-221.

8. M. Ilic-Spong, J. Medanic, "Modeling and control of slow voltage dynamics in electric power systems" ; *IFAC Conf.*, 1986.

9. J. Thorp, J. Schultz, M. Ilic-Spong, "Reactive power - voltage problem - conditions for the existence of the solution and localized disturbance propagation" ; *Electrical Power and Energy Systems*, 1986, pp. 66-74.

10. J. Thorp, M. Ilic-Spong, G. Varghese, "Conditions for localized response in decoupled voltage - var networks" ; *Proc.PSCC Conf.*, 1984., pp.664-670.

11. Blanchon, "A new aspect of studies of reactive energy and voltage on the networks" ; *Proc.PSCC Conf.*, 1972., paper 2.1./15.

12. M. Ilic-Spong, J. Medanic, "Strategies for real-time voltage var monitoring" ; *Communications and Control*, IEE, 1986.

13. Stadlin, Fletcher, "Voltage versus reactive current model for dispatch and control" ; *IEEE-PAS-101*, No.10, Oct.1982, pp. 3751-3760.

14. M. Calovic, "Modeling and analysis of ULTC transformer for control system applications" ; *Proc. PSCC Conf.*, 1984., pp.746-751.

15. C. Barbier et al., "Demands on reactive power compensation to maintain acceptable voltages on the French network - planning and method of operating the shunt capacitors" ; *RGE*, Special Issue, July 1980, pp.22-36.

16. T. J. Miller, "Reactive power control in electric power systems" ; John Wiley and Sons Inc., New York, 1982.

17. Carpentier, Girard, Scano, "Voltage collapse proximity indicators computed from an optimal load flow" ; *Proc. PSCC*, 1982., pp.671-677.

18. Zaragocin, Yan, O'Connell, Mercede, Fischl, "A Review of Methods for predicting Voltage Collapse of Power Systems" ; *Proceedings of North American Power Symposium*, Cornell University, Ithaca NY, Oct. 1986.

19. A. Tiranuchit, R.J. Thomas, "VAr Support and Voltage Instabilities in Electric Power Networks" ; *Proceedings of North American Power Symposium*, Cornell University, Ithaca NY, Oct. 1986.

20. DeMarco, Qian, "A New Result on Exit Time Calculations for Electric Power System Security Assessment" ; *Proceedings of North American Power Symposium*, Cornell University, Ithaca NY, Oct. 1986.

21. Kessel, Glavitsch, "Estimating the Volage Stability of a Power System" ; *IEEE Transactions on Power Delivery*, Vol. PWRD-1, No.3, July 1986.. pp.346-354.

22. Y. Tamura, M. Mori, H. Iwamoto, "Relationship between Voltage Instability and Multiple Load Flow Solutions in Electric Power Systems" ; *IEEE Trans.* , Vol. PAS-102, No.5, May 1983., pp.1115-1125.

23. C. DeMarco, A. Bergen, "A Security Measure for Random Load Disturbances in Nonlinear Power System Models" ; *IEEE Trans.*, Vol. CAS-34, No.12, Dec. 1987., pp.1546-1557.

24. Abe, Fukunaga, Isono, Kondo, "Power System Voltage Stability" ; *IEEE Trans.*, PAS-101, No.10, Oct. 1982., pp.3830-3840.

25. C. C. Liu, K. T. Vu, "Analysis of Tap-Changer Dynamics and Construction of Voltage Stability Regions" ; submitted to IEEE Trans. on CAS.

26. M. Brucoli, La Scala, Torelli, "A Probabilistic Approach to the Voltage Stability Analysis of Interconnected Power Systems" ; *Electric Power Systems Research*, No.10, 1986, pp.157-166.

27. R. Kaye, F. Wu, "Dynamic Security Regions of Power Systems" ; *IEEE Trans.*, Vol. CAS-29, No.9, Sep. 1982, pp. 612-623.

28. Hano, Tamura, Narita, Matsumoto, "Real Time Control of System Voltage and Reactive Power" ; *IEEE Trans.*, Vol. PAS-88, No.10, Oct. 1969, pp.1544-1559.

29. P. Kokotovic, H. Khalil, J. O'Reilly, "Singular Perturbation Methods Control Analysis and Design" ; Academic Press, 1986.

30. F. Wu, S. Kumagai, "Steady State Security Regions of Power Systems" ; *IEEE Trans.*, Vol. CAS-29, No.11, Nov. 1982, pp. 703-711.

31. F. Wu, C.C. Liu, "Characterization of Power System Small Disturbance Stability with Models Incorporating Voltage Variation" ; *IEEE Trans.*, Vol CAS-33, No.4, Apr. 1986, pp. 406-417.

32. M. Brucoli, F. Rossi, F. Torelli, M. Trovato, "A Generalized Approach to the Analysis of Voltage Stability in Electric Power Systems" ; *Electric Power Systems Research*, No. 9, 1985, pp.49-62.

33. Bijwe, Kothari, Nanda, Lingamurthy, "Optimal Voltage Control Using a Constant Sensitivity Matrix" ; *Electric Power Systems Research*, No.11, 1986., pp.195-203.

34. A. Araposthatis, S. Sastry, P. Varaiya, "Analysis of Power-flow Equation" ; *Electric Power and Energy Systems*, Vol.3, No.3, pp.115-126, July 1981.

35. A. Araposthatis, S. Sastry, P. Varaiya, "Global Analysis of Swing Dynamics" ; *IEEE CAS-29*, No.10, Oct. 1982, pp. 673-678.

36. F. Salam, J. Marsden, P. Varaiya, "Chaos and Arnold Diffusion in Dynamical Systems" ; *IEEE CAS-30*, No.9, Sep. 1983, pp.697-708.

37. F. Salam, J. Marsden, P. Varaiya, "Arnold Diffusion in the Swing Equations of a Power System" ; *IEEE Trans.*, CAS-31, No.8, Aug. 1984, pp. 673-688.

38. E. Abed, P. Varaiya, "Nonlinear Oscillations in Power Systems" ; *Electric Power Systems Research*, 1983.

39. N. Kopell, R. Washburn, "Chaotic Motions in the Two-Degree-of-Freedom Swing Equations" ; *IEEE Trans.*, CAS-29, No.11, Nov.1982, pp. 738-746.

40. H.G. Kwatny, A.K. Pasrija, L.Y. Bahar, "Static Bifurcations in Electric Power Networks - Loss of Steady State Stability and Voltage Collapse" ; *IEEE Trans.*, Vol. CAS-33, Oct. 1986, pp.981-991.

41. V.A. Venikov, V.A. Stroev, V.I. Idelchick, V.I. Tarasov, "Estimation of Electrical Power System Steady State Stability in Load Flow Calculations" ; *IEEE Trans.*, Vol. PAS-94, No.3, May/June 1975, pp.1034-1038.

42. C. DeMarco, "A Large Deviations Model for Voltage Collapse in Electric Power Systems" ; *Proc. IEEE ISCAS*, Vol.3, San Diego, 1986., pp.1011-1014.

43. Fischl, Zaragocin, Mercede, Yan, "Power System Models for Voltage Collapse" ; *Proc. IEEE ISCAS*, Vol.3, San Diego, 1986., pp.1015-1018.

44. Sauer, Rajagopolan, Pai, Varghese, "Critical Modes and Voltage Instability in Power Systems" ; *Proc. IEEE ISCAS*, Vol.3, San Diego, 1986., pp. 1019-1022.

45. Costi, Shu, Schlueter, "Power System Voltage Stability and Controllability" ; *Proc. IEEE ISCAS*, Vol.3, San Diego, 1986, pp.1023-1027.

46. C.C. Liu, "Characterization of a Voltage Collapse Mechanism due to the Effects of on-load Tap Changers" ; *Proc. IEEE ISCAS*, Vol.3, San Diego, 1986, pp. 1028-1030.

47. N. Narasimhamurthi, "Noise Induced Voltage Collapse" ; *Proc. IEEE ISCAS*, Vol.3, San Diego, 1986., pp. 1031-1034.

48. Sauer, Ahmed-Zaid, Pai, "Nonlinear Decoupling in a Class of Quadratic Two-time Scale Systems with Applications to Synchronous Machine Models" ; *Proc. 23rd CDC Conf.*, Las Vegas, Dec. 1984, pp.481-484.

49. Galiana, "Load Flow Feasibility and the Voltage Collapse Problem" ; *Proc. 23rd CDC Conf.*, Las Vegas, Dec. 1984, pp.485-487.

50. Liu, Wu, "Steady-state Voltage Stability Regions of Power Systems" ; *Proc. 23rd CDC Conf.*, Las Vegas, Dec. 1984, pp.488-493.

51. Thorp, Ilic-Spong, Varghese, "Optimal secondary Voltage-var Control using Pilot Point Information Structure" ; *Proc. 23rd CDC Conf.*, Las Vegas, Dec. 1984, pp.462-466.

52. Varghese, Levy, Kailath, "A Generalized State-Space for Singular Systems" ; *IEEE Trans. on AC*, Vol. AC-26, No.4, August 1981., pp.811-831.

53. Abe, Hamada, Isono, Okuda, "Load Flow Convergence in the Vicinity of a Voltage Stability Limit" ; *IEEE Trans.*, Vol. PAS-97, No.6, Nov/Dec 1978, pp.1983-1993.

54. H.D. Chiang, F. Wu, "On voltage Stability" ; *Proceedings of the 1986 ISCAS*, Vol.3, May 1986, pp.1339-1343.

55. R.J. Thomas, "Reasearch opportunuties focused on electric power systems" ; *Proc. 26th CDC Conf.*, Los Angeles, Dec. 1987, pp.391-392.

56. Rogers, "Methods for small signal analysis of very large power systems" ; *Proc. 26th CDC Conf.*, Los Angeles, Dec. 1987, pp.393-398.

57. Ilic, Stankovic, "Feasibility problems in transferring large reactive power over the large distances" ; *Proc. 26th CDC Conf.*, Los Angeles, Dec. 1987, pp.399-407.

58. Zaborszky, Huang, Zheng, Leung, "New results on stability monitoring on the large electric power system" ; *Proc. 26th CDC Conf.*, Los Angeles, Dec. 1987, pp.30-40.

59. Pai et al., "Application of integral manifold theory in large scale power system stability analysis" ; *Proc. 26th CDC Conf.*, Los Angeles, Dec. 1987, pp.41-44.

60. M. Ilic, F. Mak, "Mid-range voltage dynamics modeling with the load controls present" ; *Proc. 26th CDC Conf.*, Los Angeles, Dec. 1987, pp.45-52.

61. R.J. Thomas, A. Tiranuchit, "Dynamic voltage instability" ; *Proc. 26th CDC Conf.*, Los Angeles, Dec. 1987, pp.53-58.

62. Schlueter, Lo, Yazdankhah, "A fast accurate method for direct assessment of transient stability" ; *Proc. 26th CDC Conf.*, Los Angeles, Dec. 1987, pp.59-65.

63. Tsai, Parlos, "Minimizing the effects of unknown-but-bounded disturbances in power plants" ; *Proc. 26th CDC Conf.*, Los Angeles, Dec. 1987, pp.66-71.

64. H.D. Chiang, J. Thorp, "The closest unstable equilibrium point method for power system dynamic security assessment" ; *Proc. 26th CDC Conf.*, Los Angeles, Dec. 1987, pp.72-76.

65. H.Mori, S. Tsuzuki, "Estimation of Load Buses in the Proximity of Voltage Limitations" ; *Proc. of the IASTED International Symposium HIGH TECHNOLOGY IN THE POWER INDUSTRY*, Scottsdale, Arizona, March 1-4, 1988, pp.138-142.

66. M. Langevin, P. Auriol, "Load Response to Voltage Variations and Dynamic Stability" ; *IEEE PES Winter Meeting 1986*, paper 86 WM 078-0.

67. A.E. Hammad, "Analysis of Power System Stability Enhancement" ; *IEEE Trans. PWRS-1*, No.4, Nov.1986, pp.222-232.

68. W.R. Lachs, "Insecure System Reactive Power Balance Analysis and Counter Measures" ; *Trans. IEEE PAS-104*, No.9, Sep.1985, pp.2413-2419.

69. J. Zaborszky, "On-line Detection of System Instabilities" ; *DOE Report DE-AC01-84CE-76258* .

70. G.L. Mealy, "Research Progress in Disturbance Recognition and System Impact Evaluation" ; *DOE Report DE-AC01-84CE-76250* .

71. R.J. Thomas, A. Tiranuchit, "A Posture Coordinating Strategy for Large Electric Power Systems" ; *DOE Report DE-FG03-SF15784* .

72. J.H. Chow, M. Ilic et al., "Development of a Decoupling Methodology for On-line Detection of System Instabilities" ; *DOE Report DE-AC01-84CE-76249* .

73. Boeing Computer Services, "A Physically Based Methodology for Constructing Load Models for Power Systems" ; *DOE Report DOE-AC01-78ET-29020*, June 1982.

74. C. Rajagopalan, "Dynamics of Voltage Collapse" ; M.S. Thesis, University of Illinois, Urbana-Champaign, PAP-TR-85-4, October 1985.

75. J. Jarjis, F.D. Galiana, "Quantitative Analysis of Steady State Stability in Power Networks" ; *IEEE PAS-100*, No.1, Jan.1981, pp.318-326.

76. M. Chau, R. Gutman, B. Pasternak, "Understanding Voltage Collapse in Bulk Transmission Systems" ; presented at The Engineering Foundation Conference on Bulk Power System Voltage Phenomena, Voltage Stability and Security, September 18-23, 1988, Potosi, Missouri.

77. W.R. Lachs, "Planning Perspectives on Voltage Problems" ; presented at The Engineering Foundation Conference on Bulk Power System Voltage Phenomena, Voltage Stability and Security, September 18-23, 1988, Potosi, Missouri.

78. C. Concordia, "Voltage Stability and Security" ; presented at The Engineering Foundation Conference on Bulk Power System Voltage Phenomena, Voltage Stability and Security, September 18-23, 1988, Potosi, Missouri.

79. H.K. Clark, "Voltage Control Practices in North America" ; presented at The Engineering Foundation Conference on Bulk Power System Voltage Phenomena, Voltage Stability and Security, September 18-23, 1988, Potosi, Missouri.

80. J. Zaborszky, "Some Basic Issues in Voltage Stability and Viability " ; presented at The Engineering Foundation Conference on Bulk Power System Voltage Phenomena, Voltage Stability and Security, September 18-23, 1988, Potosi, Missouri.

81. M. Awad, H. Zein El-Din, C. Graham, "Preventive Measures to Voltage Collapse in Bulk Electricity Systems" ; presented at The Engineering Foundation Conference on Bulk Power System Voltage Phenomena, Voltage Stability and Security, September 18-23, 1988, Potosi, Missouri.

82. Y. Ichida, "Studies Under Way in Japan for Improved Analyses of Voltage Related System Behaviours" ; presented at The Engineering

Foundation Conference on Bulk Power System Voltage Phenomena, Voltage Stability and Security, September 18-23, 1988, Potosi, Missouri.

83. L.R. Noyes, "A Framework for the Situational Determination of Voltage and Current Constraint Thresholds and Control Priorities in the Development of Remedial Action Plans" ; presented at The Engineering Foundation Conference on Bulk Power System Voltage Phenomena, Voltage Stability and Security, September 18-23, 1988, Potosi, Missouri.

84. R. Dunnett, P. Berry, R. Ettelaie, "An Algorithm for Reactive Compensation Planning in England and Wales" ; presented at The Engineering Foundation Conference on Bulk Power System Voltage Phenomena, Voltage Stability and Security, September 18-23, 1988, Potosi, Missouri.

85. J.P. Paul, "Electricite de France Current Practice of Voltage Control" ; presented at The Engineering Foundation Conference on Bulk Power System Voltage Phenomena, Voltage Stability and Security, September 18-23, 1988, Potosi, Missouri.

86. H.G. Kwatny, "Steady State Analysis of Voltage Instability Phenomena" ; presented at The Engineering Foundation Conference on Bulk Power System Voltage Phenomena, Voltage Stability and Security, September 18-23, 1988, Potosi, Missouri.

87. F. Alvarado, T. Jung, "Direct Detection of Voltage Collapse Conditions" ; presented at The Engineering Foundation Conference on Bulk Power System Voltage Phenomena, Voltage Stability and Security, September 18-23, 1988, Potosi, Missouri.

88. Y. Tamura, K. Sakamoto, Y. Tayama, "Current Issues in the Analysis of Voltage Instability Phenomena" ; presented at The Engineering Foundation Conference on Bulk Power System Voltage Phenomena, Voltage Stability and Security, September 18-23, 1988, Potosi, Missouri.

89. Y. Sekine, A. Yokoyama, T. Kumano, "A Mehtod for Detecting a Critical State of Voltage Collapse" ; presented at The Engineering Foundation Conference on Bulk Power System Voltage Phenomena, Voltage Stability and Security, September 18-23, 1988, Potosi, Missouri.

90. Y. Sekine et al., "Mode Transition of Multiple Load Flow Solution" ; presented at The Engineering Foundation Conference on Bulk Power System Voltage Phenomena, Voltage Stability and Security, September 18-23, 1988, Potosi, Missouri.

91. A. Yokoyama, Y. Sekine, "A Static Voltage Stability Index Based on Multiple Load Flow Solutions" ; presented at The Engineering Founda-

tion Conference on Bulk Power System Voltage Phenomena, Voltage Stability and Security, September 18-23, 1988, Potosi, Missouri.

92. R. Schlueter et al., "Reactive Supply - On-line Security Criteria" ; presented at The Engineering Foundation Conference on Bulk Power System Voltage Phenomena, Voltage Stability and Security, September 18-23, 1988, Potosi, Missouri.

93. R. Navarro-Perez, B. Cory, M. Short, "Voltage Collapse Proximity Analysis Using Reactive Area Identification" ; presented at The Engineering Foundation Conference on Bulk Power System Voltage Phenomena, Voltage Stability and Security, September 18-23, 1988, Potosi, Missouri.

94. Y. Tamura et al., "Monitoring and Control Strategies of Voltage Stability Based on Voltage Instability Index" ; presented at The Engineering Foundation Conference on Bulk Power System Voltage Phenomena, Voltage Stability and Security, September 18-23, 1988, Potosi, Missouri.

95. M. Ilic, "New Approaches to Voltage/ Reactive Power Monitoring and Control" ; presented at The Engineering Foundation Conference on Bulk Power System Voltage Phenomena, Voltage Stability and Security, September 18-23, 1988, Potosi, Missouri.

96. A.R. Bergen, D.J. Hill, "A Structure Preserving Model for Power System Stability Analysis" ; *IEEE PAS-100*, No.1, Jan. 1981, pp.25-35.

97. N. Tsolas, A. Arapostathis, P. Varaiya, "A Structure Preserving Energy Function for Power System Transient Stability Analysis" ; *IEEE Trans. CAS-32*, No.10, Oct. 1985, pp. 1041-1049.

98. N. Narasimhamurthi, M. Musavi, "A generalized Energy Function for Transient Stability Analysis of Power Systems" ; *IEEE Trans. CAS-31*, No.7, July 1984, pp.637-645.

99. R.C. Burchett et al., "Developments in Optimal Power Flow" ; *Trans. IEEE PAS-101*, No.2, Feb. 1982, pp.406-413.

100. Working Group 38-01, "Static VAR Compensators" ; *CIGRE, Task Force No.2 on SVC*, 1986, Paris, France.

101. V.A. Barinov, S.A. Sovalov, V.A. Stroev, V.A. Venikov, "Load-flow and Steady State Stability Analysis of Complex Electric Power Systems with the Account of Frequency Variations" ; *CIGRE paper 38-08*, 1988, Paris, France.

102. K. Walve, "Modelling of Power System Components at Severe Disturbances" ; *CIGRE paper 38-18*, 1986, Paris, France.

103. M. Pavard, Special Report for Group 38, "Power System Analysis and Techniques" ; *CIGRE paper 38-00*, 1986, Paris, France.

104. Y. Gurevith, L. Libova, "Characteristics of Power System Loads and Their Usage for System Operating Condition Management" ; *CIGRE paper 38-17*, 1986, Paris, France.

105. P. Boremans, A. van Ranst, "A General Stability Criterion for Long Distance AC Power Transmission with Static VAR Compensation" ; *CIGRE paper 38-16*, 1986, Paris, France.

106. G. Manzoni, Special Report for Group 38, "Power System Analysis and Techniques" ; *CIGRE paper 38-00*, 1988, Paris, France.

107. J. Vithayathil, C. Taylor, M. Klinger, W. Mittelstadt, "Case Studies of Conventional and Novel Methods of Reactive Power Control on an AC Transmission System" ; *CIGRE paper 38-02*, 1988, Paris, France.

108. M. Stubbe et al., "Simulation of the Dynamic Behaviour of Electrical Power Systems in the Short and Long Terms" ; *CIGRE paper 38-03*, 1988, Paris, France.

109. B. Klerfors, T. Petersson, "Balancing Assymmetries by means of Thyristor -Controlled Static VAR Compensators" ; *CIGRE paper 38-05*, 1988, Paris, France.

110. W. Jervis, J. Scott, H. Griffiths, "Future Application of Reactive Compensation Plant on the CEGB System to Improve Transmission Network Capability" ; *CIGRE paper 38-06*, 1988, Paris, France.

111. G. Allen, V. Henner, C. Popple, "Optimisation of Static VAR Compensators and Switched Shunt Capacitors in a Long Distance Interconnection" ; *CIGRE paper 38-07*, 1988, Paris, France.

112. F. Iliceto et al., "Optimal Use of Reactive Power Resources for Voltage Control in Long Distance EHV Transmission Applications to the Turkish 420 kV System" ; *CIGRE paper 38-13*, 1988, Paris, France.

113. R. Giglioli et al., "Reactive Power Balance Optimization to Improve the Energy Transfer Through AC Transmission Systems over Very Long Distance " ; *CIGRE paper 38-16*, 1988, Paris, France.

114. B. Lereverend, "System Operation and Control" ; *CIGRE paper 39-00*, Special report of Group 39, 1988, Paris, France.

115. Y. Akimoto, T. Hayashi, "Computerized Integrated Automatic Control System for Electric Power Networks" ; *CIGRE paper 39-04*, 1988, Paris, France.

116. I. Benko et al., "Reactive Power Scheduling and Control in the Hungarian Power System" ; *CIGRE paper 39-08, 1988*, Paris, France.

117. L. Cosheev et al., "Hierarchical Stability Control System in the UPG of the USSR" ; *CIGRE paper 39-10*, 1988, Paris, France.

118. D. Denzel et al., "Optimal Power Flow and Its Real-Time Application at The RWE Energy Control Centre" ; *CIGRE paper 39-19*, 1988, Paris, France.

119. J. Guckenheimer, P. Holmes, "Nonlinear Oscillations, Dynamical Systems, and Bifurcations of Vector Fields" ; Springer-Verlag, 1983.

120. R. Bacher, W. Tinney, "Faster Local Power Flow Solution - The Zero Mismatch Approach" ; *IEEE PES Winter Meeting 1989*, paper 89-WM-129-8 PWRS.

121. M. Ilic, A. Stankovic, "Voltage Problems on Transmission NetworksSubject to Unusual Power Flow Patterns" ; *IEEE PES Winter Meeting 1989*, paper 89-WM-158-7 PWRS.

122. R. Fischl, F. Mercede, "Can Voltage Stability Indices Predict Voltage Collapse Problems in Large-Scale Power Networks?" ; *Proc. ISCAS 1988*, Finland, 1988.

123. C. DeMarco, T. Overbye, "Low Voltage Power Flow Solutions and Their Role in Exit Time Based Security Measures for Voltage Collapse" ; *Proc. 27th CDC*, Austin, Texas, Dec. 1988, pp. 2127-2131.

124. P. Sauer, M. Pai, "Steady State Stability and Load Flow" ; *Proc. 27th CDC*, Austin, Texas, Dec. 1988, pp. 2110-2113.

125. Y. Tamura, K. Sakamoto, Y. Tayama, "Voltage Instability Proximity Index (VIPI) Based on Multiple Load Flow Solutions in Ill-Conditioned Power Systems" ; *Proc. 27th CDC*, Austin, Texas, Dec. 1988, pp. 2114-2119.

126. K.T. Vu, C.C. Liu, "Analysis of Several mechanisms of Voltage Collapse" ; *Proc. 27th CDC*, Austin, Texas, Dec. 1988.

127. R. Shlueter, M. Chang, A. Costi, "Loss of Voltage Controllability as a Cause of Voltage Collapse" ; *Proc. 27th CDC*, Austin, Texas, Dec. 1988, pp.2120-2126.

128. R. Fischl, J. Chow, H. Yan, F. Mercede, F. Wu, "A Comparison of Indices for Predicting Voltage Collapse in Power Systems" ; *Proc. 27th CDC*, Austin, Texas, Dec. 1988, pp. 2098-2103.

129. H.G.Kwatny, X.Yu, "Energy Functions and Load-Induced Flutter Instability in Classical Models of Electric Power Networks" ; *Proc. 27th CDC*, Austin, Texas, Dec. 1988, pp. 690-695.

130. I. Dobson, H. D. Chiang, J. S. Thorp, L. Fekih-Ahmed, "A Model of Voltage Collapse in Electric Power Systems" ; *Proc. 27th CDC*, Austin, Texas, Dec. 1988, pp.2104-2109.

131. A. Kurita, T. Sakurai, "The Power System Failure on July 23, 1987 in Tokyo" ; *Proc. 27th CDC*, Austin, Texas, Dec. 1988, pp.2093-2097.

132. D.J. Damsker, "Control Data Networks for Power and Industrial Plants" ; IEEE Tutorial Course 86 EH0240-2-PWR.

133. IEEE, "Fundamentals of Load Management" ; IEEE Tutorial Course 89 EH0289-9-PWR.

134. G. Sheble, "Reactive Power - Basics, Problems and Solutions" ; IEEE Tutorial Course 87 EH 0262-6-PWR.

135. W. Tinney, V. Brandwajn, S. Chan, "Sparse Vector Methods" ; *IEEE PAS-104*, No.2, Feb. 1985, pp. 295-301.

136. O. Alsac, B. Stott, W. Tinney, "Sparsity-Oriented Compensation Methods for Modified Network Solutions" ; *IEEE PAS-102*, No.5, May 1983, pp. 1050-1060.

137. W. Tinney, J. Walker, "Direct Solutions of Sparse Network Equations by Optimally Ordered Triangular Factorization" ; *Proc. IEEE*, Vol.55, No.11, Nov.1967, pp.1801-1809.

138. J. Chow, J. Cullum, R. Willoughby, "A Sparsity-Based Technique for Identifying Slow-Coherent Areas in Large Power Systems" ; *IEEE PAS-103*, No.3, March 1984, pp.463-473.

139. J. Chow, P. Kokotovic, "Time Scale Modeling of Sparse Dynamic Networks" ; *IEEE Trans on Automatic Control*, Vol.AC-30, No.8, Aug.1985, pp. 714-722.

140. M. Sezer, D. Siljak, "Nested Epsilon-Decompositions and Clustering of Complex Systems" ; *Automatica*, Vol.22, No.3, 1986, pp.321-331.

141. M. Araki, M. Metwally, D. Siljak, "Generalized Decompositions for Transient Stability Analysis of Multimachine Power Systems, from - Large Scale Systems 3" ; North Holland Publishing Company, 1982, pp.111-122.

142. Lj. Jocic, D. Siljak, "On Decomposition and Transient Stability of Multimachine Power Systems" ; *Ricerche di Automatica*, Vol.8, No.1, Apr. 1977,pp.41-58.

143. M. Ikeda, D. Siljak, "Overlapping Decompositions, Expansions and Contractions of Dynamic Systems, from - Large Scale Systems 1" ; North Holland Publishing Company, 1980, pp.29-38.

144. M. Ikeda, D. Siljak, "Generalized Decompositions and Stability of Nonlinear Systems" ; *Proc. 18th Allerton Conference*, Univ. of Illinois, Monticello, Illinois, Oct. 8-10, 1980.

145. Lj. Jocic, M. Ribbens-Pavella, D. Siljak, "Multimachine Power Systems - Stability, Decomposition and Aggregation" ; *IEEE Trans. on Automatic Control*, Vol. AC-23, No.2, Apr. 1978, pp.325-331.

146. M. Ikeda, D. Siljak, D. White, "Decentralized Control with Overlapping Information Sets" ; *Journal of Optimization Theory and Applications*, Vol.34, No.2, June 1981, pp.279-310.

147. V. Vittal, N. Bhatia, A. Fouad, G. Maria, H. Zein El-Din, "Incorporation of Nonlinear Load Models in the Transient Energy Function Method" ; *IEEE PES Winter Meeting 1989*, paper 89 WM 206-4 PWRS.

148. V. Vittal, E. Zhou, C. Hwang, A. Fouad, "Derivation of Stability Limits Using Analytical Sensitivity of the Transient Energy Margin" ; *IEEE PES Winter Meeting 1989*, paper 89 WM 207-2 PWRS.

149. C. Tavora, O. Smith, "Stability Analysis of Power Systems" ; *IEEE PES Summer Meeting 1971*, paper 71 TP 591-PWR.

150. C. Tavora, O. Smith, "Equilibrium Analysis of Power Systems" ; *IEEE PES Summer Meeting*, paper 71 TP 590-PWR.

151. M. Langevin, P. Auriol, "Load Response to Voltage Variations and Dynamic Stability" ; *IEEE PES Winter Meeting 1986*, paper 86 WM 078-0.

152. Report, "Proposed Terms and Definitions for Power System Stability" ; *IEEE PAS-101*, No.7, July 1982, pp.1894-1898.

153. A. Venkataramana, J. Carr, R. Ramshaw, "Optimal Reactive Power Allocation" ; *IEEE PES Winter Meeting 1986*, paper 86 WM 103-6.

154. I. Dobson, H.D. Chiang, "Towards a Theory of Voltage Collapse in Electric Power Systems" ; preliminary draft of paper, 5/4/88, Cornell University, Ithaca, NY.

155. J. Baillieul, C. Byrnes, "Geometric Critical Point Analysis of Lossless Power System Models" ; *IEEE Trans. CAS-29*, No.11, Nov.1982, pp. 724-737.

156. R. O. Burnett , "Field Experience with Absolute Time Synchronism Between Remotely Located Fault Recorders and Sequence of Event Recorders" ; *IEEE Trans. PAS-103*, No.7, July 1984, pp.1739-1742.

157. P. Bonanomi, "Phase Angle Measurements with Synchronized Clocks - Principle and Applications" ; *IEEE Trans. PAS-100*, No.12, Dec. 1981, pp.5036-5043.

158. A. G. Phadke, J. S. Thorp, A. G. Adamiak, "A New Measurement Technique for Tracking Voltage Phasors, Local System Frequency, and Rate of Change of Frequency" ; *IEEE Trans. PAS-102*, No.5, May 1983, pp.1025-1038.

159. A. G. Phadke, J. S. Thorp, K. J. Karimi, " State Estimation with Phasor Measurements" ; *Proc. PICA 1985*, May 1985, San Francisco, CA.

160. J. S. Thorp, A. G. Phadke, K. J. Karimi, "Real-Time Voltage Phasor Measurements for Static State Estimation" ; *IEEE Trans. PAS-104* , No.11, Nov. 1985, pp.3098-3116.

161. K. J. Karimi, J. S. Thorp, A. G. Phadke, "Partitioned State Estimation and Bad Data Processing for Static State Estimators with Phasor Measurements" ; *IEEE PES Summer Meeting 1986* .

162. M. Ilic-Spong, A. G. Phadke, "Redistribution of Reactive Power Flow in Contingency Studies" ; *Proc. PICA 1985*, May 1985, San Francisco, CA, pp.336-344.

163. R. Fischl et al., "An Algorithm for Automatically Tuning The Weights of Performance Indices for Monitoring Power System Loading or Security" ; *Proc. PICA 1985*, May 1985, San Francisco, CA, pp.345-351.

164. C. S. Indulkar, B. Viswanathan, S. S. Venkata, "Maximum Power Transfer Limited by Voltage Stability In Series And Shunt Compensated Schemes For AC Transmission Systems" ; *IEEE Transactions on Power Delivery* , Vol.4, No.2, April 1989, pp.1246-1252.

165. A. Phadke, M. Begovic, V. Centeno, A. Chaudhary, V. Phaniraj, "Coherent Sampling for System-Wide Digital Relaying" ; *NSF Conference on Computer Relaying*, October 1987, Blacksburg, VA.

166. A. Phadke, M. Begovic, V. Centeno, V. Phaniraj, "Clock Synchronization for Improved Monitoring, Protection and Control" ; *Proceedings of IASTED Conference*, Phoenix, Arizona, March 1988, pp.9-13.

167. J. Thorp, A. Phadke, S. Horowitz, M. Begovic, "Some Applications of Phasor Measurements to Adaptive Protection" ; *IEEE Trans. on Power Systems*, Vol.3, No.2, May 1988, pp.791-798.

168. M. Begovic, A. Phadke, "Dynamic Simulation of Voltage Collapse" ; *Proc. of PICA 89 Conference*, May 1989, Seattle, Washington.

169. M. Begovic, A. Phadke, "Analysis of Voltage Collapse by Simulation" ; *Proc. of ISCAS 89*, Portland, Oregon, May 1989.

170. M. Begovic, A. Phadke, "Voltage Stability Assessment Through Measurement of The Reduced State Vector" ; *IEEE PES Summer Meeting 1989*, July 1989, Long Beach, California.

171. H.D. Chiang et al., "On Voltage Collapse in Electric Power Systems" ; *Proceedings PICA 89*, Seattle, Washington, May 1-5, pp.342-349.

172. Q. Wu, "Stabilitatsanalyse von Regelsystemen mit Begrenzungen" ; PhD Dissertation, ETH Zurich, Switzerland, 1986.

173. P. Kessel, "Verfahren zur Online-Beurteilung der stationaren Spannungsstabilitat in elektrischen Netzen" ; PhD Dissertation, ETH Zurich, Switzerland 1985.

174. G. Schnyder, "Verfahren zur Bestimmung des optimalen und N-1 sicheren Energieubertragungsnetzes" ; PhD Dissertation, ETH Zurich, Switzerland, 1988.

175. C. DeMarco, "Probabilistic Dynamic Security Measures for Analyzing Voltage Stability" ; presented at The Engineering Foundation Conference on Bulk Power System Voltage Phenomena, Voltage Stability and Security, September 18-23, 1988, Potosi, Missouri.

176. K. Mehlhorn, "Data Structures and Algorithms 2 - Graph Algorithms and NP-completeness" ; Springer-Verlag, New York, 1984, pp. 171-178, 191-198.

177. B. Stott, "Power System Dynamic Response Calculations" ; *Proc. of the IEEE*, Vol.67, No.2, February 1979, pp.219-241.

178. P.Anderson, A. Fouad, "Power System Control and Stability" ; Iowa State University Press, Ames, Iowa, 1977.

179. L. Johnson, R. Riess, "Numerical Analysis" ; Addison-Wesley Publishing Company, Reading, Massachusetts, 1982.

Appendix A. Parameters of Power System Model

FROM	TO	LINE RESISTANCE R [pu]	LINE REACTANCE X [pu]	SHUNT SUSCEPTANCE Y/2 [pu]	LINE #
1	2	0.0035	0.0411	0.34935	1
1	39	0.0010	0.0250	0.37500	2
2	3	0.0013	0.0151	0.12860	3
2	25	0.0070	0.0086	0.07300	4
3	4	0.0013	0.0213	0.11070	5
3	18	0.0011	0.0133	0.10690	6
4	5	0.0008	0.0128	0.06710	7
4	14	0.0008	0.0129	0.06910	8
5	6	0.0002	0.0026	0.02170	9
5	8	0.0008	0.0112	0.07380	10
6	7	0.0006	0.0092	0.05650	11
6	11	0.0007	0.0082	0.06945	12
7	8	0.0004	0.0046	0.03900	13
8	9	0.0023	0.0363	0.19020	14
9	39	0.0010	0.0250	0.60000	15
10	11	0.0004	0.0043	0.03645	16
10	13	0.0004	0.0043	0.03645	17
13	14	0.0009	0.0101	0.08615	18
14	15	0.0018	0.0217	0.18300	19
15	16	0.0009	0.0094	0.08550	20
16	17	0.0007	0.0089	0.06710	21
16	19	0.0016	0.0195	0.15200	22
16	21	0.0008	0.0135	0.12740	23
16	24	0.0003	0.0059	0.03400	24
17	18	0.0007	0.0082	0.06595	25
17	27	0.0013	0.0173	0.16080	26
21	22	0.0008	0.0140	0.12825	27
22	23	0.0006	0.0096	0.09230	28
23	24	0.0022	0.0350	0.18050	29
25	26	0.0032	0.0323	0.25650	30
26	27	0.0014	0.0147	0.11980	31
26	28	0.0043	0.0474	0.39010	32
26	29	0.0057	0.0625	0.51450	33
28	29	0.0014	0.0151	0.12450	34

Table 1. Transmission line parameters of the system model.

FROM	TO	TRANSF. RESISTANCE R [pu]	TRANSF. REACTANCE X [pu]	TRANSF. RATIO [pu/pu]	TRANSF. #
12	11	0.0016	0.0436	1.006	1
12	13	0.0016	0.0436	1.006	2
6	31	0.0000	0.0250	1.070	3
10	32	0.0000	0.0200	1.070	4
19	33	0.0007	0.0142	1.070	5
20	34	0.0009	0.0180	1.009	6
22	35	0.0000	0.0143	1.025	7
23	36	0.0005	0.0272	1.000	8
25	37	0.0006	0.0232	1.025	9
2	30	0.0000	0.0181	1.025	10
29	38	0.0008	0.0156	1.025	11
19	20	0.0007	0.0138	1.060	12

Table 2. Transformer parameters of the system model.

GEN. NODE	VOLTAGE V [pu]	ACTIVE POWER P [pu]	MIN. REACTIVE POWER Qmin [pu]	MAX. REACTIVE POWER Qmax [-pu]
30	1.048	2.500	- 1.44	1.8
31	0.982	5.729	- 8.00	10.0
32	0.983	6.500	- 3.92	4.9
33	0.997	6.320	- 3.76	4.7
34	1.012	5.080	- 3.68	4.6
35	1.049	6.500	- 3.92	4.9
36	1.063	5.600	- 3.36	4.2
37	1.028	5.400	- 3.20	4.0
38	1.026	8.300	- 4.96	6.2
39	1.030	(1.040)	- 6.00	7.5

GEN. NODE	MOMENT OF INERTIA H	DAMPING CONSTANT D	SYNCHR. REACTANCE Xq
30	42.0	4.00	0.069
31	30.3	9.75	0.282
32	35.8	10.00	0.237
33	28.6	10.00	0.258
34	26.0	3.00	0.620
35	34.8	10.00	0.241
36	26.4	8.00	0.292
37	24.3	9.00	0.280
38	34.5	14.00	0.205
39	500.0	10.00	0.019

Table 3. Generator parameters of the system model.

LOAD NODE #	ACTIVE POWER P [pu]	REACTIVE POWER Q [pu]
1	0.000	0.000
2	0.000	0.000
3	3.220	0.024
4	5.000	1.840
5	0.000	0.000
6	0.000	0.000
7	2.338	0.840
8	5.220	1.766
9	0.000	0.000
10	0.000	0.000
11	0.000	0.000
12	0.000	0.000
13	0.000	0.000
14	0.000	0.000
15	3.200	1.530
16	3.294	0.322
17	0.000	0.000
18	1.000	0.300
19	0.000	0.000

LOAD NODE #	ACTIVE POWER P [pu]	REACTIVE POWER Q [pu]
20	0.000	1.000
21	2.740	1.150
22	0.000	0.000
23	2.475	0.846
24	3.086	0.922
25	2.240	0.472
26	1.390	0.170
27	2.810	0.755
28	2.060	0.276
29	2.835	0.269

Table 4. Nominal load requirements of the system model.

NODE	VOLTAGE [pu]	ANGLE [deg]	NODE	VOLTAGE [pu]	ANGLE [deg]
1	1.04761	- 9.5820	2	1.04912	- 7.0244
3	1.03042	- 9.8701	4	1.00371	- 10.6646
5	1.00491	- 9.4768	6	1.00725	- 8.7744
7	0.99657	-10.9785	8	0.99559	- 11.4848
9	1.02803	-11.3094	10	1.01691	- 6.3897
11	1.01242	- 7.2032	12	0.99988	- 7.2190
13	1.01407	- 7.1046	14	1.01161	- 8.7747
15	1.01560	- 9.1932	16	1.03204	- 7.7896
17	1.03380	- 8.7875	18	1.03120	- 9.6282
19	1.04977	- 3.1633	20	0.99069	- 4.5753
21	1.03183	- 5.3827	22	1.04966	- 0.9329
23	1.04463	- 1.1311	24	1.03752	- 7.6699
25	1.05764	- 5.6613	26	1.05200	- 6.9172
27	1.03779	- 8.9297	28	1.04981	- 3.4032
29	1.04956	- 0.6418	30	1.04800	- 4.6067
31	0.98200	0.0000	32	0.98300	1.6091
33	0.99700	2.0560	34	1.01200	0.6179
35	1.04900	4.0309	36	1.06300	6.7271
37	1.02800	1.1212	38	1.02600	6.4279
39	1.03000	-11.1187			

Table 5. Voltage profile of the system model in normal operating regime.

The vita has been removed from the scanned document